Molecular Size of Interacting and Degrading Polysaccharides

by

Kornelia Jumel, B.Sc. (Hons.)

Thesis submitted to the University of Nottingham

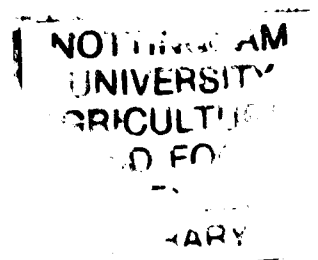for the degree of Doctor of Philosophy.

January 1994

TABLE OF CONTENTS

CHAPTER 1

CHAPTER 2

CHAPTER 3

CHAPTER 4

LIST OF FIGURES

xv

LIST OF TABLES

ACKNOWLEDGEMENTS

ABSTRACT

The use of multi angle laser light scattering on-line to size exclusion chromatography, analytical ultracentrifugation and viscosity measurements for the determination of molecular weights and conformations of polysaccharide systems is described. The use of several independent techniques for the characterization of polysaccharide systems was found to be essential due to the polydisperse nature of the materials. These techniques were used to investigate the changes in molecular size and conformation of guar gum due to irradiation. Molecular weights and viscosities were found to decrease significantly with increasing radiation dose. Conformational studies on the resulting series of homologous samples confirmed the random coil-like conformation of guar gum. Investigations on BSA/dextran complexes, obtained by dry-heating at different molar ratios showed that complex formation (most likely by a Maillard-type reaction) only took place when a low molecular weight dextran fraction was used. The highest molecular weight complexes were obtained when the BSA ratio was high, suggesting that some form of association between individual complexes and/or BSA had taken place.

CHAPTER 1

INTRODUCTION

This thesis describes the use of combined light scattering and size exclusion chromatography, ultracentrifugation, and viscosity measurements to characterize the molecular size and interactions of some polysaccharide systems. The major part of the work has been concerned with a series of guar gum samples which were irradiated to different degrees. In addition, investigations of complex formation between dry-heated mixtures of dextran and bovine serum albumin (BSA) are described. The results of the application of the combined light scattering/size exclusion chromatography technique to starch, mucin (or muco polysaccharide) and xanthan were considered worth a brief discussion and are described in appendix A to C.

This thesis will consist of six chapters. In addition to this brief introduction, Chapter 1 describes the structure and properties of the polysaccharide systems studied. This is followed in Chapter 2 by a discussion of the theory of the methods (light scattering, size exclusion chromatography, analytical ultracentrifugation and viscometry) used to characterize these materials. Chapter 3 outlines the experimental methods employed in this work. In Chapter 4 the results obtained from the irradiated guar gum samples are presented. The results from the characterization of the BSA/dextran complexes are described in Chapter 5. In the final chapter (Chapter 6) an overall view will be taken on the information obtained by the methods used in this study and some suggestions for further work on the systems studied will be made.

1.1 STRUCTURE, MOLECULAR WEIGHT AND CONFORMATION OF POLYSACCHARIDES

Polysaccharides are naturally occurring macromolecules present in most living organisms. Their main functions are either structural - cellulose and chitin are the two most ubiquitous biomolecules on the planet, or, as a source of energy like starch. The nature of their component sugars and the way in which the individual residues are linked determines secondary and higher structural properties. Food polysaccharides are used mainly to confer bulk texture to food systems and except for starch they have virtually no nutritional value (Morris, 1979).

1.1.1 Structural and Conformational Considerations

The primary structure of polysaccharides consists of 5- or (mainly) 6-membered monosaccharides in their ring form, ie. furanose or pyranose form respectively. Figure 1.1 shows the ring structure for glucose (β-D-glucopyranose). All monosaccharides contain one oxygen in the ring, any carbon atoms are then numbered in the manner indicated in Figure 1.1. Hydroxyl substituents at C-2, C-3 and C-4 can lie either in the plane of the ring, equatorial, or above or below the ring, axial. Monosaccharides are chiral, ie. have non-superimposable mirror images due to the chiral carbons at positions 5 and 1. The configuration of groups about C-5 determines whether the molecule is in its D- or L- form and the configuration of the hydroxyl group about the C-1 determines whether the molecule is an α- or β-anomer (see Figure 1.2). Monosaccharides are linked by glycosidic bonds between C-1 and (for pyranoses) O-2, O-3, O-4 or O-6 and may be either α or β.

2
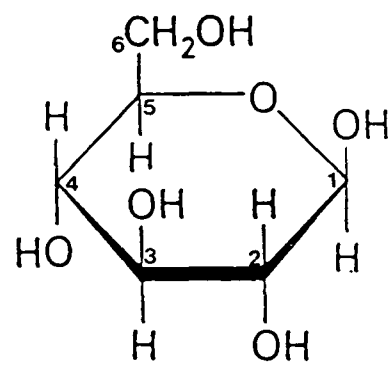
Figure 1.1: Ring structure of glucose (β-D-glucopyranose)
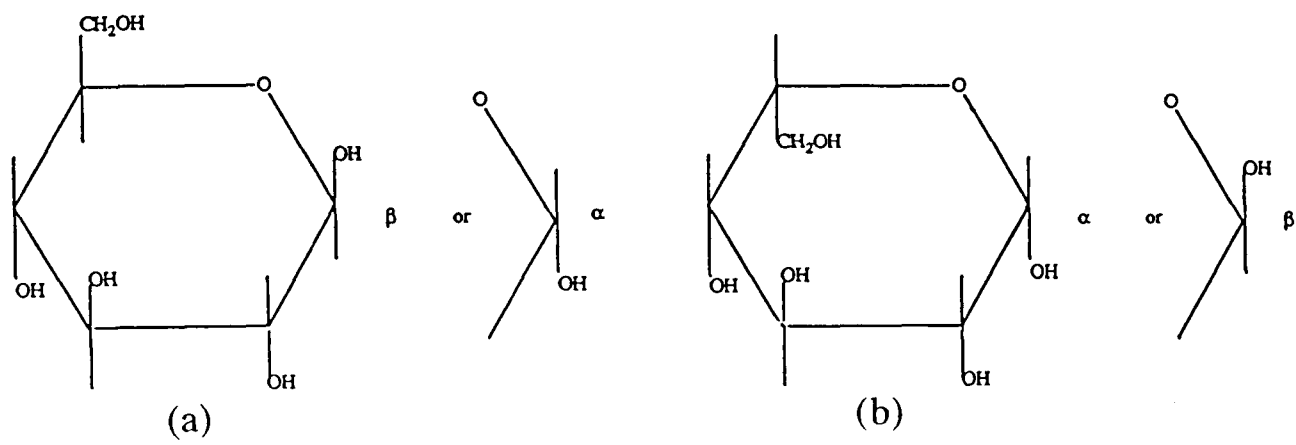
Figure 1.2: (a) D-glucopyranose, (b) L-glucopyranose
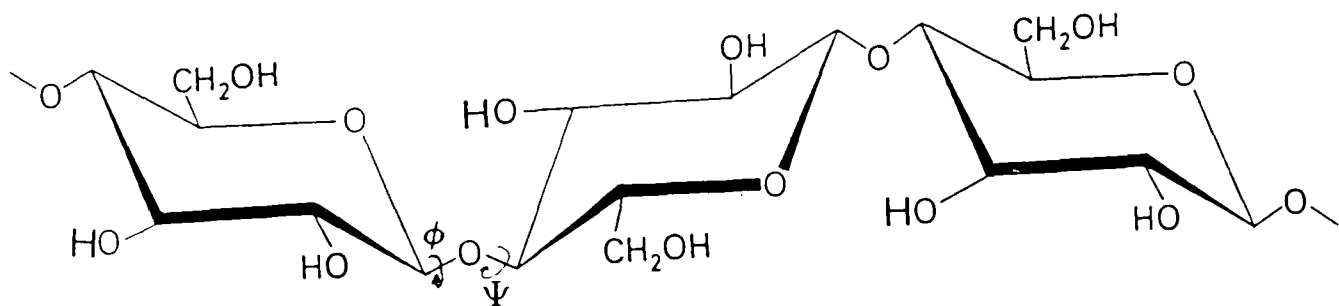
Figure 1.3: Primary structure of cellulose

3

Branching can be introduced by disubstitution of a single residue. Examples

for repeating units constituting primary structures for cellulose, guaran and

xanthan are shown in Figure 1.3, 1.10 and 1.15 respectively.

The configuration of the disaccharide (and higher saccharides) formed

through the glycosidic bond is restricted by two considerations. Firstly, it

depends on the angles of rotation ϕ and ψ about the glycosidic C-O bond (see

Figure 1.3). For example, the glycosidic link towards C-6 is very flexible

because there are three bonds instead of two for the other positions and

because there is less steric hindrance. Secondly, monosaccharide ring

structures are essentially fixed due to the steric constraints of fixed bond

lengths and angles within the molecules. The energetically most favourable

forms are the two chair conformations as depicted in Figure 1.4 for glucose.

The type of chair conformation adopted depends on steric repulsions between

the axial substituents. Hexoses generally require equatorial orientation of C-

6, D-sugars are therefore most usually found to adopt the $^4C_1$ conformation

and L-sugars the $^1C_4$ conformation (Morris, 1979). Boat-like and other

twisted conformations (see Figure 1.5) may also occur but they are usually

energetically highly unfavourable and only rarely adopted. The above

mentioned relative orientations of the component monosaccharides as defined

by the rotational angles ϕ and ψ are the major factor in determining the overall
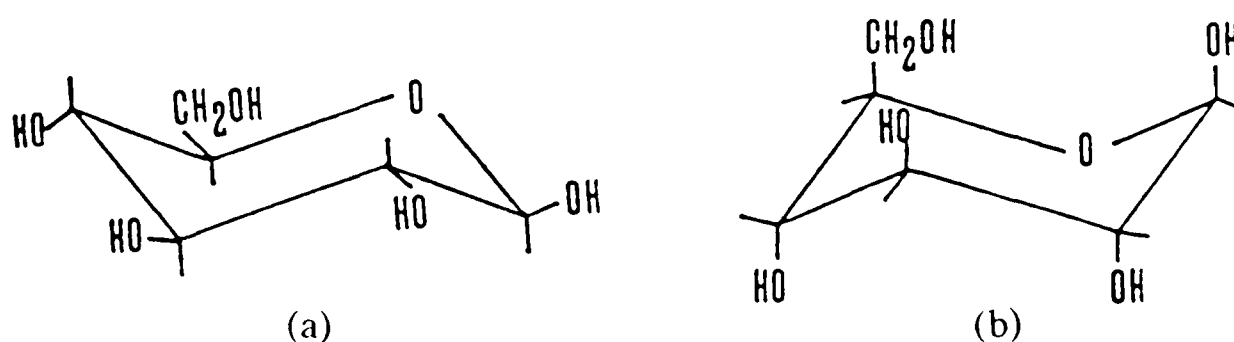
Figure 1.4: Chair conformations of pyranose monosaccharides
(a) $^4C_1$ conformation, (b) $^1C_4$ conformation

4
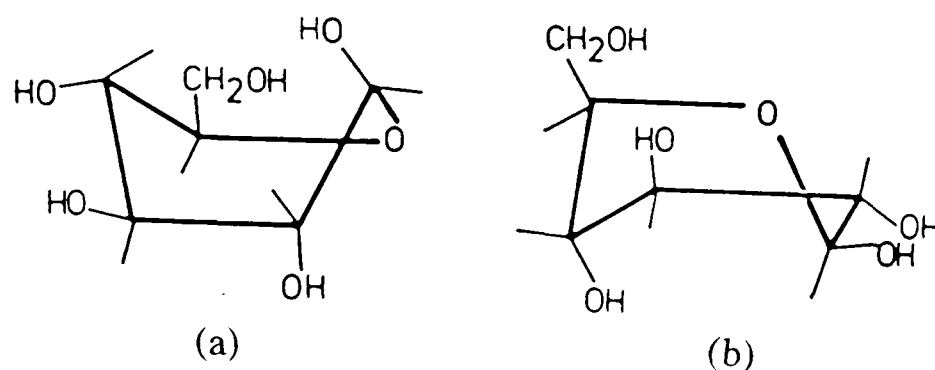
Figure 1.5: Boat like and twisted conformation of pyranose monosaccharides (a) $^{1,4}B$ boat form, (b) twisted form

conformation (ie. secondary structure) of the polysaccharide chain. Structurally regular polysaccharides adopt crystal-like conformations in the solid state which can be characterized by X-ray fibre diffraction. Such structures are determined by the fixed rotational angles between adjacent residues (ie. ϕ and ψ). Polysaccharides with a trans bonding arrangement across the sugar ring ('Type A' polysaccharides) such as cellulose show extended ribbon-like solid state conformations, whereas 'Type B' polysaccharides form hollow helices which may be in the form of compact multi-stranded structures such as the double helices of carrageenan and agarose, or a triple helix as in curdlan (Morris, 1979).

For such ordered tertiary structures to persist in solution or as fundamental structural units in gel networks, particularly favourable conditions have to prevail. Such conditions would be non-covalent interaction, inflexible secondary structure and efficiency of packing. Conditions detrimental to ordered structures in solution are loss of conformational entropy, energy of hydration, intermolecular electrostatic repulsions, structural irregularities and branching (Morris, 1979).

The existence of ordered tertiary structures in solution therefore depends on a

fine balance of solution conditions. Association of these rigid polymers to form a quarternary structure (ie. aggregate) however, is entropically less unfavourable and is to be expected unless there are repulsive forces between the molecules. It can be promoted by counterions whose radius and charge are suitable for incorporation into the aggregate. An example for this is the interchain chelation of calcium in the dimerization of poly-L-guluronate sequences forming the first step in the gelation process of alginate (Morris et al, 1978). Solutions of xanthan, a rigid rod-like molecule, exhibit pseudoplastic behaviour, ie. they behave almost like gels under zero or low shear conditions but thin with increasing shear rate (see for example, Kang and Pettitt, 1993). This is consistent with weak intermolecular associations which are disrupted when force is applied. Unlike polysaccharides with ordered conformations may also associate. Examples for mixed junction formation are interactions of agar, carrageenan and xanthan helices with unsubstituted backbone regions of galactomannans (Dea et al, 1972; 1977).

1.1.2 Molecular Weights and Average Dimensions

1.1.2.1 Molecular weight and polydispersity

Polysaccharide biosynthesis by either phosphorylation and transglycosylation or by synthesis of sugar nucleotides (Hassid, 1970) is not a very tightly controlled process due to the lack of specificity of the biosynthetic enzymes (Painter, 1967). Consequently, polysaccharides are polydisperse ie., differ in chain length and as a consequence of this, heteropolysaccharides may differ in their monosaccharide ratio from chain to chain. This lack of homogeneity results in the need for a probability function to describe these molecules. A graphical description of the different types of polydispersity is given in Figure 1.6 (Price and Dwek, 1986). Polysaccharides usually exhibit quasicontinuous polydisperse behaviour unless they are found in a mixture. Polydispersity can be described in terms of the follwing different molecular weight averages:

$$\text{Number average molecular weight,} \quad M_n = \frac{\sum M_i N_i}{\sum N_i} \qquad [1.1]$$

$$\text{Weight average molecular weight,} \quad M_w = \frac{\sum M_i^2 N_i}{\sum M_i N_i} \qquad [1.2]$$

7

$$z\text{-average molecular weight,} \qquad M_z = \frac{\sum M_i^3 N_i}{\sum M_i^2 N_i} \qquad\qquad [1.3]$$

$$z+1\text{-average molecular weight,} \qquad M_{z+1} = \frac{\sum M_i^4 N_i}{\sum M_i^3 N_i} \qquad [1.4]$$

where N_i is the number of molecules of type i and M_i is their molecular weight.

These molecular weight averages are used to define the polydispersity of a system (Tanford, 1961), ratios of M_w/M_n or M_z/M_w etc, resulting in values larger than unity describe a polydisperse system. Molecular weight averages are a useful tool for defining functional and molecular properties of a polysaccharide system. The type of molecular weight average used depends on the nature of the property investigated. M_n is determined by colligative measurements (eg. osmometry, ebulliometry, end group analysis, etc.) and basiçally 'counts' the number of molecules per molecular weight. Weight average molecular weights describe a species in terms of the relative weights of its components. Higher averages are only rarely of interest.
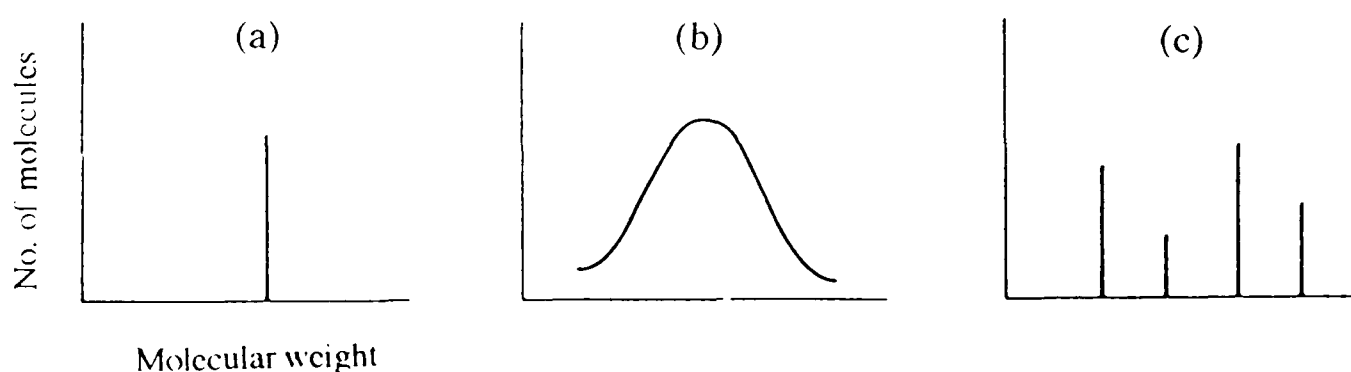
Figure 1.6: Types of polydispersity. (a) Monodisperse, (b) quasi-continuous, (c) paucidisperse

As was pointed out earlier, polysaccharides may adopt different conformations in solutions, they may exist in an extended form or densely coiled. In order to characterize molecules in such terms, average dimensions for simple models can be defined. These models are clearly defined in Tanford (1961) and only the random-flight model will be mentioned briefly in order to describe one of the most useful average dimensions, the mean square radius of gyration which can be obtained from light scattering measurements (see section 2.1).

1.1.2.2 The Random-Flight Model

The mean square radius of gyration $<R_G^2>$ is based on the random-flight model (Tanford, 1961) where it is assumed that the linear polymer in solution exists as a randomly coiled, flexible chain with spherical symmetry. The chain ends are distributed normally around the centre of this sphere. $<R_G^2>$ can now be defined by

$$<R_G^2> = \frac{\sum_i R_i^2}{N} \qquad [1.5]$$

where R_i^2 is the average square of the distance of unit i from the centre of mass of the molecule and N is the number of chain monomers (see Figure 1.7). $<R_G^2>$ can be related to the mean square end-to-end distance of the molecule $<r^2>$ by

$$<R_G^2> = \frac{<r^2>}{6} \qquad [1.6]$$

9

and since

$$r^2 = Nl^2 \tag{1.7}$$

where l is the length of a monomer unit and N is the number of monomers, r^2 is proportional to the number of links in the polymer chain (see Figure 1.8). The random-flight model has severe limitations in that all bond angles are allowed and rotation around the bonds is completely unrestricted, neither of which is strictly true, as bond angles are fixed and rotations are subject to energetic and steric restrictions. The real mean square end-to-end distance is therefore larger than r^2 given by equation [1.7]. This deviation from ideal behaviour can be quantified by the characteristic ratio, C_∞ (Flory, 1953) where

$$C_\infty = \frac{<r^2>}{Nl^2} \tag{1.8}$$

In order to allow for lack of flexibility between monomer units, the Kuhn statistical segment length, l_e can be used. This is the effective length of a number of monomers of individual length l, and can be related to $<r^2>$ via

$$<r^2> = n_e l_e^2 \tag{1.9}$$

where n_e is the total number of effective segments in a chain (see Figure 1.9). The Kuhn statistical segment length l_e is related to the Flory characteristic ratio as follows

$$C_\infty = \frac{l_e}{l} \tag{1.10}$$

10
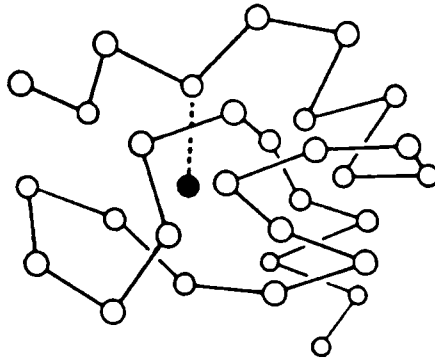
Figure 1.7: Schematic representation of the radius of gyration, (•) represents the centre of mass, (o) represent monomer units
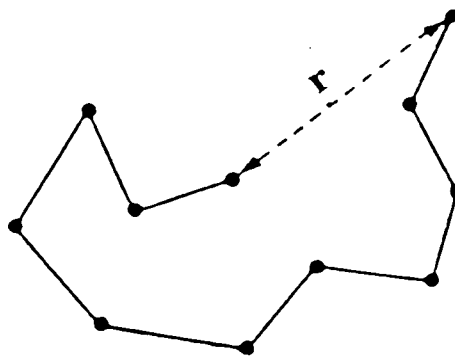
Figure 1.8: Schematic representation of the mean square end-to-end distance, $<r^2>$, (•) represent monomer units

(a)   (b)
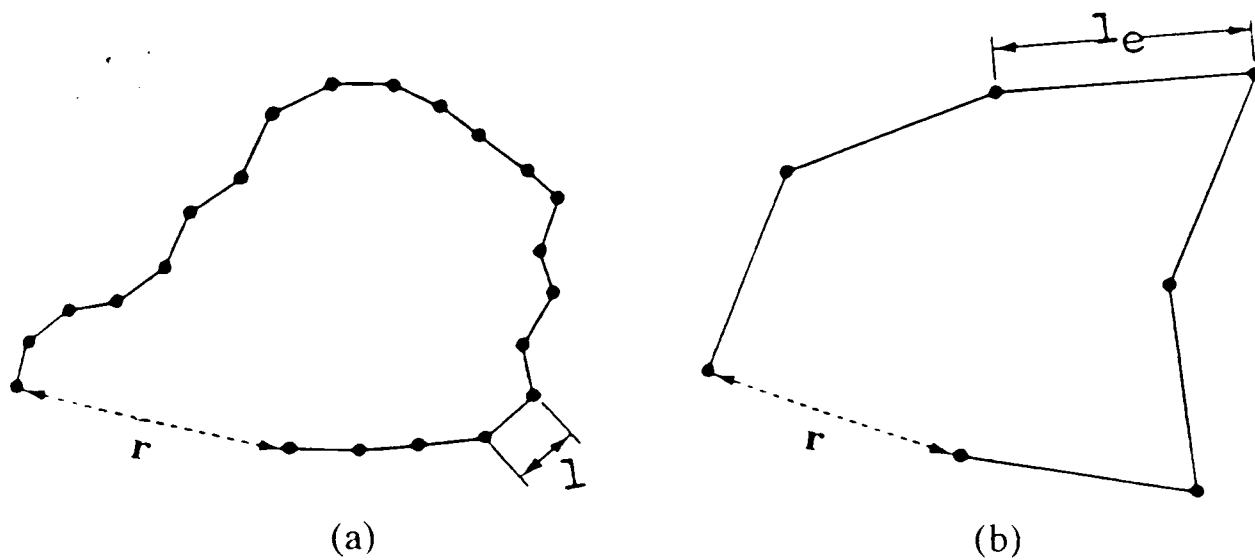
Figure 1.9: Schematic representation of the Kuhn statistical segment.(a) shows polymer consiting of monomer units (•) connected by length, l, (b) the same polymer in terms of Kuhn statistical segments connected by length, l_e

1.1.2.3 The Excluded Volume Effect and Thermodynamic Non-ideality

The above descriptions of macromolecules in solution are idealized models. Polymer configurations expand and contract depending on the solvent conditions they are exposed to. Also, it is assumed in the above models that each molecule has unlimited space within a solvent which is not true because of the presence of other molecules. Detailed mathematical description of the excluded volume effect and thermodynamic non-ideality can be found in Tanford (1961) and Launay et al (1986), the discussion here is limited to only a brief qualitative view.

In a poor solvent, the interactions between polymer and solvent are weak, which means that there can be close intramolecular contact. The resulting conformation will be fairly tight and the molecule occupies less volume than would be predicted by the average dimensions described above. However, if interactions between solvent and polymer are strong, the polymer chain will tend to adopt a more open conformation with a resulting increase in occupied volume. This is one of the major causes of thermodynamic solution non-ideality, the latter may also be caused by charge effects. Physical measurements on macromolecules have to be made at a finite concentration and excluded volume and charge effects will contribute to the final result. This contribution is usually expressed in terms of the second virial coefficient (B, in osmotic pressure and sedimentation equilibrium measurements, see section 2.4, or A_2, in light scattering measurements, see section 2.1). The expression for the osmotic pressure of a solution, correct to first order in the virial coefficient expansion is given in the following equation:

$$\frac{\pi}{c} = \left[\frac{RT}{M_n}\right](1 + BM_nc) \qquad [1.11]$$

12

Macromolecular solutions may exhibit ideal behaviour under theta (Θ)-conditions. Θ-conditions are achived when excluded voume effects and interaction effects are balanced out. However, Θ-conditions are only rarely found for polysaccharides.

1.2 GUAR GUM

1.2.1 Structure and Molecular Weight

Guaran is the functional polysaccharide of guar gum, it is a chain of β-(1->4) linked D-mannose units which are substituted on alternate groups (on average) by α-(1->6) linked D-galactose side groups. The basic structure of a guaran repeating unit is shown in Figure 1.10. Molecular weight and fine structure of guaran have been the subject of extensive research and debate in the past and a brief outline of the developments are given in the following paragraphs.
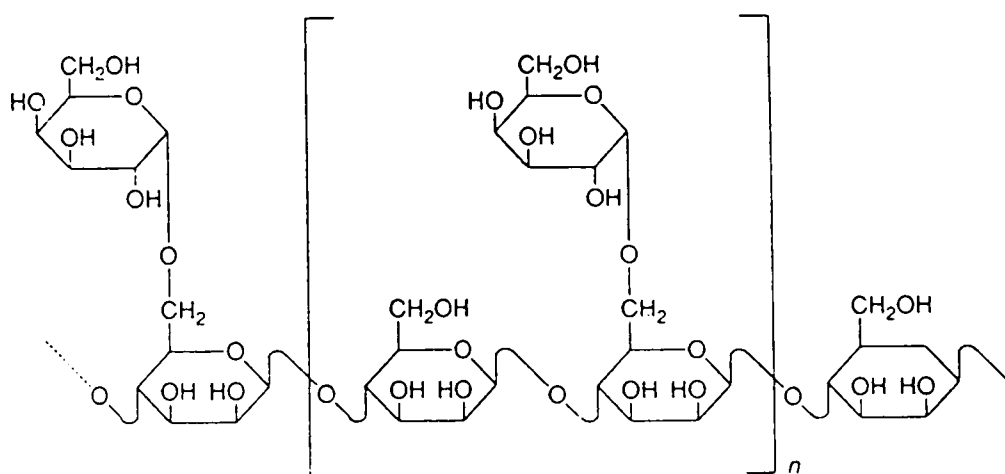
Figure 1.10: Average repeating unit of guaran

The determination of the fine structure of guaran was the subject of a prolonged debate. The D-galactose content of most guar gums ranges from 33% to 38% (McCleary et al, 1985) which could suggest a simple substitution pattern of one D-galactosyl-side chain on every alternate D-mannosyl group. Chemical studies by Baker and Whistler (1975), acetylating partially degraded p-tolylsulfones indicated that this was indeed the case. However, a specific degradation procedure developed by Hoffman and Svensson (1978) showed that the D-galactosyl side chains are distributed

14

mainly in pairs or triplets. NMR studies by Grasdalen and Painter (1980) supported a random distribution of D-galactosyl side chains. Hall and Yalpani (1980) suggested that the D-galactosyl side chains are arranged in blocks after specific derivatisation of the D-galactosyl groups and analysis by electron spin resonance (ESR) techniques.

An alternative approach to the analysis of guaran fine structure is the use of the galactomannan degrading enzymes α-D-galactosidase and β-D-mannanase. Extensive studies on the action pattern of these enzymes and the oligosaccharides produced on their hydrolysis (McCleary and Matheson, 1975, 1983; McCleary et al 1976, 1983) led to the conclusion that the D-galactosyl groups are arranged mainly in pairs and triplets (McCleary et al 1983) as suggested by Hoffman and Svensson (1978). There was no evidence of a block-arrangement of D-galactosyl groups, β-D-mannanase hydrolysis would have resulted in some fragments containing almost 50% D-galactose and some unsubstituted mannosaccharides which was not found to be the case.

A further indication of the absence of a block substituted structure of guaran is provided by the fact that guaran does not form gels without the aid of crosslinking agents. This has been attributed (Dea et al, 1977; Morris et al, 1981) to the absence of an unsubstituted region of D-mannose units and/or the absence of a region where all D-galactosyl units are on one side of the mannose backbone. In the latter case the unsubstituted face could serve as a junction zone (McCleary, 1979). Guaran may not form highly specific intermolecular associations due to the absence of a regular substitution pattern, however, its tertiary structure appears to be sufficiently stiff to align and interact with polymer chains of compatible geometry (Dea et al, 1977; Morris et al, 1981) leading to aggregate formation in dilute solution and synergistic interactions with xanthan.

1.2.2 Occurrence, Properties and Applications

Guar gum is obtained from the seed of the guar plant *Cyamopsis tetragonolobus* of the Leguminosa family. The plant is pod-bearing and has nitrogen-fixing properties (Goldstein and Alter, 1959). It is thought to originate either from Arabia or from India and Pakistan where it has been used for human and animal consumption for centuries (Whistler and Hymowitz, 1979). It was brought to the United States in the early 1900's but remained mainly a 'novelty crop' until World War II when a shortage of locust bean gum and starch initiated the search for alternatives. Guar gum was found to be an adequate substitute for these compounds for use as a strength additive in paper (Maier et al, 1993). This was the beginning of the commercial use of guar gum which has increased considerably since then, aided by the use of guar gum derivatives in the oil well drilling industry. Guar is best grown in semi-arid zones. It needs rain prior to planting and maturation of the seeds. However, rain during any other part of the growing season is detrimental to crop yields and quality. The vast majority of guar (close to 90%; Maier et al, 1993) is grown in northern India and Pakistan with a small amount being grown in the USA and in order to obtain two crops a year it has also been cultivated in Brazil, Africa and Australia (Wielinga, 1990).

A schematic diagram for the commercial production of guar gum is shown in Figure 1.11 (Wielinga, 1990). Initially, all non-seed materials such as dirt, stones, sand, etc are removed by sifting . The seeds then fall between two parallel plates moving at different speeds and are split into two endosperm halves and fine germ material. The latter is removed by further sifting and sold for animal feed. The cracked endosperm is quickly heated to 105° where the endosperm becomes rubbery and resilient while the seed coat is still brittle

16

and can be hammered off. The splits are then quickly lowered to a temperature of 60°C and the husk is removed in size reduction equipment such as attrition mills or hammer mills (Wielinga, 1990; Maier et al, 1993). Operating conditions such as temperature, moisture, pressure, shear, and throughput rates are all critical to the grade of gum obtained. Poor temperature control, particularly after the endosperm has been split, causes heat damage to the gum which results in lower yields and lower hydration rates (Maier et al, 1993).
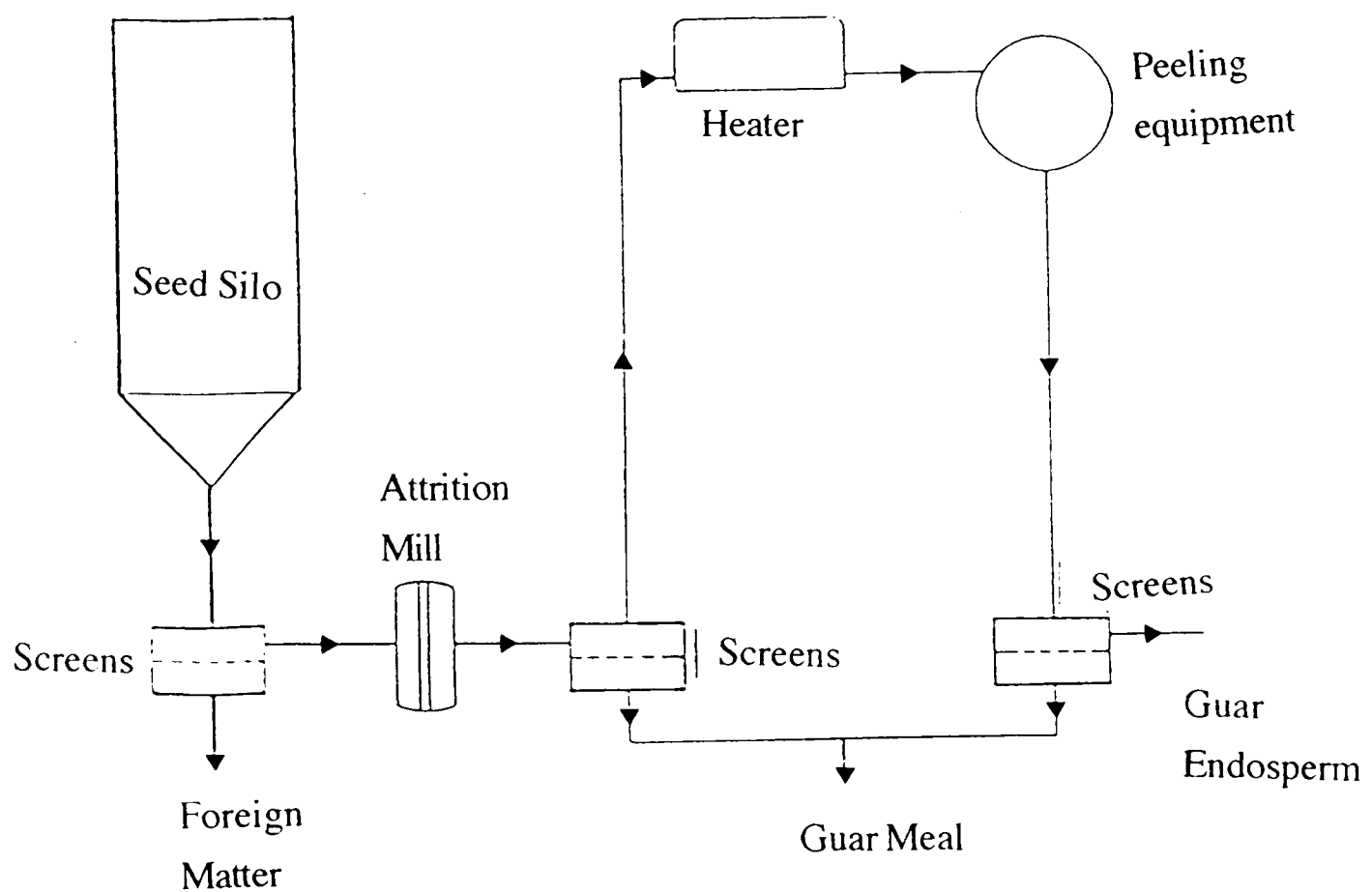
Figure 1.11: Schematic representation of the manufacturing process of guar gum from seeds. (Reproduced from Wielinga, 1990)

17

High grade guar gum is a permitted food additive (E412) and is mostly used to stabilize food preparations. The major constituent is guaran, but small amounts of edible hull, protein and cell wall components from the endosperm remain. The composition of a typical food grade guar gum is shown in Table 1.1

Table 1.1: Composition of typical food grade guar gum (from Maier et al, 1993)

Component	Approx. Amount (%)
Galactomannan	75 - 85
Moisture	8 - 14
Protein (Nx6.25)	5 - 6
Fibre	2 - 3
Ash	0.5 - 1

Guar gums for industrial use usually contain additives to control their solution properties. The need for specific properties has led to the derivatisation of guar gum in certain cases. Derivatisation is achieved by using guar meal or guar endosperm slurries, swelling the guar with aqueous bases and subsequent reaction to achieve the required derivative. Amongst the most common derivatives are hydroxypropyl guar, carboxymethylhydroxypropyl guar and carboxymethyl guar (Maier et al, 1993).

Unless guar gum is derivatised, it will swell and/or dissolve only in strongly polar solvents. The rate of dissolution increases with decreasing particle size, decreasing pH and increasing temperature. Other factors influencing the hydration rate are the presence of other solutes in the solvent.

1.2.2 Applications

The applications of guar gum and its derivatives are based on its functional properties, the most valuable of which are the thickening properties due to its large hydrodynamic volume in solution and specific intermolecular interactions (entanglements). Solutions thin on increasing temperature but regain viscosity on cooling. Interaction of guar gum with other galactomannans and some linear polysaccharides such as xanthan, κ-carrageenan and agarose lead to viscosity synergism, ie. the resultant viscosity is higher than would be predicted on the basis of the viscosity that each component would confer. Other valuable functional properties include its high salt tolerance, resistance to shear degradation and the ability to form gels via crosslinks with borates and transition metal ions (Maier et al, 1993). In oil-well drilling guar gum and some of its derivatives are used as additives for fracturing fluids. Hydraulic fracturing is a process where liquid is injected under high pressure into oil bearing rock. The initial fracture is kept open by a propping agent after the pressure is released. The polymer is degraded by a suitable agent to reduce its viscosity and the resulting fractures extending away from the well bore increase the productivity of the well.

In the textile printing and dyeing industries guar gum and its derivatives are used to thicken dye liquors and control dye mobility. This is extremely important for multicoloured materials and where special styling effects are required. Guar gum is often preferred over synthetic polymers because of high thickening efficiency, good compatibility and electrolyte tolerance.

The paper industry uses guar gum and its derivatives mainly to improve paper strength. During the pulping process lignin and hemicelluloses are removed and/or degraded, thus reducing the natural binding agents for cellulose with a resulting decrease in paper strength. Galactomannans supplement the remaining hemicelluloses in their natural fibre bonding and thus enable

19

control of the paper strength.

The flocculation properties of guar gum and its derivatives to aid separation of minerals from their crude ores are most valued in the mining industry. Absorption of guar products onto the hydrophilic surface of mineral particles causes flocs which settle rapidly and produce porous filter cakes with increased filtration rates.

Guar gum is used in explosives slurries and as a binding agent in ammonium nitrate explosive. Other applications of guar gum and derivatives include its use for wild fire control in aerial drop applications, in the building trade for paint rheology control and stabilization, in the cosmetics industry as a thickener for shampoos and in the tobacco industry as a thickener and binder.

Applications of guar gum in the food industry are varied and make use of its water-binding properties, its viscosity and its synergistic interaction with certain other polysaccharides. Processed cheeses usually contain 0.25 - 0.35% of stabilizer (guar gum and/or locust bean gum). Guar gum is used because it eliminates syneresis and by control of water distribution improves texture and flavour (Whistler and Hymowitz, 1979). The stability of its aqueous suspensions in combination with other hydrocolloids is of great advantage in ice-creams and other frozen desserts. Its function is to bind free water, thus preventing ice-crystal growth with its undesirable organoleptic effects. Hydration and stabilizing properties of guar gum at low pH are important in sauces and dressings where it also functions as an emulsion stabilizer. Addition of guar gum to bakery products such as speciality cakes and breads reduces mixing time and crumbliness and increases shelf life through moisture retention (Maier, 1993; Whistler and Hymowitz, 1979). Guar gum has also been found to reduce the total plasma cholesterol content in humans (Spiller et al, 1991). Furthermore, it is known that the addition of guar gum to glucose drinks or carbohydrate-rich meals reduces the post-

prandial rise in blood glucose (for example, Ellis et al, 1988). The use of pharmaceutical preparations of either guar gum or guar containing foods has been found to improve carbohydrate and lipid metabolism long-term in diabetic patients (Ebling et al, 1988).

1.3 PROTEIN-POLYSACCHARIDE COMPLEXES

Complex formation between proteins and polysaccharides is well known in the natural world, glycoproteins and proteoglycans are present in connective tissue and synovial fluids and plants may contain, for example, arabinogalactan-protein complexes (Fincher et al, 1983) such as gum arabic. Dickinson et al (1991) investigated the emulsifying behaviour of gum arabic and found that the protein-rich high-molecular weight component provides the functionality of an emulsifier-stabilizer. Proteins and polysaccharides also constitute the major macromolecular components of food systems and their interactions can change the rheological behaviour of an emulsion as well as its stability.

Proteins are best described as emulsifiers - their hydrophobicity and molecular flexibility allow adsorption at the oil-water interface in emulsions to form a coherent viscoelastic layer (Dickinson et al, 1988). Polysaccharides are hydrophilic and stabilize oil-in-water emulsions due to their thickening and gelling behaviour. Complexation of these two types of polymers should therefore result in a hybrid which has the emulsifying properties of a protein and enhanced stabilization due to the hydrophilic polysaccharide. Complexation can occur via various types of interaction, the major two types are (a) covalent bonding which results in a strong new permanent linkage, or (b) electrostatic associations between either oppositely charged moieties which would be quite strong, or weak associations due to interactions between anionic polysaccharides and positively charged patches on the protein (Imeson et al, 1977). Much work on protein-polysaccharide interactions has been carried out with applications to milk systems in mind. Acidic polysaccharides can inhibit protein precipitation at the isoelectric point of the proteins and they are therefore used extensively in the preparation of fruit flavoured milk drinks (see Ledward, 1979 and references cited therein).

22

One of the most widely studied interactions between milk protein and polysaccharide is that between κ-casein and κ-carrageenan, not least because it is used for a number of milk desserts. This type of interaction does not occur with any of the two other forms of casein (ie. α_{s1} or β) and is most likely due to the localization of positive charges between residues 20 and 115. In this region of the protein there are 13 positive and 3 negative charges at pH 5. In α_{s1} and β casein positive and negative charges are distributed evenly along the chains. Other examples of electrostatic interactions between proteins and polysaccharides are the formation of a milk protein - propylene glycol alginate complex, possibly aided by non-ionic attractions such as hydrogen bonding (Dickinson and Euston, 1991); and bovine serum albumin (BSA) and dextran sulphate (Gurov et al, 1988).

Electrostatic complexes can suffer from disadvantages of flocculation and phase-separation when they are due to weak, non-specific interactions (Cao et al, 1991; Dickinson, 1993). It would therefore be preferable if the two biopolymers could be covalently linked to form a stable, single entity. Such hybrids have been produced by reaction of whey proteins with propylene glycol alginate under alkaline conditions (Dickinson and Euston, 1991) and protein and alginate esters (Stainsby, 1980). It is thought that reaction occurs between the ε-amino group of lysine on the protein and the ester group on the alginate to give an amide-type bond. Reaction conditions have to be mildly alkaline so that the ε-amino groups are in their uncharged form. There is also a possibility that transesterification can take place on the hydroxyl groups of serine residues. It has been shown (Stainsby, 1980) that transesterification of alginate esters with the hydroxyl groups on starch proceed under mildly alkaline conditions.

A. Kato et al (1988) describe the preparation of an ovalbumin-dextran conjugate through cyanogen bromide activation of the dextran (average

23

molecular weight 75 000). The binding ratio dextran:ovalbumin was found to be 1:3 and the emulsifying properties of the conjugate were found to be excellent. The same activated dextran was also coupled to lysozyme and soy-protein and those conjugates showed similarly improved emulsifying properties. Coupling of proteins and polysaccharides can therefore be utilized for medical and food applications. However, for these types of application the use of chemical reagents should be avoided as much as possible and there is a naturally occuring reaction between amino acids and reducing sugars called the Maillard reaction. This reaction occurs in all foodstuffs when sugars are heated in the presence of protein. The first step in this reaction is a simple condensation between the carbonyl group of the reducing sugar and the free amino-group on the amino acid of the protein. The condensation product is converted into a Schiff's base upon loss of a molecule of water and then undergoes cyclization to the corresponding N-substitued glycosylamine. The latter are unstable and are immediately converted into the 1-amino-1-deoxy-2-ketone by the Amadori rearrangement (see for example, Mauron, 1981). This constitutes the first step in the Maillard reaction as shown in Figure 1.12. During cooking processes further steps, leading to a vast number of further reactions giving volatile or soluble substances and finally pigmentation and browning, will occur. For the purpose of protein-polysaccharide conjugate formation only the first series of reactions is important, steps 2 and 3 can lead to toxic polymers.

Y. Kato et al (1978) and Watanabe et al (1980) investigated the effect of the Maillard reaction on the chemical and conformational change in ovalbumin. In further studies (Y. Kato et al, 1981, 1988) they continued to investigate ovalbumin-glucose and ovalbumin-lactose complexes. They detected an increase of the denaturation temperature for ovalbumin when dry-heated with glucose and an increase in aggregation possibly through crosslinking.

SCHIFF BASE

⇅

ALDOSYLAMINE

⬇

AMADORI COMPOUND

(1—AMINO—1—DEOXY—2—KETOSE)

$$
\begin{array}{c}
\text{HC:O} \\
| \\
\text{(CHOH)}_n \\
| \\
\text{CH}_2\text{OH}
\end{array}
\quad \underset{\text{+RNH}_2}{\rightleftharpoons} \quad
\begin{array}{c}
\text{RNH} \\
| \\
\text{CHOH} \\
| \\
\text{(CHOH)}_n \\
| \\
\text{CH}_2\text{OH}
\end{array}
\quad \underset{\text{−H}_2\text{O}}{\rightleftharpoons} \quad
\begin{array}{c}
\text{RN} \\
\| \\
\text{CH} \\
| \\
\text{(CHOH)}_n \\
| \\
\text{CH}_2\text{OH}
\end{array}
\quad \rightleftharpoons \quad
\begin{array}{c}
\text{RNH} \\
| \\
\text{HC}\underline{} \\
| \\
\text{(CHOH)}_{n-1} \quad \text{O} \\
| \\
\text{HC}\underline{} \\
| \\
\text{CH}_2\text{OH}
\end{array}
$$

| Aldose in aldehyde form | Addition compound | Schiff base (not isolated) | N-Substituted glycosylamine |

$$
\begin{array}{c}
\text{RNH} \\
| \\
\text{HC}\underline{} \\
| \\
\text{(HCOH)}_n \quad \text{O} \\
| \\
\text{HC}\underline{} \\
| \\
\text{CH}_2\text{OH}
\end{array}
\quad \underset{\text{+H}^+}{\rightleftharpoons} \quad
\left[
\begin{array}{c}
\text{RNH} \\
\| \\
\text{CH} \\
| \\
\text{HCOH} \\
| \\
\text{(HCOH)}_n \\
| \\
\text{CH}_2\text{OH}
\end{array}
\right]^+
\quad \underset{\text{−H}^+}{\longrightarrow} \quad
\begin{array}{c}
\text{RNH} \\
| \\
\text{CH} \\
\| \\
\text{COH} \\
| \\
\text{(HCOH)}_n \\
| \\
\text{CH}_2\text{OH}
\end{array}
\quad \rightleftharpoons \quad
\begin{array}{c}
\text{RNH} \\
| \\
\text{CH}_2 \\
| \\
\text{C:O} \\
| \\
\text{(HCOH)}_n \\
| \\
\text{CH}_2\text{OH}
\end{array}
$$

| N-substituted aldosylamine | Cation of Schiff base | Enol form | N-Substituted 1-amino-1-deoxy-2-ketose, keto form |

Figure 1.12: First stage of the Maillard reaction (Mauron, 1981)

Ovalbumin-glucose complexes were also found to be susceptible to browning whereas ovalbumin-lactose systems did not exhibit browning after two weeks. Dry-heating with maltose, cellobiose, isomaltose and melibiose (Y.Kato et al, 1989) indicated a reduction in advanced Maillard reaction products for maltose, lactose and cellobiose, possibly due to the presence of terminal pyranoside groups at the C-4 OH groups of glucose retarding further degradation of the Amadori rearrangement products.

The addition of a disaccharide to a protein would not be expected to enhance the emulsifying properties of the latter as disaccharides lack the necessary long chain of hydrophilic pyranose groups to which the enhancement is attributed. However, many polysaccharides contain reducing end groups and one of those which is widely available in a pure form and well characterized is dextran. A. Kato et al (1990) stored freeze dried ovalbumin-dextran mixtures at weight ratio 1:5 under conditions of 60°C and 65% relative humidity for 3 weeks. The conjugate prepared by this method resulted in a binding ratio of ovalbumin:dextran 1:1.6 - 2.2. It exhibited excellent emulsifying properties ranging from pH 3 to pH 10, furthermore, these emulsifying properties were enhanced by pre-heating the conjugate at 100°C. Such a hybrid is therefore ideal for use in the food industry. Ovalbumin is also said to have a protective effect on lipid oxidation (Nakamura et al, 1992b) although it is not as effective as synthetic antioxidants such as butylated hydroxyanisole (BHA) and butylated hydroxy toluene (BHT). The latter, however, have the disadvantage of being suspected to be responsible for liver damage and cancer in laboratory animals (Grice, 1988). Ovalbumin-polysaccharide conjugates (ovalbumin-dextran and ovalbumin-galactomannan) showed high affinity to oil during an investigation of their emulsifying properties and it was shown (Nakamura et al, 1992b) that they can act as antioxidants. They are not quite as effective as the synthetic scavengers (when tested on salad oil) but have the added advantage of being

26

excellent emulsifiers.

Preparation of protein-polysaccharide conjugates was extended to lysozyme, another egg white protein (Nakamura et al, 1991) which can be used as a preservative for processed food. However, its lytic spectrum is limited to Gram-positive bacteria and lytic action is inert with carbohydrates and other food components (Hayashi et al, 1989). The outer membrane of Gram-negative bacteria is resistant to lysozyme and conversion of the lysozyme to an amphiphilic protein without loss of lytic activity would be expected to extend antimicrobial activity. A lysozyme-dextran conjugate obtained by dry-heating a lyophilised mixture of lysozyme and dextran (weight ratio 1:5) at 60°C for 2 weeks revealed significant antimicrobial activity for Gram-negative and Gram-positive bacteria. The binding weight ratio suggested an approximate dextran: lysozyme ratio of 2:1 in the conjugate (estimated from molecular weight data and determination of free amino groups). In addition, linkage with dextran increased the heat stability of the lysozyme activity and enhanced the emulsifying properties of native lysozyme. As dextran is a fairly expensive polysaccharide and mainly used for medical applications, replacement with a food polysaccharide would be more interesting to the food industry. Nakamura et al (1992a) reported the preparation of a galactomannan-lysozyme conjugate using the mannanase hydrolysate from guar gum and lysozyme. The hybrid showed emulsifying properties superior to commercial emulsifiers and also exhibited excellent antimicrobial properties. The complex was stable at high salt concentration and at acidic pH.

The protein-polysaccharide conjugates described above were obtained using isolated and purified proteins. Industrial processes are more likely to involve a matrix of proteins such as are to be found in egg white. It was therefore interesting to see whether conjugates similar to those obtained previously could be obtained using dried egg white. Conjugates were prepared by

27

mixing the spray dried egg white and galactomannan in water, lyophilising, and then dry-heating the mixture at 60°C (79% relative humidity) for 2 weeks (A. Kato et al, 1993). Comparison of emulsifying properties between the complexes thus obtained and commercial emulsifiers showed that the novel conjugates were superior, particularly at high salt concentration and acidic pH. Moreover, toxicity of the conjugates, which could be a problem due to compounds from advanced Maillard reaction, proved to be negative when tested for on mammalian cell cultures. This also suggests that the protein structure in the conjugate is kept in the native form. The use of dried egg white has the additional advantage of not being composed of just one protein but a mixture. The antimicrobial effect of lysozyme-polysaccharide conjugates was mentioned earlier (see Nakamura et al, 1992a). Egg white contains lysozyme, ovotransferrin, ovoinhibitor and avidin. It would therefore be expected that the dried egg white-polysaccharide conjugates also contain antimicrobial activity although this still has to be investigated.

It is important to understand the molecular composition of the above conjugates, partly in order to understand their properties and partly for future design of such compounds, and for this reason A. Kato et al (1992) studied the molecular weight distribution and composition of dextran-ovalbumin and dextran-lysozyme systems. Their results indicated that the conjugates form non-covalently linked micelle-like assemblies. Associations form proportional to salt concentration in aqueous media and are completely inhibited in the presence of the surfactant SDS. Measurements indicated that two dextran chains are usually bound to each protein and it was thought that it is the only partial covering of the protein molecule which gives the conjugate its amphiphilic properties. Hydrophobicity is a pre-requisite for the emulsifying function and covering of the whole protein moiety would reduce this. The protein might also have acquired some hydrophobicity due to partial denaturation during dry-heating.

1.4 STARCH

Starch is the most abundant food-reserve polysaccharide in plants. It occurs in seeds, fruit, leaves, tubers and bulbs of plants in amounts varying from only a few percent to over 75% as for example in cereal grain (Kennedy and White, 1983). Starch granules are composed of two polysaccharides: amylose and amylopectin.

1.4.1 Structure and Conformation

Amylose is an essentially linear α-(1->4) glucopyranose (see Figure 1.13) with molecular weights ranging from 10^4 to 10^6 and typically constitutes 15 - 35% of the carbohydrate content of most starches depending on the source although some starches may contain as little as 2% (waxy maize) or as much as 80% (amylomaize) (Kennedy et al, 1987). There is now evidence that amylose has small to moderately long chains attached through α-(1->6) branch points. Evidence for the presence of these is provided primarily by incomplete hydrolysis of amylose by the α-(1->4) specific α-amylase, in order to obtain quantitative hydrolysis a α-(1->6) specific enzyme such as pullulanase is also required (Galliard and Bowler, 1987 and references cited therein). Amylopectin also contains α-(1->4) linked glucose residues, however, these are periodically substituted by α-(1->6) branch points (Morrison and Karkalas, 1990).

X-ray powder diffraction shows three distinctive types of patterns for native starch granules, A-, B-, and C-types which depend on the botanical origin of the starch (Hizukuri et al, 1983 and references cited therein). A- and B-types are independent structures, whereas the C-type is probably a mixture of both

(Hizukuri et al, 1983). The crystallinity of starch is determined by the amylopectin structure with the ratio of A- to B-chains being important in defining the structure (Zobel, 1992).

The accepted model for amylopectin structure since the 1970's is the 'cluster model' (see Figure 1.14) credited to French (1972) which has only experienced slight modifications by other workers (Robin et al, 1974; Hizukuri, 1986; Nikuni, 1978).

The elucidation of physical characteristics such as molecular weight and structure of amylose and amylopectin from native starches has proved to be a non-trivial task, partly due to the problems with complete dissolution of starch and separation of its amylose and amylopectin components and once this has been achieved because of the polydisperse nature and large molecular sizes of these components.

Native starch granules do not dissolve readily in cold water and even at 100°C complete dissolution may not be achieved without severe agitation which may cause degradation. Dissolution at room temperature can be achieved using alkaline solutions (eg. 1M NaOH or KOH) or ~85% DMSO. However, with all these methods there is still a danger of gel formation, degradation or retrogradation of amylose (see for example Morrison and Karkalas, 1990 and references cited therein). Separation of amylose and amylopectin is usually obtained by selective precipitation and recrystallization of amylose with butan-1-ol (eg. Banks and Greenwood, 1975). The amylose-butanol complex is frequently only isolated after six or more recrystallization steps and even then contamination with amylopectin can be expected (Takeda et al, 1986) and equally important is the loss of amylose due to this procedure (Klingler and Zimbalski, 1992). Alternatively, concanavalin A has been used as a precipitant for amylopectin, however, this method has not been widely tested (Morrison and Karkalas, 1990).
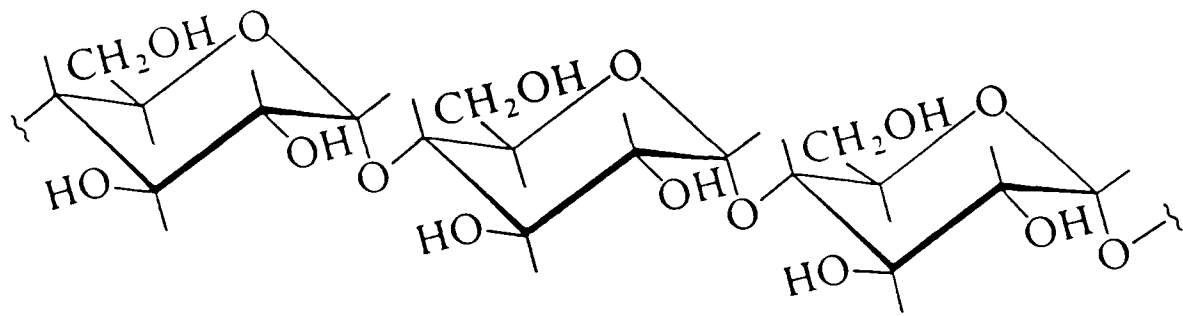
Figure 1.13: Primary structure of amylose
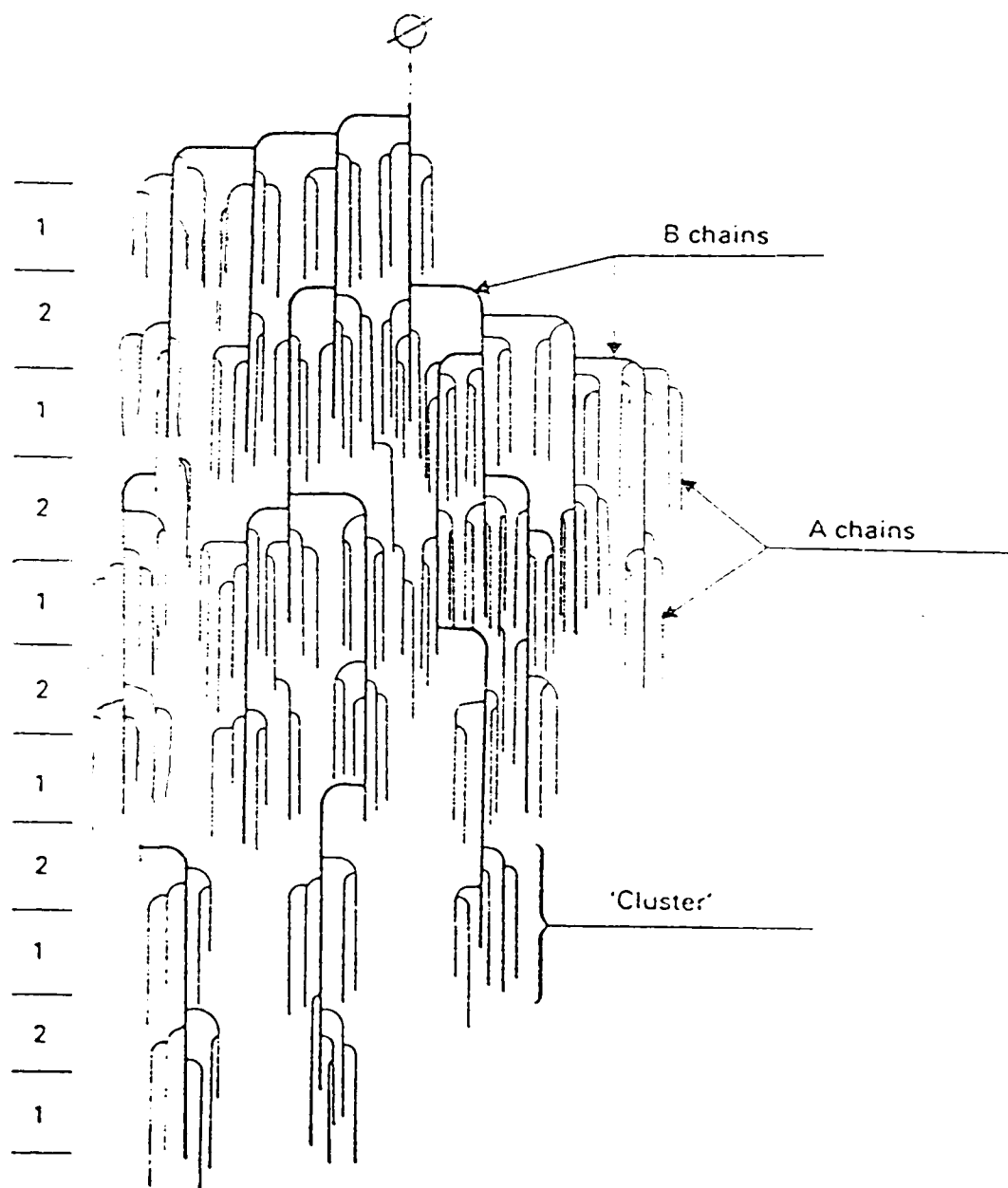
Figure 1.14: Cluster model of amylopectin according to Robin et al, 1975.

1.4.2 Applications

The major utilization of starch is as a food without separation from its surrounding plant tissue, eg potato and other vegetables, or in the form of flour which is processed to give final products such as bread, pasta, breakfast cereals and snack foods. The food industry uses starch for its gelatinization and thickening properties for sauces and pie-fillings and hydrolysed starch in the form of glucose syrups is used in vast amounts as sweetner in drinks, and confectionery. For chemical and feedstock applications starch requires to be liquefied via hydrolysis usually with α-amylase (Hong et al, 1987) and fermented to ethanol which may then be used as an alternative fuel in cars or as a starting material in the chemical industry (Kennedy et al, 1987).

As starch structure is heterogeneous, varies from botanical species to species and may depend on environmental conditions, its elucidation is extremely important. The behaviour of the starch during processing (and ultimately the resultant products) depends on its composition (ie. amylose to amylopectin ratio), structure and molecular weight and these properties are equally important in determining its behaviour towards hydrolysing enzymes.

1.5 XANTHAN

1.5.1 Structure, Conformation and Applications

Xanthan is an ionic extracellular polysaccharide produced commercially by fermentation of the bacterium *Xanthomonas campestris*. The primary structure of xanthan has been established for a number of years (Lindberg et al, 1973: Jansson et al, 1975). It consists of a β-(1->4) linked D-glucopyranosyl backbone which is substituted at every alternate unit by a trisaccharide chain at O-3. The trisaccharide chain is composed of two D-mannosyl units, separated by a D-glucuronosyl group (see Figure 1.15). The O-3 backbone linked α-D-mannopyranosyl unit contains an acetyl group at O-6 and is linked through O-2 to the β-D-glucopyranosyluronic acid unit which in turn is linked through O-4 to the terminal β-D-mannopyranosyl group. Approximately half the terminal D-mannosyl groups contain an ether linked pyruvic acid moiety (Kang and Pettitt, 1993).
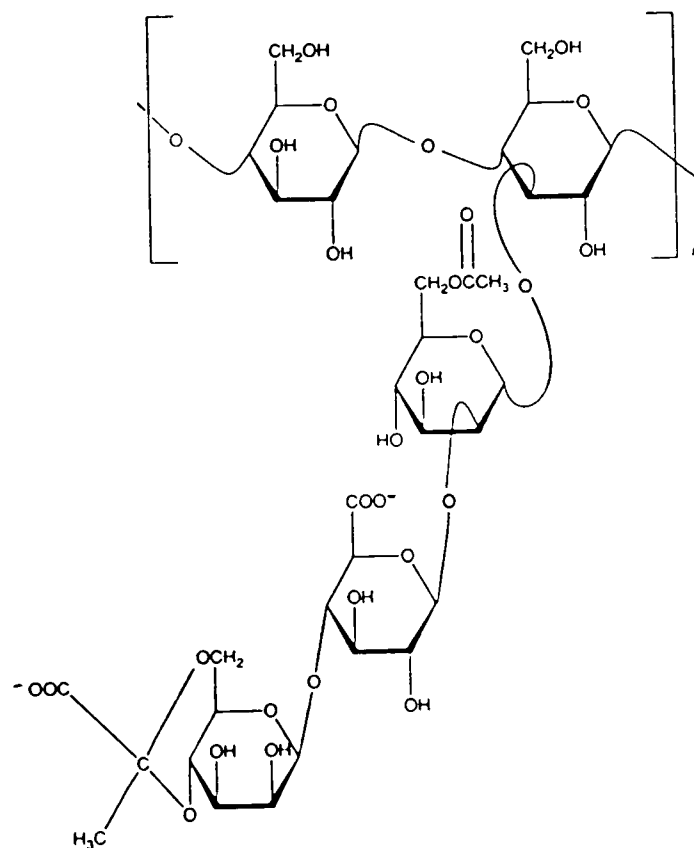
Figure 1.15: Primary structure of xanthan (Kang and Pettitt, 1993)

The secondary and tertiary structures of xanthan are not completely undisputed, molecular modelling (Moorhouse et al, 1977) suggests a five-fold single helix with side chains aligned along the polymer backbone. This is supported by light scattering and transition dynamics analysis (Norton et al, 1984). Interaction studies are divided as to the existence of a single (Moorhouse et al, 1977) or double helix. A single helical conformation has been suggested by Norton et al (1984) whereas other light scattering data seem to support the notion of a double helical conformation (Sato et al, 1984). Solution conformation studies (Sato et al, 1984; Norton et al, 1984; Holzwarth, 1976) point to a rod-like ordered conformation or a worm-like chain with limited flexibility. Associations between xanthan molecules have also been studied (Tako and Nakamura, 1984), however, these studies are not yet conclusive and require further consideration.

1.5.2. Properties and Applications

The applications of xanthan are mainly due to its unusual viscosity and rheological characteristics. It dissolves readily in hot or cold water, giving highly viscous solutions at low concentrations which are important for its use as a suspending and thickening agent. Solutions exhibit very pronounced pseudoplasticity, ie. viscosity decreases with increasing shear rate. Xanthan solutions are stable between pH 1 and 13 and solution viscosity is not impaired by temperatures up to 93°C. Xanthan is susceptible to biodegradation from enzymes formed by microorganisms under certain environmental conditions, but it is stable against enzymic degradation by "laboratory" enzymes (Kang and Pettitt, 1993). Xanthan interacts with galactomannans to give a synergistic increase in solution viscosity and in the case of locust bean gum, gelation (Dea et al, 1972; 1977; Lopes et al, 1992).

Xanthan is used extensively in oil-well drilling and enhanced oil-recovery operations where its pseudoplasticity means that it is easy to pump but recovers viscosity when pressure is removed. It also reduces friction pressure in turbulent flow areas and it tolerates most drilling additives and salts. Food applications of xanthan vary from salad dressings, to dry mixes, syrups, sauces and dairy products to baked products and rely on its excellent suspending properties, its stability to temperature, its high viscosity at low concentrations and its unique rheological properties (Kang and Pettitt, 1993). Other applications are in the textile, printing and dyeing industries as a thickener, in ceramic glazes to aid suspension of insoluble components, in cleaning agents and slurry explosives.

1.6 MUCIN

Mucus is a complex mixture of glycoprotein, water, salts, lipids and cellular materials. Mucins (mucin polysaccharides, mucus glycoproteins) are the components of mucus secretions lining respiratory, urogenital and digestive tracts which are responsible for their viscoelastic and lubricating properties (Gerken, 1993). Physical properties of mucins appear to be independent of source (Silberberg and Meyer, 1982) leading to the assumption that their basic structures are identical and that they vary only in molecular size (Carlstedt and Sheehan, 1984). Mucins typically have molecular weights above $2x10^6$ and exhibit expanded solution structure (Harding et al, 1983). Mucins are composed of a polypeptide backbone containing highly glycosylated regions and 'naked' protein regions, the protein content is approximately 20%, whereas the carbohydrate content constitutes 70-80% of the molecule (see for example, Harding, 1989 and references cited therein). The macromolecule consists of several subunits which in turn consist of several 'basic units' (see Figure 1.16). A basic unit consists of a highly glycosylated backbone region which is resistant to proteolysis and one or two naked protein regions. The latter are sensitive to proteolytic degradation. Subunits are obtained by thiol reduction of the native mucin and they may have molecular weights of up to $2x10^6$. These subunits can be digested with proteases (eg. trypsin or papain) to yield the basic units which typically exhibit molecular weight values of ~$0.5x10^4$ (Harding, 1989 and references cited therein). In the glycosylated region the protein backbone contains large amounts of threonine, serine and proline and it is serine and threonine which facilitate the link to the oligosaccharide side chains through a specific O-glycosidic link to N-acetylgalactosamine. Proline molecules appear to be responsible for the formation of the loosely coiled structure due to their ability

Glycosylated region

'Naked' protein region

○	GalNAc
●	GlcNAc
□	Gal
△	Fuc
▲	Sialic acid

(a)

(b)

(c)
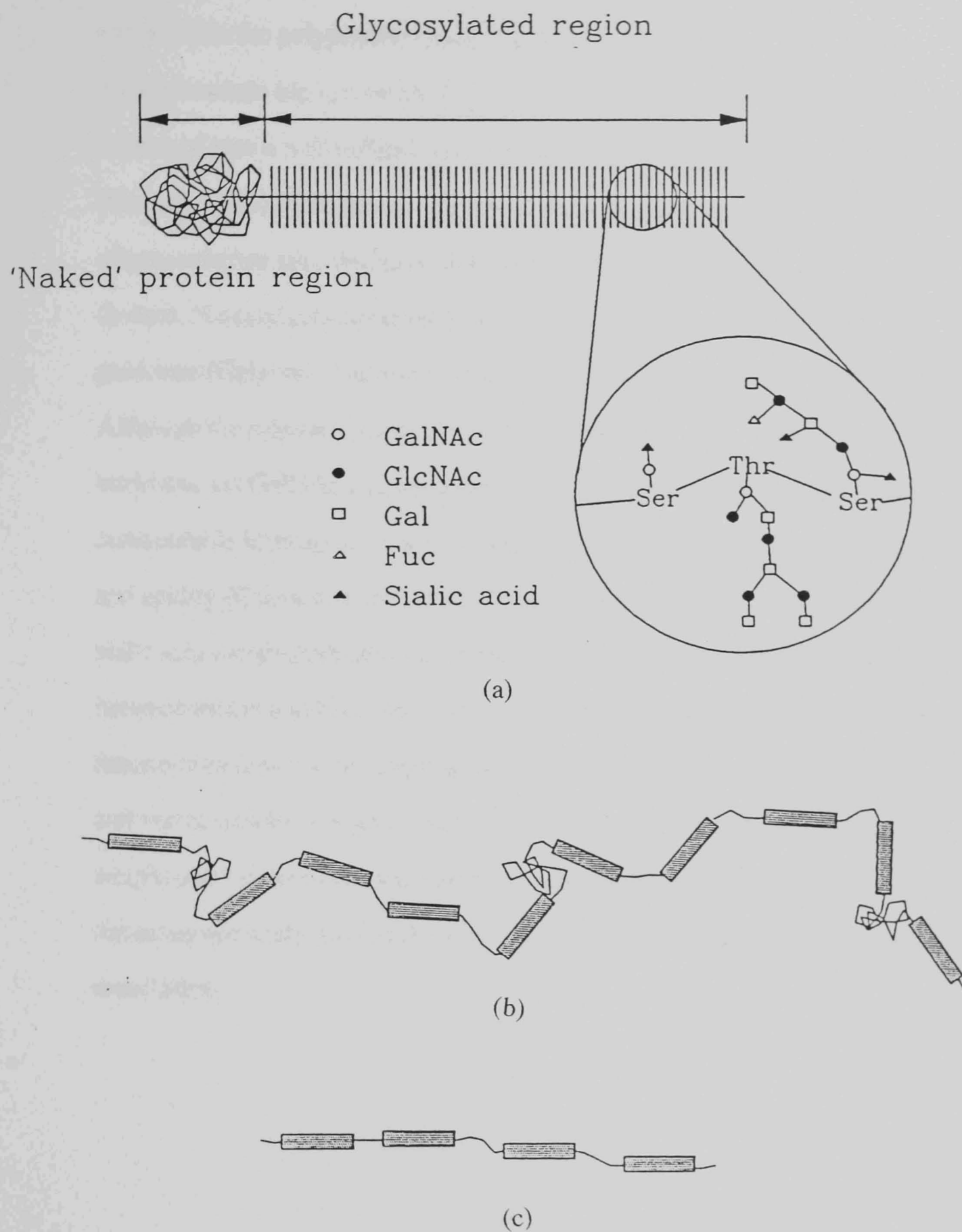
Figure 1.16: Schematic representation of a mucin molecule
(Carlstedt et al, 1985)
(a) basic unit (Mol. wt. ~ 500 000)
(b) mucin polymer (Mol. wt. >2.5x10^6)
(c) subunit resulting from thiol reduction (Mol. wt. ~2x10^6)

to adopt a compact conformation which facilitates the production of bends and turns in the polypeptide chain (Harding, 1989). The 'naked' protein regions contain high proportions of cystein residues and are thought to be organised into a well defined globular shape, stabilized by disulphide bridges (Gerken, 1993). This domain appears to be susceptible to proteolysis. The oligosaccharide side chains are composed of five monosaccharides: L-fucose (L-fuc), N-acetylgalactosamine (GalNAc), N-acetylglucosamine (GlcNAc), galactose (Gal) and N-acetylneuraminic acid (NeuAc) (Harding, 1989). Although the oligosaccharide side chains are always linked to the peptide backbone via GalNAc and often terminated by L-fuc or NeuAc, they exhibit considerable heterogeneity with regards to composition, length , branching and acidity (Carlstedt et al, 1985). The net negative charge which is due to the sialic acid components plays an important part in the mucoadhesive forces between mucin and positively charged bioadhesive polymers. Mucins are the determining factor in the physical properties of mucus, ie. its high viscosity and viscoelasticity and gel characteristics. However, elucidation of molecular weight and solution conformation is no easy task due to its thermodynamically non-ideal behaviour, its polydispersity and possible self-association.

1.7 Radiation Induced Changes in Polysaccharides

The polysaccharides discussed in this thesis are used to confer certain functional properties to food systems. They frequently originate from countries with tropical or sub-tropical climates and require transport and may be subjected to prolonged storage prior to use resulting in the need for disinfestation and sterilisation. Thermal treatments may be effective, however, they may cause degradation of unstable materials. In the past, gums such as guar gum have been sterilized using ethylene oxide or ethylene dibromide. However, suggestions that small residual amounts of these gases may be ingested by the consumer have led to restrictions in their use. For example, the reaction of ethylene chloride with moisture and chloride ions in foods can lead to epichlorohydrin which is considered to be mutagenic. Alternative methods of preservation for food polysaccharides are therefore to be found. One such method is irradiation. Food irradiation was patented as early as 1930 but scientific research into the subject did not start until after 1945 and the technical application of the process did not commence until the 1950's and 60's (Jukes, 1991 and references cited therein). Investigations regarding the safety of food irradiation particularly with respect to the wholesomeness of irradiated foods were initialized in a joint meeting sponsored by the Food and Agricultural Organisation (FAO), International Atomic Energy Agency (IAEA) and the World Health Organisation (WHO) (Jukes, 1991). This Joint Expert Committee on Irradiated Food (JECIF) reported in 1980 after extensive animal feeding studies and identification of irradiation products from foods had been carried out, that radiation processing of food with doses up to 10kGy was safe in relation to all aspects of the wholesomeness of food (Joint FAO/IAEA/WHO Expert Committee, 1981). However, despite these findings the acceptance of this process for food stuffs is still very much debated by governments and consumers alike

due to it being associated with nuclear energy (Jukes, 1991, Rayas-Duarte and Rupnow, 1989 and references cited therein).

The process of irradiation is carried out by using electromagnetic (ionizing) radiation from either X-ray or gamma (γ)-ray sources or electron accelerators. Radiation from these sources reacts with matter by several processes, the most important of which is the Compton effect which is an elastic scattering process (von Sonntag, 1987; Swallow, 1977) as shown in Figure 1.17. The photon gives up part of its energy by ejecting an electron from an atom and then continues in a different direction, and interacts with another atom. The ejected electron will excite and ionize other molecules along its path. The initial ionization thus induces a large number of excited and ionized molecules. The other interaction mechanisms are the photoelectric effect , pair formation, and nuclear reaction. In the photoelectric effect the photon gives up all its energy by ejecting an electron from an atom. This effect occurs nearer the nucleus (see Figure 1.18) and is more important for high atomic number elements and low energy γ- or X-radiation. Pair formation describes the conversion of the photon into a positron-electron pair. This process can only take place when the photon energy is greater than the rest masses of electron and positron, ie. greater than 1.02 MeV. It is of significance for high atomic number elements and high energy radiation only. Nuclear reactions occur when γ- or X-rays interact with certain atomic nuclei and emit neutrons or other particles, producing radioactivity. This process only takes place when the photon energy is above a certain threshold for the nucleus and its effects are generally negligible. However, in order to avoid radioactivity, an upper limit must be imposed on the energy of radiation permitted to treat foods.
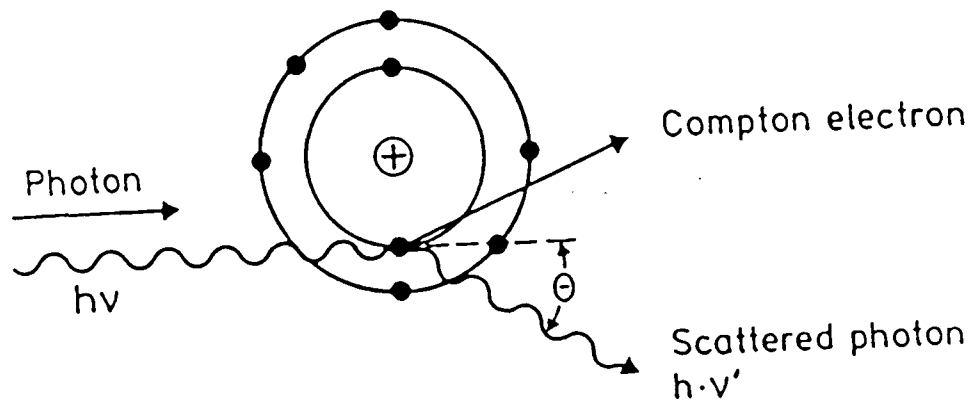
Figure 1.17: Schematic representation of the Compton effect
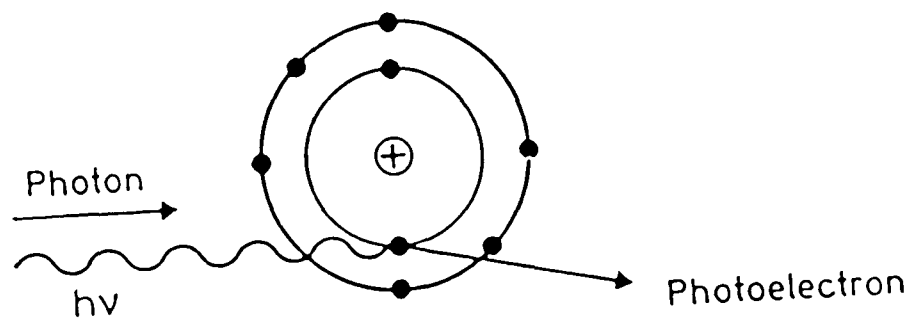
Figure 1.18: Schematic representation of the photoelectric effect
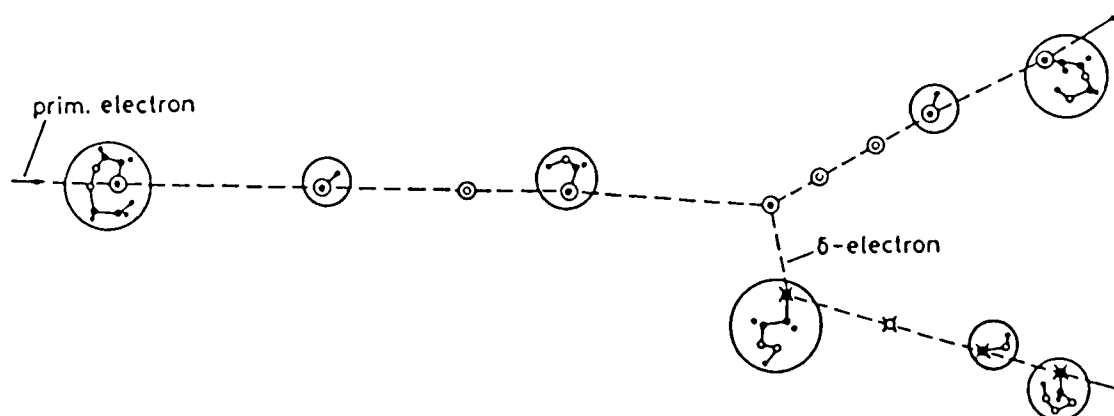
Figure 1.19: Schematic representation of the 'spur model'

As mentioned earlier, the interaction of matter with fast electrons gives rise to a large amount of excitation and ionization along the electron track. If electrons which have been ejected have sufficient energy to cause excitation and ionization close to the original ionization they give rise to groups of events called 'spurs'. Some of the electrons will have sufficient energy to leave the main path of the particle and form separate tracks of their own. These are called δ-electrons or δ-rays. A schematic diagram of the spur model is shown in Figure 1.19 (von Sonntag, 1987).

The most common radiation sources for foods are the radionuclides Cobalt-60 (^{60}Co) and Caesium-137 (^{137}Cs) or electron generators. The amount of radiation used is expressed as the 'dose' and measured in units of Gray (Gy) where $1Gy = 1Jkg^{-1}$. Irradiation dose may vary with the required objective. Inhibition of sprouting, insect disinfestation and delay of ripening can be achieved with applications up to 1kGy (low dose). At doses between 1 and 10kGy (medium dose) the number of non-sporing pathogenic micro-organisms and microbial load can be reduced, and technical properties of food can be improved. Applications at high doses (10 - 70kGy) eliminates viruses and gives sterilization (Joint FAO/IAEA/WHO Expert Committee, 1981).

The radiation chemical yield is the chemical effect of radiation in terms of the numbers of molecules (or transformations) effected per 100eV absorbed in the medium. This is commonly termed the G-value in units of molecules $(100eV)^{-1}$ (von Sonntag, 1987; Swallow, 1977).

Fast electrons as produced by γ-radiation excite or ionize molecules along their track. Reactions of excited molecules are known from photochemistry and include molecular decomposition resulting in new molecular products of free radicals, transfer of excitation energy, internal conversion to lower excited states, intersystem crossing to give triplet states, hydrogen atom

transfer and electron transfer.

Positive ions (from ionization) may initiate transfer of electrons, protons, hydrogen atoms and hydride ions. Electrons ejected during the formation of the positive ions can become trapped in suitable vacancies in crystal lattices or may be captured by molecules with positive electron affinity or may recombine with positive ions. All the above processes are extremely short-lived and will be over within 10^{-8} seconds or less (Swallow, 1977). However, their reaction products, ie. newly formed molecules or free radicals, will be present in the irradiated material. The free radicals produced in the above primary steps after ionization can undergo a variety of reactions such as addition to double bonds, electron transfer, hydrogen transfer etc.

As is clear form the preceding paragraph, there is a vast number of chemical reactions which may originate from irradiation of polysaccharides. These reactions have been reviewed by several authors (for example, Phillips, 1961, 1972; von Sonntag, 1980) and there is no need to review them further at this point. The radiation induced changes in polysaccharides relevant to this thesis are primarily the effects on molecular size. It has been found (Phillips, 1961 and references cited) that irradiation of polysaccharides in the solid state or in solution results in degradation of these materials as the most predominant feature. However, the radiation dose required to cause a significant change in solid polysaccharides is larger than for the equivalent changes in solution (Whistler and Ingle, 1965). Irradiation in dilute solutions causes molecular transformations predominantly as a result of interaction of intermediates of water hydrolysis, ie. OH , e_{aq}, H . In dry solids unstable radicals may not migrate as freely, resulting in relatively long life-times (Rayas-Duarte and Rupnow, 1989).

The effect of irradiation on starches of various origins has been investigated and reviewed by a number of researchers (Raffi et al 1981a, b, c; Rayas-

Duarte and Rupnow, 1989; Adam, 1983). The change in the amount of low molecular weight reaction products such as hydrogen peroxide, formic acid and carbonyl compounds with increasing radiation dose was reported by Raffi et al (1981a, b, c). Rayas-Duarte and Rupnow (1989) reported a marked decrease of the viscosity of pastes from irradiated Great Northern beans at radiation doses of 20kGy but also found a 55% decrease in viscosity when the radiation dose was reduced to 2.5kGy.

Decreases in viscosity of irradiated cellulose and pectin in solution (Clegg and Kertesz, 1956) was one of the earliest indications of degradation of irradiated polysaccharides. Kusama et al (1976) investigated the effect of γ-radiation on the molecular weight distribution of various types of cellulose. A radiation dose of 50kGy under vacuum at room temperature reduced the weight average molecular weight of Mexican cotton cellulose (Cellulose I) to a much greater extent than that of polynosic rayon (Cellulose II). Furthermore, molecular weights of microcrystalline celluloses of type I and II decreased much less than their originals, particularly for cellulose I. This implies that the degradation behaviour depends on the micro-structure of the polysaccharide. The effect of γ-irradiation of cellulose in wood was investigated by McLaren (1978) who found that there is some initial protection against radiation possibly from some natural constituents of the wood (eg. lignin, hemicelluloses) which is overcome as the radiation dose increases.

γ-irradiation is already used as a means of preservation for fresh fruit in some countries. There is therefore a need to be able to differentiate between irradiated and unirradiated fruit. Sjöberg (1987) studied the effect of γ-radiation on apple pectin in the whole fruit and pectin isolated prior to irradiation and some standard apple pectins. She found that there was no significant change in pectin molecular weight of the whole fruit, whereas molecular weight of isolated and standard pectins decreased significantly. She

44

attributed the absence of depolymerization in the whole-fruit pectin to the presence of the protective effect of sugars in the apples. It is known that sugars are better OH radical scavengers than polysaccharides (Phillips, 1980). There was a slight decrease in viscosity of the whole-fruit pectin after irradiation at doses above the limit for fresh fruits. The most significant irradiation induced change of the whole-fruit pectin was found to be in its degree of methylation which decreased more than that of the isolated and standard pectins, implying that there might be a change in the primary structure under these conditions which could be used to differentiate between irradiated and unirradiated whole fruit.

Gums are used to a large degree in the food industry as stabilizers and some also as emulsifiers. The primary goal of irradiating these materials is to sterilize them and reduce microorganisms and bacterial growth on storage. A study by Blake et al (1988) on the effect of γ-radiation on molecular weight and emulsifying properties of three differently treated (raw, kibbled and spray dried) samples of gum arabic revealed that intrinsic viscosity and molecular weight were reduced with increasing radiation dose for the kibbled and spray dried samples, whereas these properties were not affected in the raw material. The emulsifying properties of gum arabic were unchanged for all three samples.

The water-swelling properties of karaya gum after γ-irradiation were studied by LeCerf et al (1991). They found an increase in water solubility of karaya gum from 20 to approx. 70% after a dose of 5kGy without any decrease in molecular weight. However, they found a decrease in viscosity and swelling properties and suggested that this may be due to radiation affecting the branching and thus reducing aggregate formation.

King and Gray (1993) reported the effect of γ-irradiation on guar gum, locust bean gum, gum tragacanth and gum karaya. They attributed the rapid

45

decreases in viscosity of guar and locust bean gum to a decrease in polymer aggregation at low radiation doses which was then followed by a more gradual decrease in viscosity due to hydrolysis of the polymer at high doses. ESR spectra indicated two groups of free radicals generated during irradiation which may relate to the mechanism in viscosity decrease. Viscosity measurements of irradiated gum karaya and tragacanth showed different behaviour and led to the conclusion that these polymers were hydrolysed in a random fashion. Solubility of these polymers was increased at low radiation doses, stabilizing or increasing viscosity, whereas at high doses polymer hydrolysis caused a decrease in viscosity. ESR spectra of these gums only changed with respect to signal strength indicating an increase in free radical production with dose.

CHAPTER 2

THEORY AND APPLICATIONS OF METHODS

2.1 COMBINED SIZE EXCLUSION CHROMATOGRAPHY AND CLASSICAL LIGHT SCATTERING

The technique of combined size exclusion chromatography and classical light scattering has been established since the 1970's (Ouano, 1976) and is best described as on-line monitoring of the solute fractionated by size exclusion columns by light scattering resulting in absolute molecular weights and molecular weight distributions.

The theory of each technique is presented separately, followed by a brief review of the application of the combined technique to polysaccharides and related systems.

2.1.1 Classical Light Scattering

The term 'Classical (or 'Static') Light Scattering' refers to the scattering of incident radiation in the visible region from macromolecules in solution. It is theoretically rigourously founded and one of the few absolute methods for the determination of molar mass and molecular size.

It was Lord Rayleigh (Strutt, 1871) who first published the theory of the scattering of light by an ideal gas. Einstein (1910), Raman (1927), Debye (1944) and Zimm (1945) are probably the most noted scientists responsible

for the advancement of this theory and its application towards macromolecular systems. Developments since then have been concerned with refinements in theory and instrumentation.

Extensive descriptions of the theory of classical light scattering can be found in Tanford (1961), Kratochvil (1987), Billingham (1977), and others, only the fundamental principles will be covered here.

2.1.1.1 Light scattering from small molecules

The intensity of light scattered by a small, isotropic molecule (ie. $R_G < \lambda/20$) from a plane polarized beam can be shown to be (Billingham, 1977)

$$i_\theta = \frac{I_0 n}{r^2} \frac{16\pi^4 \alpha^2}{\lambda^4} \cos^2\theta \qquad [2.1]$$

where

θ = scattering angle to the incident beam

i_θ = the intensity of the scattered light

I_0 = the incident light intensity

r = the distance between the scattering molecule and the detector

n = the refractive index of the solution

α = the polarizability of the scattering molecule

λ = the wavelength of the incident light in vacuo

By combining parameters relating to particular experimental arrangements and introducing the scattering volume, V, containing n scattering centres, the Rayleigh ratio (or Rayleigh factor), R_θ can be defined

48

$$R_\theta = \frac{16\pi^4\alpha^2 n}{\lambda^4 V}$$

[2.2]

The polarizability α, can be described in terms of the refractive index through

$$\alpha = \frac{Mn_0}{2\pi N_A}(dn/dc)$$

[2.3]

where M is the molar mass, N_A is Avogadro's number and dn/dc is the specific refractive index increment, which describes the change in refractive index with concentration and n_0 is the refractive index. This parameter can be measured independently. Using this equation and defining the total number of scattering centres within a certain scattering volume by

$$n/V = cN_A/M$$

[2.4]

and substituting into equation [2.2] we obtain

$$R_\theta = \frac{2\pi^2 M n_0^2 c}{N_A \lambda^4}(dn/dc)^2$$

[2.5]

and by grouping the constant terms (for a given polymer) on the right hand side together using

$$K = \frac{2\pi^2 n_0^2}{\lambda^4 N_A}(dn/dc)^2$$

[2.6]

we now obtain

$$R_\theta = KMc$$

[2.7]

It can be shown that for polydisperse samples the molecular weight average obtained from light scattering measurements is the weight average molecular weight (Billingham, 1977).

Equation [2.7] is highly idealized and in real systems external interference which reduces the scattering intensiy has to be taken into account. This has been done by Debye (1944) who based his thermodynamic treatment on the assumption that the scatter from a solution originates from local concentration fluctuations of the solute. If the solvent scatter is due to the density fluctuations, the solute scatter must be due to the concentration fluctuations. This can be described in terms of the free energy required to create a concentration gradient in a solution via the osmotic pressure, π, and leads to

$$\frac{Kc}{R_\theta} = \frac{1}{RT} \frac{\delta\pi}{\delta c} \qquad [2.8]$$

π can be expressed in the form of a virial expansion, and equation [2.8] becomes

$$\frac{Kc}{R_\theta} = \frac{1}{M} + 2A_2c + 3A_3c^2 + \ldots \ldots \qquad [2.9]$$

where A_2, A_3 etc are the second, third, etc. virial coefficients. The virial coefficients quantitatively characterize thermodynamic interactions among solute molecules. In dilute solution measurements the third and higher virial coefficients are usually neglibly small and can be ignored.

If $A_2 > 0$ it means that polymer-solvent interactions are favoured. When A_2 (and/or higher virial coefficients) is zero, polymer-solvent interactions and polymer-polymer interactions are energetically equivalent and the solution behaves in some respects as an ideal solution. Solvents meeting the

50

requirements for zero virial coefficients are called theta (θ)-solvents and the temperature at which these requirements are fulfilled is the θ-temperature. A negative value of A_2 indicates preferred polymer-polymer interactions and therefore, that the solvent is poor for that particular polymer.

2.1.1.2 Light scattering from large molecules

The use of the equations established in section 2.1.1.1 depends on the assumption that the particles are sufficiently small (ie. $<\lambda/20$) to act as point scattering centres. Macromolecules with molecular weights larger than approx. 30 000 have solution dimensions which are considerably larger than $\lambda/20$. The scattering from different points of such a molecule will reach the detector with different phases. The beams scattered from different points of a particle are coherent and therefore capable of interference. If two beams which are out of phase interfere, the intensity of the resulting radiation is smaller than the sum of the intensities of the constituent beams. As this interference is caused by different points in the same particle it is termed internal (or intramolecular or intraparticle) interference. As a consequence of this, the scattered intensity at any angle to the forward direction of the beam is greater than that at the corresponding angle to the backward direction of the beam and as a result, R_θ becomes a function of θ. The scattered intensity is reduced due to internal interference at all angles except zero. It is possible to eliminate the internal interference by taking measurements at several low angles and extrapolating to zero angle. However, as internal interference originates from the difference in distance between the scattering centres of the molecule, ie. its size and shape, the variation in scattering intensities with θ should be able to give some information regarding the size and shape of the molecule.

51

2.1.1.3 Angular dependence of light scattering

The angular dependence of the scattering intensity for large particles can be described by the scattering function $P(\theta)$ which is defined as

$$P(\theta) = R_\theta/R_0 \qquad\qquad [2.10]$$

At zero angle the effect of internal interference is always zero and therefore, $P(0) = 1$. The value for R_0 cannot be measured experimentally as most of the incident light is transmitted through the solution. R_0 is therefore determined by extrapolation to zero angle. Also, light scattered from different solute molecules can interfere, reducing the sum of the individual scattering intensities of the solute molecules. This intermolecular interference effect is eliminated by extrapolation to zero concentration.

Particle scattering functions can be directly related to the radius of gyration of a molecule (see for example, Tanford 1961) without having to make any assumption regarding the shape of the molecule

$$\lim_{\theta \to 0} P(\theta) = 1 - \frac{\mu^2 <R_G^2>}{3} \qquad\qquad [2.11]$$

where $\mu = \left(\frac{4\pi}{\lambda}\right) \sin\frac{\theta}{2}$

This is unique in that all other physical measurements of radius of gyration require some assumption regarding molecular shape.

The above can be rearranged to give

$$\lim_{\theta \to 0} P(\theta)^{-1} = 1 + \frac{16\pi^2}{3\lambda^2} <R_G^2> \sin^2\frac{\theta}{2} \qquad\qquad [2.12]$$

52

and at zero concentration and zero angle $Kc/R_\theta = 1/M$, therefore,

$$\lim_{(\theta \to 0),(c \to 0)} \frac{Kc}{R_\theta} = \frac{1}{MP(\theta)} = \frac{1}{M}\left(1 + \frac{16\pi^2}{3\lambda^2}\right) <R_G^2> \sin^2\frac{\theta}{2} \qquad [2.13]$$

The limits of the equation, ie. $\theta \to 0$ and $c \to 0$ can be achieved by the method developed by Zimm (1948) (an example is shown in Figure 2.1) where extrapolations to zero angle and zero concentration are plotted in the same graph. Extrapolating to $\theta = 0$ a plot of Kc/R_θ vs kc (k is an arbitrary scale factor) is obtained with the intercept being $1/M$ and the slope giving the second virial coefficient. Extrapolation to zero concentration results in a plot of Kc/R_θ versus $\sin^2(\theta/2)$ with the limiting slope being a direct measure of R_G (cf. limiting slope/intercept = $(16\pi^2/3\lambda^2)<R_G^2>$).
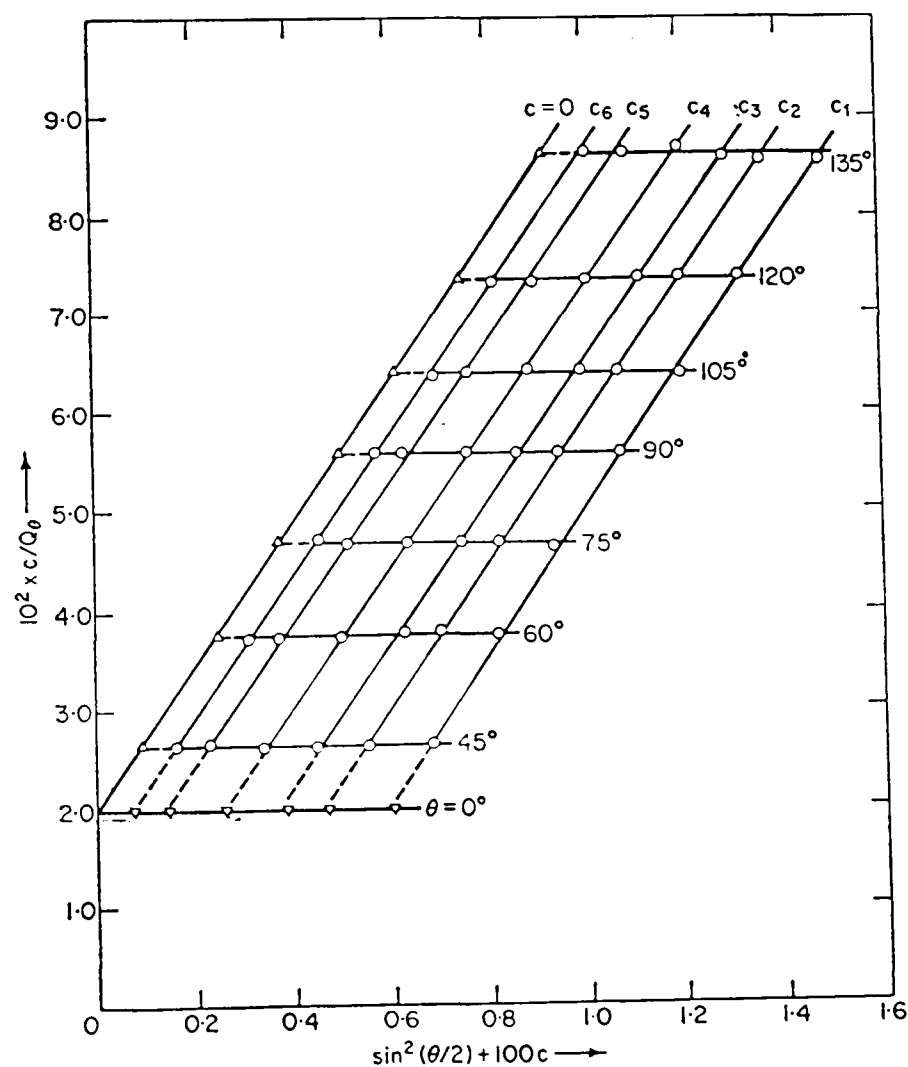
Figure 2.1: Typical Zimm plot (from Evans, 1972, wherein experimental details and scale parameters are described)

53

Particle scattering functions for basic particle shapes can be derived (see Kratochvil, 1987; Tanford, 1961) and are illustrated in Figure 2.2 However, it is recommended to evaluate particle size from the radius of gyration (Kratochvil, 1987). For the three basic models for macromolecular shape, the following simple relationships hold

For a random coil $\quad <R_G^2> = \dfrac{<r^2>}{6}$ $\quad\quad\quad\quad$ [2.14]

For a thin rod $\quad\quad <R_G^2> = \dfrac{L^2}{12}$ $\quad\quad\quad\quad$ [2.15]

For a hard sphere $\quad <R_G^2> = \dfrac{3a^2}{5}$ $\quad\quad\quad\quad$ [2.16]

where a is the radius of a sphere, r^2 is the mean square end-to-end distance of a random coil and L is the length of a thin rod.
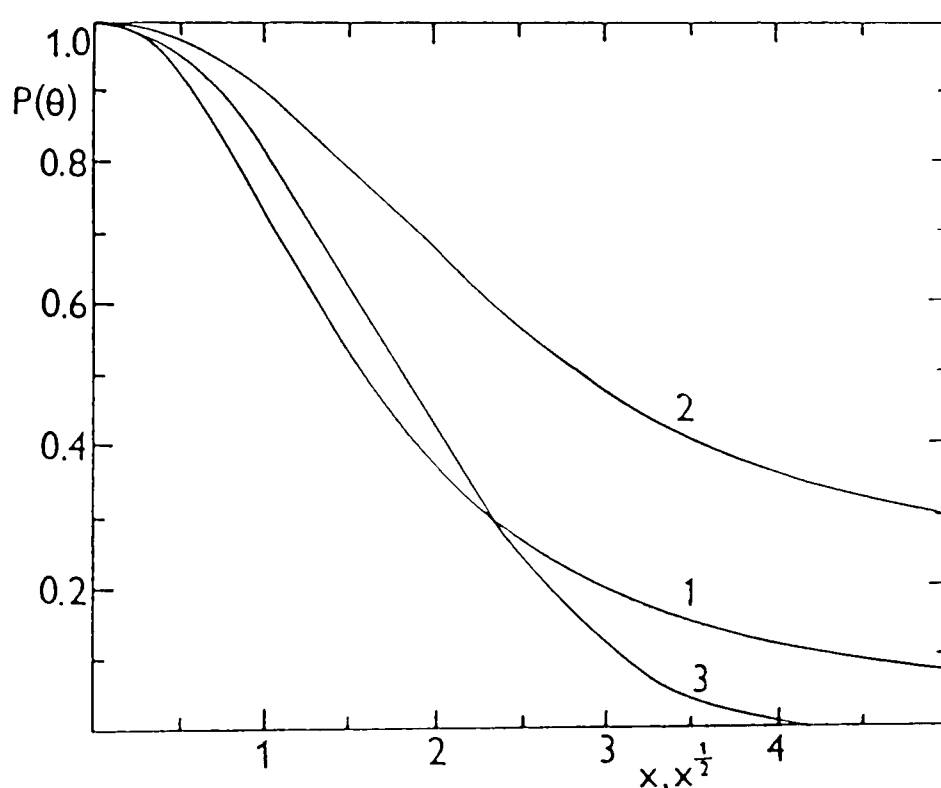
Figure 2.2: Particle scattering functions, $P(\theta)$ for basic particle shapes. Curve 1 is for monodisperse linear random coils, curve 2 for infinitely thin rods, curve 3 for homogeneous spheres (x and $x^{1/2}$ are products from dimensional and angular factors and differ depending on particle shape) (from Kratochvil, 1987).

The above has demonstrated that any information about particle size and sometimes shape is a result of the angular dependence of the scattering intensity which can be described by $P(\theta)$. To represent this graphically, plots of $P^{-1}(\theta)$ versus $\sin^2(\theta/2)$ or a parameter proportional to $\sin^2(\theta/2)$ (eg. $\mu^2 <R_G^2> = (16\pi^2/\lambda^2) <R_G^2>\sin^2(\theta/2)$ are constructed. Similarly, Kc/R_θ instead of $P^{-1}(\theta)$ versus $\sin^2(\theta/2)$ can be plotted, allowing elucidation of the weight average molecular weight. If angular dependences of samples with different molecular weights are to be compared, it is preferable to use a plot of $P^{-1}(\theta)$ versus $\sin^2(\theta/2)$. There are three typical shapes for $P^{-1}(\theta)$ shown in Figure 2.3. Line a corresponds to the angular dependence of small molecules which is of course unity, ie. R_θ is independent of θ. For molecules with dimensions comparable to the wavelength of the incident light, the angular dependence may be linear with a positive slope or moderately curved (line b). Highly polydisperse solutions or those containing small amounts of large particles, result in the strongly curved line c.

The curvature of line c can be explained in the following way: there is no angular dependence of R_θ for small particles, however, for large particles R_θ decreases with increasing angle of observation, resulting in a strong curvature at low angles which diminishes at higher angles. The situation is similar for broad continuous distributions of molecular size and shape. For such systems it may be impossible to extract any information from $P^{-1}(\theta)$ functions as the effect of polydispersity may outweigh the effect of particle shape.
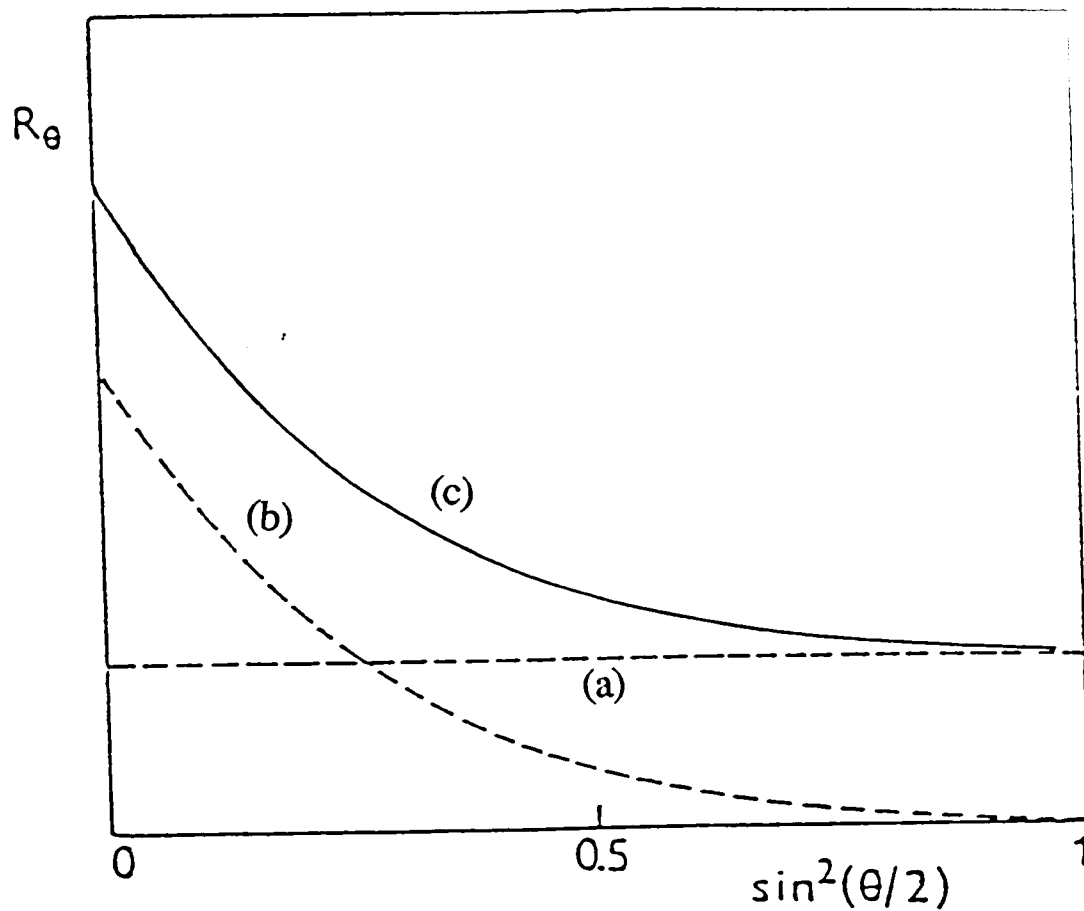
Figure 2.3: Angular dependence of the Rayleigh ratio, R_θ, for a two-component (large and small particles) system. Line a represents the contribution of the small particles, line b represents the contribution of the large particles and line c shows the total excess Rayleigh ratio (from Kratochvil, 1987).

2.1.2 SIZE EXCLUSION CHROMATOGRAPHY

Solutions of macromolecules rarely contain monodisperse species, most frequently the polymers although structurally identical will be of a large variety of different sizes, ie. the system will be polydisperse. The physical properties of a polymer will be significantly influenced by its molecular weight distribution, and point average molecular weights as determined by classical methods of molecular weight determination are frequently not sufficient in describing a macromolecular system.

One of the most successful and popular techniques for investigating whole molecular weight distributions is size exclusion chromatography (SEC). Porath and Flodin (1959) were the first to demonstrate that by eluting a polymer solution through a column packed with a swollen cross-linked dextran, fractionation of the components of such a solution would occur. Since this time, development of a large variety of column packing materials and chromatography hardware for conventional SEC and high performance SEC (HPSEC) have led to the great popularity of the method.

2.1.2.1 Retention Mechanism

The basic principle behind SEC is the separation of molecules according to size. The column packing matrix consists of porous polymer beads and solute molecules will penetrate in and out of these pores, thus establishing an equilibrium between the solute concentration inside the polymer beads and the eluent.

The volumes of the mobile phase inside and outside the pores of the gel matrix are grouped together into one volume term, V_M (Yau et al, 1979; Laurent and Killander, 1964). The stagnant part of the mobile phase residing in the pores is in effect the stationary phase, ie., the internal pore volume, V_i. The remaining

57

mobile phase is the void volume, V_0, which is the interstitial liquid volume between the packing particles.

Therefore,

$$V_M = V_0 + V_i \qquad [2.17]$$

Size separation in SEC is the result of the differential distribution of solute between the internal pore volume and the solvent outside the pores (Yau et al, 1979) and this distribution can be described by the SEC distribution coefficient K_D which is the ratio of average solute concentration inside the pores to that outside the pores. This means that the total accessible volume for the solute is $(V_0 + K_D V_i)$ and SEC retention volume, V_R can be described by

$$V_R = V_0 + K_D V_i \qquad [2.18]$$

The SEC distribution coefficient is the most universal parameter to quote for a component separated by SEC as it is not influenced by flow rate fluctuations or differences in column lengths. For any SEC column, $K_D = 0$ for a molecule that is too large to diffuse into the porous matrix, ie. $V_R = V_0$; this point is called the total exclusion volume, and $K_D = 1$ for a polymer that can penetrate the entire bed volume, ie., $V_R = V_M$, this point is called the total permeation volume.

The retention mechanism in SEC is controlled by entropy changes between the phases (Dawkins, 1976) ie., the extent of partition rather than the rate of partition. This was confirmed by studies by Yau et al (1968, 1970) who showed that retention is independent of flow rate and that the K_D (from SEC) of a particular solute compares well with the solute distribution coefficient when the solute is mixed with the polymer packing in a static mixing experiment.

2.1.2.2 Calibration

The major problem with SEC is that the retention mechanism is based on molecular size which may vary depending on solvent conditions whereas the information most usually sought is the molecular weight. There are three types of calibration in SEC (Yau et al, 1979): calibration with narrow molecular weight standards, universal calibration, and calibration with broad molecular weight standards.

The first method relies on determining the peak elution volume or K_D of a series of narrow standards and plotting this against the logarithm (to the base 10) of the molecular weight (see Figure 2.4). Such a calibration curve is only valid for a given set of experimental conditions and it is also based on the assumption that the standards behave in a similar way to the unknown sample (Yau et al, 1979) which is frequently not the case. However, this method is often used despite the lack of well defined standards and the uncertainty surrounding the predicted behaviour of an unknown polymer due to the ease and speed with which information, albeit limited, can be obtained.

A universal calibration taking into account differences in behaviour due to solute and pore shape would, therefore, be ideal in relating K_D or (V_R) to molecular weight. A number of attempts have been made to find a universally acceptable calibration for all types of polymers, some of which are statistical theories based on radius of gyration (Yau and Bly, 1980; Coll and Prusinowski, 1967) or other steric constraints on configurational space (Giddings et al., 1968; Cassassa, 1976). Grubisic et al (1967) employed Flory's relationship (Flory, 1953) between intrinsic viscosity and molecular weight to construct a calibration curve by plotting the product of log[η] and M_w versus elution volume. Such a calibration has been found to be valid for neutral polymers in
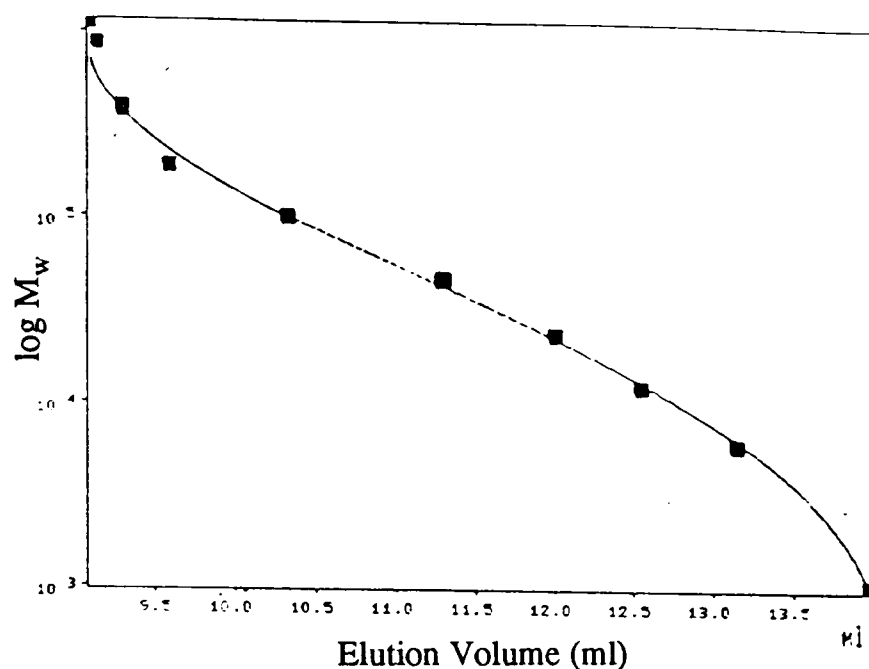
Figure 2.4: SEC calibration curve using dextran standards on gels having 1000 and 100Å pore sizes (Reproduced from PSS GmbH sales literature).

non-polar solvents (Corona and Rollings,1988). However, biological macromolecules are usually polar or ionic and it has been found that gels with inert pores cannot be universally calibrated for all kinds of macromolecules (leMaire et al, 1989)

Calibration with broad molecular weight standards requires knowledge regarding the complete molecular weight distribution curve of the polymer standard either by experimentally determining the molecular weight of many different fractions of the polymer or by using theoretical polymer molecular weight distributions and average molecular weights (Weiss and Cohn-Ginsberg, 1970). The latter method has been applied to water-soluble and organic-soluble polymers and is based on the assumption that many polymers follow predictable molecular weight distribution curve shapes which depend on the type and condition of polymerisation.

All three calibration procedures can only give molecular weight values which are based on a number of assumptions regarding solute behaviour.

2.1.2.3 Non-size exclusion effects

Additional problems in SEC are encountered due to non-size exclusion effects. These secondary separation mechanisms may occur in neutral or charged polymer systems, however, they are more usual in charged systems eg. polyelectrolytes. They are due to ionic interactions between the polymer in solution and the porous support matrix. These interactions have been reviewed by Stenlund (1976), they can lead to adsorption, ion exclusion and ion inclusion effects.

Other non-size exclusion effects include shear degradation (see for example, Giddings, 1982; Barth and Carlin, 1984) and concentration effects. Shear forces inside the column packing, injection valve, capillary tubing and column frits are all responsible for this phenomenon. Other factors influencing shear degradation are polymer configuration in solution and flow rate (Nakano and Minovra, 1975, 1978; Giddings, 1982; Huber and Lederer, 1980). The problem applies foremost to high molecular weight polymers.

Concentration effects appear as distortions on the SEC chromatogram. They are generally attributed to differences in viscosity between the eluting sample and the eluent and can be reduced by a decrease in sample concentration and if the sample consists of polyelectrolytes, addition of a small amount of electrolyte to the solvent (Rinaudo and Desbriers, 1980).

2.1.3 COMBINED SIZE EXCLUSION CHROMATOGRAPHY AND CLASSICAL LIGHT SCATTERING

The preceding two sections describe the techniques of classical light scattering and size exclusion chromatography . Each of these techniques has its own shortcomings - in SEC molecules are separated and molecular size distributions can be obtained for polydisperse samples . However, any molecular weight values obtained from SEC can only be relative. Molecular weights from light scattering experiments are absolute, however, they are only averages over the whole molecular weight distribution. Polymer solutions are usually polydisperse unless previously fractionated and an ideal system for molecular weight determination of polymers would be one which could combine the separation of molecules according to size and characterization of the resultant fractions by an absolute method such as light scattering. Frequently, SEC is used preparatively and the resulting fractions are then characterized independently (see for example, Berth, 1988). However, this is a laborious process and new instruments have been developed which combine SEC and light scattering on-line. A schematic diagram of such combined SEC/light scattering instrumentation is shown in Figure 2.5. The solution eluting from the column system is monitored first by the light scattering instrument and secondly by a concentration detector, usually a differential refractive index detector (DRI) or a UV detector. Chromatograms therefore consist of two traces, one due to the light scattering detector and the second due to the concentration detector (see Figure 2.6). After adjusting for the delay time for the fraction to reach the second detector, the excess scattering intensity at point i corresponds to the concentration at point i on the concentration curve. Absolute molecular weight

62
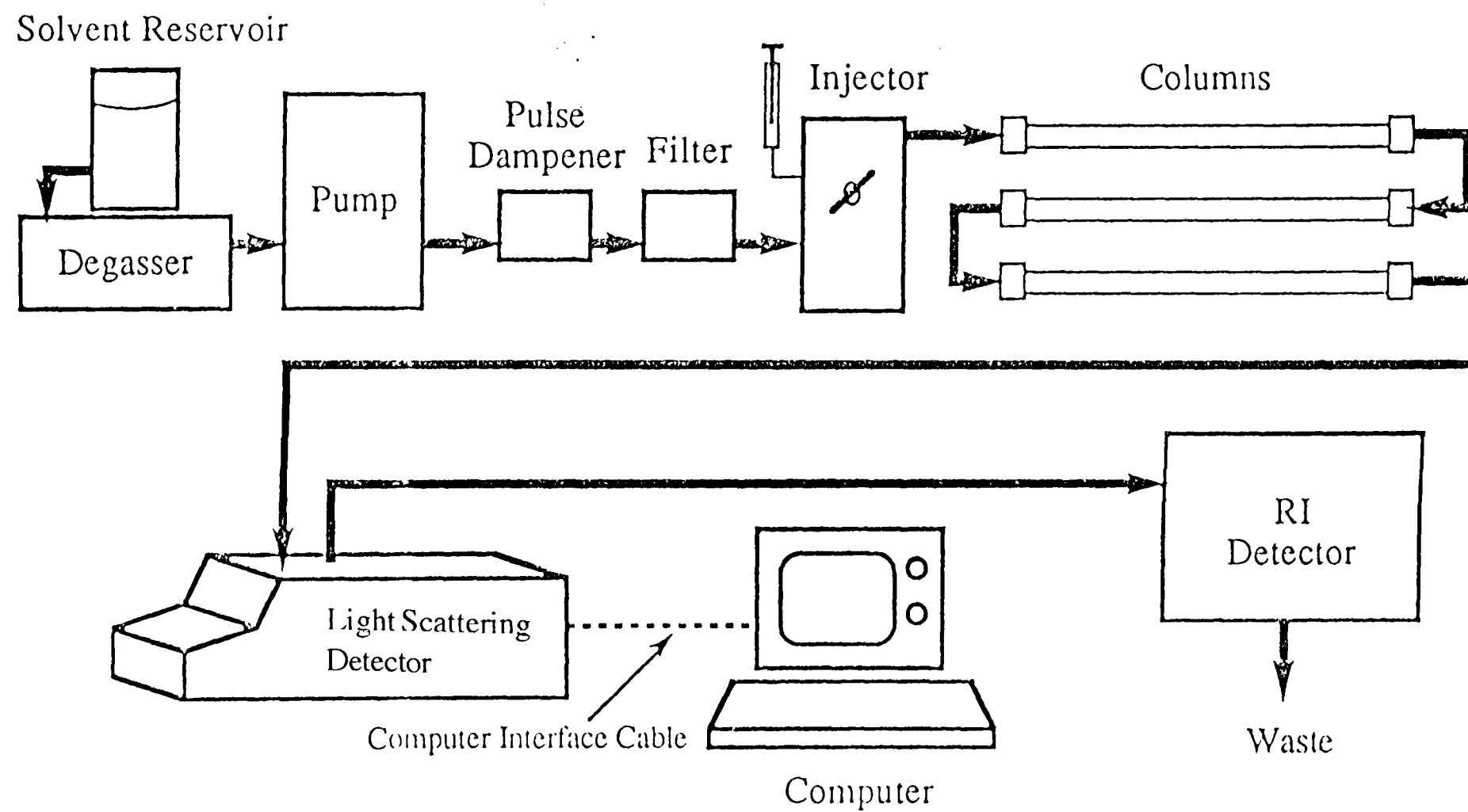
Figure 2.5: Schematic diagram of SEC/light scattering instrumentation. (Reproduced from Dawn F manual, Wyatt Technology)
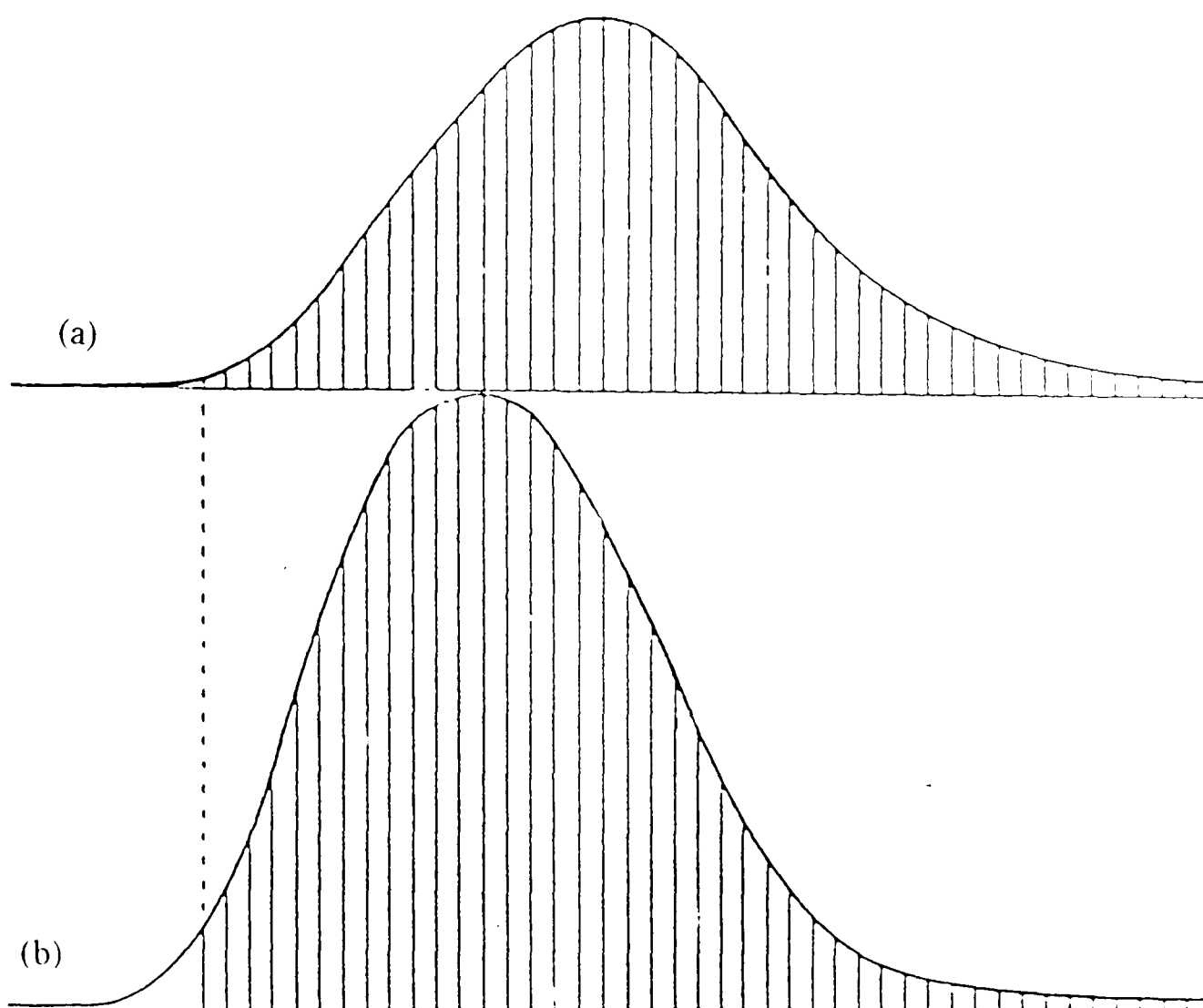
Figure 2.6: Examples of elution traces from SEC/light scattering instrumentation, (a) from concentration detector, (b) from light scattering detector. Responses from each detector at the corresponding slices are used to calculate molecular weight and radius of gyration averages.

and radius of gyration can therefore be calculated at each of those points according to:

$$\frac{Kc_i}{R_\theta} = \frac{1}{M_{wi}P(\theta)} + 2A_2c_i \qquad\qquad [2.19]$$

and both M_{wi}, and R_{Gi} are used to calculate molecular weight averages and radius of gyration distributions over the entire sample peak using the usual expressions

$$M_n = \frac{\sum c_i}{\sum \frac{c_i}{M_i}} \qquad\qquad <r^2>_n = \frac{\sum <r_g^2>_i c_i/M_i}{\sum c_i/M_i}$$

$$M_w = \frac{\sum c_i M_i}{\sum c_i} \qquad\qquad <r^2>_w = \frac{\sum <r_g^2>_i c_i}{\sum c_i}$$

$$M_z = \frac{\sum c_i M_i^2}{\sum c_i M_i} \qquad\qquad <r^2>_z = \frac{\sum <r_g^2>_i c_i M_i}{\sum c_i M_i}$$

2.1.3.1 Applications of Combined SEC/Light Scattering

Advances in light scattering instrumentation, initially using a single low angle laser light scattering photometer (LALLS) (Kaye et al., 1971, Kaye and Havlik, 1973) in the early 1970's allowed direct connection from the column system to the light scattering cell (Ouano, 1976). According to equation [2.10] section 2.1, P(θ) tends to unity in the limit of zero scattering angle. This means that information regarding radius of gyration and molecular shape is lost, however, the instrument can determine absolute molecular weight averages.

A multi angle laser light scattering (MALLS) photometer was developed by Wyatt in the late 1980's (Wyatt et al, 1988). This instrument has a flow cell which is surrounded by 18 photodiode detectors. The information obtained from a SEC/MALLS set-up will yield absolute molecular weight data and radius of gyration values.

The combined techniques of SEC and light scattering have had many applications especially in the field of biopolymers (for extensive reviews see: Yu and Rollings, 1987; Corona and Rollings, 1988; Stuting et al, 1989; Takagi, 1990; Jumel et al, 1992; Wyatt, 1993; Williams et al, 1992; Jackson et al, 1989) and a small selection is presented here.

The determination of absolute molecular weight distributions of guar gum by SEC/low angle laser light scattering (LALLS) was reported by Vijayendran and Bone (1984). The absolute weight average molecular weight of an extensively filtered guar sample was found to be 2.2×10^6 with a polydispersity of 1.9. The former agreed well with static light scattering experiments on the same sample. The authors point out the difficulties associated with elucidating the guar molecular weight (and distribution) namely, that due to the extensive pre-injection sample clean-up required and approximately 10% adsorption on the column packing material, the whole guar fraction could not be investigated. Lecacheux et al (1985) demonstrated the value of SEC/LALLS for the molecular

weight determination of carrageenans. They paid particular attention to experimental conditions in order to eliminate shear degradation. Molecular weight distributions were found to be highly reproducible and weight average molecular weights from SEC/LALLS compared well with those from static experiments. Large molecular weight differences between native (food-grade) and acid degraded carrageenans were found. Lecacheux et al (1986) also reported absolute weight average molecular weights for a series of extracellular microbial polysaccharides including scleroglucan, schizophyllan and xanthan, all very high molecular weight materials. Weight average molecular weights were found to range between $2x10^6$ and $5x10^6$ depending on the sample. The authors mention a polydispersity for most of these materials of close to unity. In my opinion this is quite likely due to poor resolution of the column packing material in the very high molecular weight region. Molecular weight determination of xanthan by SEC/LALLS had been reported earlier (Lambert et al, 1982) mentioning the above problem with column resolution. Weight average molecular weights of native and partially degraded xanthans were found to be $3x10^6$ and $2.2x10^5$ respectively. Apple pectin molecular weights were investigated by Kontominas and Kokini (1990) and were found to be higher than $5x10^6$ with a polydispersity of 15.4. These values were higher than those reported in the literature, but different isolation techniques were thought to be responsible for the differences in molecular weight values obtained. The major drawback with LALLS is that large aggregates will affect the scattering intensity at low angles significantly (see for example, Berth, 1992). Molecular weight values may, therefore, be high due to small amounts of large particles and as there is no way of obtaining angular dependences with LALLS, these effects cannot be investigated closely.

A systematic study of the SEC/MALLS technique assessing accuracy and precision of the instrumentation for characterizing chitosan was published by Beri et al (1993). Assessment of the instrument using dextran standards showed

low standard deviations and good agreement with manufacturers molecular weight values. Results from the chitosan samples indicated that SEC/MALLS provided reliable molecular weight distribution data for polymers in the molecular weight range 10 000 - 500 000. Information regarding the radius of gyration was found to be reliable only for molecules with molecular weights above 100 000.

The use of combined SEC and light scattering instrumentation for characterization of starches and their derivatives is widespread. Hizukuri and Takagi (1984) and Takagi and Hizukuri (1984) characterized amylose molecular weights and molecular weight distributions from various botanical sources and found significant differences between their molecular weights. Also, from comparison of molecular weight and elution volume relationships between amylose and pullulan (also a linear polysaccharide) they suggested that amylose molecules are less expanded than pullulan molecules. Hong et al (1987) monitored the enzymatic depolymerization of starch with respect to the solution conformation of the starch. Qualitative structural differences of two hydroxyethyl starches were reported by Sommermeyer et al (1992). Comparison of results from SEC/MALLS and hydrodynamic measurements showed that both materials were highly branched.

The above examples indicate that a combination of SEC and light scattering can yield valuable information, especially regarding absolute molecular weight distributions and radius of gyration. Obtaining these data by other absolute methods is usually very time-consuming and tedious.

2.2 ANALYTICAL ULTRACENTRIFUGATION

The development of the ultracentrifuge by Theodor Svedberg between 1923 and 1926 laid the foundations for macromolecular characterization as this was the first method to allow the unambiguous measurement of molecular weights and heterogeneity of macromolecules.

Analytical ultracentrifugation can be divided into two techniques: sedimentation velocity which measures the rate of movement of solute through a solution in a centrifugal field and sedimentation equilibrium where there is no net movement of the solute due to centrifugal and diffusional forces being equal as long as the rotor speed is not changed. In sedimentation equilibrium it is the concentration gradient of the solute at equilibrium which is the determining factor.

The complete theoretical background and derivations for both sedimentation ultracentrifugation techniques can be found for example in Tanford (1961), van Holde (1985), Fujita (1975), only the basic equations will be reviewed here.
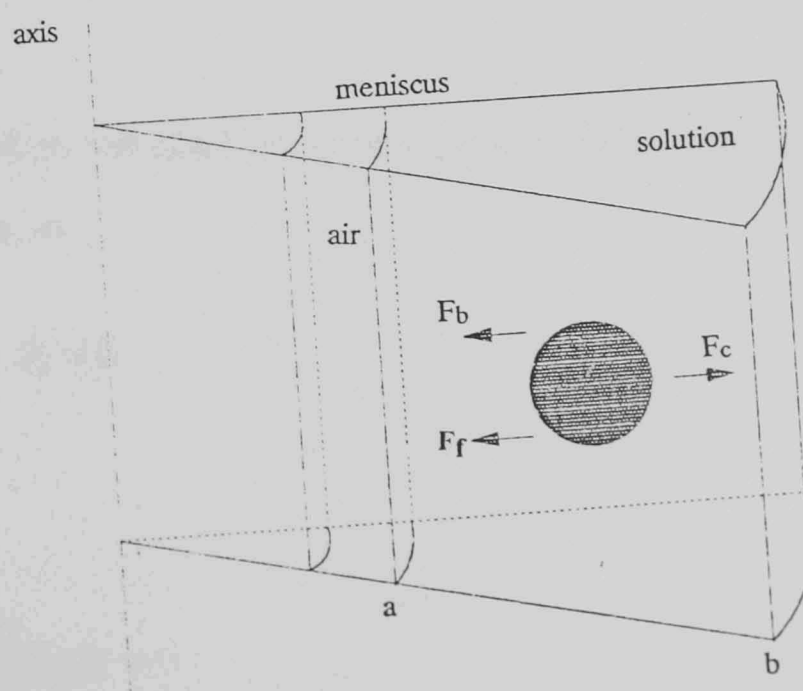
Figure 2.7: Forces acting on a solute molecule in an ultracentrifugation cell

2.2.1 Sedimentation Velocity

There are three types of forces which act on a solute molecule in a spinning rotor (see Figure 2.7). If the rotor turns with an angular velocity, ω, (radians per second) the molecule will experience a centrifugal force which is proportional to its mass (m) and the distance (r) from the centre of rotation, ie.

$$F_c = \omega^2 r m \qquad [2.20]$$

The buoyant force is equal to the force which would be exerted on the mass of solvent displaced (m_0) by the solute molecule, ie.

$$F_b = -\omega^2 r m_0 \qquad [2.21]$$

The molecule also experiences a viscous drag through the solution as the velocity (v) increases which results in the frictional force

$$F_f = -fv \qquad [2.22]$$

where f is the frictional coefficient.

This situation will result in the molecule acquiring a velocity to make the total force zero. ie.

$$F_c + F_b + F_f = 0 \qquad [2.23]$$

or,

$$\omega^2 r m (1 - \bar{v}\rho) - fv = 0 \qquad [2.24]$$

where

m = mass of particle

$\bar{v}$ = partial specific volume of particle

ρ = density of solvent

Rearranging and multiplying by Avogadro's number (N) gives

$$\frac{M(1-\bar{v}\rho)}{Nf} = \frac{v}{\omega^2\rho} = s \qquad\qquad [2.25]$$

where s is the sedimentation coefficient in units of seconds, and 1×10^{-13} is one Svedberg and denoted S

As a centrifugal field is applied to a solution, the solute molecules will start to migrate through the cell. The distribution is no longer uniform, in fact, there will be a region near the meniscus which will be completely devoid of solute molecules and a region towards the bottom of the cell where the solute concentration is uniform - the plateau region. Between this plateau region and the supernatant there is a transition region where solute concentration varies with distance from the axis of rotation. This region is called the boundary and it is the rate of movement of this boundary which is observed in sedimentation velocity experiments and allows calculation of the sedimentation coefficient through (see for example, van Holde, 1985)

$$\ln \frac{r_b(t)}{r_b(t_0)} = \omega^2 s \, (t - t_0) \qquad\qquad [2.26]$$

where $r_b(t)$ is the position of the boundary at time t. A plot of $\ln[r_b(t)/r_b(t_0)]$ versus $(t - t_0)$ will give $\omega^2 rs$ and hence s.

The above is a purely mechanical treatment of the concept of sedimentation

71

velocity. A more precise treatment can be obtained by the thermodynamic treatment described below.

The equilibrium condition for a system in a field of force is that its total potential is defined as the sum of the chemical potential and the potential energy (per mole) of the material in the field. In a centrifugal field, 1 mole of solute with molecular weight M will have a potential energy of $(-\frac{1}{2} M\omega^2 r^2)$ and the total potential, μ_t will be

$$\mu_t = \mu_c - \frac{1}{2} M\omega^2 r^2 \qquad [2.27]$$

The condition for equilibrium is

$$\frac{\delta\mu_t}{\delta r} = \frac{\delta\mu_c}{\delta r} - M\omega^2 r = 0 \qquad [2.28]$$

leading to the flow equation for the solute in a two-component mixture which after evaluating μ as a function of pressure, temperature and concentration (see van Holde, 1985) leads to

$$J = L \left[\omega^2 r M (1 - \bar{v}\rho) - \frac{RT}{c} \frac{\delta c}{\delta r} \right] \qquad [2.29]$$

The coefficient L can be expressed in terms of the frictional coefficient, f, giving $L = \frac{c}{Nf}$

and

$$J = \frac{M(1-\bar{v}\rho)}{Nf} \omega^2 r c - \frac{RT}{Nf} \frac{\delta c}{\delta r} \qquad [2.30]$$

72

This is the Lamm equation of flow (Fujita, 1975; Creeth and Pain, 1967) which includes sedimentation and diffusion coefficients, ie.

$$J = s\omega^2 rc - D\frac{\delta c}{\delta r}$$ [2.31]

The concentration dependence of s is due to interactions between the solute molecules interfering with each other and thus the frictional coefficient will increase. If

$$f = f^0 (1 + kc + ...)$$ [2.32]

and

$$f^0 = f_{c=0},$$

then

$$s = s_0(1 - kc) \text{ or, } \frac{1}{s} = \frac{1}{s_0}(1 + k_s c)$$ [2.33]

(see Creeth and Pain, 1967; van Holde, 1985) and a plot of sedimentation coefficient versus concentration will extrapolate to s_0 at the intercept and k is the concentration dependence regression factor.

As sedimentation coefficients are also temperature and solvent dependent, it is convention to quote the s value corrected to standard conditions at 20°C and water, using

$$s_{20,w} = \frac{((1 - \bar{v}\rho)_{20,w})}{((1 - \bar{v}\rho)_{T,b})} \frac{(\eta_{T,b})}{(\eta_{20,w})} s_{T,b}$$ [2.34]

where subscripts T and b refer to experimental temperature and buffer (assuming that a buffer was used as a solvent). The correction is dependent on the frictional coefficient, f, being proportional to solvent viscosity, η. The partial specific volume of the solute, $\bar{v}$, may be considered to remain constant over the experimental conditions (Cassassa and Eisenberg, 1961). After extrapolation to zero concentration and correction for temperature and solvent conditions, the sedimentation coefficient is now denoted $s^0_{20,w}$.

Values of $s^0_{20,w}$ and k_s can be used for analysis of molecular weight and conformation. Molecular weights may be obtained through the Svedberg equation

$$\frac{s^0}{D^0} = \frac{M(1-\bar{v}\rho)}{RT} \qquad [2.35]$$

where D^0 is the diffusion coefficient extrapolated to zero concentration and obtained either by sedimentation or dynamic light scattering experiments. Ordinarily, this would mean the combination of the weight average derived sedimentation coefficient and the z-average diffusion coefficient to give the weight average molecular weight. This has been done for example for galactomannans by Sharman et al (1978) and mucus glycoprotein (Sheehan and Carlstedt, 1984), however, Tanford (1961) points out that it is preferrable to obtain weight average molecular weights from light scattering or sedimentation equilibrium experiments for such polydisperse systems.

The value of k_s can be used as a guide to gross conformation via the Wales-van Holde ratio $k_s/[\eta]$. This ratio has been found empirically to give a value of ~1.6 for compact spheres and random coils and lower values for more extended conformations. Lavrenko et al (1992) discusses this ratio with particular reference to cellulose and its derivatives as well as some other polysaccharides.

Further, information regarding molecular weight and/or conformation can be obtained from the sedimentation coefficient via the Mark-Houwink-Kuhn-Sakurada (MHKS) relationship (as described in Harding, 1992) of the form

$$s^0_{20,w} = K''M^b \qquad\qquad\qquad [2.36]$$

Thus, if coefficients K'' and b are known the molecular weight can be obtained. Alternatively, the slope from a double log plot of $s^0_{20,w}$ versus M_w gives a value for b which is indicative of the gross conformation. Thus, b values of ~0.67 correspond to spheres, 0.4 - 0.5 to random coils, and ~0.15 to rigid rods (Smidsrod and Andresen, 1979). Kawahara et al (1984) investigated the hydrodynamic properties of pullulan fractions and obtained a b value of 0.445 from the MHKS plot which corresponds to a random coil conformation. Investigation on citrus pectin (Harding et al, 1991a) gave a value of 0.17±0.07 for citrus pectin which is consistent with an extended conformation. A change in the molecular weight dependence of s_0 over a molecular weight range was found for xanthan (Sato et al, 1984). At M_w below 4×10^5 the relation was linear and consistent with an essentially rigid and straight conformation. s_0 increased more dramatically with higher molecular weights which was interpreted as a result of the xanthan helix becoming semiflexible, which was also consistent with radius of gyration data for the same samples.

2.2.2 Sedimentation Equilibrium

As mentioned in section 2.2.1, the total potential of a solute in a field of force will tend towards equilibrium. If the centrifugal force is low enough, there will be a finite, and at equilibrium unchanging solute concentration gradient

throughout the cell through which the molecular weight of the solute and information regarding polydispersity and ideality of a system can be obtained (Creeth and Harding, 1982a).

When equilibrium is established in a centrifugal field, all net flow must vanish provided the ultracentrifuge continues to operate at the same angular velocity and temperature. The concentration gradient at equilibrium for a single solute component in an ideal two-component system can then be described by

$$J = L \left[\omega^2 r M (1 - \bar{v} \rho) - \frac{RT}{c} \frac{\delta c}{\delta r} \right] = 0 \qquad [2.37]$$

The partial derivative $(\frac{\delta c}{\delta r})$ can now be replaced by the total derivative since concentration is no longer a function of time but only of r and, therefore,

$$\frac{1}{c} \frac{dc}{dr} = \frac{\omega^2 M (1 - \bar{v} \rho)}{RT} \qquad [2.38]$$

Integrating between the meniscus and some point r, the dependence of c on r is found to be:

$$\ln \frac{c(r)}{c(a)} = \frac{\omega^2 M (1 - \bar{v} \rho)(r^2 - a^2)}{RT} \qquad [2.39]$$

where c(a) is the concentration at the meniscus

or, after differentiation

$$\frac{d \ln c}{d(r^2)} = \frac{\omega^2 M (1 - \bar{v} \rho)}{2RT} \qquad [2.40]$$

A plot of lnc versus r^2 should give a straight line with a slope of $\frac{\omega^2 M (1 - \bar{v} \rho)}{2RT}$

76

The concentration, c, at different points in the cell can be determined in several ways, the two most common ones are (a) an absorption optical system and (b) an interferometric optical system. The former system will give absolute concentration, however, it is only applicable to molecules which absorb in the measurable region and it also has the disadvantage of being less accurate than the interferometric optical system. The latter system will give fringe patterns (see Figure 3.5, section 3.3.2.1.1) which can be measured with great precision (Rowe et al, 1989). However, concentration data obtained from interference optics are relative to the meniscus as a function of radial displacement which considerably complicates the determination of concentration. The usual equations (see Creeth and Pain, 1967) in terms of concentration [2.41a] and corresponding fringe number concentration [2.41b] are not applicable to polysaccharides because of the difficulties in obtaining accurate initial cell loading concentrations (ie. c_0 or J_0) and cell base concentrations (c_b or j_b).

$$M^0_{w,app} = \frac{1}{k}\left[\frac{c_b - c_a}{c_0(b^2 - a^2)}\right] \qquad\qquad [2.41a]$$

$$M^0_{w,app} = \frac{1}{k}\left[\frac{J_b - J_a}{J_0(b^2 - a^2)}\right] = \frac{1}{k}\left[\frac{j_b}{J_0(b^2 - a^2)}\right] \qquad\qquad [2.41b]$$

For polydisperse systems Creeth and Harding (1982b) reported the use of the reduced point average molecular weight A^*. A^* has several properties which are as follows: A^* at the cell base = reduced weight average molecular weight over the whole cell, A^0_w. A^* at the meniscus = A_w at the meniscus. A^* at zero concentration = reduced number average molecular weight, A_n.

The latter property is particularly useful enabling the extraction of $J_{(a)}$. The formal definition of A^* and the mathematical derivation to arrive at the following equations are described in Creeth and Harding (1982b).

Since

$$\frac{j(r)}{A^*(r)} = J(a)\ (r^2 - a^2) + 2\int_a^r rj dr \qquad\qquad [2.42]$$

In the limit of the radial position being equal to the meniscus

$$\lim_{(r\to a)} \frac{j}{(r^2 - a^2)} = 2A^*(a)J(a) \qquad\qquad [2.43]$$

Therefore, a plot of

$$\frac{j}{(r^2 - a^2)} \quad \text{versus} \quad \int_a^r rj dr/(r^2 - a^2) \qquad\qquad [2.44]$$

has a limiting slope of $2A^*(a)$ and an intercept of $A^*(a)J(a)$, thus allowing determination of $J(a)$, the absolute meniscus concentration and A^*. This is simple for monodisperse, ideal systems, polydisperse and/or non-ideal systems require automatic data capture and multiple data analysis (Harding, 1992).

A^* is the reduced point average molecular weight, conversion to apparent point average molecular weight is obtained by $M^* = A^*k$ where k is the operational constant for the run, ie.,

$$k = \frac{\omega^2(1 - \bar{v}\rho)}{2RT} \qquad\qquad [2.45]$$

Thus M^* takes all the properties of A^*, one of the most important of which is M^* at the cell base $= M^0_w$, ie. apparent cell weight average molecular weight. Apparent point average molecular weights are obtained using $M_w = \frac{d\ln J}{dr^2}$ Macromolecular systems are rarely homogeneous, mostly they contain a mixture of species which differ in one or more molecular characteristics - most

frequently size. Provided that $\bar{v}$ can be assumed to be equal for all the components in the mixture, it can be shown (see eg. van Holde, 1985) that the point molecular weight average obtained from sedimentation equilibrium experiments is the weight average molecular weight, M_w.

The above expressions for molecular weight have not taken into account thermodynamic non-ideality which is particularly prevalent in polysaccharide systems, molecular weights obtained as described in the above section are therefore only apparent molecular weights. The relationship between apparent and ideal molecular weights is given by the expression

$$\frac{1}{M_{wapp}} = \frac{1}{M_w} [1 + 2BMc + \dots\dots]$$
[2.46]

where B is the colligative second virial coefficient (higher terms in the expansion can be ignored as they become negligible).

If the initial cell loading conditions, c^0, are used, the complete equation for non-ideal systems includes a speed dependence term which may be significant at high speeds and for large solution column lengths (Fujita, 1975)

$$B_{eff} = B(1 + \lambda^2 M_z^2/12)$$
[2.47]

where B_{eff} is the effective second virial coefficient and

$$\lambda = (1 - \bar{v}\rho)\omega^2(b^2 - a^2)/2RT$$
[2.48]

2.2.2.1 Applications of sedimentation equilibrium to polysaccharides and glycoproteins

Sedimentation equilibrium is a method, which compared to other techniques, is not frequently used for the characterization of polysaccharide molecular weights (Harding et al, 1991b). A possible reason for this might be the rather old-fashioned instrumentation and exaggerated run-times required (usually 24 - 48 hours). Also, as polysaccharides and glycoprotein systems are frequently not only polydisperse but also thermodynamically non-ideal, data interpretation can be quite hazardous. However, a number of examples of sedimentation equilibrium experiments for the above systems are available.

Kawahara et al (1984) used sedimentation equilibrium to determine weight average molecular weights of narrow pullulan fractions. Similarly defined fractions are now used as standards for SEC. Narrow and well defined dextran fractions are also used as calibration standards in SEC. Molecular weight values of these fractions have been obtained using sedimentation equilibrium (Edmond et al, 1968) and good agreement was found between that method and light scattering measurements. Ball et al (1990) describe the use of combined SEC/sedimentation equilibrium to obtain an absolute molecular weight distribution for an unfractionated dextran T500 and Harding et al (1991a) used the same technique to determine the absolute molecular weight of a fractionated citrus pectin. The molecular weight data agreed very well with those obtained from light scattering measurements of the same fractions. The application of the sedimentation equilibrium method for pectins is of particular value as classical light scattering as an alternative is fraught with problems of clarification for this class of compounds (see for example, Berth, 1992). Changes in pectins from tomato cell wall in the ripening process were monitored by low speed sedimentation equilibrium (Seymour and Harding, 1987).

The galactomannans locust bean gum and guar gum were investigated by

Gaisford et al (1986). The whole cell average molecular weight of the hot water soluble fraction from locust bean gum was found to be slightly lower than that of the cold water soluble fraction. Guar gum gave a whole cell weight average molecular weight of 630 000 which is lower than values obtained from light scattering studies (on different samples) (Robinson et al, 1982). The latter authors reported problems with supramolecular particles which could have moved to the cell base during the sedimentation experiment and, therefore, not have affected the final molecular weight averages.

Horton et al (1980) examined the polysaccharide components of the hydrolysed lipopolysaccharide antigens from *Pseudomonas aeruginosa* by sedimentation equilibrium. They found the molecular weights to range from 14 000 to 24 000 for the different immunotypes. Apparent weight average molecular weights of β-D-glucans from barley endosperm were determined by Woodward et al (1983) as part of a full hydrodynamic characterization of a purified and a commercial sample.

Mucin, the carbohydrate rich glycoprotein from mucus secretions, is highly heterogeneous (a) because the carbohydrate composition on the protein backbone may vary and (b) because of the variability in numbers of subunits (Harding, 1989). They are also thermodynamically non-ideal mainly due to their very high solvent association. Sedimentation equilibrium has provided a powerful means of characterizing heterogeneity of mucins with respect to polydispersity by using the technique of non-overlap of point weight average molecular weight versus concentration plots for different loading concentrations (Harding, 1984; Creeth and Cooper, 1984). Furthermore, self-association phenomena were investigated by the same workers by blocking possible interactive sites and comparing molecular weight values from experiments with and without blocking of these sites. The evidence suggested that self-association is not a major contributor to the heterogeneity of mucins.

2.3. VISCOMETRY

Viscosity is the resistance of a fluid to flow. Macromolecular solutes contribute to the viscosity of a solution depending on the volume they occupy. The theories describing viscosity were developed by Einstein (1906, 1911), they describe the viscosity of a solution containing rigid, spherical solute particles (van Holde, 1985).

2.3.1 THEORY

The mechanics of viscous flow can be envisaged by considering the situation shown in Figure 2.8. A liquid is held between two infinitely large parallel plates. One of these plates is moved in the x-direction at a constant velocity, v.
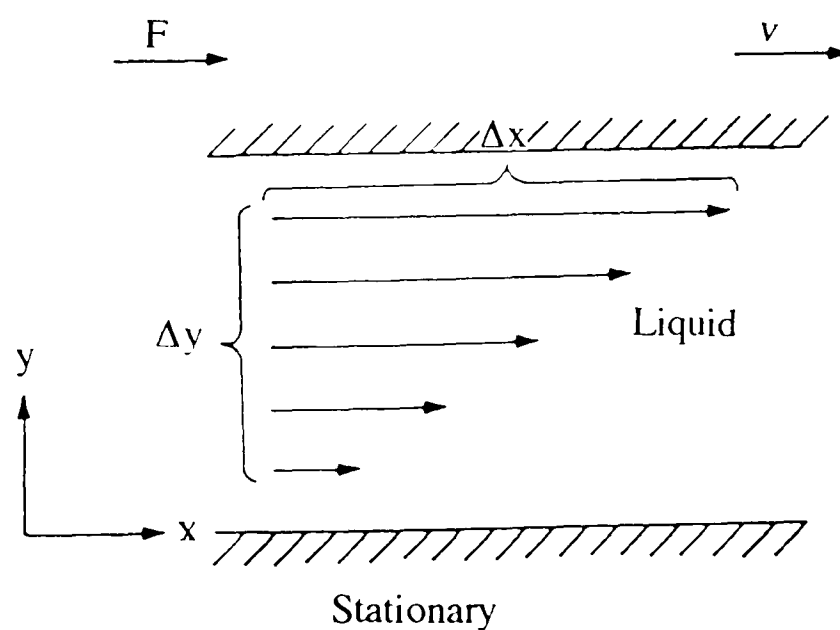
Figure 2.8: Schematic description of shearing of a Newtonian liquid between parallel plates

The two layers directly in contact with the plates will stick to the plates, causing the intervening layers of liquid to slide over each other. This treatment causes the liquid to experience a shear strain at any point defined by $\frac{dx}{dy}$ and also a shear stress (σ) which is defined as the force (F) pushing the top plate in the x direction, divided by the area (A) over which that force acts, ie. $\frac{Fdx}{A}$. The relationship between shear stress and the rate of shear strain for Newtonian liquids (ie. liquids where viscosity is independent of shear stress) is

$$\frac{F}{A} = \sigma = \eta \; \frac{d}{dt} \frac{dx}{dy} \qquad [2.49]$$

where η is the viscosity.

Viscosity can also be described in terms of the rate of energy dissipation in flow. If shear rate is defined $v/\Delta y$ and both sides of equation [2.49] are multiplied by this,

$$\frac{F}{A\Delta y} \frac{dx}{dt} = \eta \left(\frac{v}{\Delta y}\right)^2 \qquad [2.50]$$

The left hand side of equation [2.50] represents the rate of energy dissipation per unit volume of fluid $\delta E/\delta t$ which is proportional to the square of the shear rate ie.,

$$\frac{dE}{dt} = \eta \left(\frac{v}{\Delta y}\right)^2 \qquad [2.51]$$

If rigid solute particles occupying a fraction, φ, of the solution volume are introduced into the solution, the force required to maintain the shear rate is greater, because the rate of energy dissipation per unit volume is greater which is due to the same deformation having to be achieved in a smaller volume of

83

fluid. At very low volume fractions

$$\left(\frac{dE}{dt}\right)_s = \left(\frac{dE}{dt}\right)_0 (1 - \nu\phi)^{-1} = \left(\frac{dE}{dt}\right)_0 (1 + \nu\phi)$$

[2.52]

and the ratios of viscosities are therefore

$$\frac{\eta_s}{\eta_0} = 1 + \nu\phi$$

[2.53]

where ν is a numerical factor which depends on the shape of the molecule. Einstein (1906) showed that for spherical particles $\nu = \frac{5}{2}$.

In order to include solute-solute interactions, equation [2.52] has to be expanded to higher terms in concentration, therefore,

$$\eta_r = 1 + \nu\phi + \kappa\phi^2 + ...$$

[2.54]

where η_r is the relative viscosity $\frac{\eta_s}{\eta_0}$ and κ is a virial expansion coefficient.

The specific viscosity η_{sp} is a measure of the fractional change in viscosity due to the addition of solute and is defined by

$$\eta_{sp} = \eta_r - 1 = \frac{\eta_s - \eta_0}{\eta_0} = \nu\phi + \kappa\phi^2 + ...$$

[2.55]

Concentration terms are easier to work with than volume fraction concentrations and by using $\phi = \upsilon c$ where υ is the specific volume of the solute and c its concentration in g/ml.

$$\eta_{sp} = \nu\upsilon c + \kappa\upsilon^2 c^2 + ...$$

[2.56]

and

$$\frac{\eta_{sp}}{c} = v\upsilon + \kappa\upsilon c + \ldots$$ [2.57]

and under the limiting conditions of c approaching zero

$$[\eta] = \left(\frac{\eta_{sp}}{c}\right)_{c\to0} = v\upsilon$$ [2.58]

where $[\eta]$ is the intrinsic viscosity which now describes the property of an isolated macromolecule as interaction effects have been eliminated by extrapolation. The expressions for these extrapolations were defined by Huggins (1942)

$$\frac{\eta_{sp}}{c} = [\eta] + k_H[\eta]^2 c$$ [2.59]

and Kraemer (1938)

$$\frac{\ln(\eta_{rel})}{c} = [\eta] + k_K[\eta]^2 c$$ [2.60]

where k_H and k_K are the Huggins and Kraemer constants respectively. The intercepts of the extrapolations will give the intrinsic viscosity. Frequently both extrapolations are plotted on the same graph - the intercepts should meet at the same point on the y-axis.

Equation [2.58] demonstrates that the intrinsic viscosity depends on the shape (through v) and the specific volume of the macromolecule. However, the specific volume has to include the fact that macromolecules are hydrated. It is possible to use information from a combination of intrinsic viscosity, frictional

85

coefficient and other coefficients to make an educated guess as to the shape and hydration of a macromolecule (see for example Sheraga and Mandelkern equation for prolate and oblate ellipsoids as described in van Holde, 1985).

Random coils occupy very much greater volumes than do compact structures such as spheres and an expression for $[\eta]$ can be obtained by assuming that the effective radius of the polymer coil is of the same order of magnitude as its radius of gyration, R_G.

If equation [2.58] is rewritten on a volume per mole basis it becomes

$$[\eta] = vN\frac{\upsilon_m}{M} \qquad [2.61]$$

where υ_m is the volume of one molecule and M the molecular weight.

If $\upsilon_m = K''R_G{}^3$

$$[\eta] = K'\frac{R_G{}^3}{M} \qquad [2.62]$$

For a series of different molecular weight samples of a given polymer, R_G will be a function of chain length and therefore molecular weight. If the polymer is dissolved in a θ-solvent, the radius of gyration is proportional to the square root of the molecular weight (Tanford, 1961) and

$$[\eta] = KM^{1/2} \qquad [2.63]$$

If the polymer is dissolved in a solvent better than a θ-solvent,

$$[\eta] = KM^a \qquad [2.64]$$

K and a are determined by measuring intrinsic viscosities of a series of polymer

samples with different molecular weights and plotting $\log[\eta]$ versus $\log M$.

Once these constants are known for a particular solute-solvent system, the

molecular weight of an identical solute of unknown molecular weight may be

determined (in that solvent). It must be noted that for compact particles there is

no dependence of $[\eta]$ on molecular weight.

2.3.2 VISCOSITY MEASUREMENTS

2.3.2.1 Intrinsic Viscosity

Viscosity measurements have to be of very high precision as the relative

viscosities may sometimes be very small. Capillary viscometers can provide

very accurate comparison of solution and solvent viscosities.

The most common type of capillary viscometer is the Ostwald viscometer

shown in Figure 2.9. It enables measurement of the time required for a given

volume of liquid, V, to flow through the capillary. The volume rate of flow of a

liquid through a capillary of radius, a, and length, l, when driven by a pressure,

p, is given by Poiseuilles's law

$$\frac{dV}{dt} = \frac{\pi a^4 p}{8\eta l}$$

[2.65]

The liquid is driven by the hydrostatic pressure head $p = hg\rho$ (g is the

gravitational constant) where the height, h, is subject to slight variations

between limits h_1 and h_2 as the bulb empties. Integration of equation [2.65]

yields the following expression for the flow time
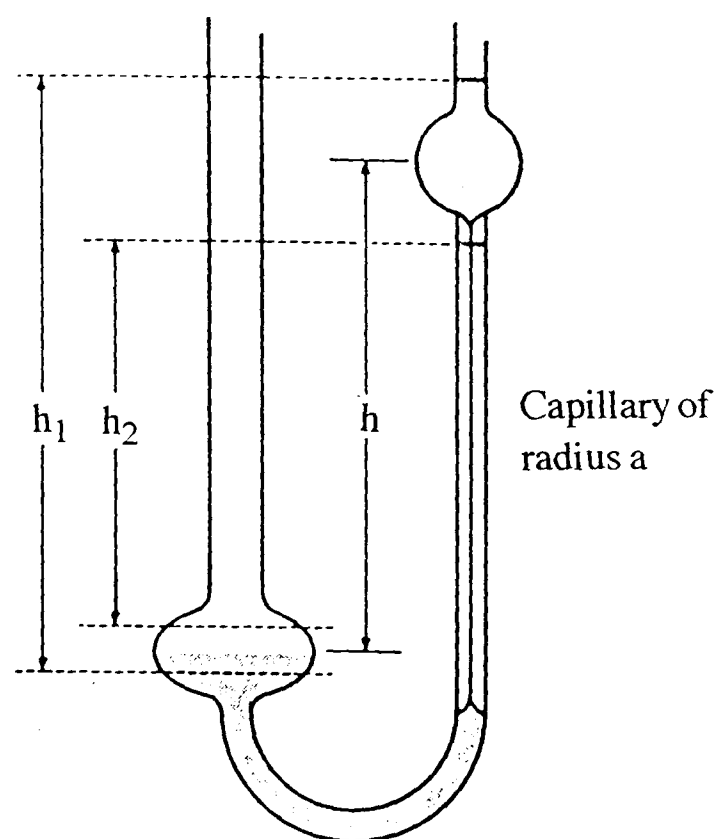
Figure 2.9: The Ostwald Viscometer

$$t = \frac{\eta}{\rho} \left(\frac{8l}{\pi g a^4} \int_{h_1}^{h_2} \frac{dV}{h} \right) \qquad [2.66]$$

The factors in parentheses can be regarded as instrument constants. The expression

$$\frac{t_s}{t_0} = \frac{\eta_s}{\eta_0} \frac{\rho_s}{\rho_0} \qquad [2.67]$$

can be used for the measurement of relative viscosity (subscript zeros refer to solvent properties). If the density ratio is known, the ratio of flow times are used to calculate the relative viscosity. Provided that there is good temperature control, the relative viscosity can be measured very precisely.

2.3.2.2 Concentrated Solution Viscosity

Capillary viscometers may be able to measure relative viscosities very accurately, however, in such viscometers the shear rate varies throughout the liquid. This is an important limitation for non-Newtonian liquids where viscosities are shear-rate dependent.

There are a variety of viscometers available for the measurement of shear-rate dependence. Many of these viscometers rely on rotational motion to achieve a simple shearing flow. Flow can be induced by either driving one member and measuring the resulting couple or by applying the couple and measuring the rotation rate. A schematic diagram of a cone-and-plate viscometer is shown in Figure 2.10.
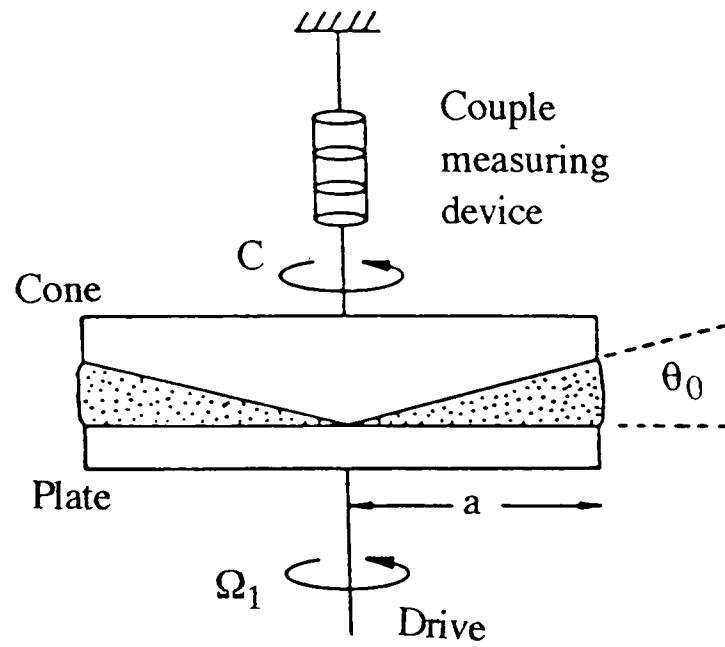
Figure 2.10: Schematic diagram of a cone-and-plate viscometer

Provided that the gap angle θ_0 is small, the shear rate is very nearly uniform in the entire liquid and is given by

$$\dot{\gamma} = \frac{\Omega_1}{\theta_0} \qquad [2.68]$$

where Ω_1 is the angular velocity of the rotating platten.

The shear stress is given by

$$\sigma = \frac{3c}{2\pi a^3} \qquad [2.69]$$

where a is the radius of the cone and c is the torque experienced by the cone or plate. The viscosity is therefore given by

$$\eta = \frac{3c\theta_0}{2\pi a^3 \Omega_1}$$

[2.70]

In order to fit the shape of the general flow curve for polymer solutions, at least four parameters are needed. The Cross equation (Cross, 1965) is one of the most useful semi-empirical relations. It is given by

$$\frac{\eta - \eta_\infty}{\eta_0 - \eta_\infty} = \frac{1}{(1 + (K\dot{\gamma}^m))} \quad \text{or} \quad \frac{\eta_0 - \eta}{\eta - \eta_\infty} = (K\dot{\gamma})^m$$

[2.71]

where η_0 and η_∞ refer to the asymptotic values of viscosity at very low and very high shear rates respectively. K is a constant with dimension of time and m is a dimensionless constant.

In order to demonstrate the use of zero shear viscosity (η_0) measurements in conjunction with intrinsic viscosity measurements as an indicator of coil overlap and specific junction formation of polysaccharides with random coil conformation, the study by Morris et al (1981) is described below. These authors studied the flow behaviour of a variety of polysaccharides. The concentration dependence of the zero shear specific viscosity ($\eta_{sp,0}$) showed a distinct increase in gradient above a certain 'critical' concentration, c^*. c^* is defined as the onset of significant coil overlap of polymer molecules in a solution. A schematic description of the transition from isolated coils in dilute solutions to a situation where the hydrodynamic volume of the chains exceeds the solution volume is shown in Figure 2.11 and plots of $\log\eta_{sp,0}$ versus $\log c$ for four polymers are shown in Figure 2.12.
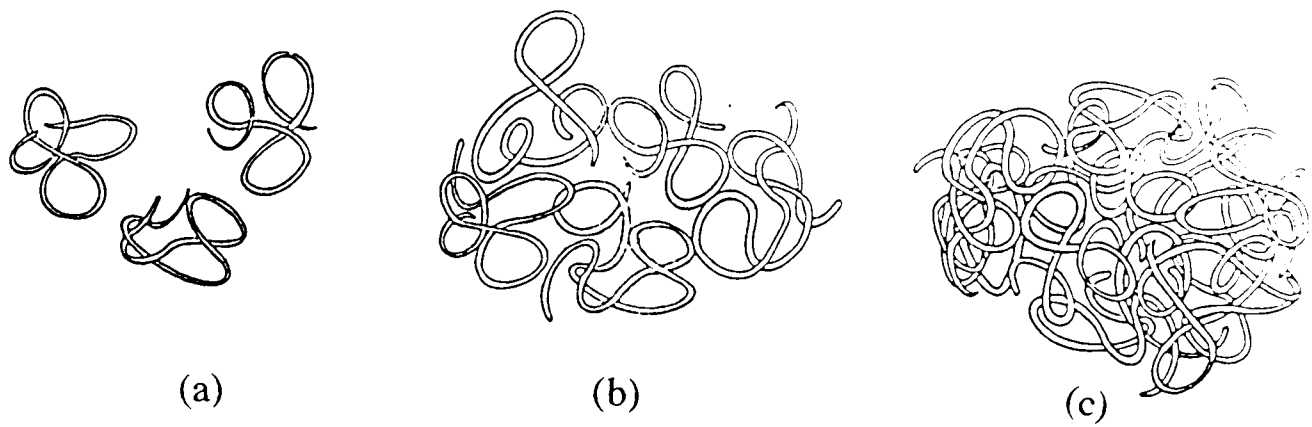
Figure 2.11: Schematic description of transition from isolated macromolecules, ie., c<c* (a), via incipient overlap of molecules, where c ≈ c* (b), to uniform overlapping of polymer segments c>c* (c) (from Robinson et al, 1982).
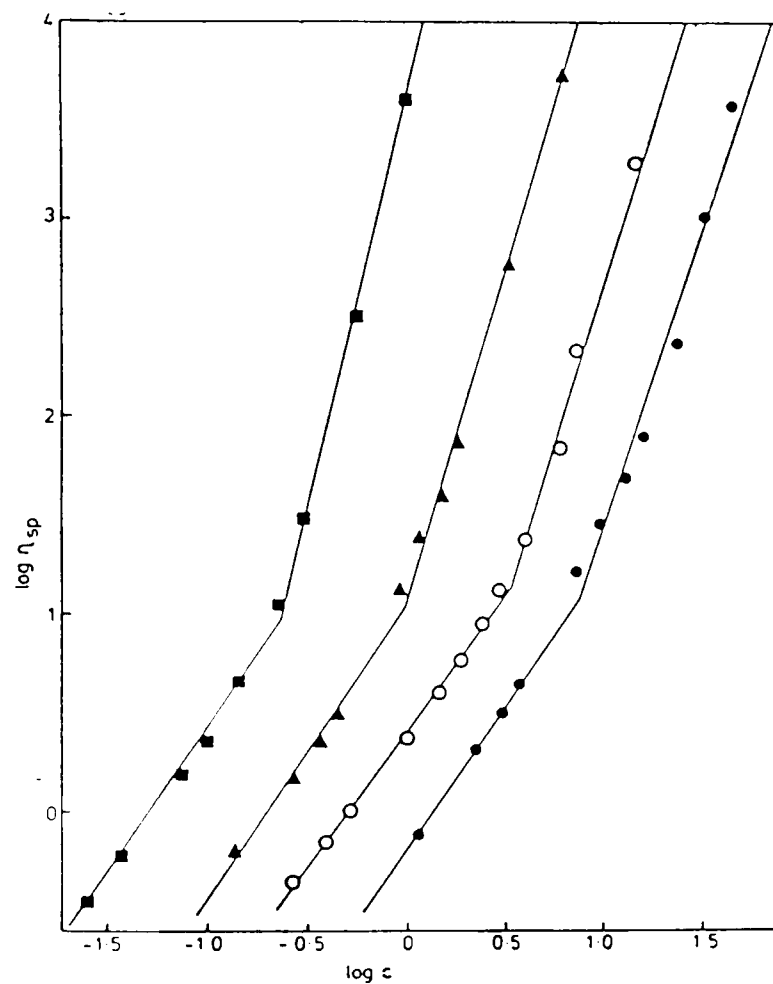
Figure 2.12: Double log plot of $\eta_{sp,0}$ versus concentration for (■) guar gum, (▲) alginate, (●) dextran and (○) polystyrene in toluene (from Morris et al, 1981)

As intrinsic viscosity is a measure of polymer dimension through R_G and M via the Fox-Flory relationship (Flory, 1953)

$$[\eta] = \Phi 6^{3/2} R_G^3 / M \qquad\qquad [2.72]$$

where Φ is a constant, the space occupied by the polymer can be described by the 'coil overlap parameter' $c[\eta]$. A plot of $\log \eta_{sp}$ versus $c[\eta]$ showed that except for the galactomannans and hyaluronte at low pH and high ionic strength, the c* transition occurs at the same value (ie., $c[\eta] \approx 4$) and $\eta_{sp,0}$ at this transition was found to be close to 10. The galactomannans and hyaluronate systems displayed the onset of concentrated solution behaviour at $c[\eta] \approx 2.5$. This behaviour was attributed to the possibility of the formation of specific junction zones between molecules in addition to the physical overlap of coils.

2.4 COMBINATION OF HYDRODYNAMIC MEASUREMENTS

The above methods have been discussed mainly in isolation, however, a combination of results from the various methods provides a powerful means of (a) defining the hydrodynamic behaviour of molecules and (b) verification of individual results from one method by a second method (eg. absolute molecular weight values from light scattering and sedimentation equilibrium). Measurements of molecular weights and their combination with sedimentation velocity and/or viscosity and diffusion data results in information regarding the conformation of molecules, ie., whether they behave like spheres, flexible coils or rods via Mark-Houwink-Kuhn-Sakurada (MHKS) double logarithmic plots of sedimentation coefficient, intrinsic viscosity or radius of gyration versus molecular weight and through the Wales-van Holde parameter of sedimentation regression coefficient (k_s) versus intrinsic viscosities. A few examples describing comprehensive characterization of polysaccharides and glycoproteins are given below.

Sheehan and Carlstedt (1984) describe the characterization of human cervical-mucin by light scattering (classical and quasi-elastic), sedimentation velocity, and rotary viscometry. Molecular weight determination of the whole mucin, subunits and tryptic digests resulted in values of $10 - 15x10^6$, $2x10^6$ and $0.4x10^6$ respectively, which was very much in keeping with expectations. Stokes radius from diffusion coefficient and radius of gyration from classical light scattering were also in good agreement when the concept of the equivalent hydrodynamic sphere was used. The Wales-van Holde ratio was found to be 1.42, an indication that mucin occupies a spheroidal domain in solution. MHKS relationships of intrinsic viscosity, sedimentation coefficient and diffusion coefficient with molecular weight were consistent with the model of linear

flexible macromolecules.

The conformation of amylose in dimethylsulfoxide (DMSO) has been investigated using a combination of methods (Fujii et al, 1973). In contrast to the Gaussian random coil chain conformation of amylose in aqueous electrolyte solution, the molecule was found to adopt a predominantly helical conformation in DMSO. Amylopectin in aqueous solution was similarly investigated (Banks et al, 1972). Molecular weight measurements confirmed the large size of the molecule. Comparison of hydrodynamic behaviour between the closely related glycogen and amylopectin revealed differences which were attributed to the more 'flexible, coil-like nature of amylopectin'. Variation in solvent conditions showed that under certain conditions a helix to coil transition can be observed. Kawahara et al (1984) describe a full hydrodynamic study on various pullulan fractions. These samples were found to be stable in solution, their hydrodynamic behaviour was that of expanded random coils at molecular weights above 20 000. The conformation and molecular weight distribution of a citrus pectin was studied by Harding et al (1991a). Molecular weights of chromatographically separated fractions were obtained by low speed sedimentation equilibrium ultracentrifugation and sedimentation velocity and intrinsic viscosity data were related to the molecular weights via the MHKS equations. The coefficients obtained were consistent with a rigid rod-like model. The Wales-van Holde parameter ($k_s/[\eta]$) for all the fractions was found to be consistent with an extended conformation. Comparison of the experimental data with those obtained from theoretical predictions using rod-like and worm-like coil models led to the conclusion that, within the range of molecular weights investigated and under the experimental conditions used, citrus pectin exhibits rod-like characteristics.

The final example for a full hydrodynamic investigation of a polysaccharide is that of xanthan (Sato et al, 1984). 12 different xanthan samples were used and plots of sedimentation coefficients, radii of gyration and intrinsic viscosities as

functions of molecular weight indicated a double helix conformation for xanthan in 0.1M NaCl. Analysis of the data in terms of rigid rod and worm-like chain models confirmed that the double helical structure of xanthan in NaCl is essentially identical to that in the crystalline state.

CHAPTER 3

MATERIALS AND METHODS

3.1 SAMPLES

3.1.1 Irradiated Guar Gum

Irradiated guar gum samples were a gift from Dr.Karen King of Queen's University of Belfast. The original guar gum had been obtained from Sigma Chemical Co. (G-4129; Lot No 77F-0639). The samples were irradiated by the following method: powdered gum samples (~10 g) were sealed in glass vials (5.0x2.5cm) and subjected to given doses ranging from 0.1 to 10kGy using a Cobalt 60 source (Gamma-beam 650, Nordion International Inc., Kanata, Ontario, Canada). The dose rate was 1.38kGyh^{-1} and the ambient temperature was kept between 16 and 18°C during irradiation. Gammachrome YR dosimeters (UK Atomic Energy Authority, Harwell, UK) were attached to vials receiving 0.1-3kGy and amber perspex dosimeters (type 3042 B, UK Atomic Energy Authority) were attached to all other samples. The intended and actual irradiation doses are shown in Table 3.1. Samples were stored in sealed vials at room temperature until further use.

Table 3.1: Intended and actual irradiation doses for Guar Gum and standard deviation for 3 replicates

Intended Dose (kGy)	Actual Dose (kGy)	Standard deviation from 3 replicates
0.1	0.113	0.003
0.2	0.204	0.014
0.4	0.373	0.019
0.6	0.498	0.018
0.8	0.649	0.017
1.0	0.860	0.027
2.0	1.700	0.073
5.0	5.072	0.250
10.0	9.071	0.651

Samples were routinely dissolved by adding an accurately weighed portion of the gum into the vortex of magnetically stirred aqueous phosphate/chloride buffer (ionic strength 0.1, pH 6.8; Green, 1933) to give a final concentration of approx. 3mg/ml, and stirred for one hour. The samples were then left to hydrate overnight in a refrigerator and stirred for a further one hour period the following morning.

The insoluble fraction was removed by centrifugation (4000rpm, 2500g, 20 minutes) using an MSE Multex (Measuring and Scientific Equipment Ltd., Crawley, UK) bench top centrifuge. Supernatants were carefully decanted into sample vials, further pre-analysis treatment depending on the analytical method used.

For measurements of intrinsic viscosities samples were dissolved in double-distilled water with magnetic stirring for 2 hours and then centrifuged as above.

Concentrated (ie. 1% w/v) guar gum solutions were prepared by adding the powder to the vortex of double-distilled water which was stirred by a high speed paddle mixer and then stirring for a further two hours.

3.1.2 Protein/Polysaccharide Composites

Protein/polysaccharide composites were a gift from Prof. E. Dickinson at the University of Leeds. Mixtures of protein and polysaccharide in the required proportions were dissolved in double-distilled water, freeze dried and then stored at 60°C and 40% relative humidity for three weeks unless otherwise stated.

The following dry heated protein/polysaccharide composites were investigated during this work:

• Bovine Serum Albumin/Dextran T40 molar ratio 1: 5, 1:3.4, 1:3, 1:1.7,

1:0.85, 1:0.5

• BSA/Dextran T500 fraction, molar ratio 1:3, 1:0.33

The following materials were investigated as controls:

• BSA native, BSA dry-heated for one, two, or three weeks

• Dextran T40 fraction native, Dextran T40 dry-heated for one, two or three

weeks

• Dextran T500 native

• BSA/Dextran T40 dry heated for two or three weeks

• Mixture of BSA and Dextran T40, molar ratio 1:5

Samples were dissolved in phosphate/chloride buffer at an ionic strength = 0.1 and pH 6.8 (Green, 1933) immediately prior to experimental measurements. Samples used for molecular weight determination by SEC/MALLS were filtered through 0.45µm membrane filters (Millex-HV, Millipore, Watford, UK). For molecular weight determination by sedimentation equilibrium samples were dialysed against pure buffer over night.

3.1.3 Starch Samples

Unmodified wheat and potato starches were purchased from the Sigma Chemical Co. (St. Louis, USA). Waxy rice and cassava starches were obtained from Cairn Foods (Chesham, UK) and Ajinomoto, Malaysia, respectively. Starch samples were debranched by a modified method described by Hizukuri (1985).

An accurately weighed portion (approx. 75mg) was dispersed in 3.71 ml of double-distilled water and heated at 100°C for 6 minutes. After the mixture had cooled to 45°C, 0.25ml of 1M acetate buffer at pH 3.5 and 55µl isoamylase (equivalent to 3245 U) were added and the mixture was incubated at 45°C for 2.5 hours. 1ml of 0.5M sodium phosphate buffer containing 0.1% sodium azide was added and the solution heated at 100°C for 3 minutes.The hot solution was centrifuged at 2000rpm (630g) for 20 minutes using a Multex bench top centrifuge and the supernatant was immediately injected into the SEC/MALLS system.

3.1.4 MUCIN SAMPLES

3.1.4.1 Pig Gastric Mucin

Fresh pig gastric mucus glycoprotein (PGM) was purified by Mr. I. Fiebrig by the following method: fresh PGM from fresh solubilised pig gastric mucus was purified by preparative caesium chloride isopycnic density gradient ultracentrifugation in an enzyme inhibitor cocktail according to a modified procedure by Hutton et al (1990). This was followed by size exclusion chromatography of the glycoprotein fraction on a Sepharose CL-2B column. The totally excluded volume fractions were pooled and concentrated by ultrafiltration, dialysed against distilled water and 1ml aliquots were kept frozen at -20°C or freeze-dried. The mucin preparation was gently defrosted and dialysed into the buffer or redissolved in buffer before use. Purity of the mucin preparation was checked by analytical isopycnic density gradient ultracentrifugation by the procedures of Creeth et al (1977). Samples are identified by the code given in Table 3.2. Samples were diluted in a phosphate/chloride buffer (ionic strength = 0.1, pH 6.8) containing 0.04% diaminotetraacetic acid- disodium salt (Na_2EDTA) and 0.01% sodium azide and filtered through 0.45μm filter membranes (Millex HV-type, Millipore, Watford, UK) prior to injection into the SEC/MALLS system.

101

Table 3.2: Sample description and sample codes for mucin preparations

Sample Code	Sample
	Pig gastric mucin
PGM 1	Sigma Cat. No. M1778, partially purified from porcine stomach
PGM 2	Sigma Cat. No. M1778, subjected to ultrafiltration prior to analysis
PGM 3	Partially pepsin digested mucin from Orthana Kemisk Fabrik, Denmark
PGM 4A	Freshly prepared pig gastric mucin, as descibed above, Batch 1
PGM 4B	As for PGM 4A but further purified by preparative SEC on Sepharose 2B column
PGM 4C	As for PGM 4B but additional Caesium chloride density gradient ultracentrifugation
PGM 5B1	As for PGM 4B, Batch 2
PGM 5B2	As for PGM 5B1 but SEC was carried out several weeks later
	Pig colonic mucin
PCM A1	Pig colonic mucin purified as described by Hutton et al (1990)
PCM A2	As for PCM A1
PCM A3	As for PCM A1
PCM P1	As for PCM A1 but then papain digested
PCM P2	As for PCM P1
PCM R1	As for PCM A1 but then reduced using β-mercaptoethanol
PCM R2	As for PCM R1

3.1.4.2 Pig Colonic Mucin

Fresh pig colonic mucus glycoprotein was prepared by Ms F. Fogg at the University of Newcastle from fresh pig colonic mucus according to the method of Hutton et al (1990). Portions of the fresh pig colonic mucin were subjected to papain digestion or β-mercaptoethanol reduction as described by Hutton et al (1990). Samples are identified by the code given in Table 3.2. Samples were diluted and filtered as described in Section 3.1.4.1 prior to injection into the SEC/MALLS system.

3.1.5 Xanthan

Three xanthan samples of different grades were gifts from Kelco International Ltd. (London, UK) and are identified as follows:

• Keltrol RD (readily dispersable)

• Keltrol BT (brine tolerant)

• Keltrol FG (food grade)

Samples were dissolved by adding the accurately weighed material into the vortex of magnetically stirred double-distilled water (final concentration 1mg/ml). Solutions were then left to stir overnight. The solutions were dialysed overnight into a phosphate/chloride buffer of ionic strength 0.3 and pH 7.0 (Green, 1933). Prior to injection into the SEC/MALLS system, the samples were centrifuged on a bench top centrifuge for 10 minutes at 13 000rpm, and filtered through 0.45μm filter membranes (Millex HV-type, 4mm, Millipore, Watford, UK) to remove any particulate matter.

3.2 CHEMICALS

- Blue dextran was purchased from the Sigma Chemical Co. (St. Louis, USA) (average $M_w \sim 2\,000\,000$).

- Dextran T500 ($M_w \sim 500\,000$, Edmond et al, 1968) was obtained from Pharmacia, (Uppsala, Sweden).

All other chemicals were obtained from Fisons plc (Loughborough, UK) and were of Analytical Grade or higher purity.

3.3 METHODS

3.3.1 SIZE EXCLUSION CHROMATOGRAPHY/MULTI ANGLE LASER LIGHT SCATTERING (SEC/MALLS)

A photo of the SEC/MALLS system used for some of the experimental work is shown in Figure 3.1. It is similar to the set-up described in Wyatt (1993). The eluent is drawn through a 0.45μm in-line filter in order to remove any particulate matter, and through a degasser (Degasys, DG-1200, uniflow, HPLC Technology, Macclesfield, UK). Degassing of solvents is important for several reasons: air dissolved in the solvent may separate due to pressure or temperature changes - deaeration occurring in the pump would cause fluctuations in flow and therefore unstable baselines. Air bubbles entering the column packing matrix could cause voids thus damaging the column. Small air bubbles entering the light scattering detector would cause spikes in the light scattering traces and air in the differential refractive index detector would cause baseline fluctuations.

The eluent was pumped through the system by a high performance pump
(Model 590 Programmable Solvent Delivery Module, Waters, Millipore,
Watford, UK) at a flow rate of 0.8ml/min for all samples except starches and
xanthans which were run at flow rates of 0.5ml/min.

Centrifuged guar gum samples were filtered consecutively through 0.45μm
(Millex-HV type, 25mm, Millipore) 0.45μm (Millex-HV type, 4mm,
Millipore), and 0.25μm (Millex-GV, 13mm, Millipore) membrane filters prior
to injection via a Rheodyne Model 7125 injection valve (Rheodyne, Inc.,
Cotati, CA, USA) fitted with a 100μl injection loop.
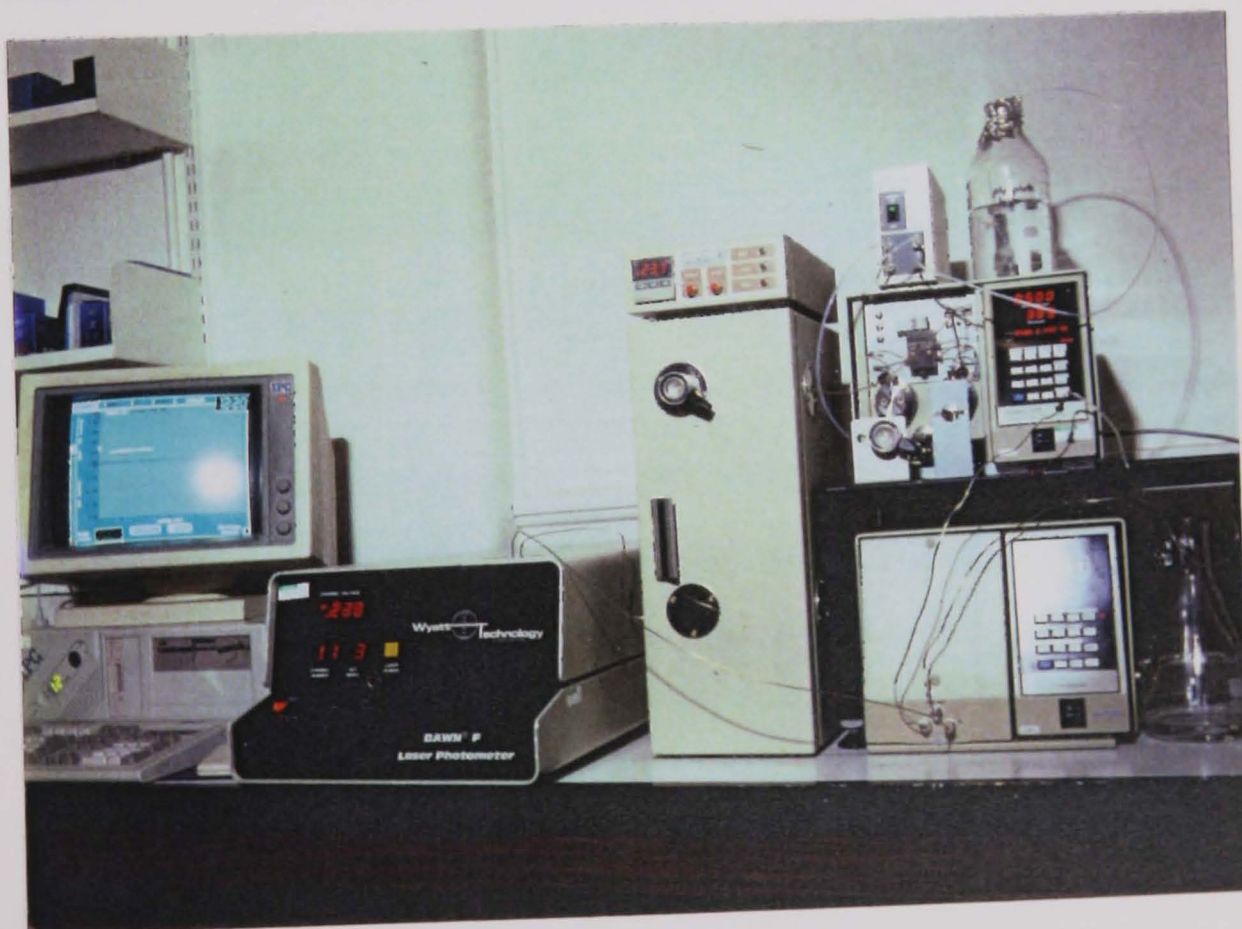
Figure 3.1: The SEC/MALLS system

3.3.1.1 Column Systems

Column system 1:

This consisted of one Ultrahydrogel linear column (Waters, Millipore, Watford, UK) with dimensions 300x7.8mm, having an exclusion limit of 7×10^6 for polyethylene oxide, and a PSS Hema Bio 40 column (Polymer Standards Services GmbH (PSS), Mainz, Germany) having an exclusion limit of 40 000 for dextrans. The packing material of the Ultrahydrogel column consisted of hydroxylated polymethylmethacrylate and that of the PSS column consisted of a co-polymer of hydroxyethylmethacrylate cross-linked with ethyleneglycol dimethacrylate and modified with polar groups to improve the resolution of hydrophilic biopolymers. The analytical columns were connected in the following order: Ultahydrogel -> PSS Hema Bio 40 and protected by a guard column (Ultrahydrogel Guard Column). Void volume and total permeation volume of the column system were found to be 7.9ml and 18.8ml respectively.

Column system 2:

This system consisted of one PSS Hema Bio Linear and one PSS Hema Bio 40 column (both columns were obtained from Polymer Standards Service GmbH, Mainz, Germany). Column dimensions were 300x7.5mm, with the first column (PSS Hema Bio Linear) having an exclusion limit for dextrans of 7×10^6 and the second column (PSS Hema Bio 40) an exclusion limit for dextrans of 40 000. The macroporous gel matrix of both columns consisted of a co-polymer of hydroxyethylmethacrylate cross-linked with ethyleneglycoldimethacrylate and modified with polar groups to improve the resolution of hydrophilic bio-polymers. The analytical columns were connected in the following order: PSS Hema linear -> PSS Hema Bio 40 and protected by a guard column (Ultrahydrogel Guard Column). Void volume and total permeation volume of the column system were found to be 9.2ml and 21.4ml respectively.

Column system 3:

This column system was exclusively used for the starch samples and consisted of a guard column (TSK Gel PWXL: 40mmx6mm) and 5 analytical columns (TSK Gel G3000PWXL, Asahipak GS-320H (x2), TSK Gel G2500PWXL and TSK G-Oligo PWXL) connected in that order and kept at a temperature of 40°C in a column oven (Anachem Ltd., Luton UK). TSK columns with dimensions 300mmx7.5mm were purchased from Anachem Ltd., Luton UK, and Asahipak columns with dimensions 250mmx7.5mm were purchased from Rhône-Poulenc, Manchester, UK. Void volume and total permeation volume of the column system were found to be 23.8ml and 48.0ml respectively. Column effluent was monitored using a Dawn F laser light scattering photometer (Wyatt Technology, Santa Barbara, USA) and a differential refractive index detector (Model 410, Water, Millipore, Watford, UK). The theory of combined SEC/light scattering has been reviewed in Section 2.1. Figure 3.2 shows a diagram of the read head of the Dawn F laser light scattering photometer. This is where the sample cell (see Figure 3.3) is held precisely, the scattered light is collimated and the detectors are aligned and held in place. The read head structure holds the 19 hybrid transimpedence photodiodes. This structure is designed to minimize any stray light effects - each detector's field of view is limited by its own collimator, thus only the centre of the illuminated sample scatters light into the detector.

The signal from 15 of these detectors is collected simultaneously, digitised, and analysed by an IPC 286XS IBM-compatible PC using ASTRA and EASI software (Wyatt Technology, Santa Barbara, USA)™

The differential refractive index detector is a concentration detector and operates according to Snell's law which defines the relationship between the angle of incidence and the angle of refraction as a beam of light passes from one medium to another.
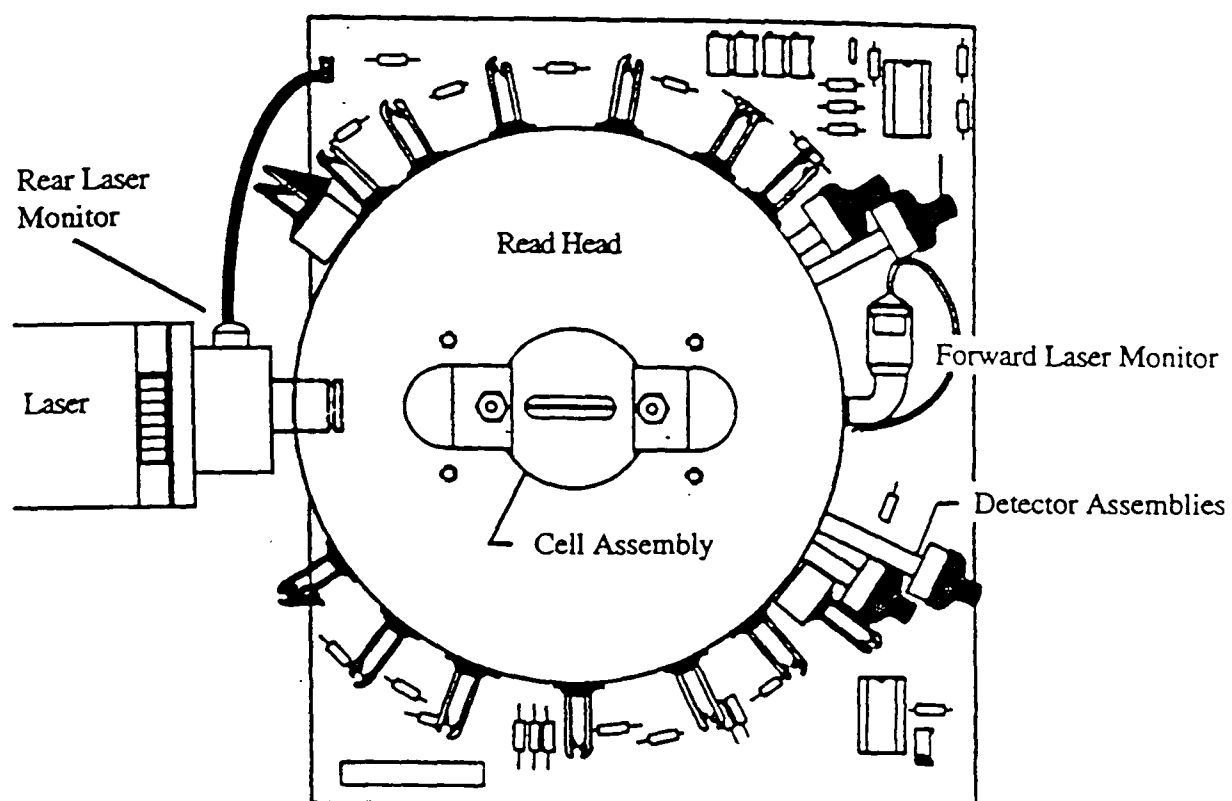
Figure 3.2: Top view of the read head of the Dawn F laser light scattering photometer (Reproduced from Dawn F instruction manual)
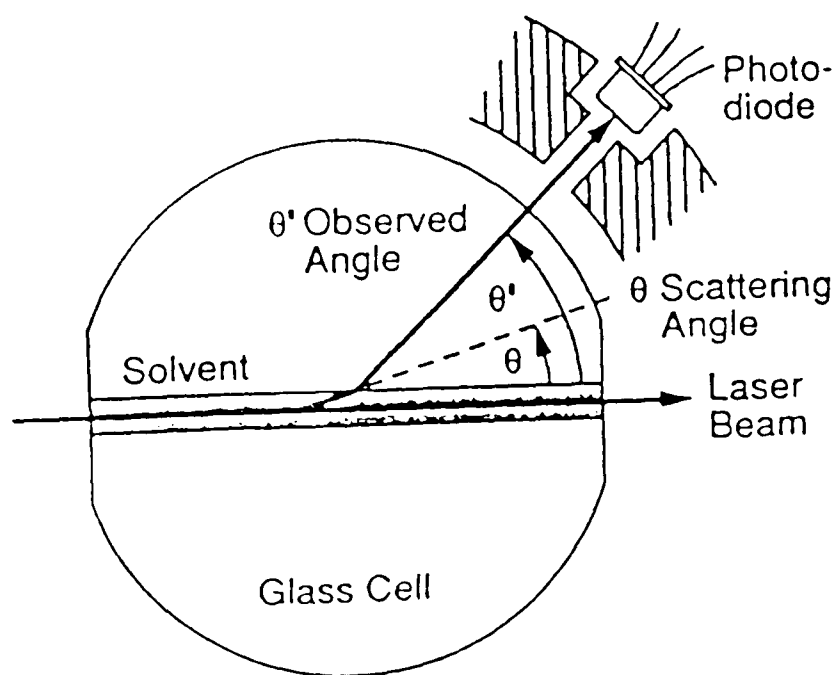
Figure 3.3: Schematic representation of the sample cell of the Dawn F laser light scattering photometer, showing refraction of scattered light within cell (Reproduced from Wyatt, 1993)

3.3.2 ANALYTICAL ULTRACENTRIFUGATION

3.3.2.1 Sedimentation Equilibrium Experiments Using the Beckman Model E Analytical Ultracentrifuge

All sedimentation equilibrium runs carried out were low speed sedimentation equilibrium runs. The analytical ultracentrifuge used was a Model E (Beckman Instruments Inc., Palo Alto, California) fitted with a Rayleigh Interference optical system (see Figure 3.4) and a Rotor Temperature Indicator and Control (RTIC) device . The light source used was either a 5mW Helium-Neon laser of wavelength 632.8nm or a Mercury arc light source with a green filter. Interference fringes (as shown in Figure 3.5) were recorded on photographic film (Kodak technical pan film) and scanned on an Ultroscan XL Enhanced Laser Densitometer (LKB, Bromme, Sweden). Fringe shifts were obtained using the ANALYSER Software and raw data were transferred via the JANET link to the IBM-3081 mainframe computer at Cambridge where fringe shift data were further analysed.

Sample cells (30mm double sector, Kel-F centrepiece, or 30mm multichannel as shown in Harding, 1989) were assembled as shown (Figure 3.6) and tightened with a torque wrench to $120lb/inch^2$. Both types of cell were loaded with 250μl solution (after dialysis against pure buffer over night) and 260μl dialysis buffer in sample and solvent channels respectively.

Typically, experiments were performed at 20°C, with rotor speeds ranging between 2000 and 5600rpm depending on the estimated molecular weight of the sample.

For investigations concerning speed and concentration dependence the 0.6kGy dose irradiated guar gum sample was run at speeds of 2000, 3000, 4000, and 5200rpm and at concentrations of 0.4, 0.6, 0.8, and 1.0mg/ml.
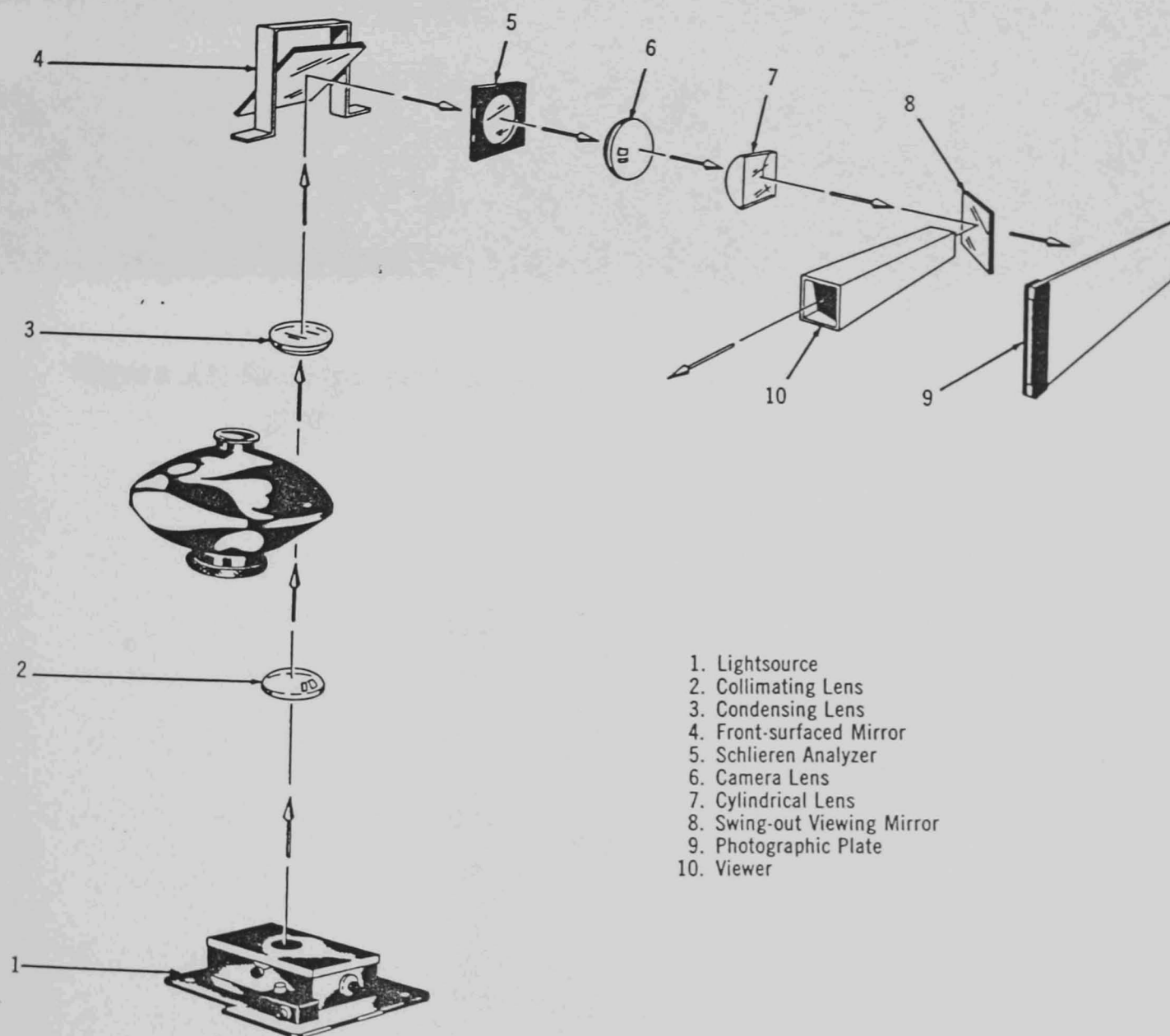
Figure 3.4: Schematic representation of Rayleigh interference optics in the Beckman Model E analytical ultracentrifuge. (Reproduced from Beckman Model E manual)

1. Lightsource
2. Collimating Lens
3. Condensing Lens
4. Front-surfaced Mirror
5. Schlieren Analyzer
6. Camera Lens
7. Cylindrical Lens
8. Swing-out Viewing Mirror
9. Photographic Plate
10. Viewer
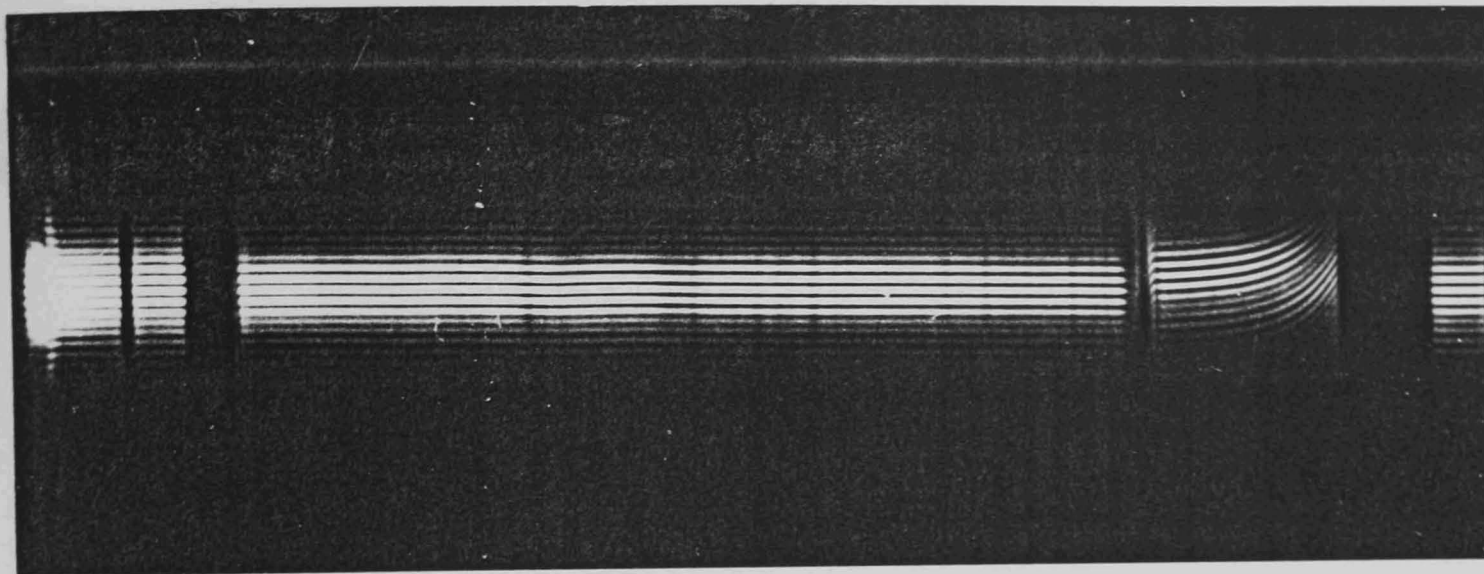
Figure 3.5: Rayleigh interference fringes (Sample: Irradiated (10.0kGy) guar gum)

Screw Ring
Screw Ring Gasket
Upper Window Holder
Window Gasket
Window Liner
Window
Centerpiece Gasket
Aluminum Centerpiece
Centerpiece Gasket
Window
Window Liner
Window Gasket
Lower Window Holder
Cell Housing
Housing Plug Gasket
Housing Plug
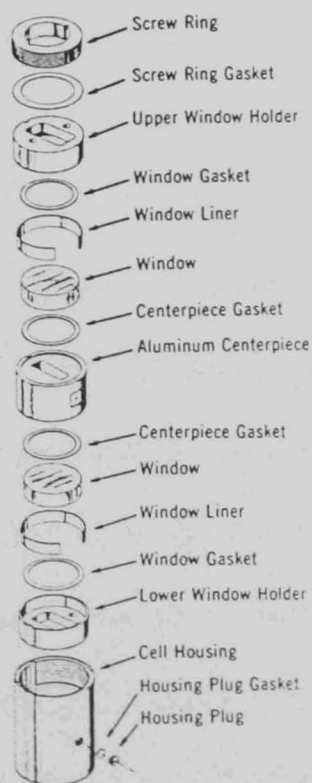
Figure 3.6: Components and assembly of a sample cell for Beckman Model E analytical ultracentrifuge. (Reproduced from Beckman Model E manual)

111

3.3.2.2 Sedimentation Equilibrium Experiments Using the Optima XL-A Analytical Ultracentrifuge

A detailed description of this instrument can be found in Ralston (1993), only a brief summary is given here. The Optima XL-A analytical ultracentrifuge contains an absorption optical system within a detachable monochromator arm as shown in figure 3.7 and automated, computer controlled data capture.

The light -source is a UV-enhanced Xenon flashlamp which allows scanning at a range of wavelengths from 190nm to 800nm. The light source is fired as the sector of interest passes directly over the detector, with the duration of the flash lasting about one microsecond. Data is thus taken one sector at a time.

Temperature control is accomplished via an isothermal radiometer temperature-sensing system. Heating and cooling of the rotor are achieved by a refrigeration can which surrounds the rotor, which is in turn heated and cooled by thermoelectric modules.

This instrument was used for sedimentation equilibrium runs of dry-heated BSA and BSA/dextran T40. A 12mm multichannel cell was loaded with 80µl of BSA/dextran T40 (2:1 molar ratio) composite and 80µl of 3 weeks heat treated BSA in two of the sample channels and 80µl of dialysis buffer in their respective solvent channels. The run was performed at 20°C and 6000rpm. The Optima XL-A is a software driven instrument and after initially keying in the necessary run details such as temperature, speed, and the wavelength at which scans are to be taken, no further manipulation of the instrument is required. In order to identify whether equilibrium had been attained, scans were taken after 18, 20, and 24 hours, by which time scans could be perfectly overlaid indicating that equilibrium had been reached.
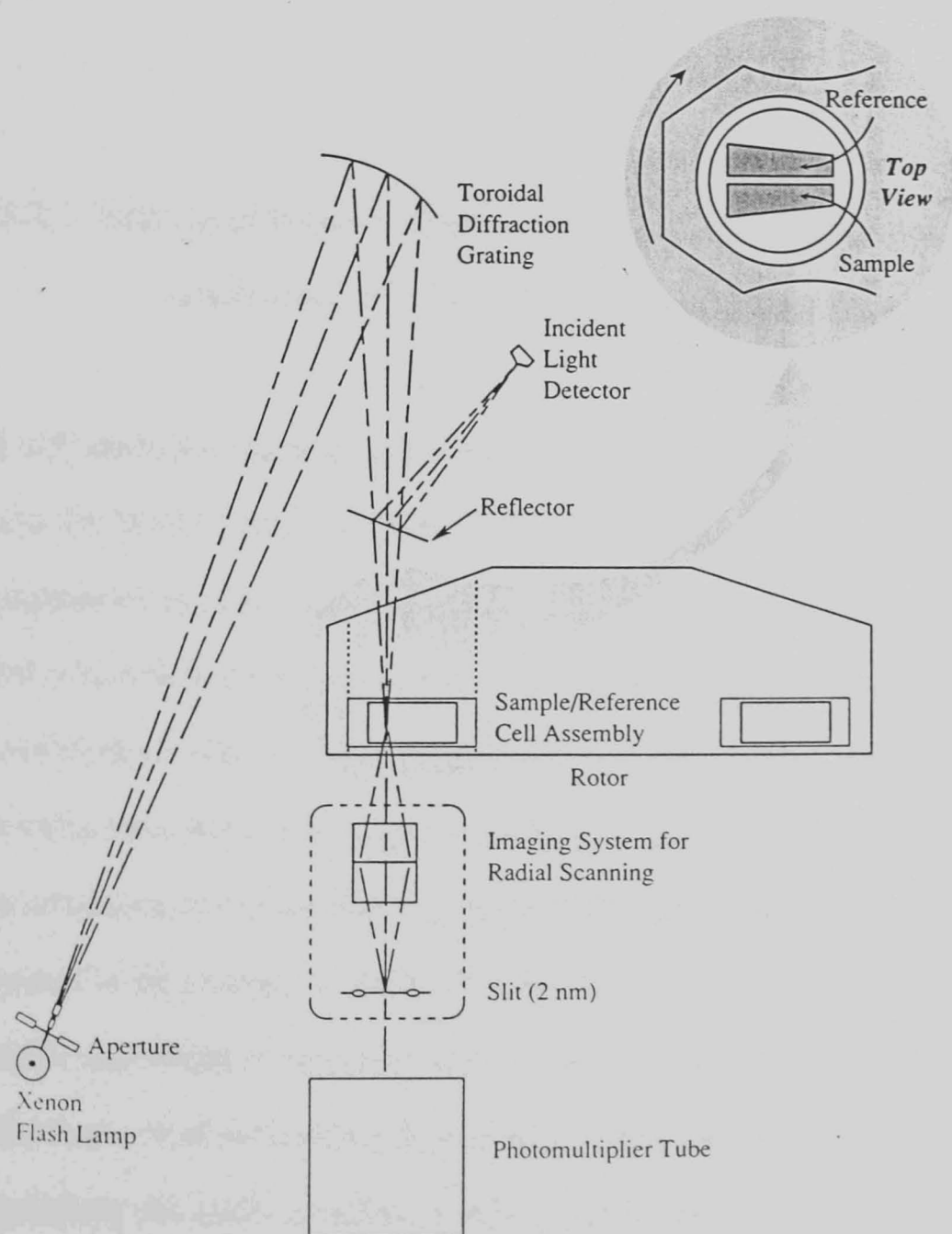
Figure 3.7: Absorption optical system in the Optima XL-A analytical ultracentrifuge (Reproduced from Ralston, 1993)

113

Raw absorption versus radial displacement data were manipulated using the XL-A software to achieve an absorption versus radial displacement plot. These data were then transferred to the IBM-3081 mainframe computer at Cambridge via the JANET link where they were analysed further to give apparent weight average molecular weights using the 'MSTAR' program (Harding et al, 1992) which had been adapted by Dr. J.C.Horton to suit the requirements for the XL-A software output.

3.3.2.3 Sedimentation Velocity Experiments Using the MSE Centriscan 75 Analytical Ultracentrifuge

All sedimentation velocity experiments on the guar gum samples were carried out in the MSE Centriscan 75 ultracentrifuge (Measuring and Scientific Equipment Ltd., Crawley, UK). The MSE Centriscan 75 ultracentrifuge is fitted with a Schlieren optical system using a monochromatic filter at a wavelength of 546nm. The Schlieren optical system relies on the comparison of two cells, therefore, only single channel cells were used in these experiments. The scrupulously clean cells (all 20mm MSE cells) were assembled and then tightened with a torque wrench to 130lb/inch^2. Cells were loaded with 800μl of solution and 900μl of reference buffer (it is necessary to use more reference buffer than solution to ensure satisfactory subtraction of the reference buffer signal along the entire solution column length). Solute concentrations ranged from 1.2 to 3.0mg/ml. Using a six-place rotor, four sample cells, a solvent cell and a counterpoise were run at any one time. The counterpoise contains two reference slits 1.603cm apart which were registered on every scan in order to calibrate actual radial displacements for data analysis. The samples were run at a temperature of 20°C and a speed of 47 000rpm. A series of five to eight scans

114

were taken at fixed time intervals. Temperature was controlled and monitored with a built-in infra-red sensor, fixed at a standard distance from the rotor. The speed was monitored using a digital frequency meter. The distance between scans was measured using a digitising tablet connected to an Apple personal computer and data were analysed using software written by Dr. A. Rowe (Leicester University). The following information was obtained from the above analysis:

(i) the sedimentation coefficient, $s_{T,b}$, for the sample under the experimental conditions prevailing at that time (ie. temperature, concentration, buffer), (ii) the standard error for a given set of scans, (iii) the average radial dilution - a result of the sector shape of the solution column.

$s_{T,b}$ was then converted into $s_{20,w}$ according to equation [2.34] and the concentrations as calculated for the dissolved fractions were corrected by multiplication by the radial dilution factor. A graph of $s_{20,w}$ versus concentration for each sample was plotted and extrapolated to zero concentration and a value for $s^0_{20,w}$ and k_s (the concentration dependent regression factor) was obtained for each sample.

3.3.2.4 Sedimentation Velocity Experiments Using the Optima XL-A Analytical Ultracentrifuge

Sedimentation coefficients for the BSA/dextran mixtures were obtained using the Beckman XL-A analytical ultracentrifuge (Beckman, Palo Alto, California, USA). Sample cells were 12mm double sector cells. 300μl of sample solution was loaded into the sample channel and 350μl of buffer into the solvent channel. Each cell was then tightened to 120lb/inch^2 with a torque wrench. The AN-Ti 60 is a four-place rotor, allowing three sample cells and a counterpoise to be loaded. Sedimentation velocity experiments were performed at 35 000rpm

and 20(±0.5)°C and movement of the sedimenting boundary was monitored at a wavelength of 280nm. The absorption versus radial distance traces were stored on the IBM PC computer hard disc. For data analysis the following points on the traces were marked and/or noted:

(a) the meniscus position (r_0)

(b) the radial displacement of the boundary (r_{infl}) and the time (t) at which the scan was taken

The data obtained were then used in the following calculation:

$$s_{T,b} = \frac{\ln\frac{r_{infl}}{r_0}}{\omega^2 t}$$

where

$$\omega^2 t = \left(\frac{2\pi rpm}{60}\right)^2$$

values were calculated for each scan and the average value quoted as $s_{T,b}$

3.3.3 VISCOMETRY

The theoretical background to viscosity measurements has been discussed in Section 2.3.

3.3.3.1 Intrinsic Viscosity

Intrinsic viscosities [η] were determined for each irradiated guar gum sample by measuring relative viscosities ($\eta_r = \frac{\text{flow time of solution}}{\text{flow time of solvent}}$), converting to

116

specific viscosity and extrapolating to zero concentration using Huggins and Kraemer relationships as described in equation [2.59] and equation [2.60] respectively.

Measurements were performed using an Automated Viscosity Measuring Unit AVS 310 (Schott Geräte, Hofheim, Germany).

Guar gum samples were prepared as described in Section 3.1.1 and run at five different concentrations ranging from 0.5mg/ml to 1.5mg/ml at 25 (±0.1)°C. An accurately measured amount of sample liquid was placed into the low shear Ostwald-type capillary viscometer which was then mounted into the fixing frame. After allowing the sample to reach temperature equilibrium it was automatically pumped up the capillary viscometer, past two light barriers which act as measuring levels. Shortly after the meniscus passes the upper measuring level, the pump unit switches off, the viscometer is vented and the sample liquid starts running back. As the meniscus passes the upper light barrier, the light intensity is changed - this change is converted into a digital electrical signal which starts the internal crystal-controlled clock. Time measurement is stopped when the meniscus passes the lower measuring level. The measured time is shown on the display and stored internally. Ten measurements were performed for each sample concentration and the mean value for each concentration was obtained.

3.3.3.2 Shear Viscosity

Shear viscosities were measured using the computer controlled, software driven Bohlin C.S. Rheometer (Bohlin Reologi AB, Lund, Sweden) with the cone and plate measuring geometry CP4/40 (a 40mm diameter cone having an angle of 4°), consisting of a rotating upper cone and a fixed lower plate with the sample contained between them. The temperature was at 24.8°C within limits of ±0.5°.

117

The cone and plate geometry was set up with the required gap width of 150μm. A small amount of sample was placed between the two components and the program was pre-set to record the effect of ten different shear rates on the solution viscosities. Data was collected for each irradiated sample and analysed using the dedicated Bohlin software which produced plots of viscosity versus shear rate. Zero shear viscosities were obtained using the Cross equation (Cross, 1965).

3.3.4 REFRACTOMETRY

The value of the differential refractive index increment (dn/dc) is an essential requirement for the determination of molecular weights from light scattering.

Measurements were performed using the Optilab 903 interferometric differential refractive index detector (Wyatt Technology Corp., Santa Barbara, California, USA) in the laboratories of Optochem Ltd. (Schotten, UK). A schematic diagram of the instrument is shown in Figure 3.8.

The detector is based on a wave front shearing technique. The beam from a collimated light source is plane polarized at 45° to the horizontal and then split into two components by the first Wollaston prism. The beam passing through the sample cell is vertically polarized, whereas that passing through the reference cell is horizontally polarized. The beams are recombined in the second Wollaston prism, the quarterwave plate and the analyser. Any difference in refractive index between sample and reference results in a phase shift of one beam relative to the other which is directly proportional to the difference in refractive index of the two liquids.
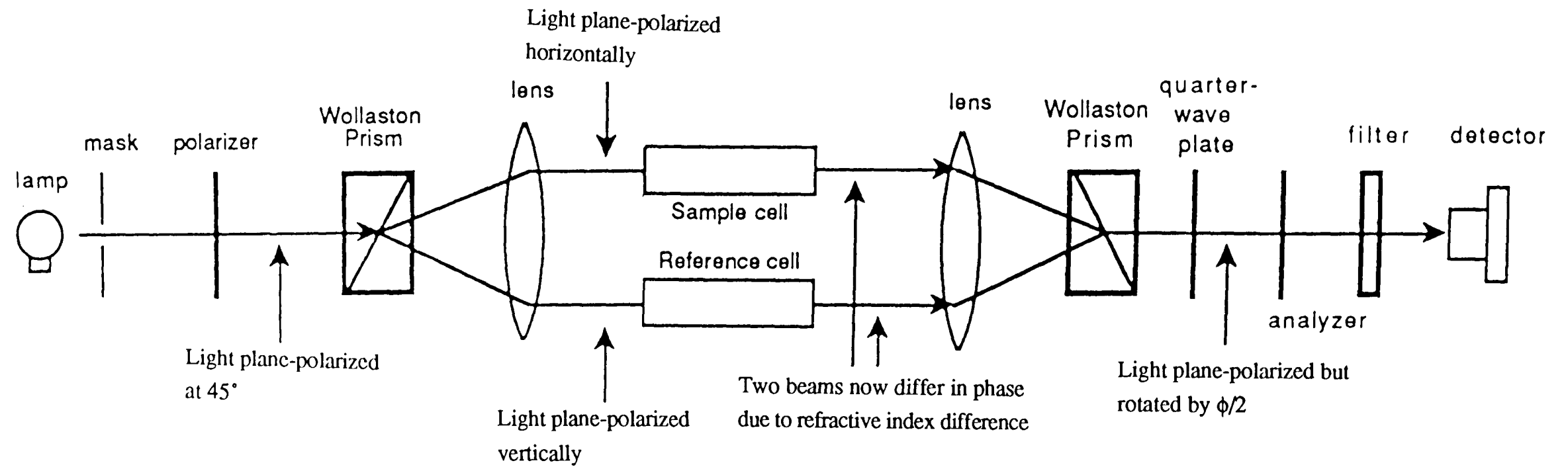
Figure 3.8: Schematic diagram of an interferometric differential refractometer (from Wyatt, 1993)

Dn/dc measurements were performed by slowly pushing sample through the sample cell, the reference cell already contained the buffer identical to that used for dissolving the sample. The sample was run through the sample cell until the signal for the refractive index remained stable (approx. 2ml). For each sample a minimum of four concentrations in the range 0.1 to 0.3mg/ml was used. Signals were digitised and analysed using the Dn/Dc software™ (Wyatt Technology Corp, Santa Barbara, California, USA).

3.3.5 MOISTURE CONTENT

Moisture content was determined using approx. 0.5g of guar gum sample and drying at 70°C in a vacuum oven to constant weight. Measurements were performed in triplicate.

3.3.6 SOLUBLE FRACTION

The amount of soluble material in the guar gum samples was determined gravimetrically. Samples were dissolved and centrifuged as described in Section 3.1.1 and aliquots (10.0ml) were transferred into aluminium pans and dried to constant weight in a vacuum oven (70°C). Measurements for three replicates were obtained.

3.3.7 CHEMICAL METHODS

3.3.7.1 Total Carbohydrate Content

The carbohydrate content of the irradiated guar gum samples was determined by the scaled down version of the phenol-sulphuric acid colorimetric method according to Dubois et al. (1956). One volume of sample (100µl) was added to one volume (100µl) of a 5% aqueous phenol solution. The solutions were mixed and five volumes of concentrated sulphuric acid (1000µl) were carefully added to the mixture. 100µl of the mixture was transferred into the wells of a micro titre plate and the absorbance was read at 485nm on a Dynatech DMP 5000 plate reader, using Biolinks™ software.

3.3.7.2 Galactose/Mannose ratio

Galactose/mannose ratios of the irradiated guar gum samples and control were determined according to the method by Albersheim et al (1967).

3.3.7.2.1 Hydrolysis

Approximately 50mg of each irradiated guar gum sample was hydrolysed using 1M sulphuric acid for 2 hours in a water bath at 100°C. These samples are then stable and were left in cold storage until further work-up.

121

3.3.7.2.2 Derivatisation

Aliquots (3.0ml) of the hydrolysates were taken and 0.5ml of internal standard (allose at a concentration of 1mg/ml in 50% benzoic acid) was added. Then 1.2ml of 12M ammonium hydroxide were added and the samples were reduced by adding a freshly prepared solution of 3M ammonium hydroxide containing sodium borohydride at a concentration of 50mg/ml. After mixing, the solutions were left at 40°C for one hour after which 0.5ml of glacial acetic acid was added.

To 0.5ml of the acidified solution, 0.5ml of 1-methylimidazole and 5ml of acetic anhydride were added and then mixed. After 10 minutes, 0.8ml of ethanol was added and the mixture left for 5 minutes. Then 5ml of water were added, the solutions were mixed and left to stand for a further 5 minutes and then 0.5ml of bromophenol blue solution (0.04%) was added. The samples were placed into a cold water bath to aid the dispersal of heat and 5ml of potassium hydroxide (7.5M) were added. After a few minutes a further 5ml of 7.5M potassium hydroxide were added. The tubes were capped and mixed by inversion. The mixtures were left until separation into two phases had occurred. The upper layer was drawn into a pipette and transferred into a small vial for analysis by gas liquid chromatography.

3.3.7.2.3 Gas Liquid Chromatography

Gas liquid chromatography (glc) was performed using a Perkin Elmer (Beaconsfield, UK) GC8500 apparatus, data were evaluated using a Pye Unicam PU4810 Computing Integrator. An aliquot of the sample (0.5μl) was applied to a Supelco SP2330 capillary column, dimensions: 30m x 0.75mm id., 0.2μm film (ie. column "packing" was coated onto column). The sample was

carried through the column with nitrogen at a flow rate of 5.4ml/min. The temperature program was set to stay at 200°C for 2 minutes, increase to 240°C at a rate of 4° per minute and then stay at 240°C for a further 2 minutes.

.

3.3.7.3 Protein Content

Duplicate determinations of the protein content of the guar gum samples were carried out using the Kjeldahl method as described in Kirk and Sawyer (1991).

CHAPTER 4

ANALYSIS OF IRRADIATED GUAR GUM SAMPLES

Irradiated guar gum samples were a gift from Dr. K. King of Queen's University of Belfast. For the purpose of this study the irradation doses referred to are the nominal rather than the actual doses (see Table 3.1). The samples were investigated for two reasons: (a) to study the effect of γ-irradiation on the molecular size and solution properties of guar gum, and (b) they provided a homologous series of samples of different molecular weights facilitating conformational analysis.

4.1 COMPOSITION AND PHYSICAL CONSTANTS

The guar gums used had not been purified previously and were not purified in this laboratory prior to analysis. This means that the samples still contained some non-carbohydrate constituents. For this reason preliminary studies were undertaken to quantify moisture content, the amount of material in the soluble fraction, the amount of carbohydrate, galactose to mannose ratio, and protein content. In addition, dn/dc values (for light scattering measurements) were determined for some of the samples. Samples were dissolved as described in Section 3.1.1. Average results are shown in Table 4.1.

Table 4.1: Average compositional parameters and dn/dc value determined for irradiated (and control) guar gum samples

Moisture content (%)	11.23±0.46[a]
Soluble fraction (% of total weight)	80.57±7.37[a]
Carbohydrate content (% of total weight)	86.93±9.76[b]
Galactose/Mannose ratio	38/62[a]
Protein content (%)	3.08±0.17[c]
dn/dc (ml/g)	0.146±0.009[b]

[a] average from ten samples

[b] average from seven samples

[c] average from four samples

The relative moisture contents of our samples determined at 70°C in a vacuum oven were in good agreement with literature values (Maier et al, 1993; see Table 1.1). The average amount of soluble fraction resulted in a large standard deviation. It might be expected that depolymerisation of guar gum at higher radiation doses would lead to an increase in solubility with increasing irradiation. However, variations were not systematic which suggests that they are associated with the dissolution process rather than changes on a molecular level. This should have had implications for the dn/dc measurements as accurate knowledge of solute concentration is important for these. However, our values are relatively close to the literature value of 0.143ml/g (Doublier and Launay, 1981) and the average value from our own determinations (ie. 0.146ml/g) was used for light scattering measurements. A plot of $\Delta n/c$ versus c is shown in Figure 4.1. Dn/dc is determined by extrapolating to zero concentration using a zero slope.

The carbohydrate content of the samples that were tested was determined using a scaled-down version of the phenol-sulphuric acid method. The

chromophore was developed in the wells of a micro titre plate. Differences in absorbance between different samples were very small, a small error could therefore lead to significant uncertainty in the final result and it must be assumed that this is the reason for the very high average value obtained. These values were not used for any concentration corrections.

The galactose to mannose ratios obtained were consistent over the range of our samples and in good agreement with literature.

The protein content obtained by the Kjeldahl method was found to be lower than reported in the literature for guar gum (see Table 1.1) which may be a reflection of the variability of the native material.
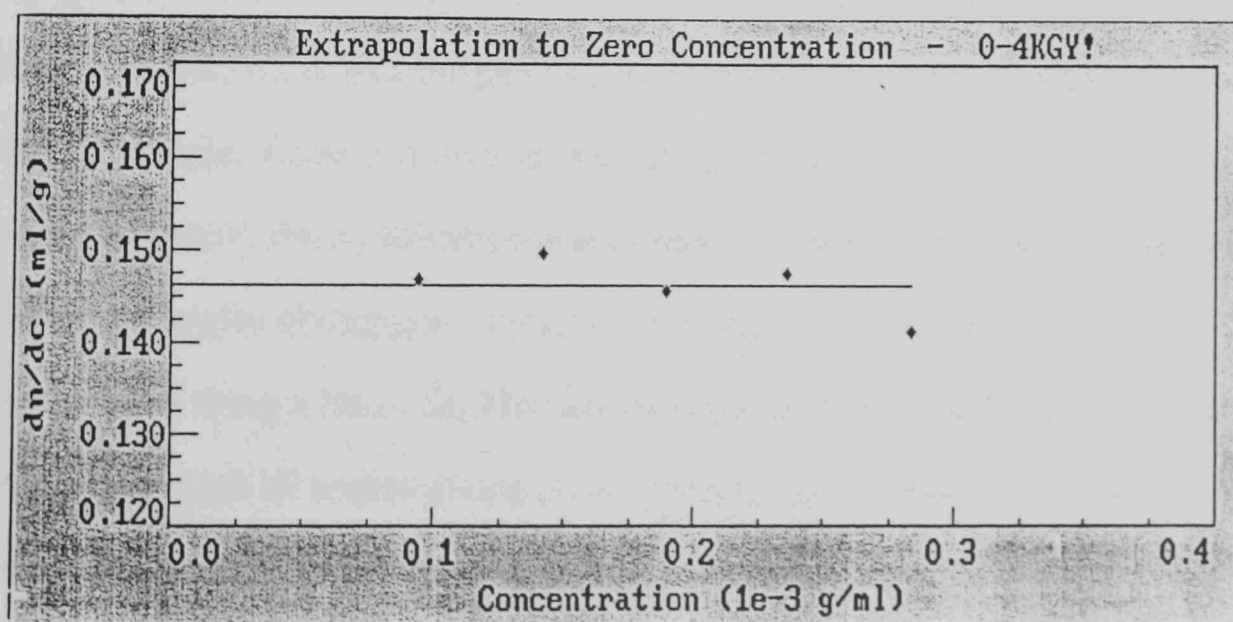
Figure 4.1: Plot of Δn/c versus c for 0.4kGy sample. Concentration range 0.1 to 0.3 mg/ml in phosphate/chloride buffer pH 6.8, ionic strength 0.1.

4.2 SEC/MALLS RESULTS

Samples were dissolved as described in Section 3.1.1 and triplicate runs were performed. Elution profiles of the control and two irradiated samples are shown in Figures 4.2 to 4.4. These are representative of the trends in all samples. Qualitative inspection of the elution profiles indicates one main peak which for the control material appears bimodal, and for samples up to 1.0kGy has a shoulder on the low molecular weight side and two minor peaks at high elution volume (17.7 and 19.1ml). The latter two peaks appear to be characteristic of the guar gum preparations and do not change significantly in area from sample to sample. They are most likely due to the small amounts of protein and other impurities present in the gum, as their appearance does not change with changing radiation dose it is unlikely, in my opinion, that they are due to low molecular weight radiation products. The maximum of the main peak is shifted slightly to higher elution volumes as the radiation dose increases which is indicative of a slight decrease in molecular size of the eluting material.

The determination of molecular weight and radius of gyration averages was found to be somewhat tricky. Figure 4.5 shows the Debye plot (R_θ/Kc versus $\sin^2\theta/2$) for one of the peak fractions (elution volume 11.44ml) of the 5.0kGy sample. There is a very strong curvature observed at low angles. Due to this curvature, three different extrapolations to zero angle were performed. Firstly, all angles giving good signal to noise ratios were used and extrapolated using a linear fit. The second procedure involved using a second order fit through all angles giving good signal to noise ratios. For the third extrapolation, only angles prior to the onset of the upturn in the Debye plots were used (angles at and above 65°). Weight average molecular weights (M_w) and their associated errors from all three extrapolations are given in Table 4.2. The M_w values from the first two extrapolation procedures are very high

Figure 4.2: Elution profiles from light scattering (90° detector) and differential refractive index detectors for non-irradiated guar gum. Sample concentration = 1mg/ml, injection volume = 100µl, dn/dc = 0.146ml/g, flow rate = 0.8ml/min, eluent = phosphate/chloride buffer (I = 0.1, pH6.8) (Green,1933), column system 2.

128

Figure 4.3: Elution profiles from light scattering (90° detector) and differential refractive index detectors for 1.0kGy sample. Sample concentration and chromatographic conditions as in Figure 4.2.
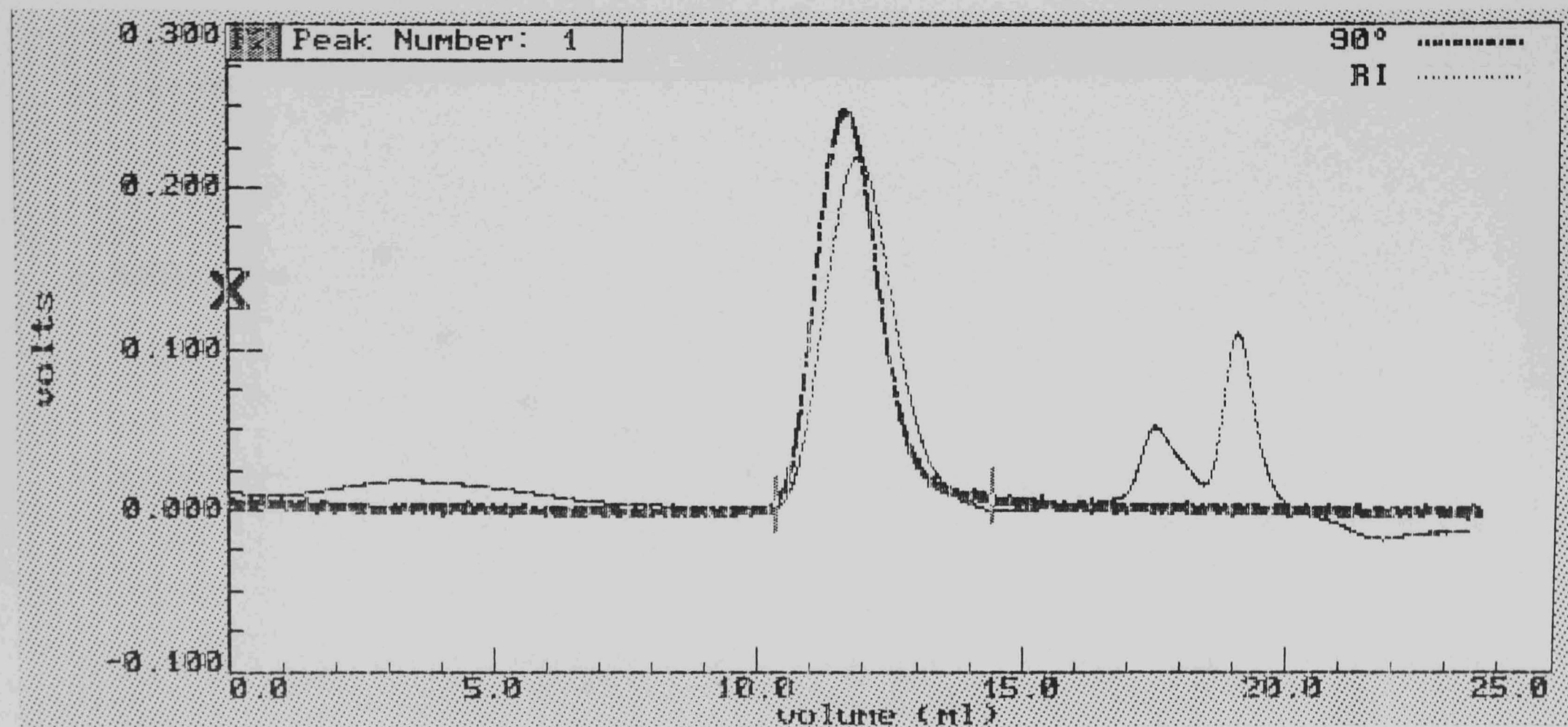
Figure 4.4: Elution profiles from light scattering (90° detector) and differential refractive index detectors for 10.0kGy sample. Sample concentration and chromatographic conditions as in Figure 4.2.
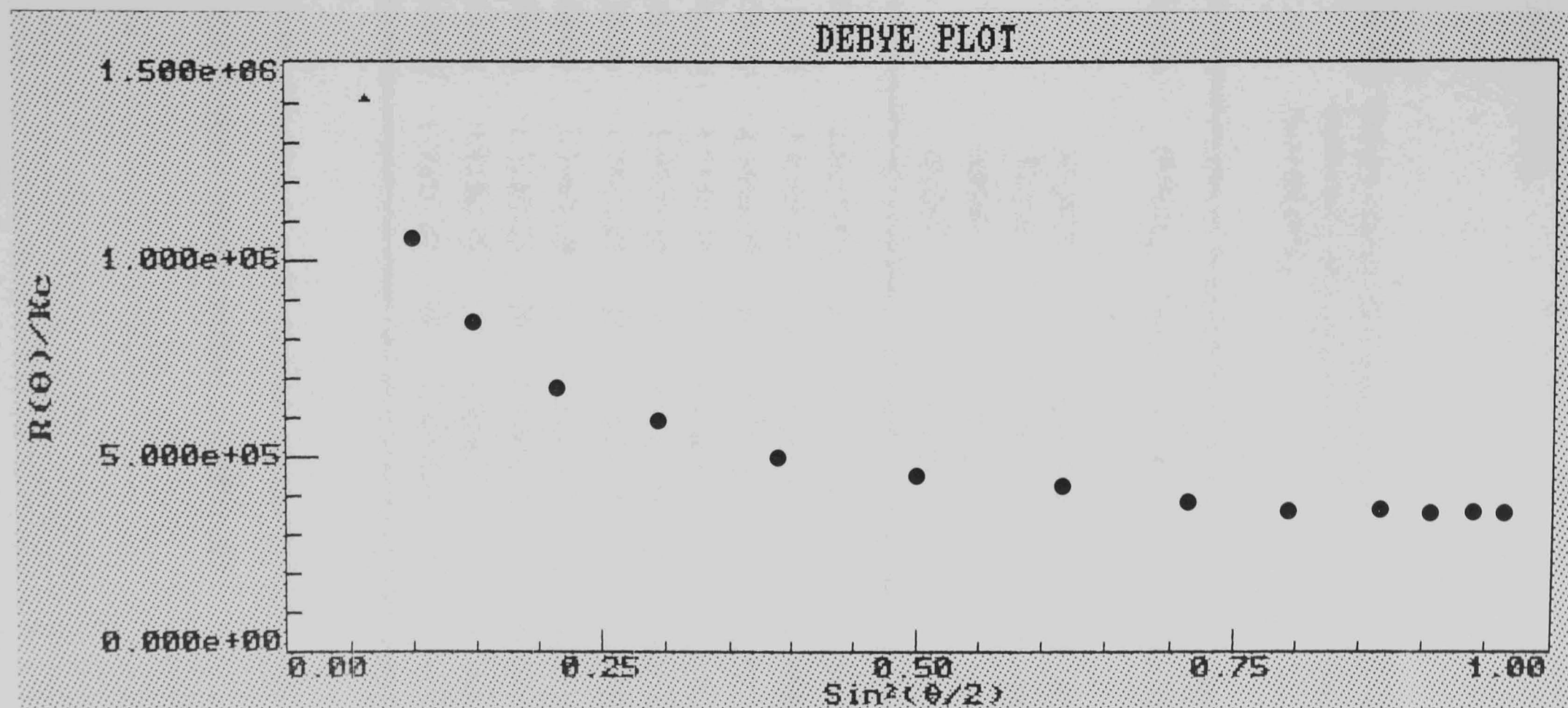
Figure 4.5: Debye plot for peak fraction (elution volume 11.44ml) of 5.0kGy sample.

and have unacceptably high errors (weight average molecular weights of chitosans and dextrans have been shown to have errors of less than 10% (Beri et al, 1993)).

Table 4.2: Weight average molecular weight values from control and irradiated guar gum preparations using three different extrapolations

Sample	$10^{-6}xM_w$ 1st Order Fit (all useable angles)	Error (%)	$10^{-6}xM_w$ 2nd Order Fit (all useable angles)	Error (%)	$10^{-6}xM_w$ 1st Order Fit (angles >65°)	Error (%)
Blank	2.61±0.62	24	4.28±1.16	27	1.08±0.12	11
0.1kGy	2.22±0.31	14	3.56±0.63	18	0.99±0.06	6
0.2kGy	2.85±0.53	19	4.90±1.2	24	0.99±0.08	8
0.4kgGy	1.78±0.16	9	2.83±0.34	12	0.84±0.01	2
0.6kGy	1.91±0.30	16	3.03±0.54	18	0.87±0.08	10
0.8kGy	1.75±0.47	27	2.80±1.10	35	0.80±0.03	4
1.0kGy	1.74±0.38	22	2.78±0.87	31	0.82±0.03	4
2.0kGy	1.11±0.22	20	1.59±0.37	23	0.68±0.08	13
5.0kGy	0.87±0.19	22	1.42±0.15	10	0.58±0.06	10
10.0kGy	0.72±0.07	10	1.10±0.13	12	0.40±0.02	4

Errors are calculated from the standard deviation from three runs divided by the mean molecular weight expressed as a percentage

According to Banks et al (1969) the angular dependence at low angles may be due to either of the following: (a) the presence of microgels or aggregates, (b) a wide molecular weight distribution within the sample, (c) branching, (d) presence of dust. The extrapolation procedure (and ultimately the molecular weight values) depends on the cause of the curvature. If the curvature is real, it cannot be ignored and the molecular weight values will be quite high. If the curvature is only due to artefacts like dust, it can be ignored and extrapolation can start at angles above the onset of the upturn.

Dust causes serious problems in classical static light scattering where relatively large amounts of solution (in order of mls) are used in cuvettes. However, in a flow-through system such as the one used in the present experiments, these problems should have been eliminated because, firstly, eluent and samples are filtered through $0.22\mu m$ membrane filters, secondly, the columns act as filters and thirdly, the scattering volume is extremely small (in the order of μls). Also, the presence of dust would be recognized in the chromatograms as 'spikes' which do not influence the calculations to any significant extent and were not observed in any of our traces. Robinson et al (1982) ascribed the curvature in their Zimm plots from static light scattering for commercial guar gums to small amounts of supramolecular particles and ignored this curvature. Such particles, even if present in only tiny amounts, can distort the angular dependence significantly (Kratochvil, 1972; 1987) and create large uncertainties in the weight average molecular weight values and radii of gyration. This is also most likely one of the reasons for the curvature at low angles in our Debye plots.

The second reason is probably associated with polydispersity. The guar gum samples used are very large and elute at or very close to the exclusion volume of the column system. For the non-irradiated sample and those irradiated with low doses, there is a very steep rise in the elution traces (see Figures 4.2 and 4.6), indicating the onset of size separation. Molecules larger than the
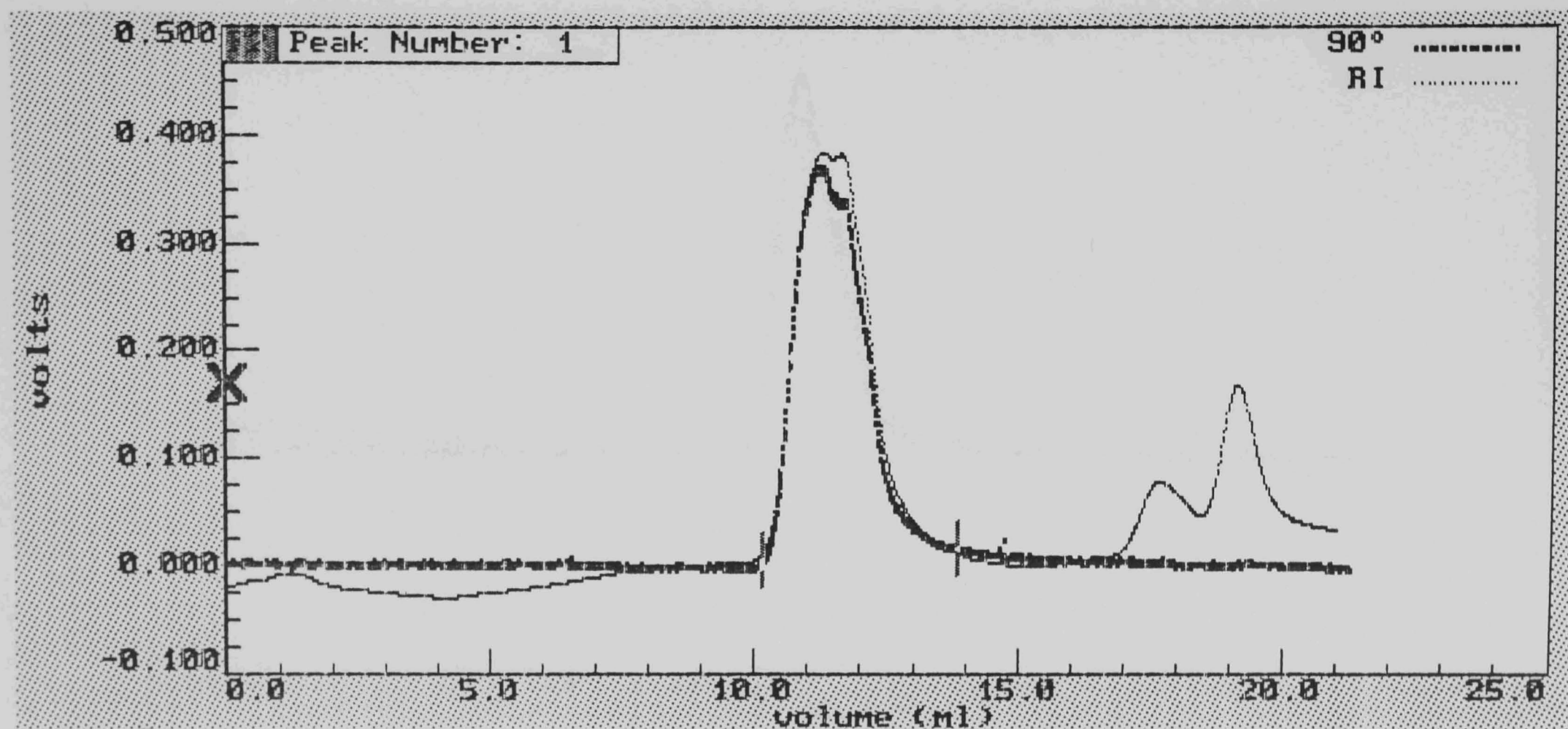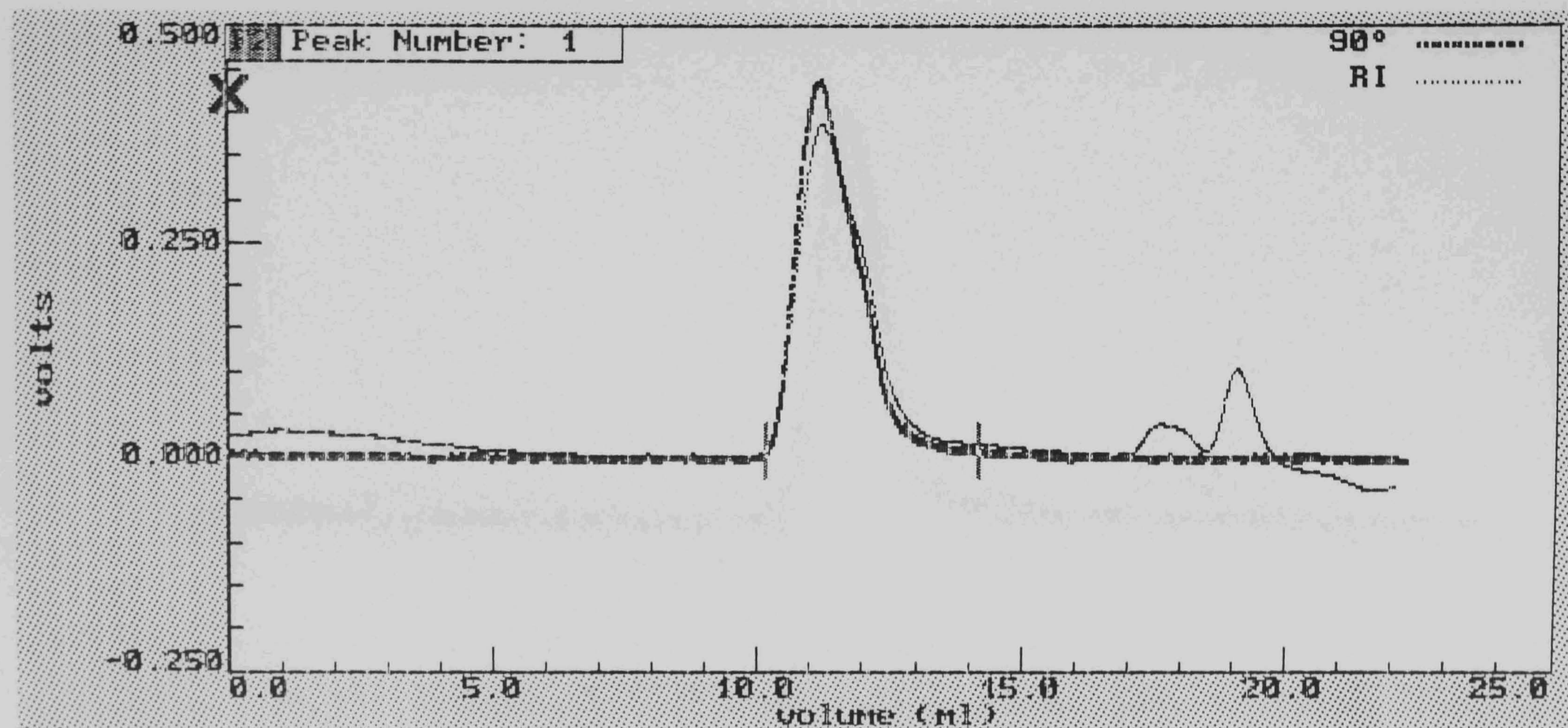
133
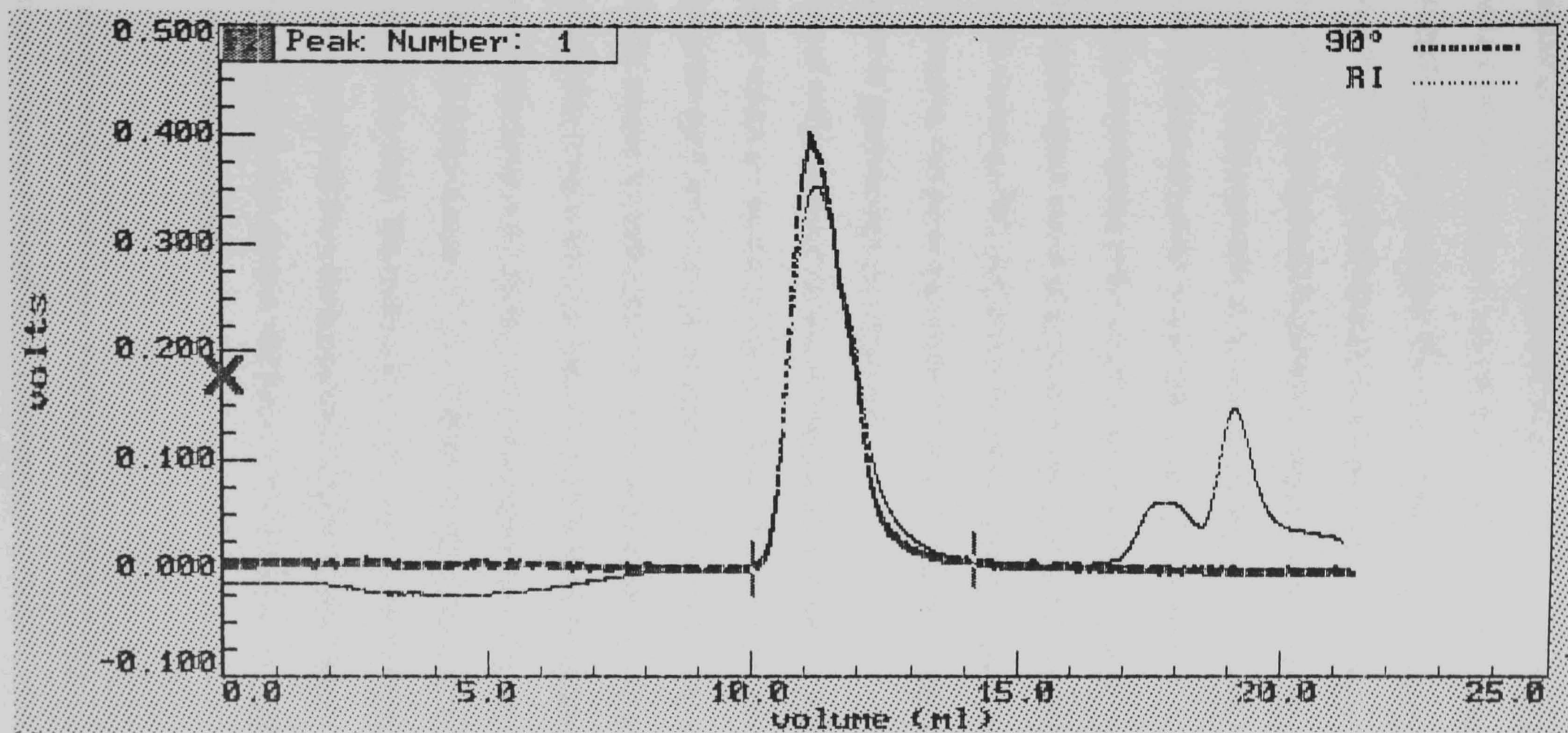
Figure 4.6: Elution profiles from light scattering (90° detector) and differential refractive index detectors for 0.4kGy sample. Sample concentration and chromatographic conditions as in Figure 4.2.

exclusion size will also elute at this point, effectively diminishing the separation. This can be illustrated using molecular weight versus elution volume plots in Figures 4.7 to 4.9 for the non-irradiated, 1.0kGy and 10.0kGy irradiated samples. The slope obtained for the control sample is very flat indicating that virtually no separation has taken place. The slopes for the samples in Figures 4.8 and 4.9 are larger and show some separation. Polydispersity, especially at the low irradiation doses, must therefore be considered as one of the factors influencing the curvature in the Debye plots, causing uncertainties in the weight average molecular weight values.

The mean-square radius of gyration is obtained from the initial slope of the R_θ/Kc versus $\sin^2\theta/2$ plot, however, due to the distinct curvature in our Debye plots, this parameter could not be determined with any certainty and radius of gyration data are not quoted.

Plots of weight average molecular weight versus radiation dose for all three sets of values are shown in Figures 4.10 to 4.12. The plots are fairly similar except for the 0.2kGy sample which shows an increase in M_w over the 0.1kGy sample for both extrapolations which include the curvature whereas this increase is not evident for the extrapolation from higher angles only. The second difference is the slightly more rapid decrease in M_w for the more highly irradiated samples (2.0 to 10.0kGy) using extrapolation from the higher angles only. The molecular weights used in the following discussions are those obtained from extrapolation of angles 65° and higher. The jusitification for this decison will become evident from the conformational studies described below.

Molecular weight distributions for the control and the irradiated samples are shown in Figures 4.13 and 4.14. The narrow distribution of the control sample is most likely due to the lack of separation for molecules which are too large for the column packing material to separate.

135
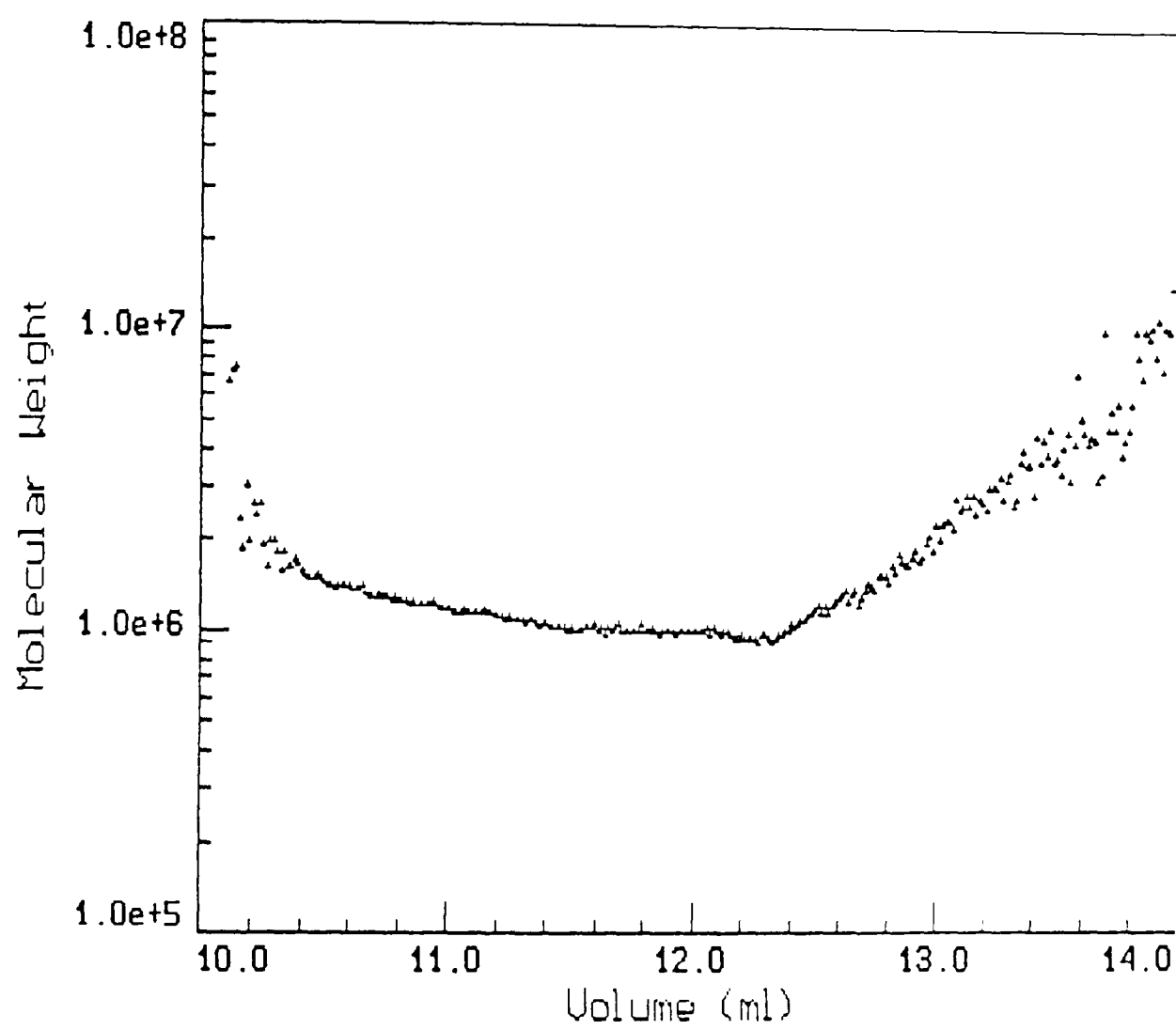
Figure 4.7: Plot of molecular weight versus elution volume for non-irradiated guar gum sample

136
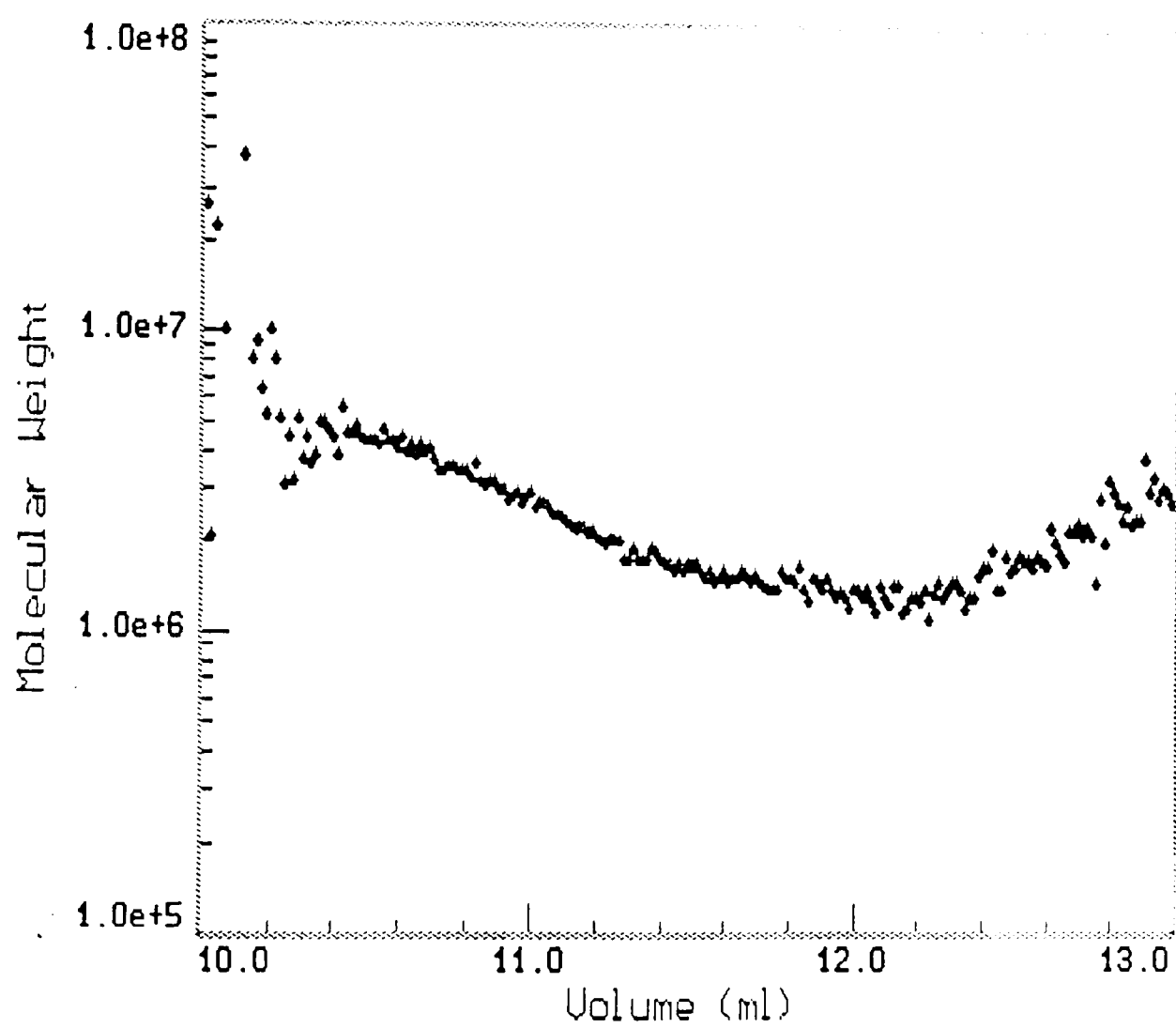
Figure 4.8: Plot of molecular weight versus elution volume for 1.0kGy guar gum sample
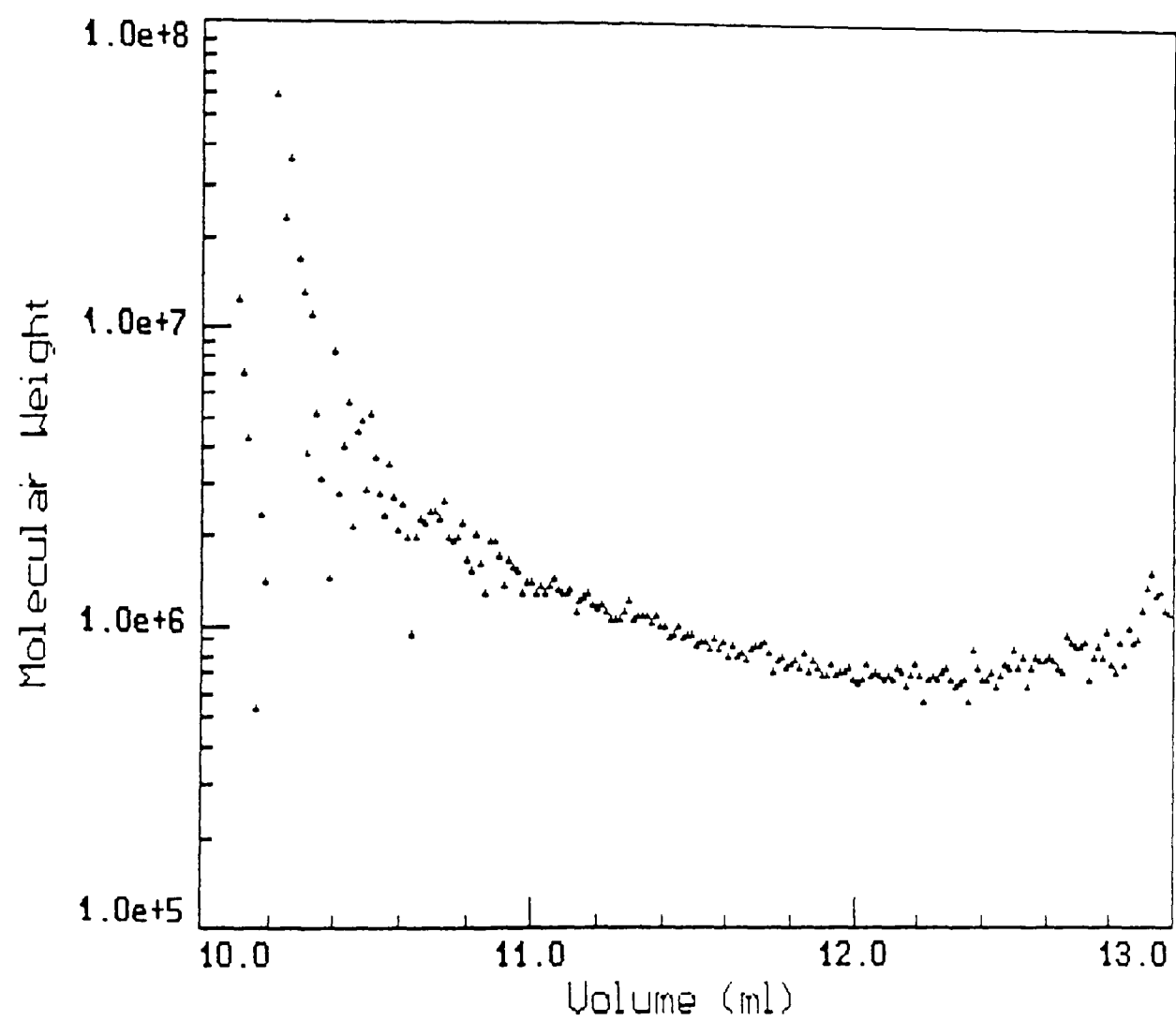
Figure 4.9: Plot of molecular weight versus elution volume for 10.0kGy guar gum sample.
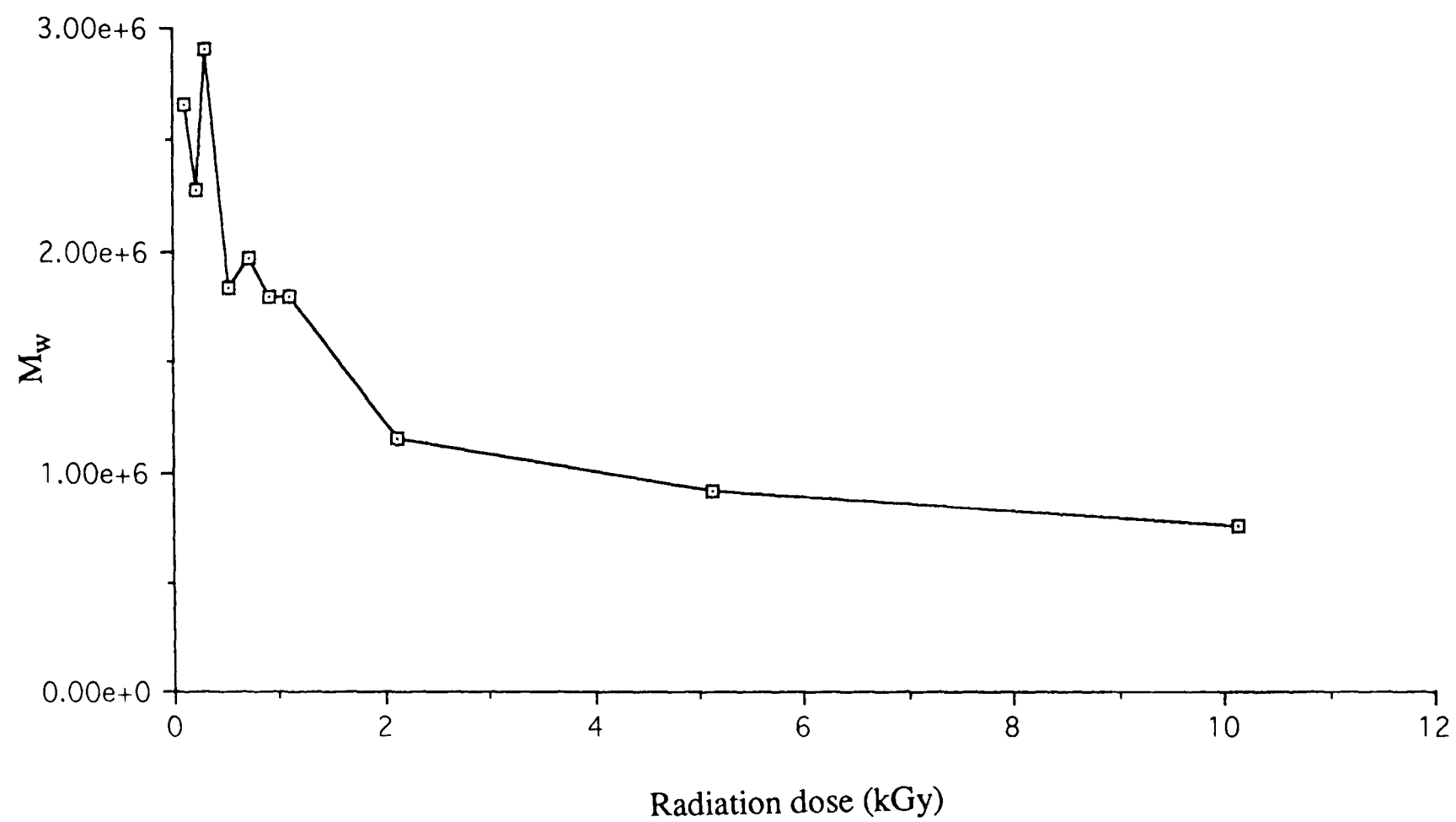
Figure 4.10: Weight average molecular weight (from SEC/MALLS using 1st order fit through all useable angles) versus radiation dose.
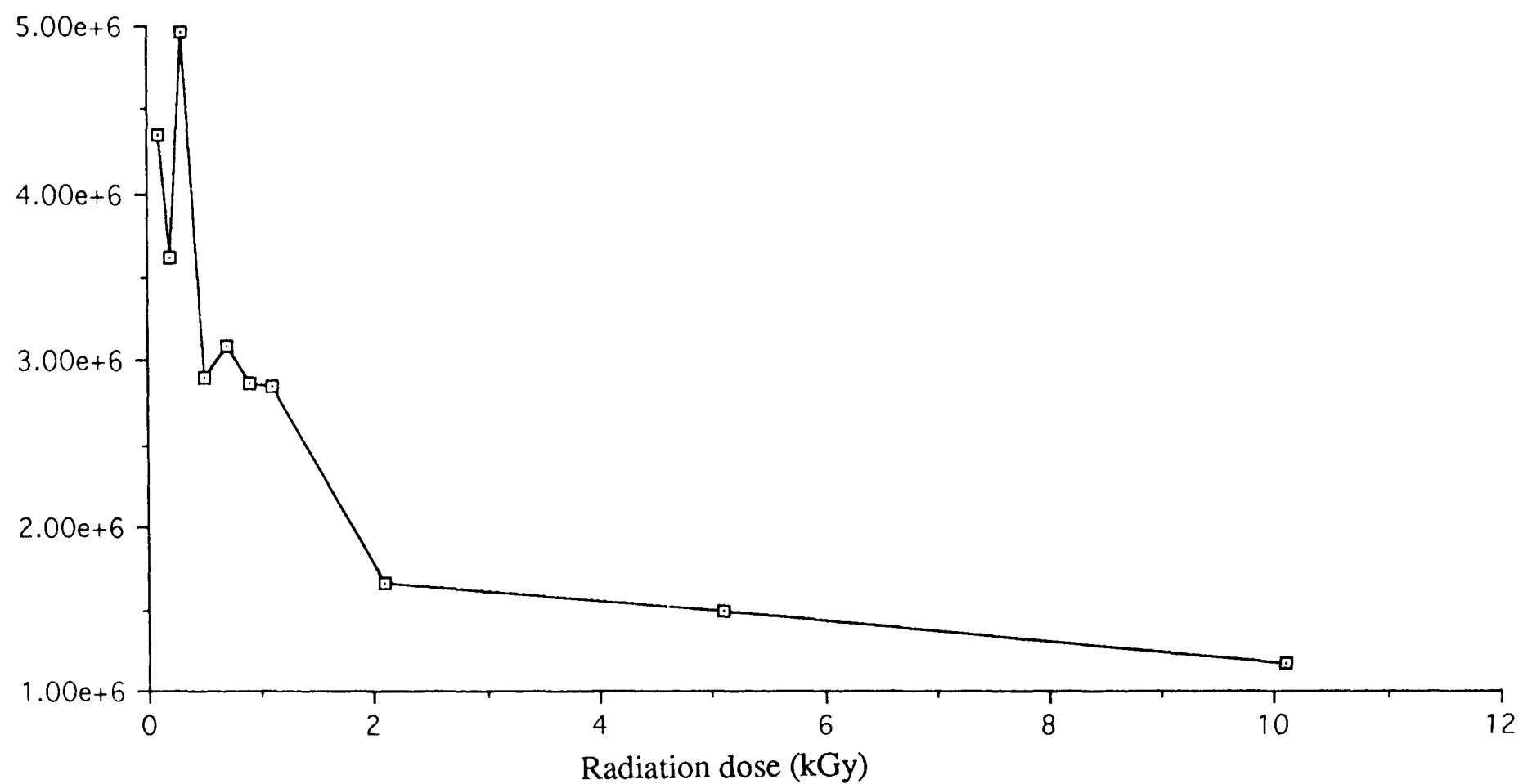
Figure 4.11: Weight average molecular weight (from SEC/MALLS using 2nd order fit through all useable angles) versus radiation dose.
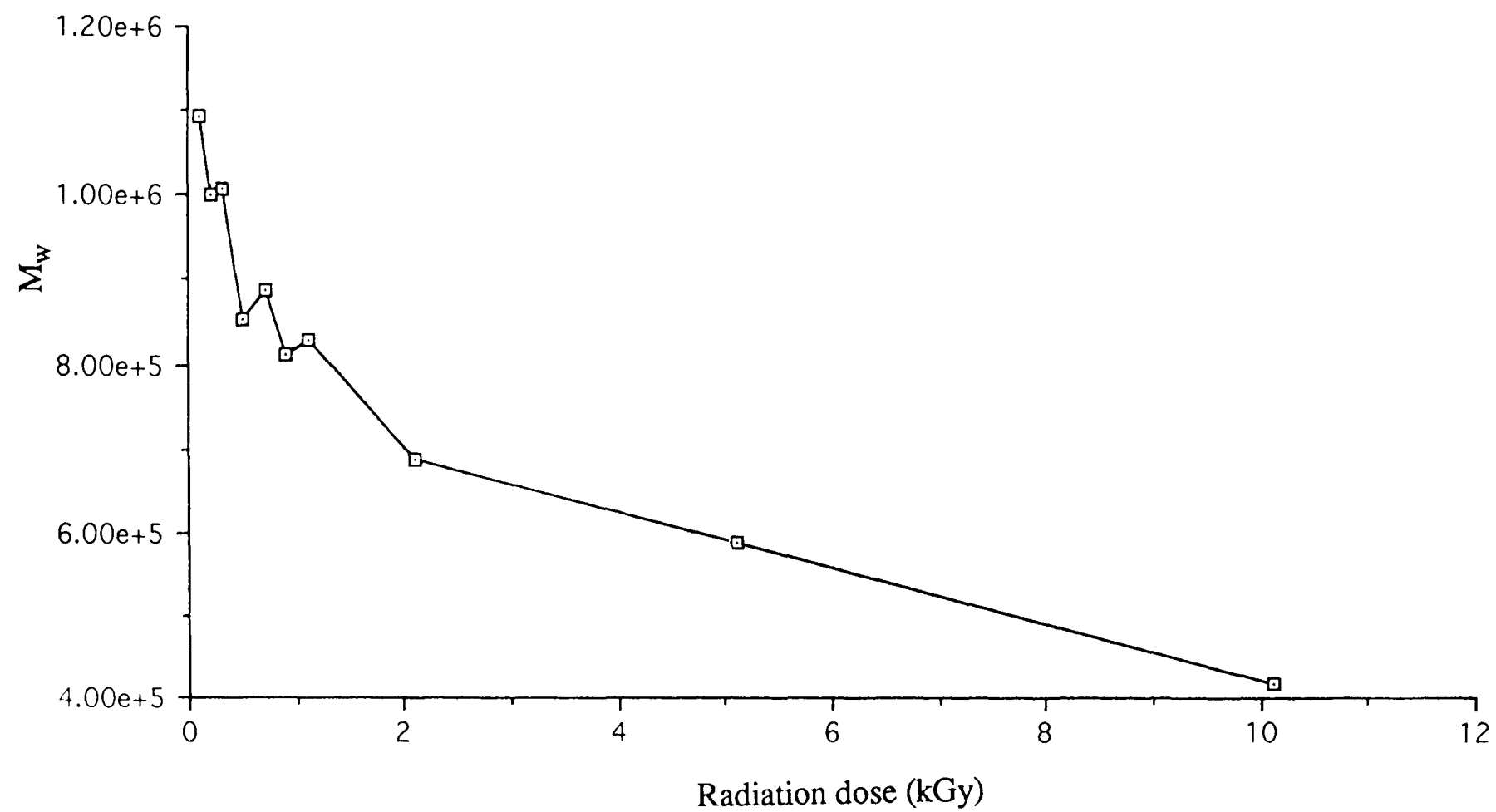
Figure 4.12: Weight average molecular weight (from SEC/MALLS using 1st order fit through angles at or above 65°) versus radiation dose.
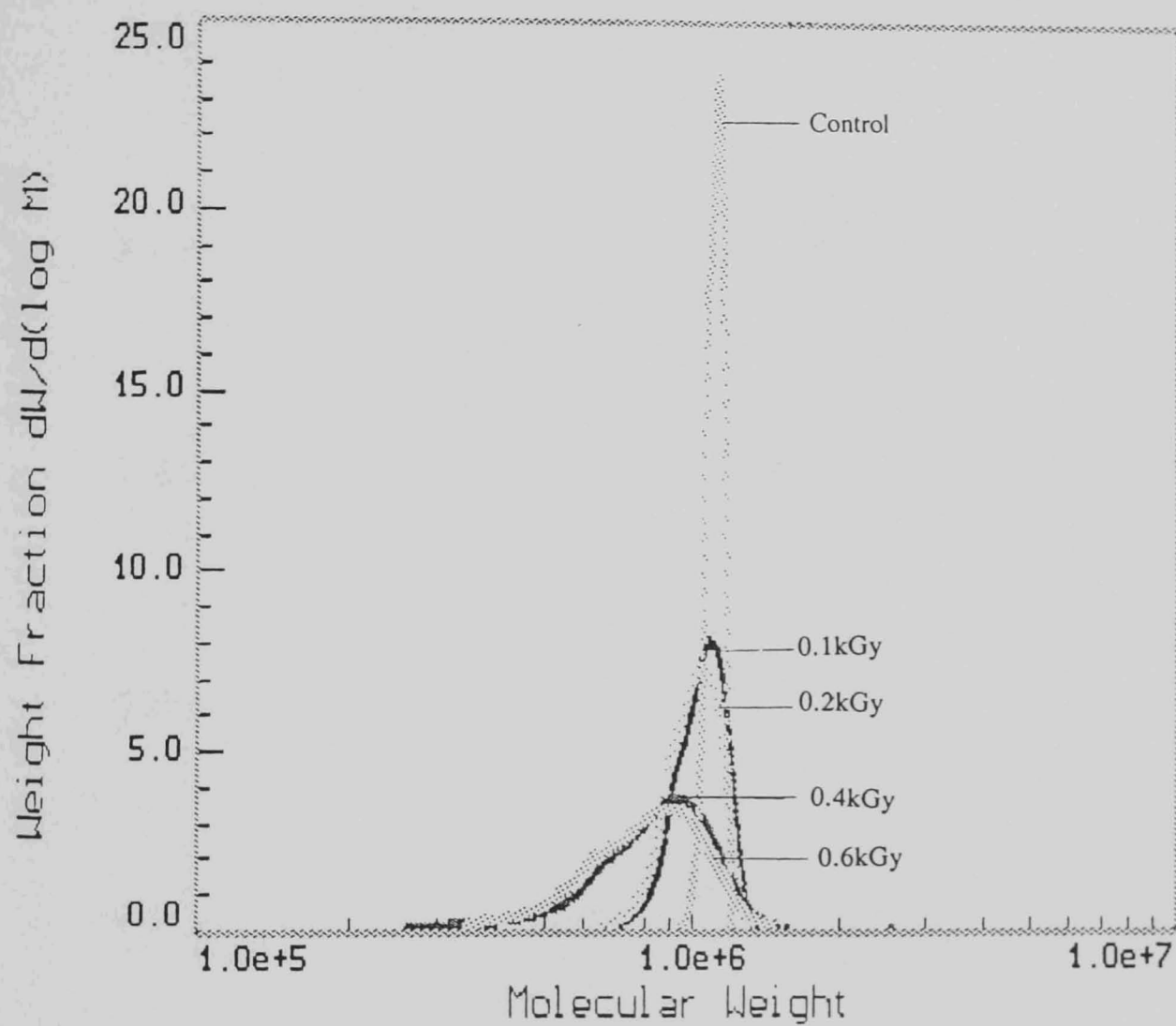
Figure 4.13: Molecular weight distributions for control and irradiated samples. Radiation doses as indicated in plot.
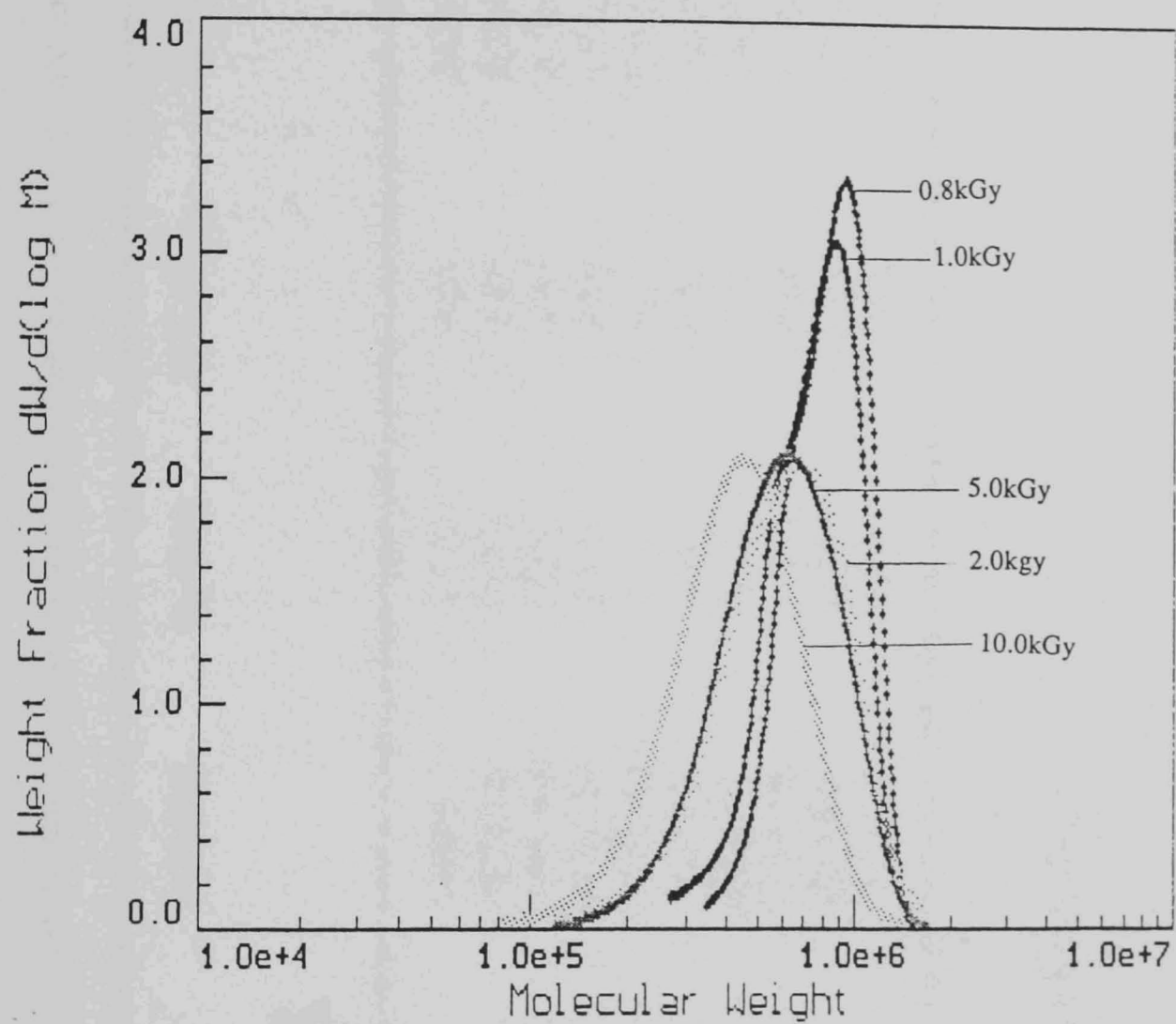
Figure 4.14: Molecular weight distributions for 0.8 to 10.0kGy irradiated samples. Radiation doses as indicated in plot.

Table 4.3: Weight average molecular weights and hydrodynamic parameters for control and irradiated guar gum samples

Sample	$10^{-6} \times M_w$		$[\eta]$(ml/g)	η_0 (Pas)	$10^{13} \times s^0_{20,w}$	k_s(ml/g)	$k_s/[\eta]$
	Light Scattering[a]	Sedimentation Equilibrium [b]					
Control	1.08±0.12	1.45±0.02	1160±14	21.4	4.58	242±17	0.209±0.018
0.1	0.987±0.063	1.1±0.2	1020±36	19.87	5.00	222±26	0.218±0.032
0.2	0.993±0.081	1.5±0.1	1100±628	12.91	4.65	211±67	0.192±0.109
0.4	0.839±0.014	1.13±0.03	1200±224	8.27	4.95	241±31	0.201±0.054
0.6	0.873±0.084	1.17±0.1	1150±112	5.18	4.23	190±26	0.165±0.035
0.8	0.8±0.031	0.5±0.05	900±31	4.64	4.44	223±23	0.248±0.04
1.0	0.816±0.032	1.09±0.03	860±152	5.17	5.17	288±32	0.335±0.082
2.0	0.675±0.088	1.05±0.1	1010±246	1.71	4.88	233±22	0.231±0.063
5.0	0.576±0.057	0.6±0.01	790±408	0.46	3.85	157±19	0.199±0.083
10.0	0.404±0.015	0.32±0.03	650±9	0.12	3.78	191±20	0.294±0.035

(a) Light scattering data from extrapolation of angles higher than 65°

(b) Apparent molecular weight values

144

4.3 VISCOSITY MEASUREMENTS

4.3.1 INTRINSIC VISCOSITY

Examples of combined Kraemer and Huggins plots for three irradiated guar gum samples are shown in Figures 4.15 to 4.17. The intrinsic viscosities quoted were obtained from the Kraemer plots and are given in Table 4.3. The variation in intrinsic viscosity [η] with radiation dose is shown in Figure 4.18 The general trends of molecular weight and intrinsic viscosity change with radiation dose are in fairly good agreement, however, it appears that there is a much larger decrease in intrinsic viscosity than molecular weight with radiation dose at the lower doses which then stabilizes and decreases again at 10.0kGy. With the intrinsic viscosity versus radiation dose plot however, there seems to be a 'plateau' in the region between 0.4kGy and 1.0kGy of the irradiated samples which then decreases as the radiation dose is increased to 2.0kGy.
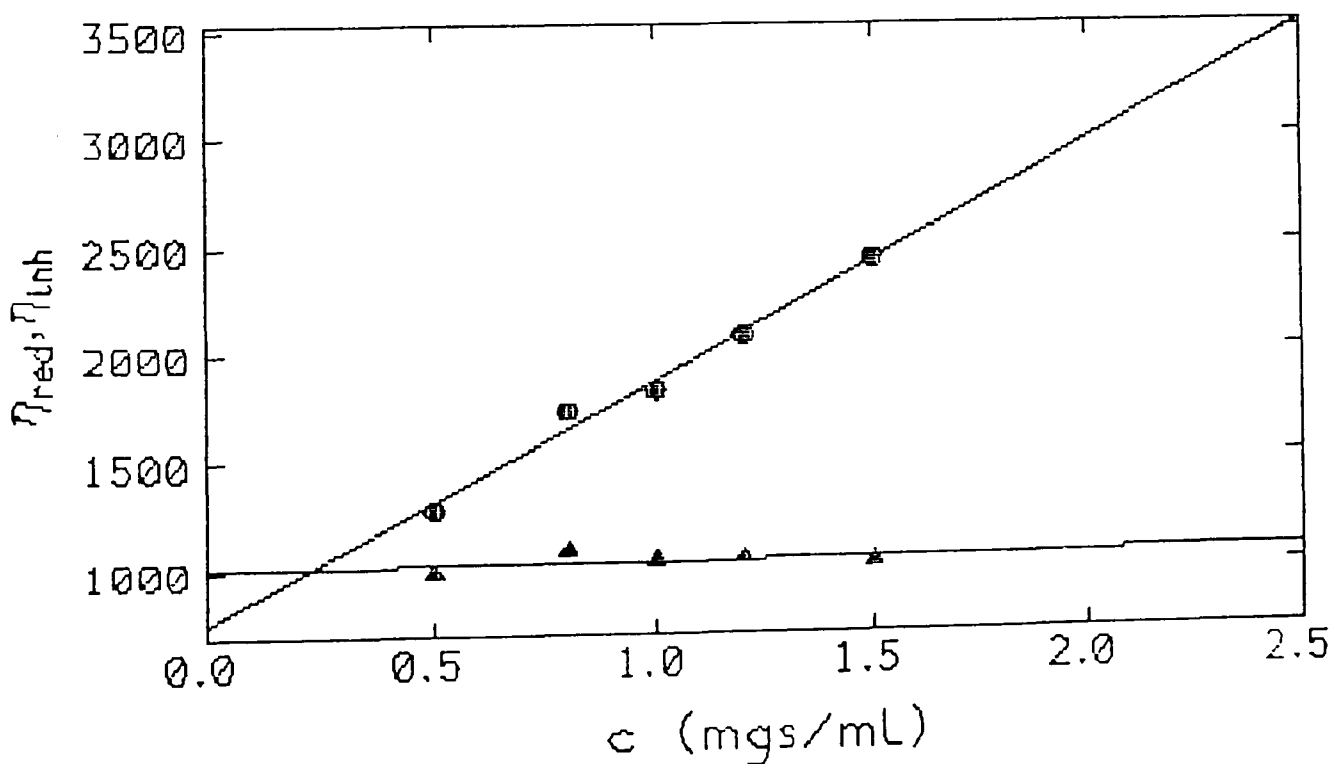
Figure 4.15: Combined Huggins and Kraemer plots for 0.1kGy sample.
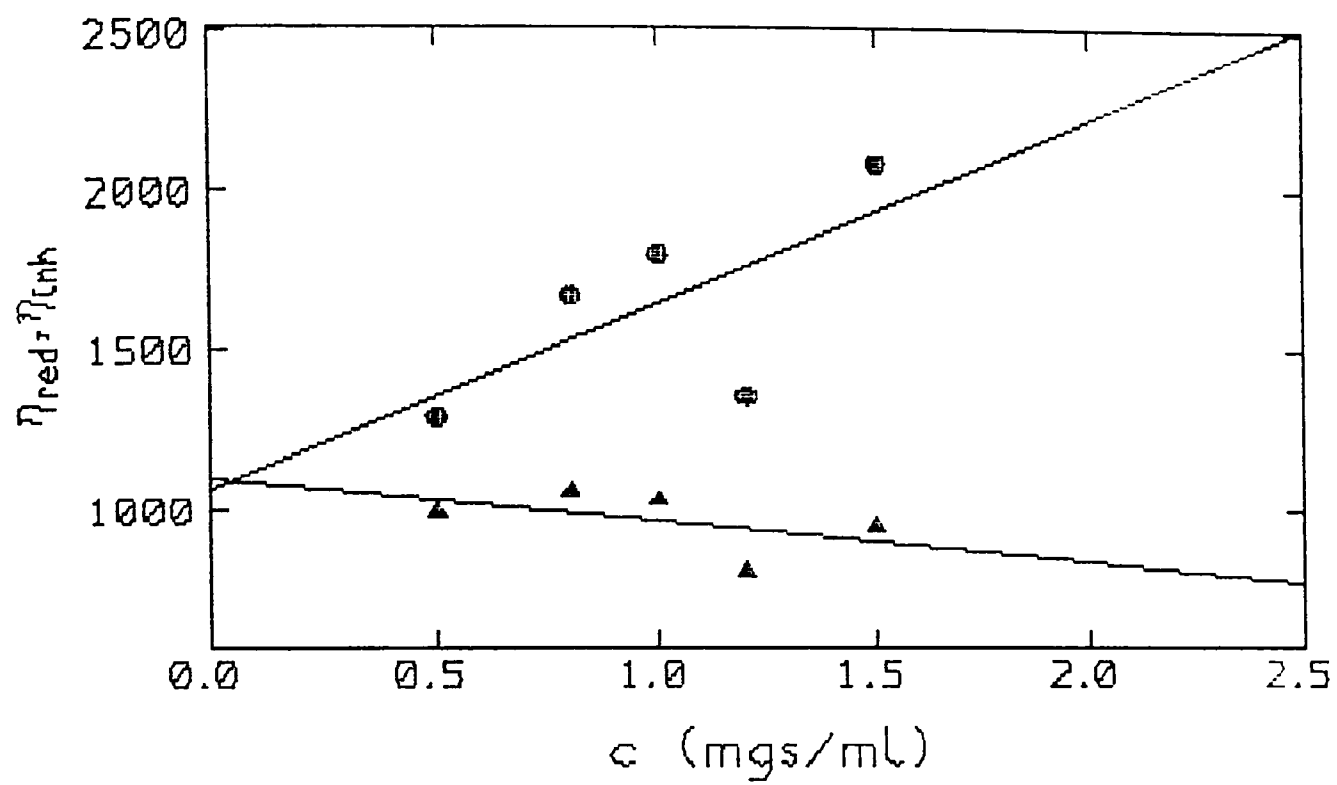
Figure 4.16: Combined Huggins and Kraemer plots for 0.2kGy sample
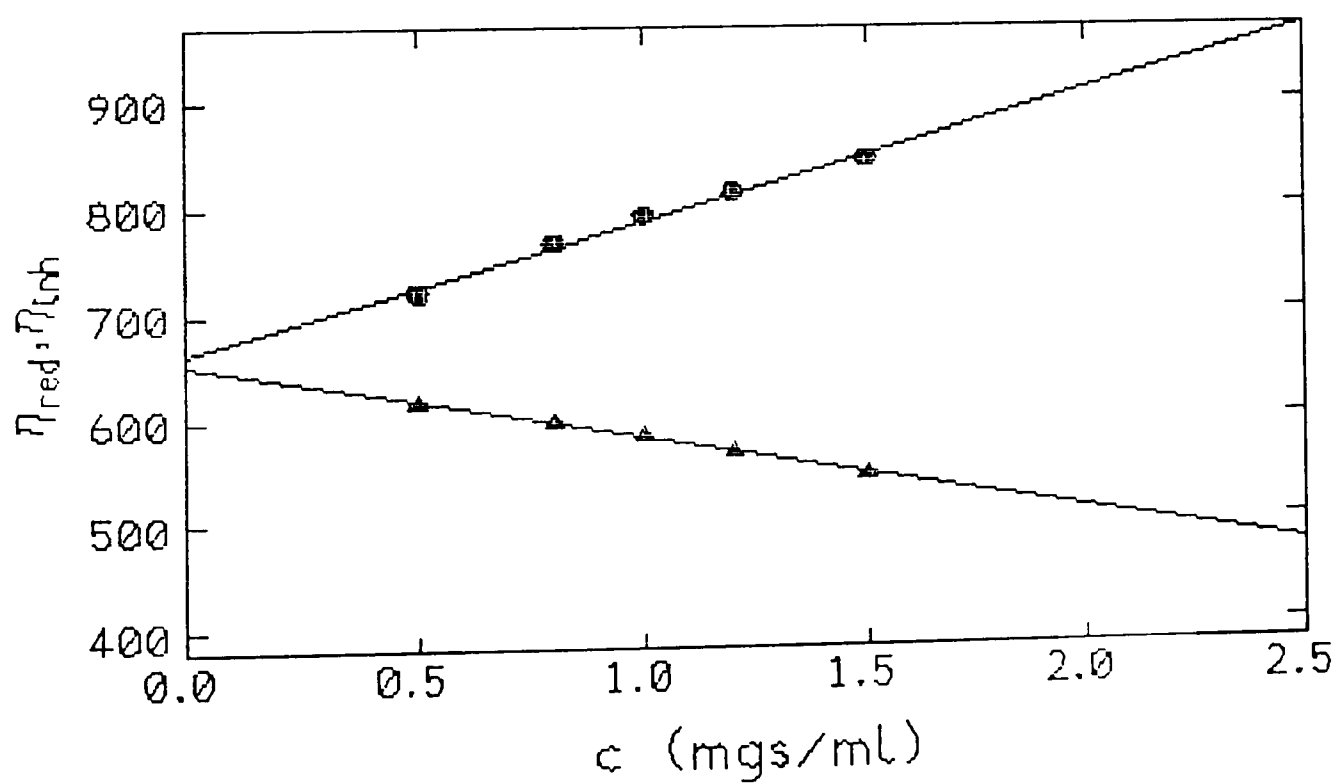
Figure 4.17: Combined Huggins and Kraemer plots for 10.0kGy sample

146
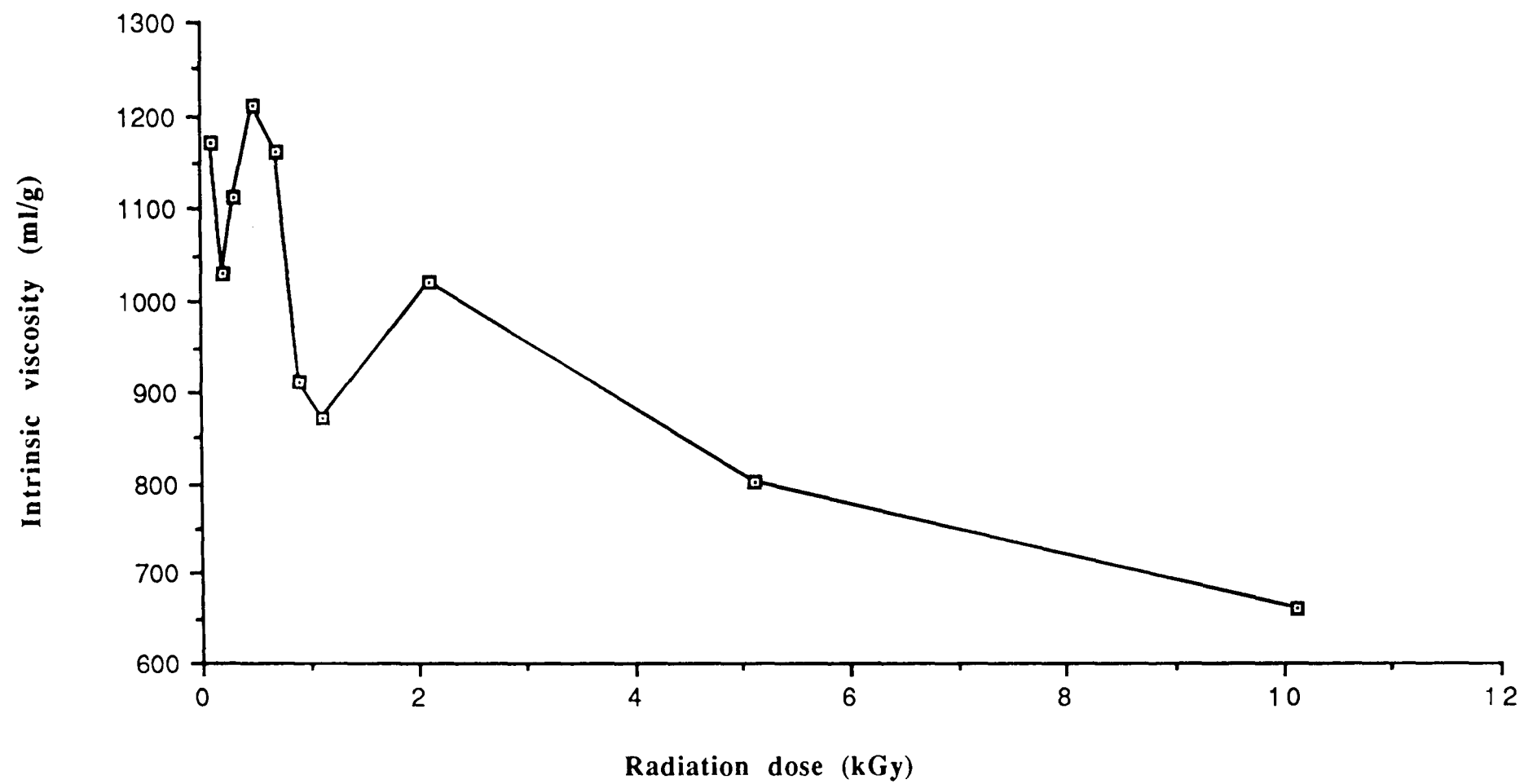
Figure 4.18: Radiation induced changes of intrinsic viscosity of control and irradiated guar gum preparations.

4.3.2 CONCENTRATED SOLUTION VISCOSITIES

Measurements of the shear rate dependence of viscosity of the concentrated solutions were obtained using a Bohlin rheometer fitted with cone and plate geometry. Examples of three flow curves are shown in Figure 4.19. The non-Newtonian behaviour of the guar solutions is evident for the samples irradiated at low doses, even at low shear rates, whereas for the 5.0 and 10.0 kGy samples the decrease in viscosity with shear rate is much more gradual in the low shear rate region. The variation of zero shear viscosity (η_0) with radiation dose is illustrated in Figure 4.20. The decrease in η_0 with radiation dose is quite sharp between 0.1 and 0.6kGy after which it decreases more gradually.
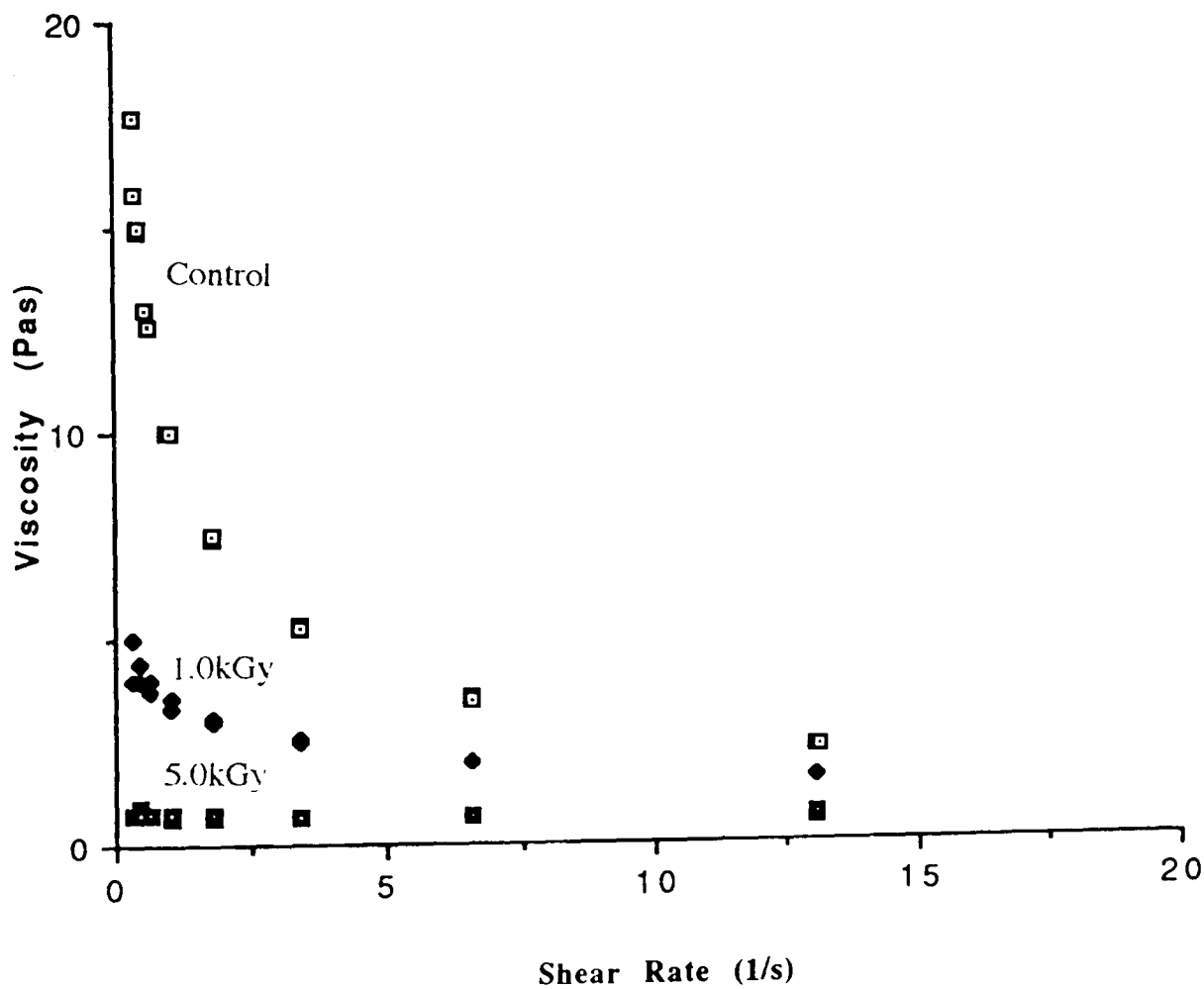
Figure 4.19: Flow curves for control and 1.0kGy and 5.0kGy irradiated samples at shear rates below 20s^{-1}

148
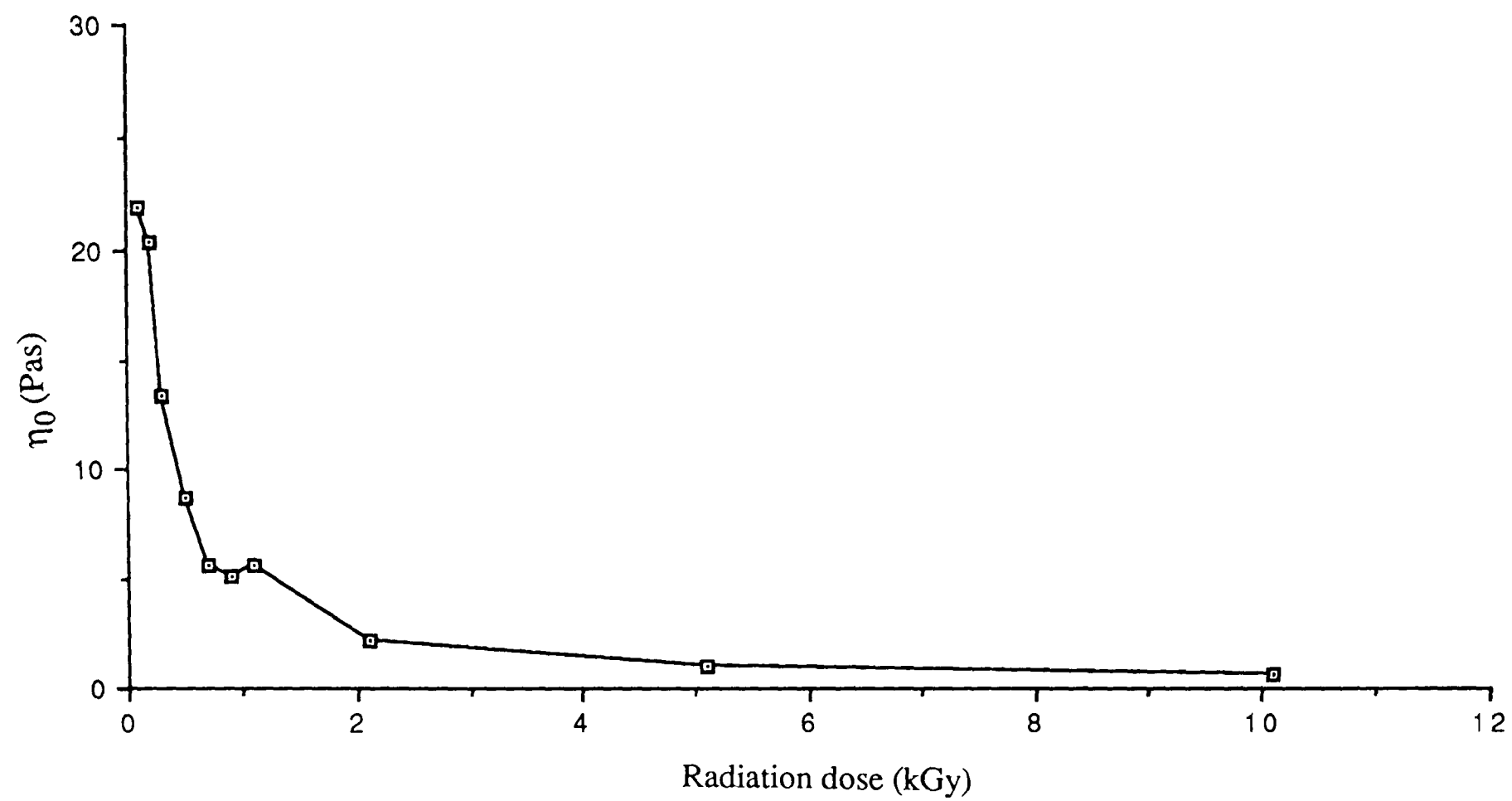
Figure 4.20: Radiation induced changes of zero shear viscosity of control and irradiated guar gum preparations.

4.4 SEDIMENTATION ANALYSIS

4.4.1 SEDIMENTATION EQUILIBRIUM

Sedimentation equilibrium studies were carried out using rotor speeds ranging from ~2000 to ~5600rpm depending on the expected molecular weight of the sample. A range of chosen rotor speeds depending on the sample were considered necessary due to the polydisperse nature of the samples. High rotor speeds could cause some of the high molecular weight material to sediment to the cell base, which would then not be included in the molecular weight averages. Loading concentrations for all samples were ~0.4mg/ml. Solute distributions were recorded as Rayleigh interference fringes and then analysed giving plots of lnJ versus ξ, M^* versus ξ and M_w versus ξ, where ξ is the normalized radial displacement $\dfrac{r^2 - a^2}{b^2 - a^2}$, where r is the radial displacement of a given point in the cell and a and b are the radial displacements at the meniscus and cell base respectively, J is the absolute concentration in terms of fringe displacement numbers and M^* versus ξ is used to get the apparent whole cell weight average molecular weight, M^0_w, as $\xi \rightarrow 1$. The plots shown in Figures 4.21 to 4.26 are for the 5.0 and 0.4kGy samples and are representative for all the samples.

Rayleigh interference fringes (an example is shown in Figure 3.4) were analysed and gave a plot of lnJ versus ξ (Figure 4.21) with a distinct upward curvature indicating that the sample was heterogeneous. The apparent whole cell weight average molecular weight, $M_{w,app}$ (600 000±10 000) was obtained from extrapolation of the M^* versus ξ plot to the cell base (ie. $\xi \rightarrow 1$) (Creeth and Harding, 1982b) (see Figure 4.22). The variation in point weight average molecular weights with radial displacement is shown in Figure 4.23.

150

Figure 4.21: Plot of lnJ versus ξ for 5.0kGy sample. Initial loading concentration = 0.4mg/ml, rotor speed = 5200rpm, temperature = 20°C

Figure 4.22: Plot of M^* versus ξ for 5.0kGy sample. Conditions as in Figure 4.21

151

Figure 4.23: Plot of M_W versus ξ for 5.0kGy sample.
Conditions as in Figure 4.21

Figure 4.24: Plot of lnJ versus ξ for 0.4kGy sample. Initial
loading concentration = 0.4mg/ml, rotor speed =
3013rpm, temperature = 20°C
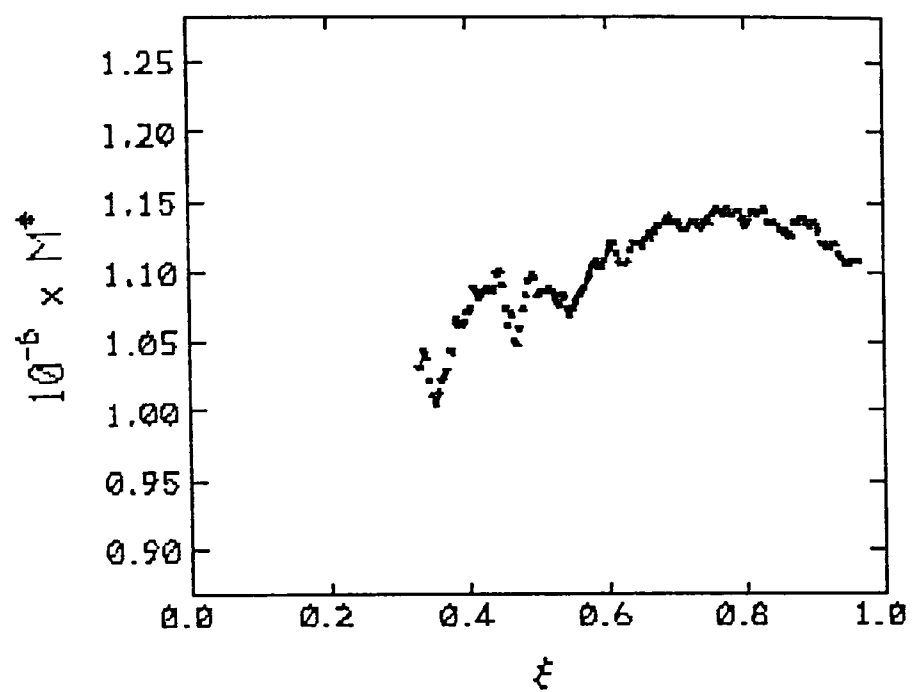
Figure 4.25: Plot of M* versus ξ for 0.4kGy sample. Conditions as in Figure 4.24
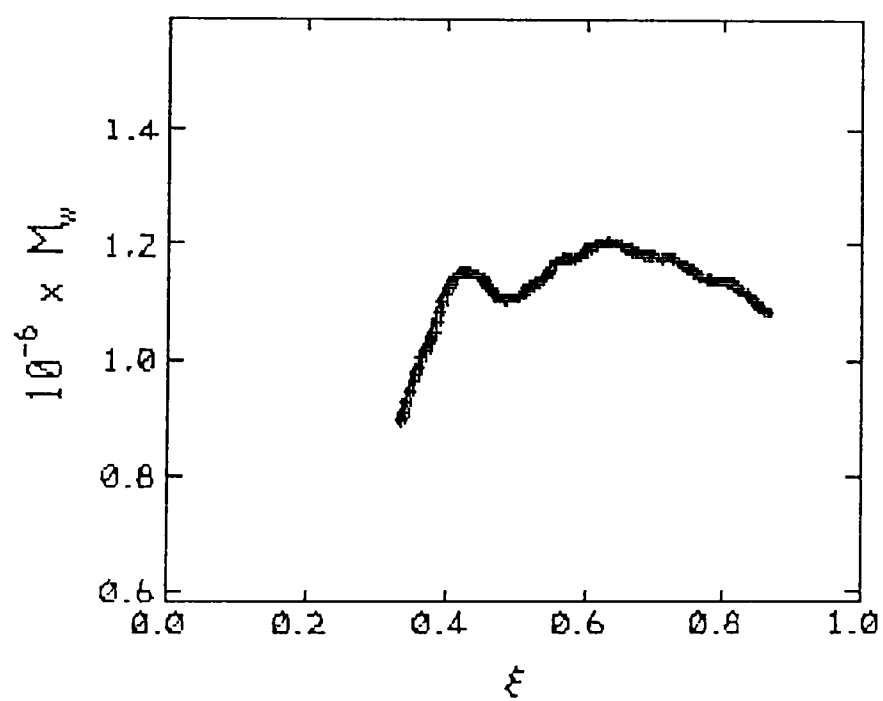
Figure 4.26: Plot of M$_w$ versus ξ for 0.4kGy sample. Conditions as in Figure 4.24

153

Information regarding the non-ideality and/or polydispersity of a macromolecular system can be obtained from the lnJ versus ξ plots. Downward curvature is indicative of a thermodynamically non-ideal system and upward curvature is due to polydispersity (see for example Harding et al, 1991b). If a system is both polydisperse and non-ideal the opposed curves may cancel, giving the appearance of a pseudo-ideal system. An example for this behaviour is shown in Figure 4.24 which was obtained from the data analysis for the 0.4kGy sample. Figures 4.25 and 4.26 give the corresponding plots of M^* versus ξ (used to get M^0_w, ie., the whole cell weight average molecular weight from $M^*(\xi\text{->}1)$) and M_w, ie., the point, or at that particular radial position local, weight average molecular weight, versus ξ. Apparent whole cell weight average molecular weight extrapolated from the M^* plot was found to be $(1.13\pm0.03)\times10^6$. Evidence for the existence of both polydispersity and non-ideal behaviour of macromolecules can be indicated by a maximum in the plot of point average molecular weight versus radial displacement (see for example, Harding, 1992). Such a maximum was evident in many of the samples such as that for the 0.4kGy sample shown in Figure 4.26.

Due to the evidence for non-ideality despite the low loading concentrations it was considered desirable to follow the concentration dependence of at least one of the irradiated (0.6kGy) samples. The ideal (ie., zero concentration) weight average molecular weight $(1.18 \pm0.01)\times10^6$ was obtained in the standard way (see Tanford, 1961) by extrapolating reciprocals of the apparent whole cell average molecular weights from the M^* plots to zero concentration (see Figure 4.27).
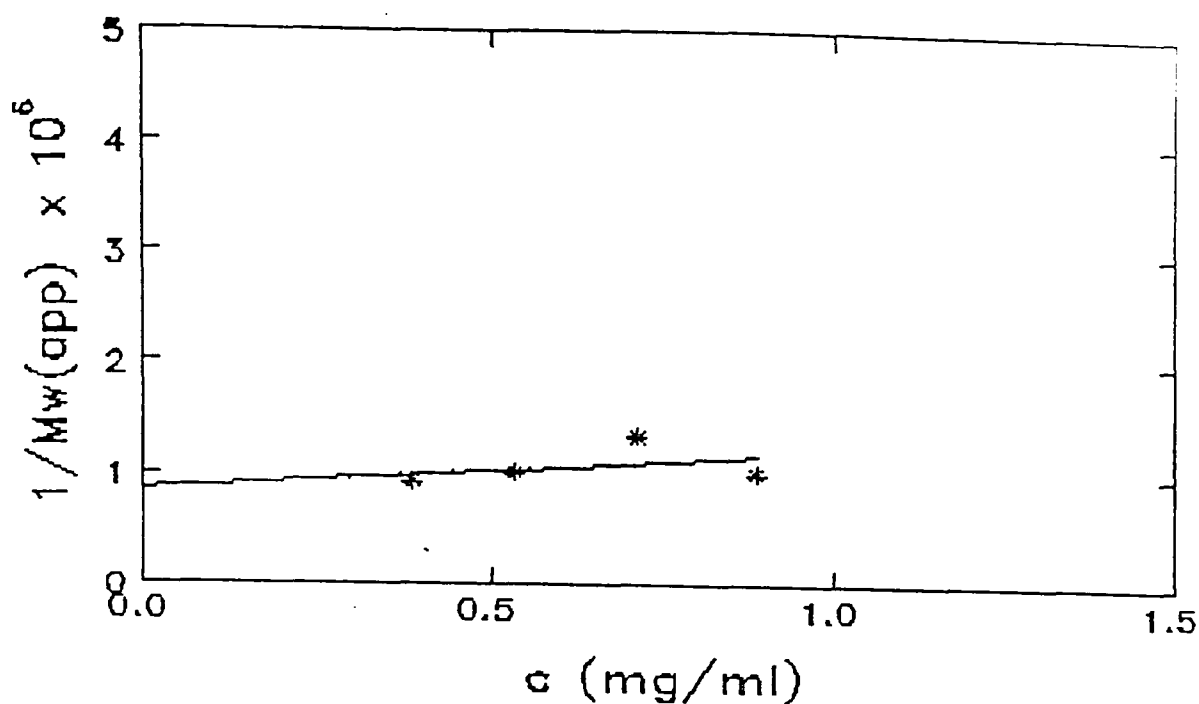
Figure: 4.27: Plot of $1/M_w$ versus concentration for 0.6kGy sample, rotor speed = 3000rpm

The rotor speeds at which the samples were run differred depending on the expected molecular size of the sample. In order to ascertain whether these differences had any real effect on the (ideal) molecular weight determined, the 0.6kGy sample was run at four different rotor speeds and apparent weight average molecular weights at each of these speeds were obtained to check if any high molecular weight components were being lost at the cell base. Sedimentation velocity studies (see below) resulted in $s^0_{20,w}$ values of 4 - 5S. It is therefore unlikely that molecules would move to the cell base at rotor speeds of 5200rpm and less, on the other hand, if too low a speed is chosen, the fringe increment between meniscus and base is too small and the precision of the molecular weight obtained is poor. Encouragingly, Table 4.4. shows no real trend although the 4000rpm result seems anomalousy high. Figures 4.28 to 4.35 give the M^* versus ξ and M_w versus ξ plots for the range of speeds used for sample 0.6kGy at loading concentrations of 0.4mg/ml. At the two lower rotor speeds non-ideality appears to be the dominating effect (Figures 4.29 and 4.31), the distribution of molecular weights is relatively

155
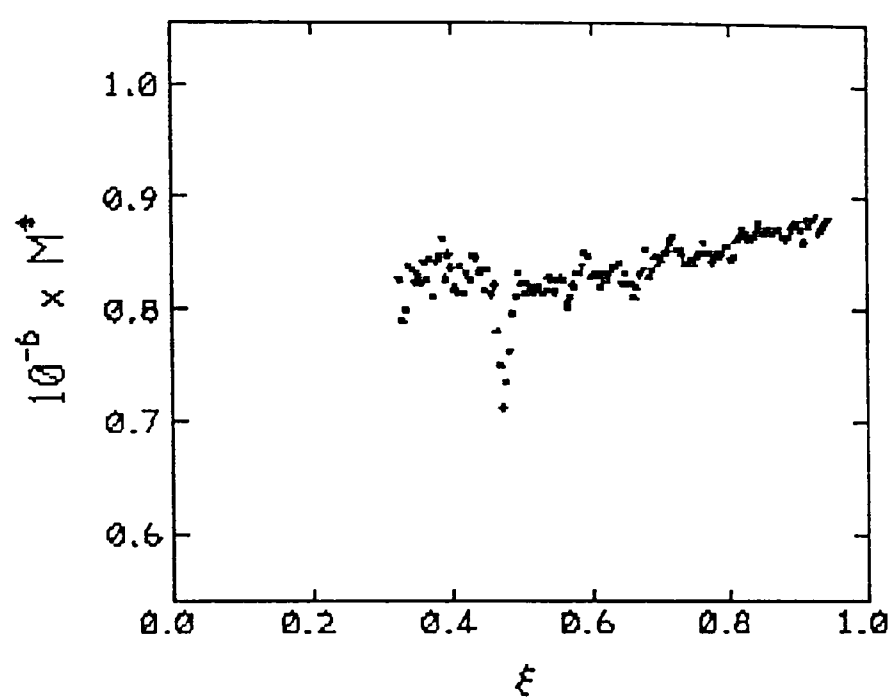
Figure 4.28: Plot of M^* versus ξ for 0.6kGy sample. Initial
loading concentration = 0.4mg/ml, rotor speed =
2000rpm, temperature = 20°C
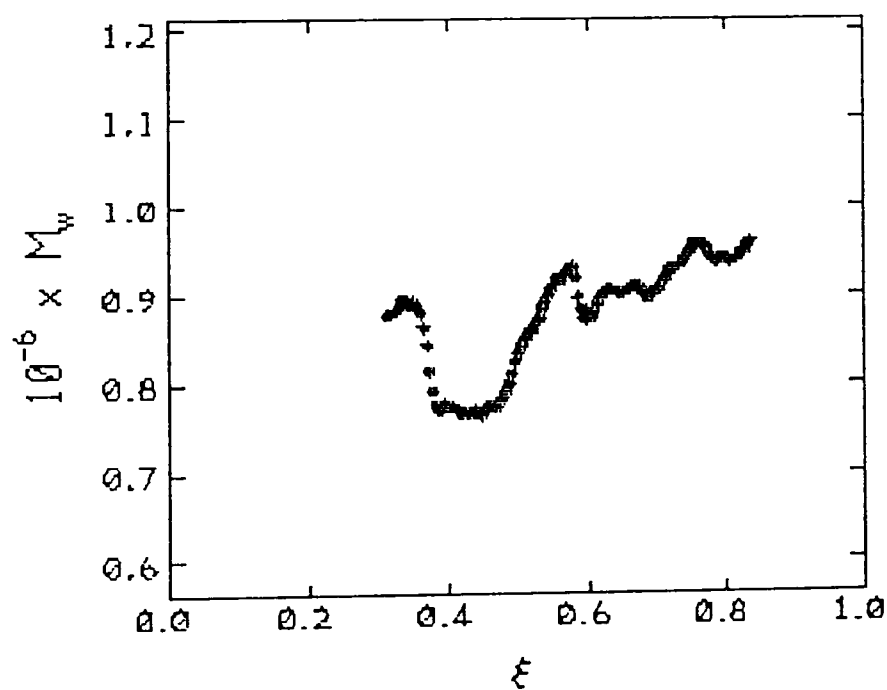
Figure 4.29: Plot of M_w versus ξ for 0.6kGy sample.
Conditions as in Figure 4.28
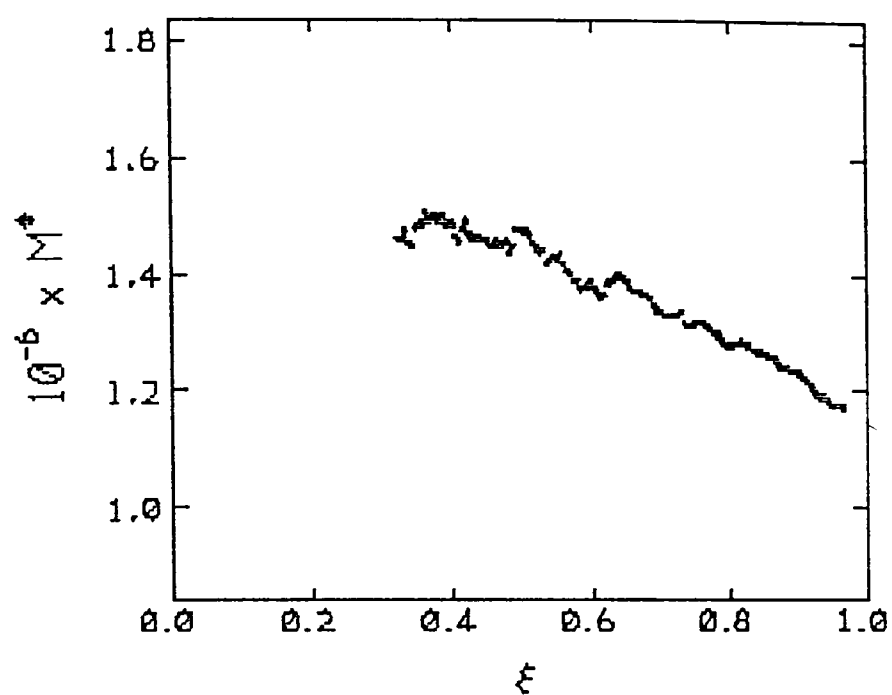
Figure 4.30: Plot of M^* versus ξ for 0.6kGy sample. Initial loading concentration = 0.4mg/ml, rotor speed = 3000rpm, temperature = 20°C
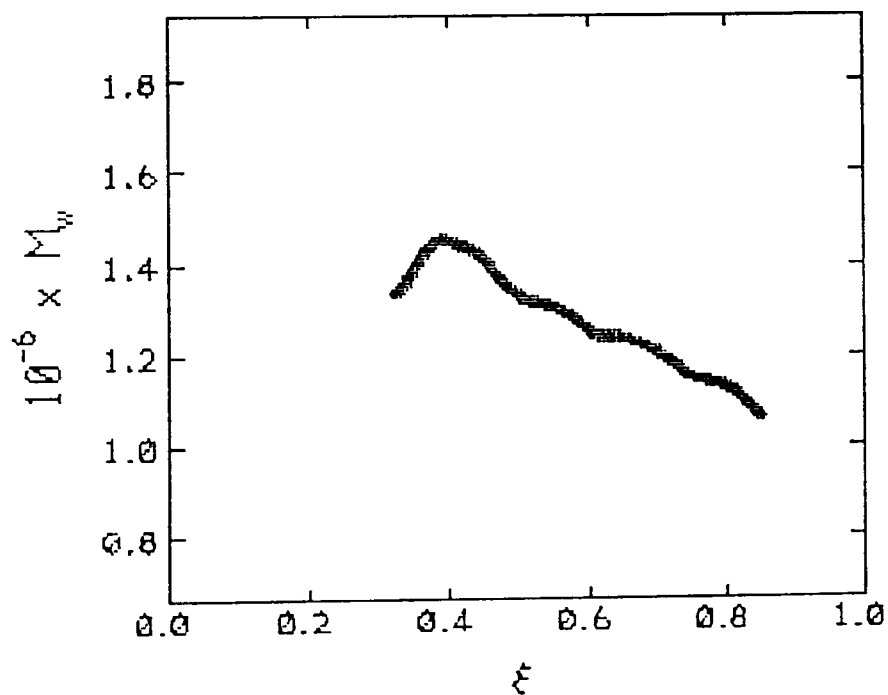
Figure 4.31: Plot of M_w versus ξ for 0.6kGy sample. Conditions as in Figure 4.30
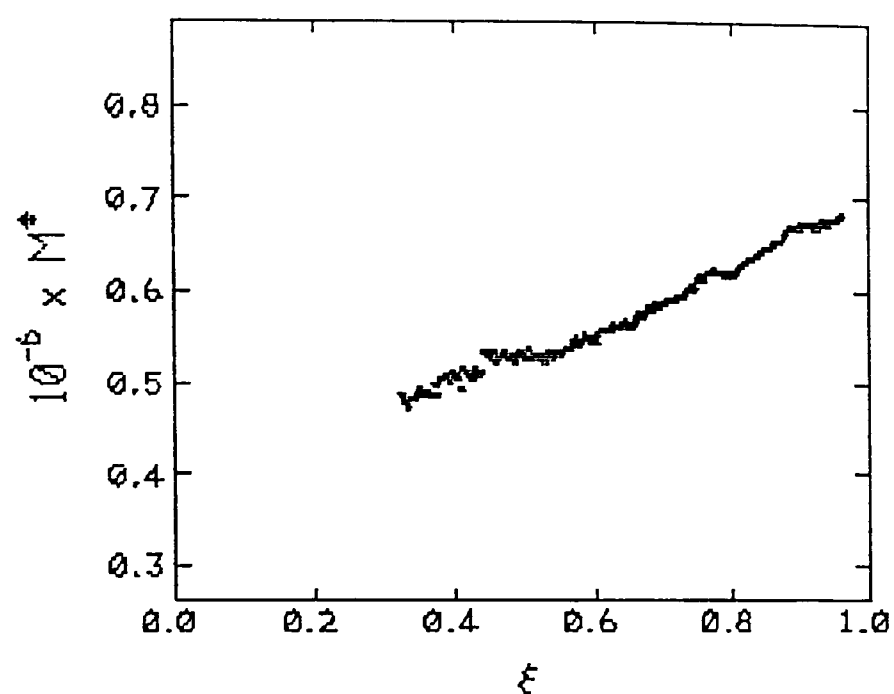
Figure 4.32: Plot of M^* versus ξ for 0.6kGy sample. Initial
loading concentration = 0.4mg/ml, rotor speed =
4000rpm, temperature = 20°C
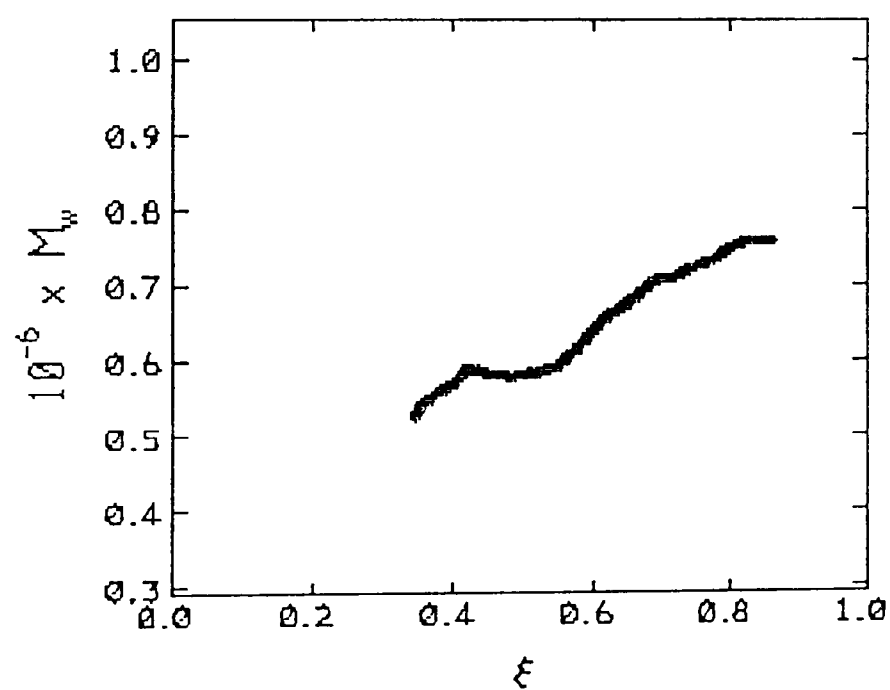
Figure 4.33: Plot of M_w versus ξ for 0.6kGy sample.
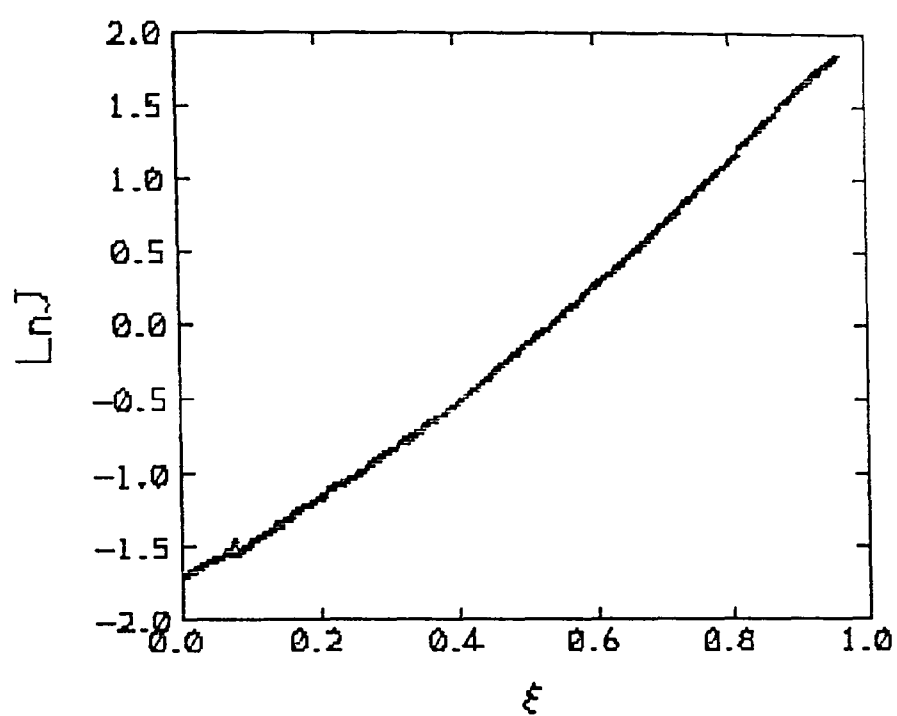Conditions as in Figure 4.32

158
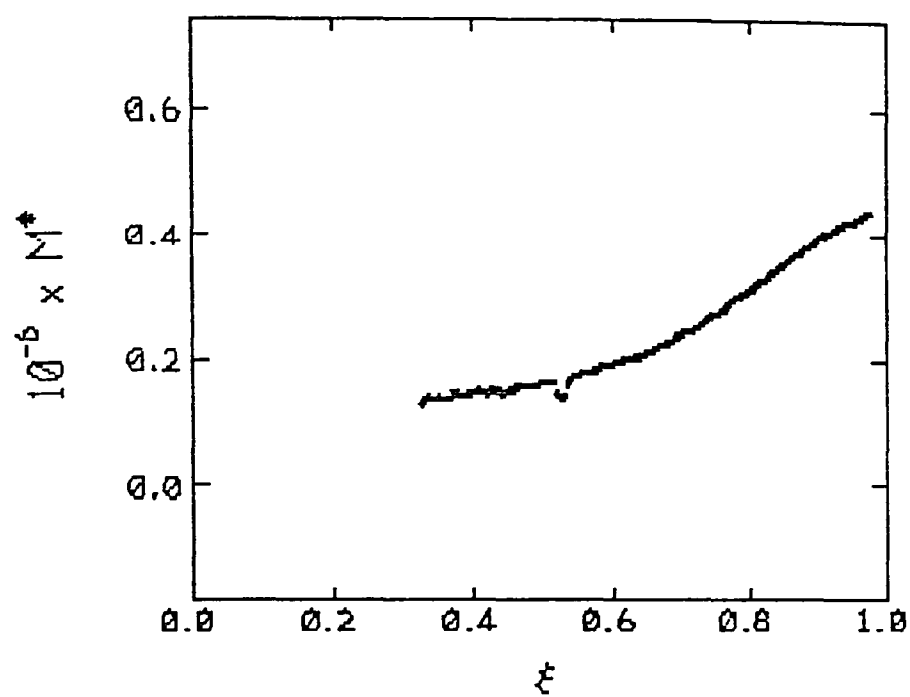
Figure 4.34: Plot of M^* versus ξ for 0.6kGy sample. Initial loading concentration = 0.4mg/ml, rotor speed = 5200rpm, temperature = 20°C
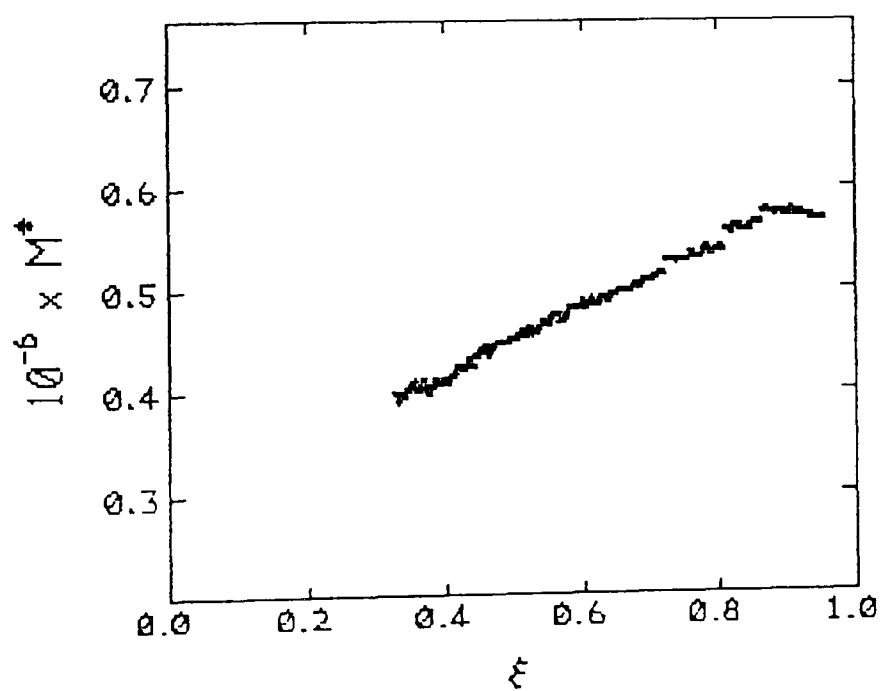

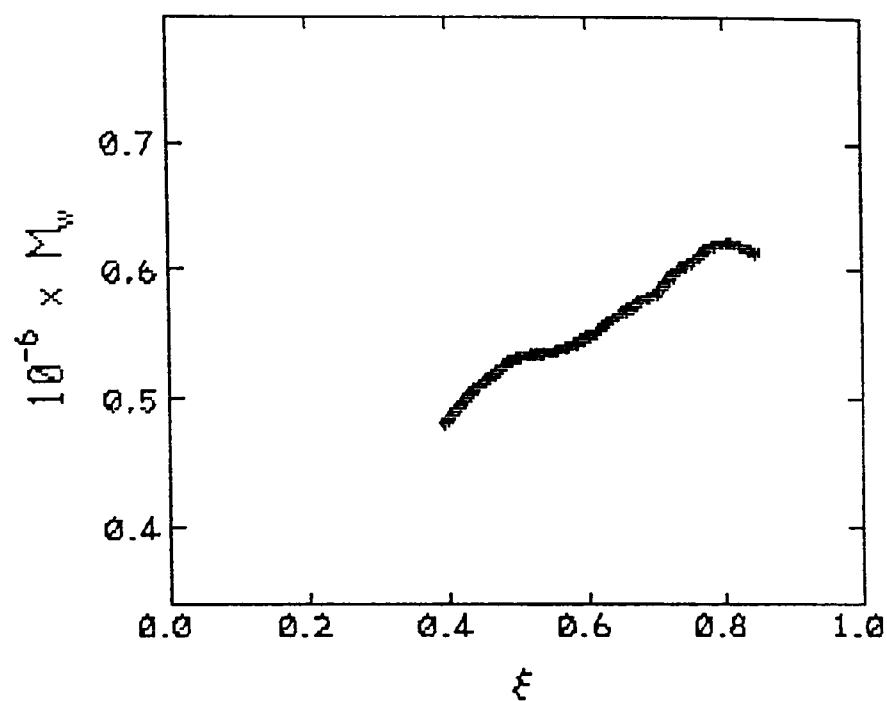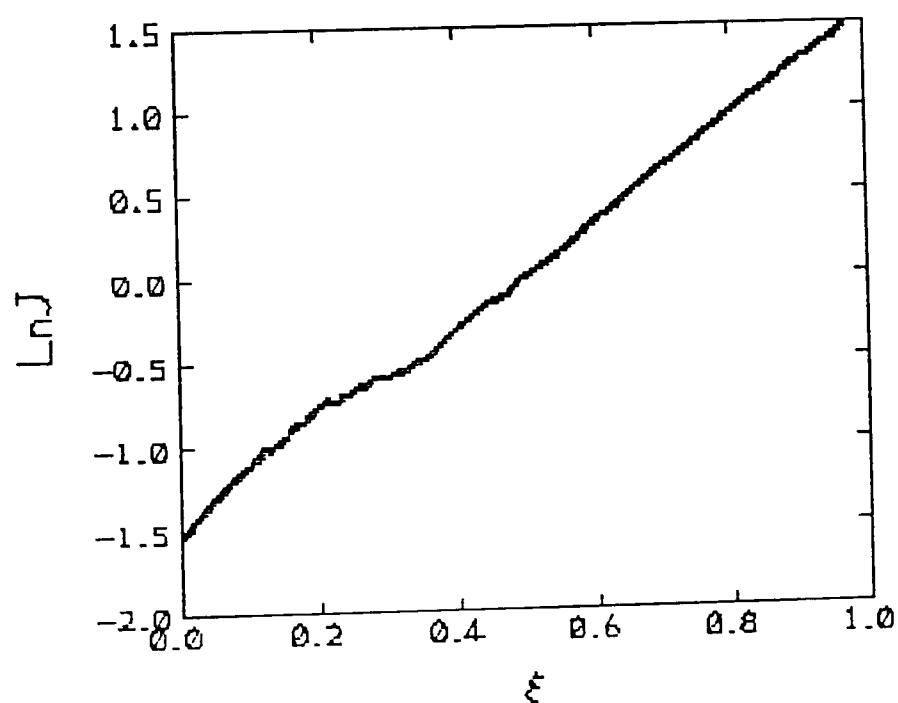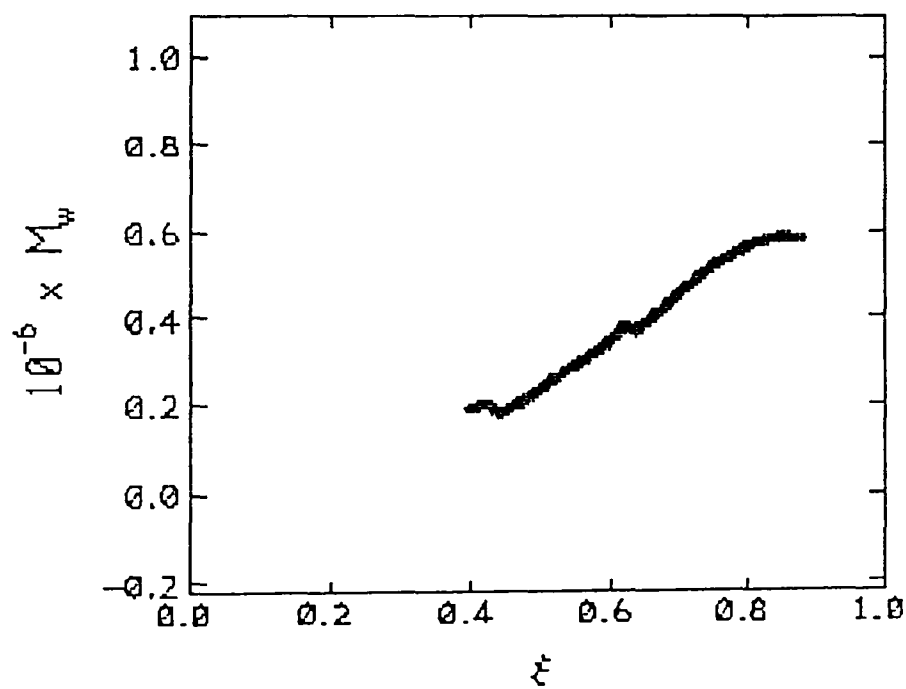**Figure 4.35**: Plot of M_w versus ξ for 0.6kGy sample. Conditions as in Figure 4.34

even throughout the cell particularly for the 2000rpm run. This is not the case for the samples run at 4000 and 5200rpm. The molecular weight distribution is much wider and dominates the M_w versus ξ plots. The consideration of these effects when analysing molecular weight data of such highly non-ideal and polydisperse materials is therefore very important and may influence the outcome of the results considerably.

Table 4.4: Variation of ideal (ie., extrapolated to zero concentration) weight average molecular weight for sample 0.6kGy

Speed (rpm)	$10^{-6}xM_w^{0}$
2000	0.71
3000	1.18
4000	2.06
5200	0.74

The apparent whole cell weight average molecular weight values from sedimentation equilibrium ultracentrifugation for all irradiated samples are shown in Table 4.3. The variation in apparent weight average molecular weight with radiation dose (Figure 4.36) appears somewhat noisy if compared with the values of molecular weight obtained from light scattering, the intrinsic viscosity and zero shear viscosity data. Nevertheless, despite the one or two noisy points (Figure 4.36) it confirms the very rapid decrease in molecular weight at the high irradiation doses. The rather noisy variation of molecular weight with radiation dose is most likely due to the uncertainties in the interpretation of the sedimentation equilibrium runs due to the dual problems of non-ideality and heterogeneity experienced with guar gum.
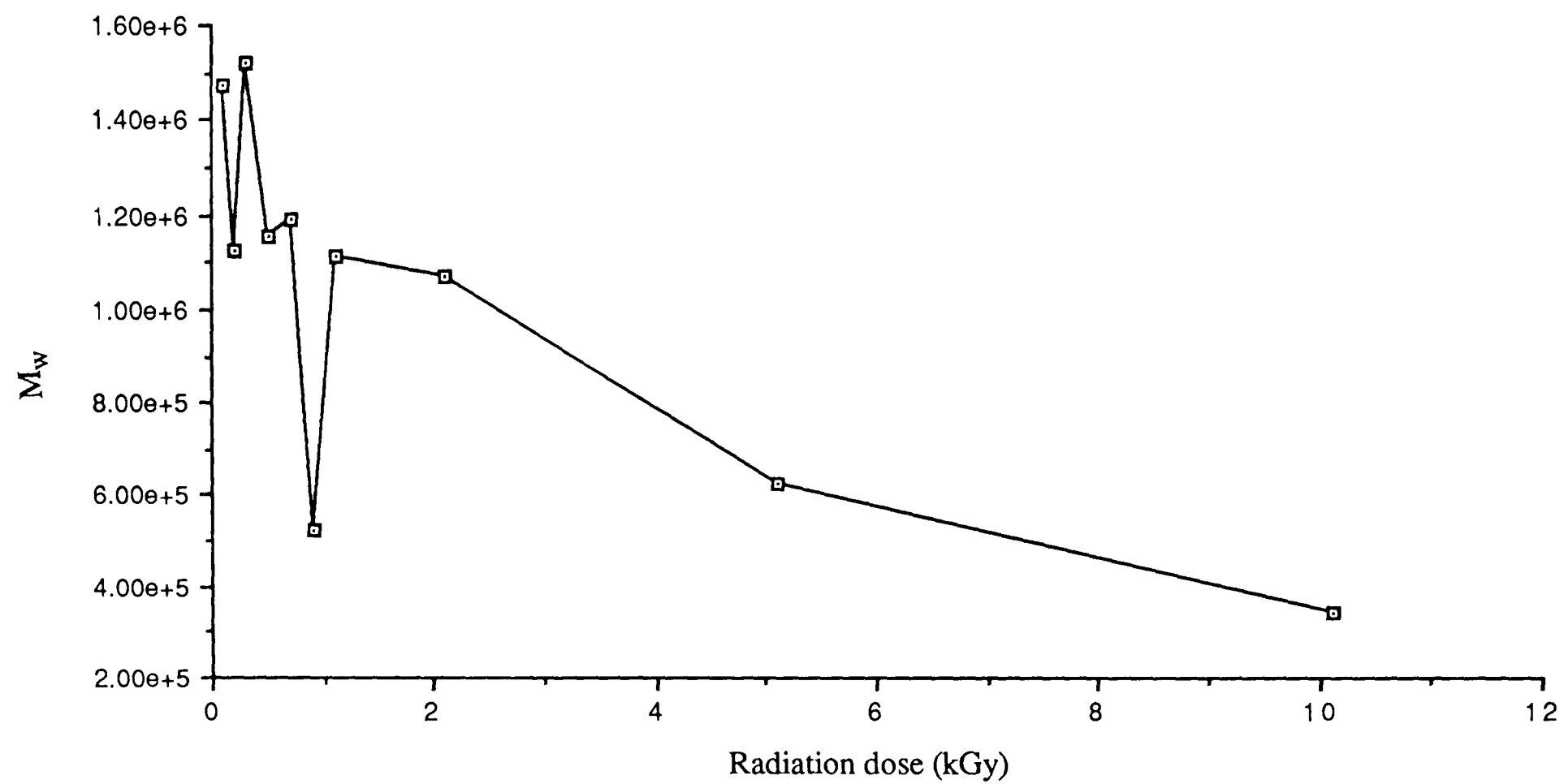
Figure 4.36: Variation in apparent whole cell weight average molecular weight with radiation dose for irradiated and control guar gum preparations

4.4.2 SEDIMENTATION VELOCITY

Sedimentation velocity experiments were carried out using an MSE Centriscan analytical ultracentrifuge fitted with a Schlieren optical system as described in Section 3.3.2.3 and two representative Schlieren boundary traces are shown in Figure 4.37 and Figure 4.38. Sedimentation coefficients were obtained using a digitising tablet and then corrected to standard conditions (ie., water at 20°C) and for radial dilution, and $s_{20,w}$ values were extrapolated to zero concentration (van Holde, 1985). Typical plots of $s_{20,w}$ versus concentration are shown in Figure 4.39 and Figure 4.40 and $s^0_{20,w}$ and k_S values are tabulated in Table 4.3.

The Schlieren traces show very sharp symmetric boundaries symptomatic of a very non-ideal system (see for example, Creeth and Knight, 1965). This self-sharpening can also obscure the effects of continuous types of polydispersity. $s^0_{20,w}$ values in the order of 4 to 5 Svedbergs for the molecular weights obtained (Table 4.3) are indicative (qualitatively) of large, highly asymmetric molecules.

Combination of the molecular weight data with sedimentation coefficients and intrinsic viscosities can be used to elucidate the conformational behaviour of macromolecules in solution using (a) the Mark-Houwink-Kuhn-Sakurada (MHKS) relationships which describe the change in intrinsic viscosity and/or sedimentation coefficient with molecular weight and (b) the Wales-van Holde ratio which describes the deviation from spheroidal conformation (Wales and van Holde, 1954).
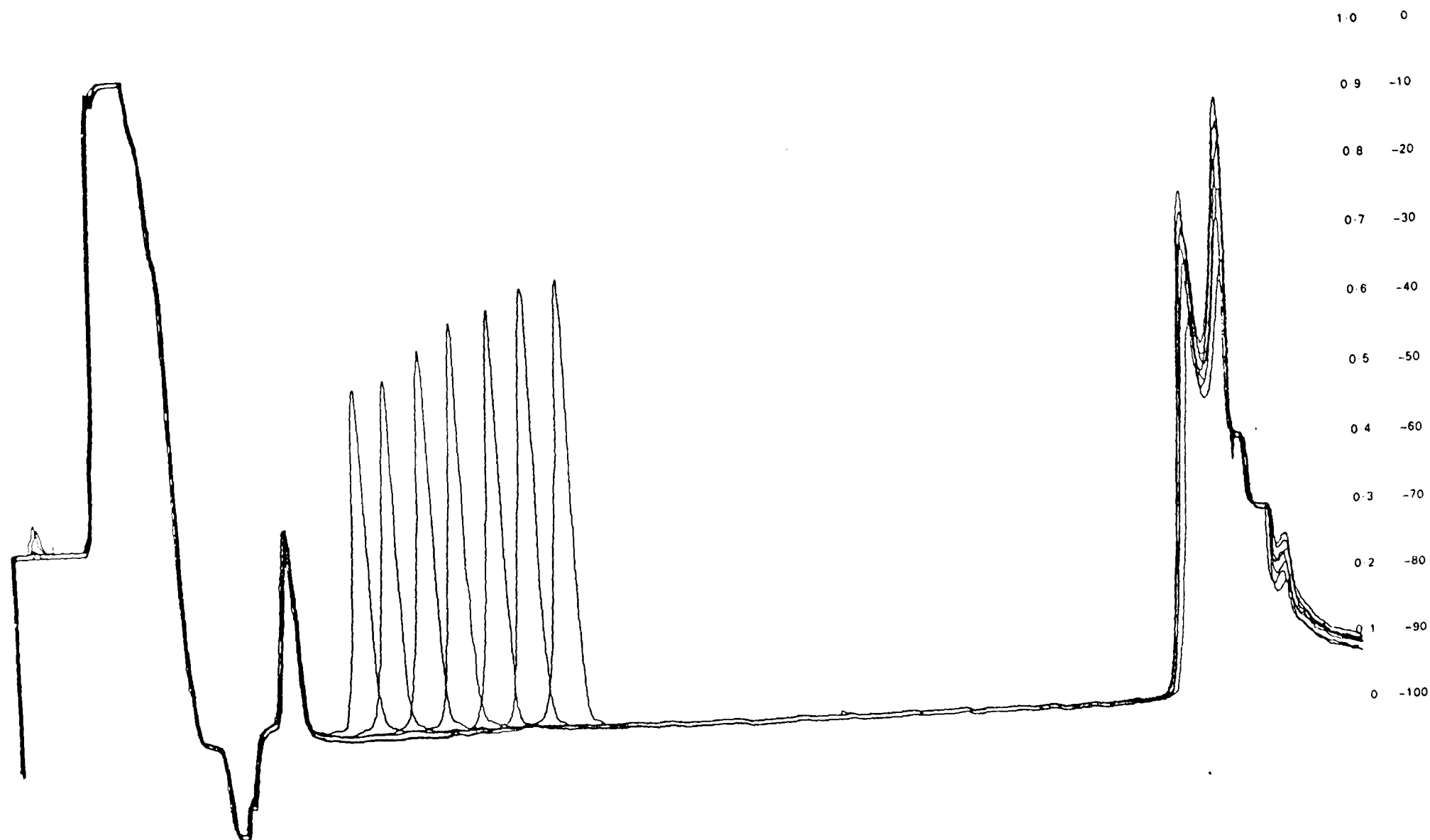
Figure 4.37: Sedimentation velocity profile (Schlieren optics) from 0.8kGy sample. Sample concentration = 1.8mg/ml, rotor speed = 47 000rpm, temperature = 20°C.

163
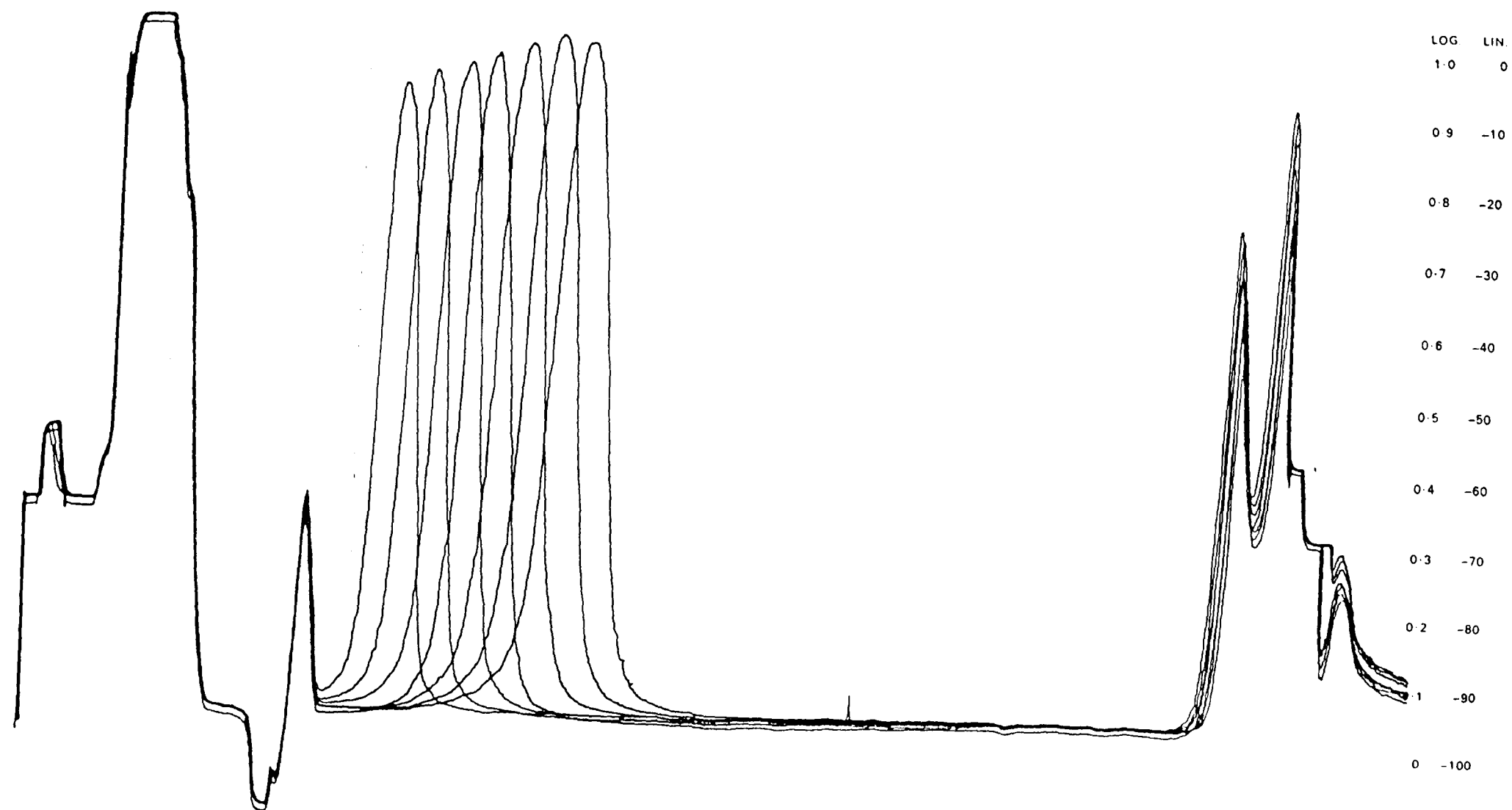
Figure 4.38: Sedimentation velocity profile (Schlieren optics) from 10.0kGy sample. Sample concentration = 1.8mg/ml, rotor speed = 47 000rpm, temperature = 20°C.
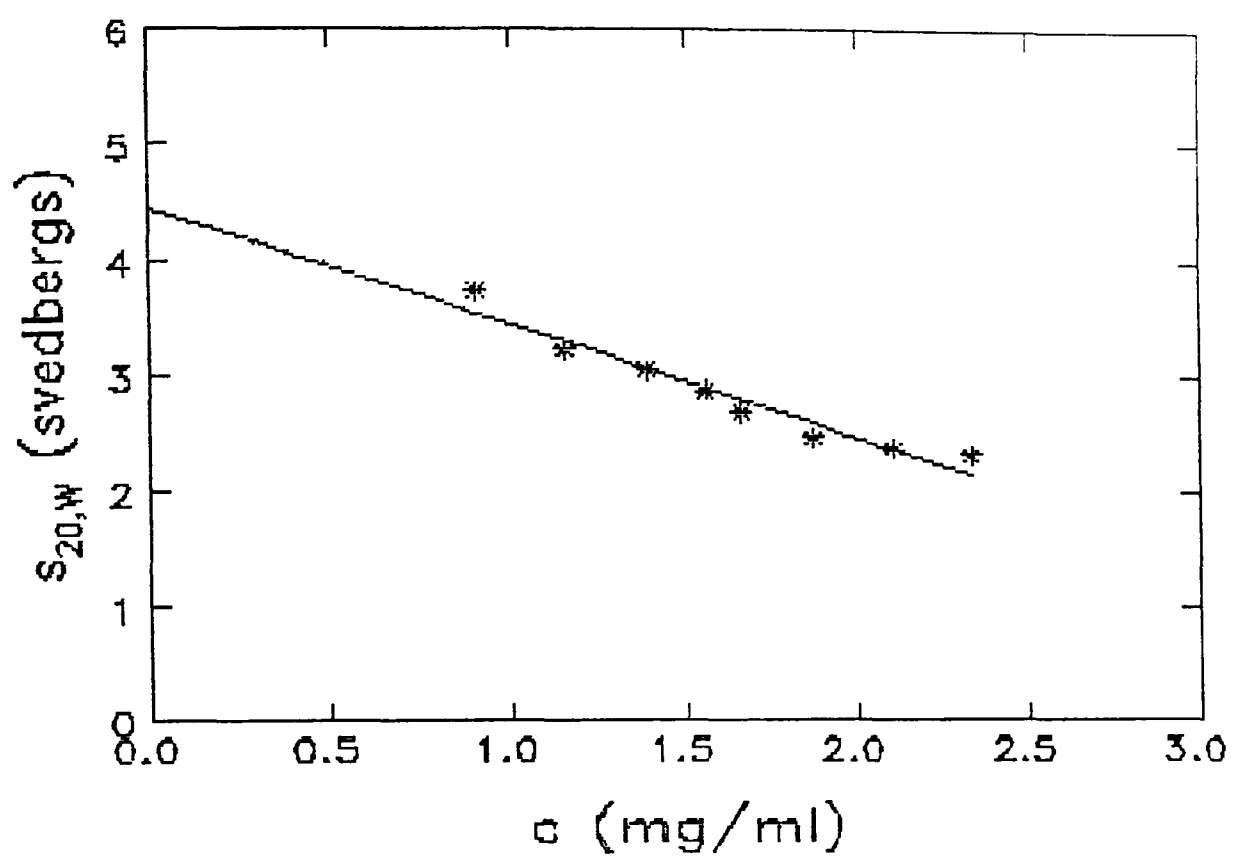
Figure 4.39: Plot of $s_{20,w}$ versus concentration for 0.8kGy sample
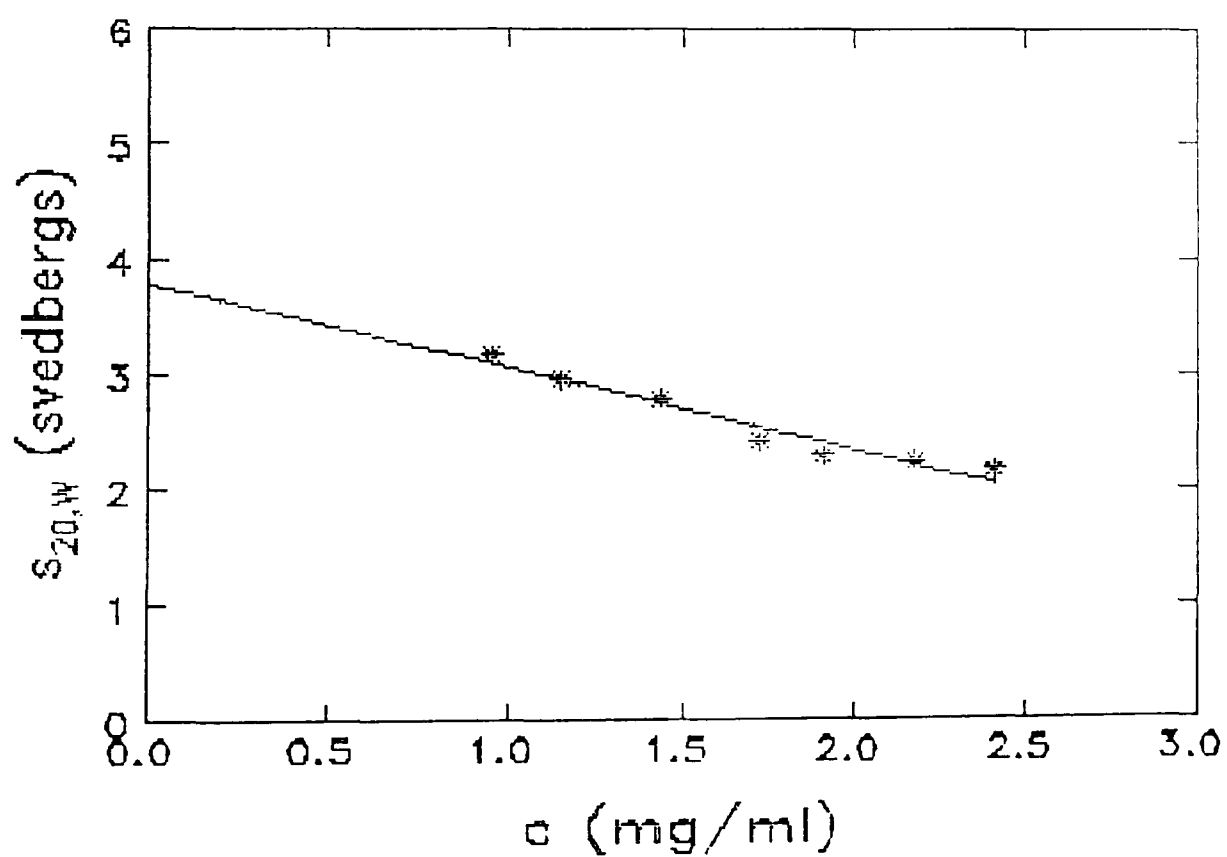
Figure 4.40: Plot of $s_{20,w}$ versus concentration for 10.0kGy sample

The MHKS expressions for intrinsic viscosity and sedimentation coefficient respectively are (see for example, Harding et al, 1991b)

$$[\eta] = K'M^a$$

and

$$s^0_{20,w} = K''M^b$$

The parameters a and/or b give information regarding the chain rigidity of the polymer and may aid in defining the solution conformation of macromolecules. Values for a (or b) are obtained from double logarithmic plots of $[\eta]$ (or $s^0_{20,w}$) versus molecular weight. A schematic description of the variation in a (and b) with changing conformation is conveniently represented by Haug's triangle (Smidsrod and Andresen, 1979; see Figure 4.41) and values are quoted in Table 4.5 (see for example, Harding et al, 1991b).

Table 4.5: MHKS coefficients for different conformations from intrinsic viscosity and sedimentation velocity measurements (from Harding et al, 1991b)

Configuration	MHKS a coefficient	MHKS b coefficient
Rod	1.8	0.15
Random coil (good solvent)	0.8	0.4
(theta solvent)	0.5	0.5
Compact sphere	0.0	0.667

Compact Sphere

a = 0.0   b = 0.667

Random Coil

a = 0.5 - 0.8   b = 0.4 - 0.5

Rigid Rod

a = 1.8   b = 0.15
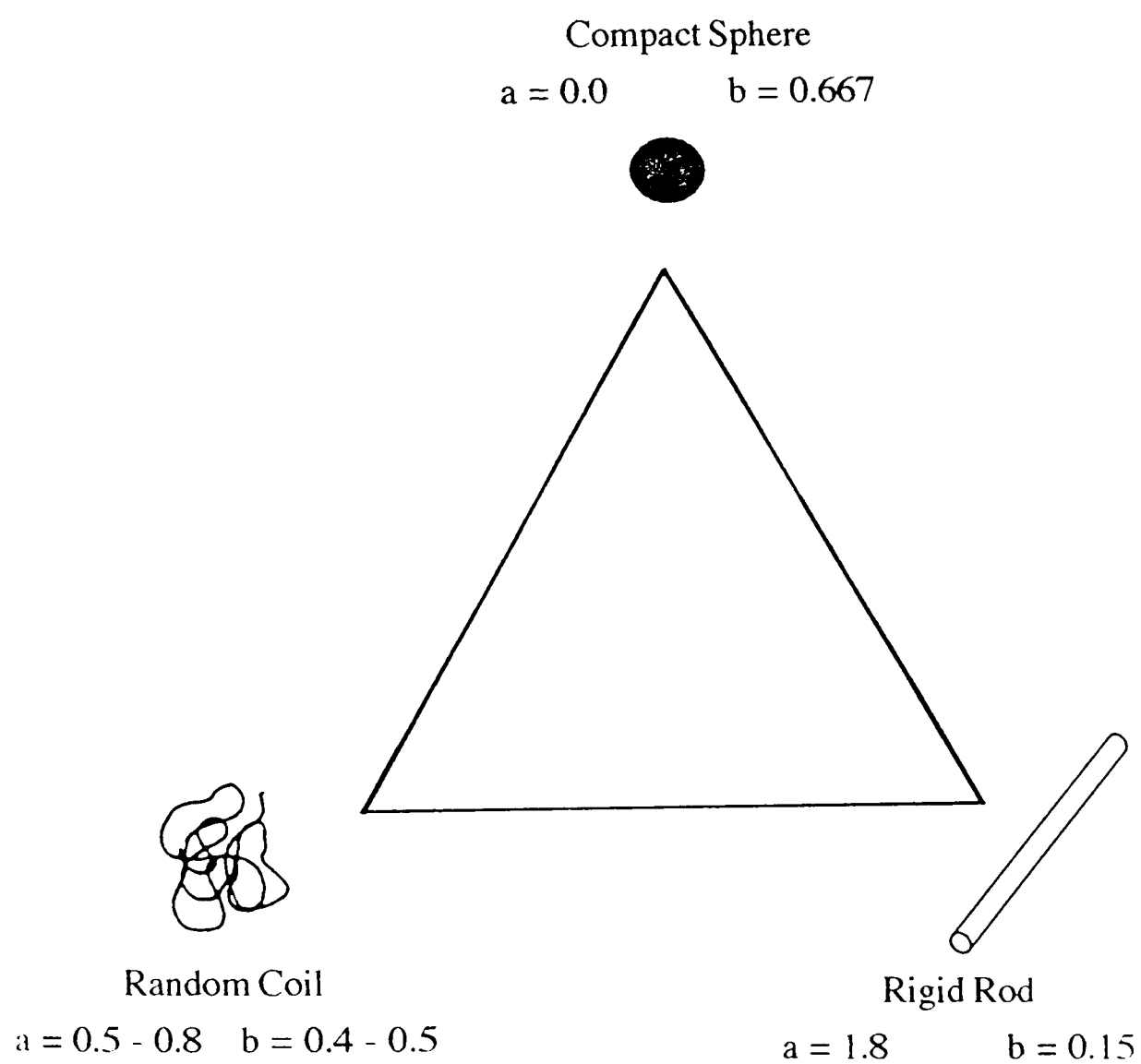
Figure 4.41: The 'Haug Triangle' representation of macromolecular gross
solution conformation (from Smidsrod and Andresen, 1979)

Plots of intrinsic viscosity versus molecular weight were obtained for the different sets of molecular weights from the different extrapolations of the angular dependences from light scattering experiments (Figure 4.42 to 4.44). None of the data give a good linear fit, however, the values from the extrapolation at the higher angles gave the best (albeit low) correlation and a value for a of 0.603 which is consistent with the well established model for the guar gum solution conformation (see for example, Robinson et al, 1982), namely an extended random coil. Our value for a is lower than the literature values, ie., a = 0.723 (Robinson et al, 1982), a = 0.98 (Doublier and Launay, 1981), a = 0.641 (Sharman et al, 1978) but it still fits in well with the random coil model for guar.

The coefficients from both other extrapolations are not consistent with any of the conformational models. This was the major factor in deciding to ignore the lower angles in the Debye plots. However, it is important to realize that the supramolecular portion of the guar sample has not been included in any further considerations and that for a full characterization of the material it may be necessary to obtain molecular weights from light scattering experiments where the angular dependence has been taken into account by calculating a fit which takes all the conformations believed to be present in the solution into account (Dautzenberg, 1992).

The MHKS plot of sedimentation coefficient versus molecular weight is shown in Figure 4.45 and a value of 0.221 is obtained for the coefficient b. Although this value does not correlate directly with any of the predicted values for a random coil, rigid rod or compact sphere, it lies between a rod and a random coil conformation on Haug's triangle (see Figure 4.41) and is therefore in very good agreement with a predicted extended random coil conformation for guar gum.

168
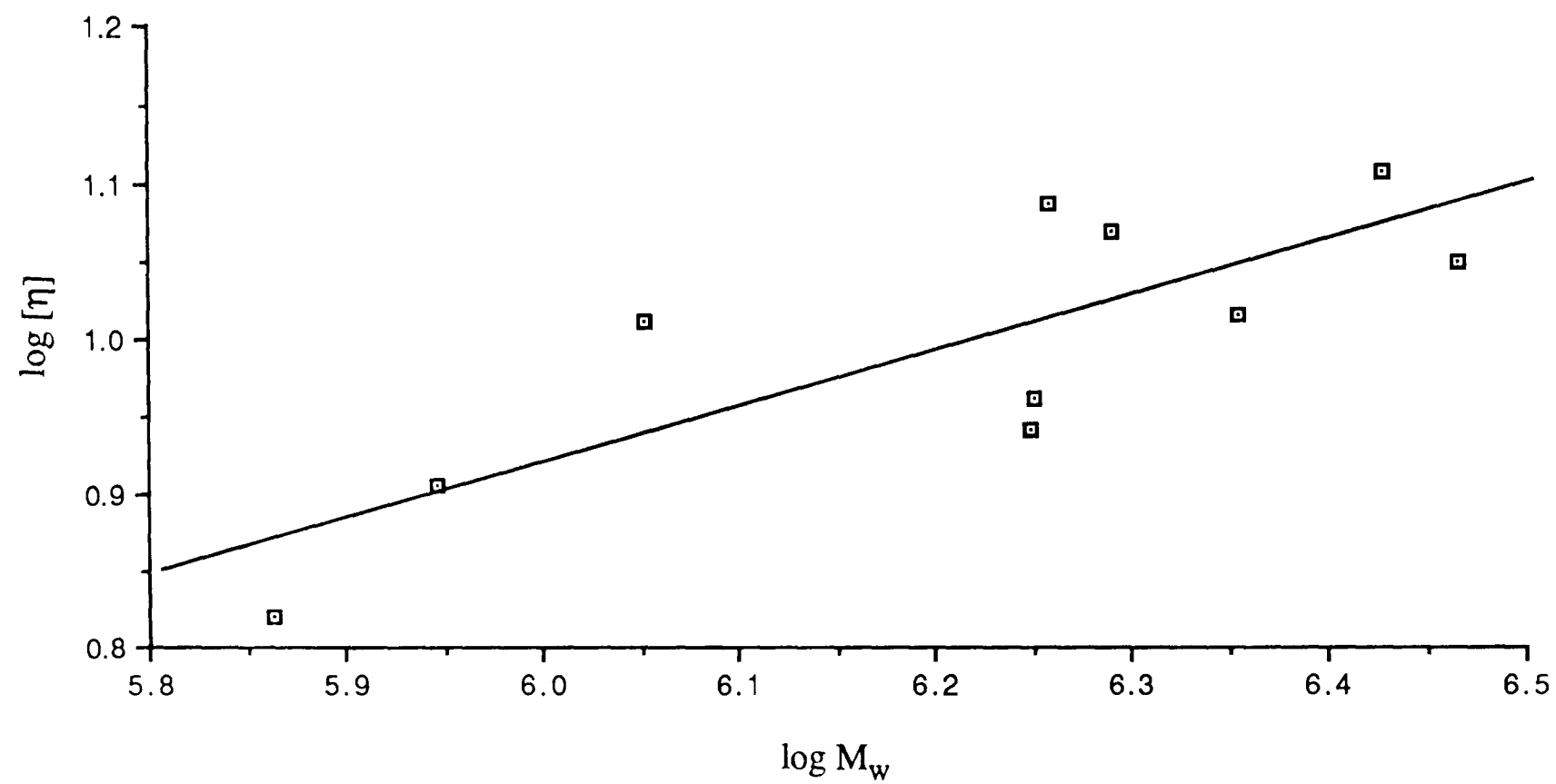
Figure 4.42: Double-log plot of intrinsic viscosity versus molecular weight (from SEC/MALLS using 1st order fit through all useable angles)
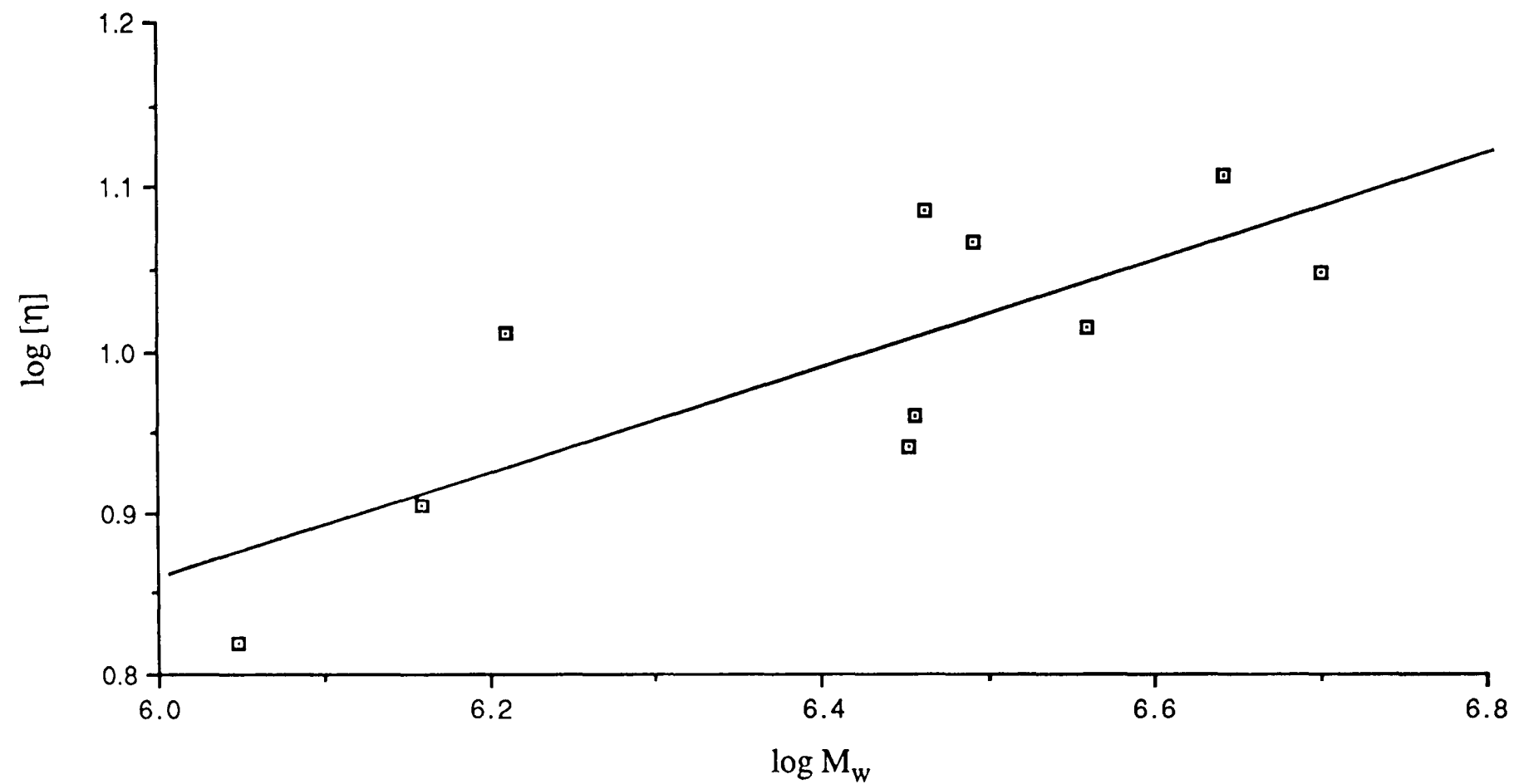
Figure 4.43: Double-log plot of intrinsic viscosity versus molecular weight (from SEC/MALLS using 2nd order fit through all useable angles)
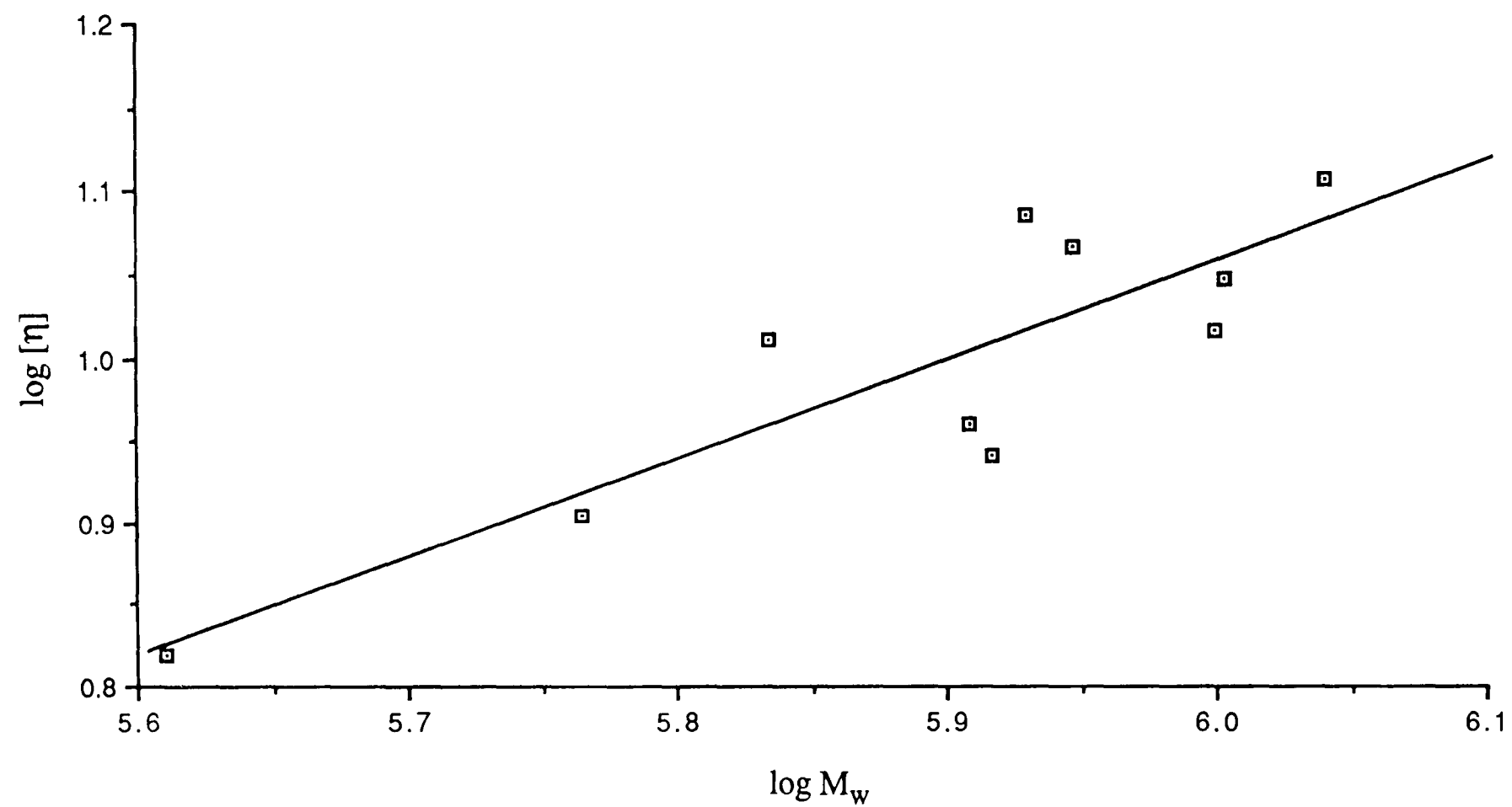
Figure 4.44: Double-log plot of intrinsic viscosity versus molecular weight (from SEC/MALLS using 1st order fit through angles at and above 65°)

In order to obtain some further indication as to the gross conformation via the Wales-van Holde ratio, values of $k_s/[\eta]$ were calculated for all the samples studied and are shown in Table 4.3. Empirically, $k_s/[\eta]$ values have been found to be near 1.6 for spheres and much lower for more extended conformations. The values obtained for the irradiated guar gum samples range from 0.14 to 0.32 which means they are all consistent with an extended conformation (see Lavrenko et al, 1992 and references cited therein).

The concentration dependence of zero shear rate viscosity is commonly plotted using double logarithmic plots of η_0 versus $c[\eta]$ (the coil overlap parameter). A master curve was established by Morris et al (1981), and Robinson et al (1982) used the η_0 versus $c[\eta]$ plot to demonstrate the coil overlap dependence of zero shear rate viscosity for their commercial guar samples. The data obtained for the irradiated guar gum samples are added to this graph (see Figure 4.45 and are found to be in good agreement with the Robinson et al (1982) data.
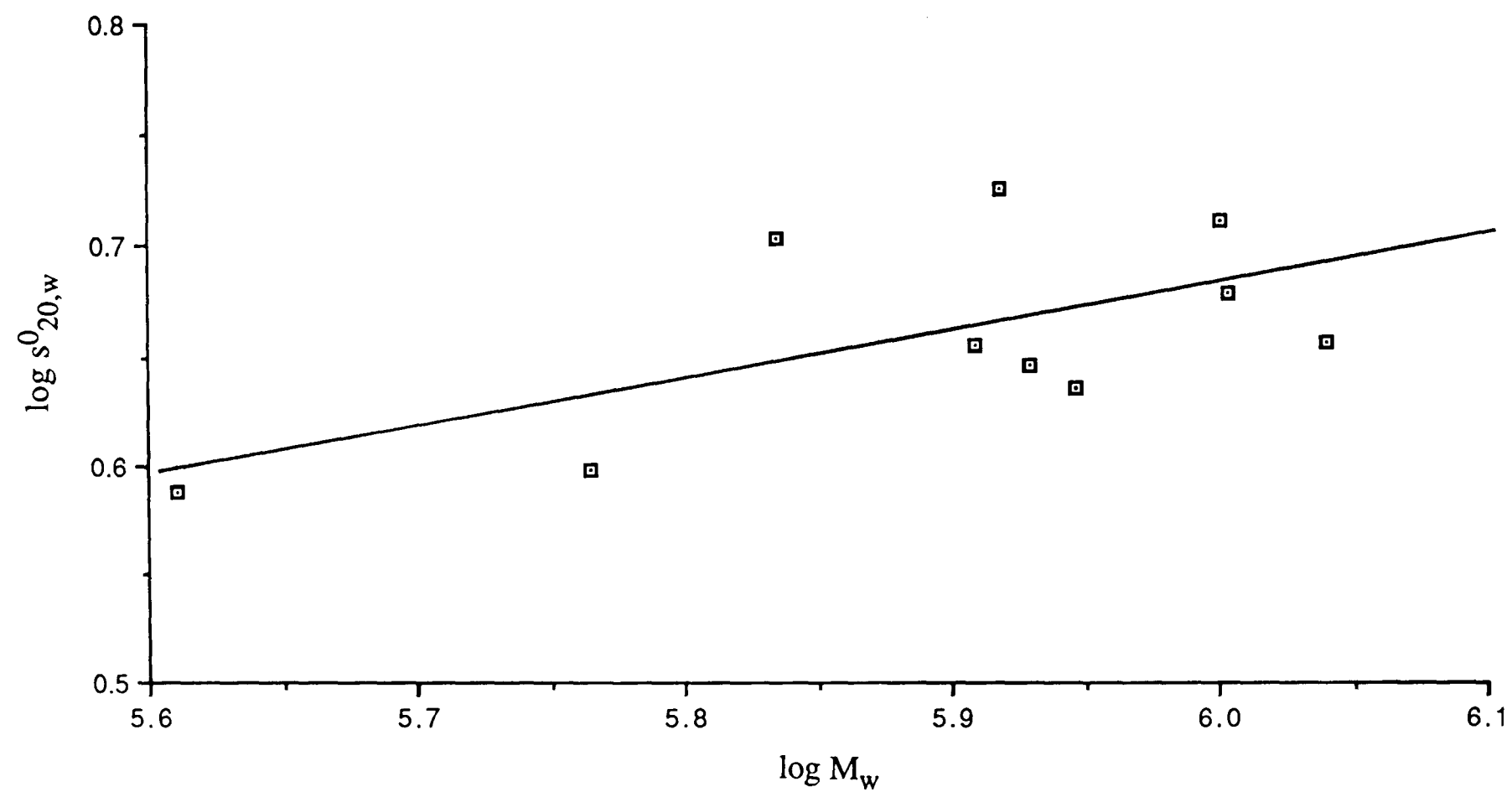
Figure 4.45: Double-log plot of $s^0_{20,w}$ versus molecular weight (from SEC/MALLS using 1st order fit through angles at and above 65°)
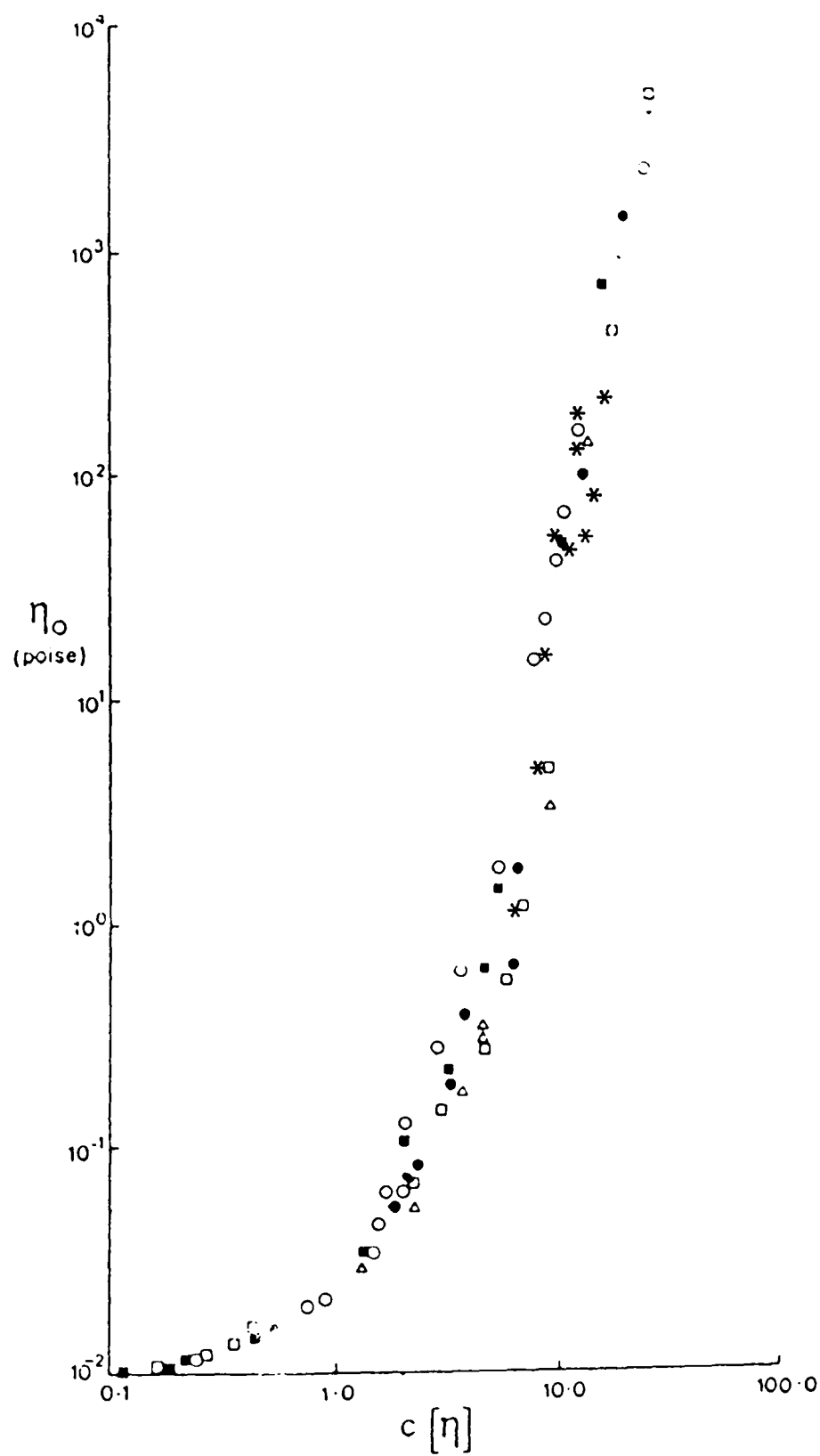
Figure 4.46: Double logarithmic plot of zero shear viscosity (η_0) versus coil overlap parameter c[η]. (Reproduced from Robinson et al. 1982). Own data marked (*)

The irradiated guar gum samples were investigated using a variety of techniques and the results obtained from these different techniques all showed very similar trends. An increase in radiation dose causes a decrease in molecular weight and a decrease in viscosity. However, the interpretation of results was not always found to be easy due to the nature of the material investigated.

Polydispersity was found to be a major problem in the interpretation of the SEC/MALLS data. Molecules with uniform conformation but different molecular weight are separated by SEC columns of the appropriate separation range. Differences in conformation are not so easily recognized - a high molecular weight molecule of spherical conformation may easily co-elute with a molecule in a more extended conformation (eg. a random coil) of lower molecular weight. Light scattering measurements then become subject to angular dependencies which cannot be attributed to one definite origin. The resulting molecular weight values are therefore uncertain to some degree and information regarding the radius of gyration is lost, as this value is extracted from the initial slope of the extrapolation to zero angle and therefore even more sensitive to slight variations in this extrapolation.

Sedimentation equilibrium measurements are affected by solution non-ideality, polydispersity, and/or self-association phenomena (see for example, Harding et al, 1991b). Guar gum solutions suffer from all of these and this was borne out by the difficulties in interpretating the data. The molecular weights resulting from measurements of the irradiated samples and the control show the same basic trend as molecular weights from light scattering measurements, however, they are considerably more noisy than the latter. Investigations regarding the effect different rotor speeds might have on the apparent weight average molecular weights obtained did not result in a particular trend. However, it was found that the molecular weight

distributions within the cell differed depending on the rotor speed chosen and that non-ideality appeared as the dominating effect at the lower speeds.

Both, intrinsic viscosity and concentrated solution viscosity decreased more rapidly with increasing radiation dose than the molecular weights obtained from either of the techniques discussed in the preceeding paragraphs. This may be regarded as evidence for the presence of high molecular weight spheroids within the guar gum solutions. The viscosity of molecules with compact spherical conformation is only slightly molecular weight dependent, whereas the results from both absolute techniques are significantly affected by heterogeneity.

Conformational analysis using molecular weights obtained from light scattering and viscosity and sedimentation velocity measurements was found to agree very well with values reported in the literature despite the difficulties described above.

CHAPTER 5

ANALYSIS OF PROTEIN-POLYSACCHARIDE COMPOSITES

BSA/dextran mixtures were prepared by Professor Dickinson's group in Leeds. They had investigated emulsifying properties of protein-polysaccharide systems and found that dry-heated protein-dextran and protein-amylopectin systems were good emulsifiers having the added advantage for food systems of not containing any other chemicals (Dickinson and Galazka, 1991; 1992). Our group was called upon to determine the molecular weights of these complexes. The initial study concerned only two BSA/dextran T40 mixtures which had been mixed and dry-heated at molar ratios of 1:5. The results obtained for the protein and polysaccharide alone and the non-heated and heated mixtures are shown in Table 5.1. This and the elution profiles of complexes and non-heated controls (see Figure 5.1 to Figure 5.4) indicate that a shift to higher molecular weight has taken place on heating and this is borne out by the weight average molecular weight data obtained (see Table 5.1).

It appears that the BSA control material is largely dimerized under the experimental conditions used. This is not surprising, dimerization of BSA is known to occur under various conditions (Tombs, 1970), although perhaps surprising at the low concentrations here (typically 3mg/ml). It also seems that the BSA in the non-heated BSA and dextran T40 mixture is in its monomeric form, a further demonstration that solvent conditions are important in determining the state of association of BSA.

177
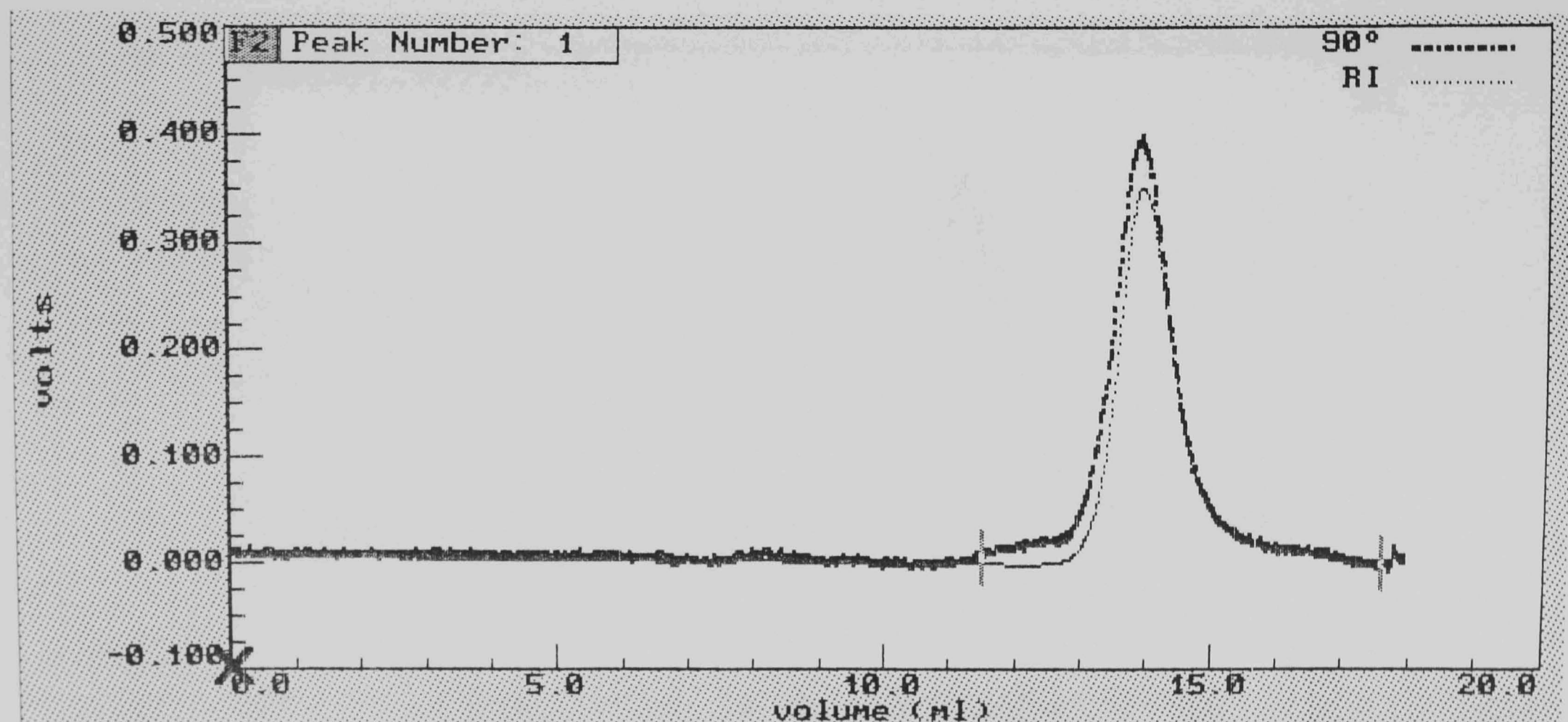
Figure 5.1: Light scattering (90° detector) and refractive index detector elution profiles for native BSA (Batch 1). Sample concentration = 3mg/ml, injection volume = 100µl, dn/dc = 0.185ml/g, flow rate = 0.8ml/min, eluent = phosphate/chloride buffer (I = 0.1, pH 6.8) (Green 1933). Column system 1.
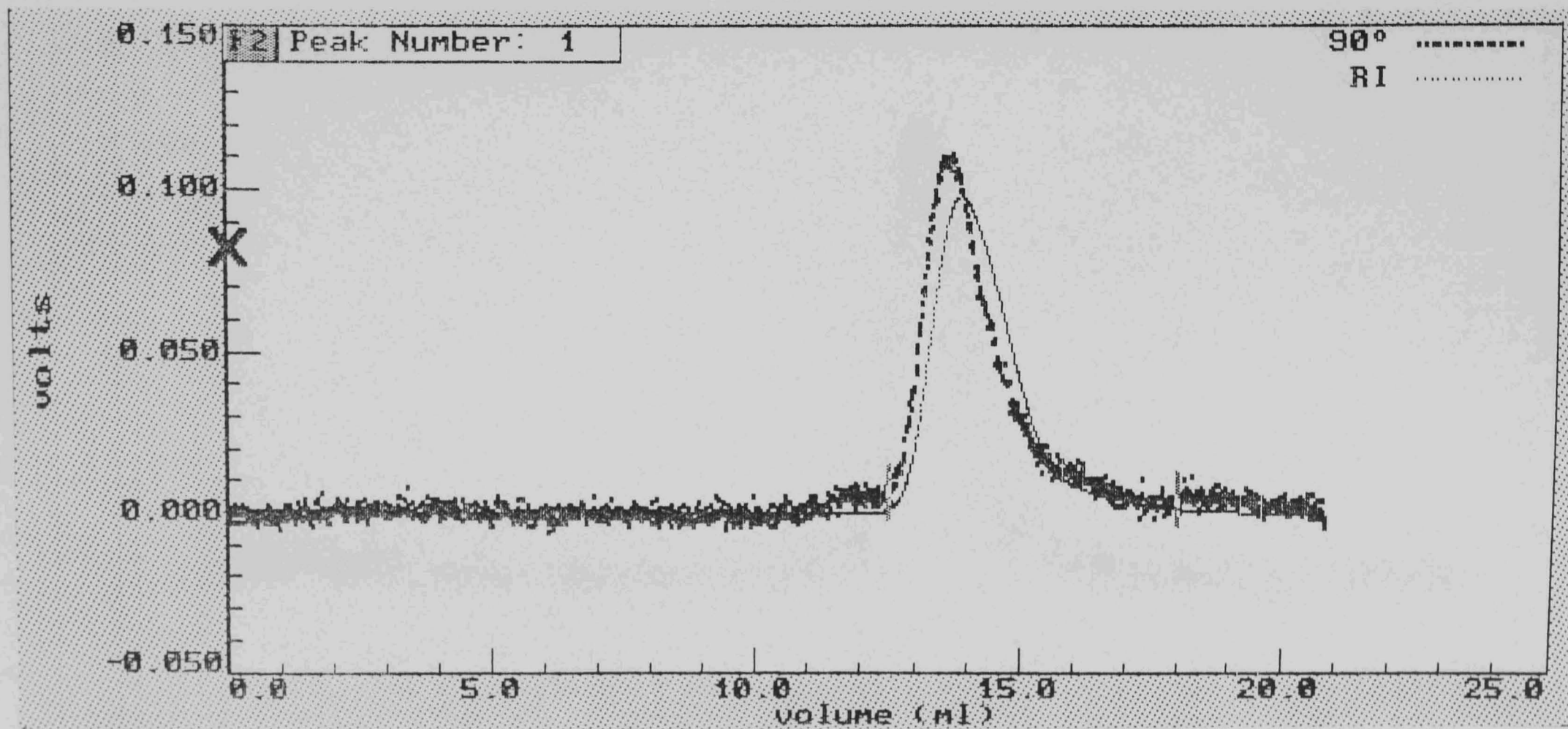
Figure 5.2: Light scattering (90° detector) and refractive index detector elution profiles for native dextran T40 (Batch 1). dn/dc = 0.147ml/g, all other conditions as described in Figure 5.1
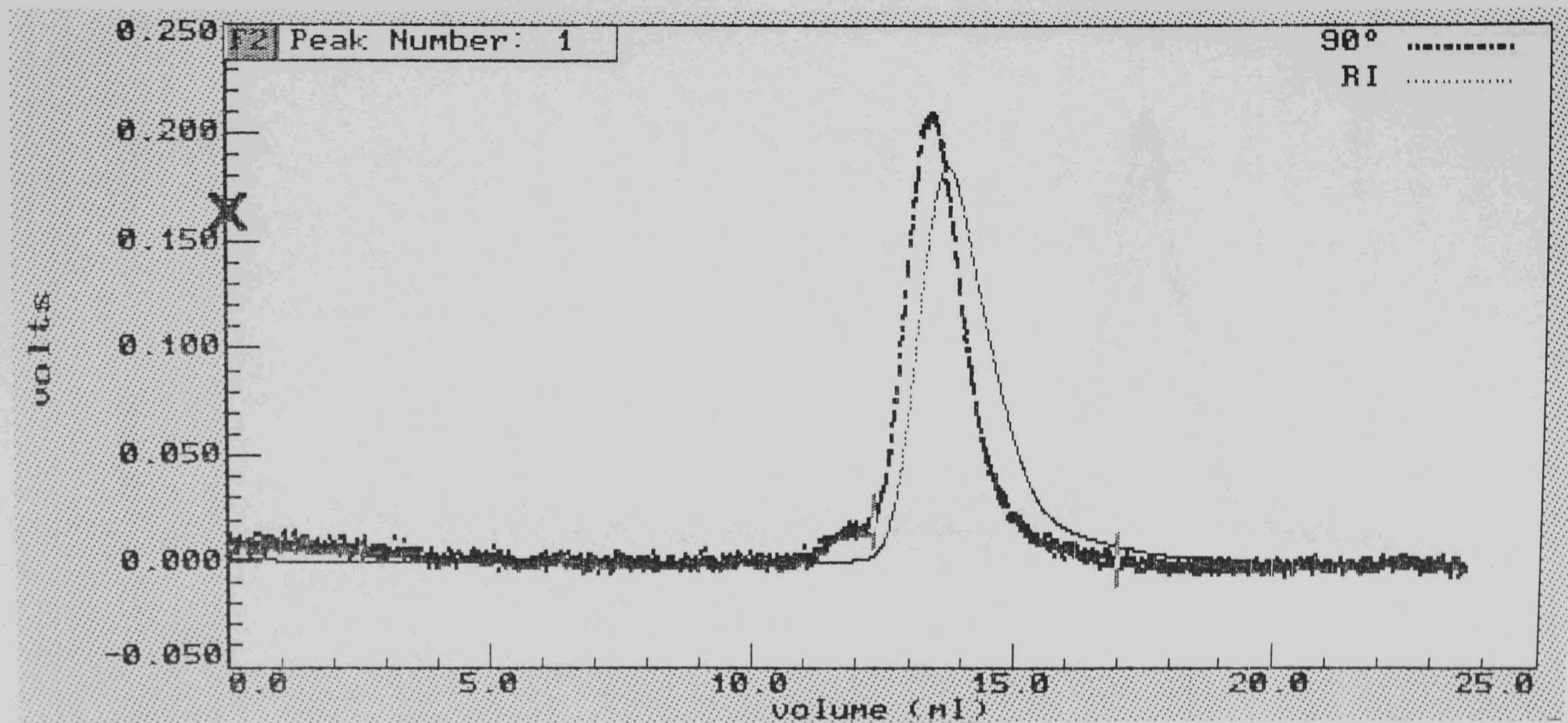
Figure 5.3: Light scattering (90° detector) and refractive index detector elution profiles for 3 weeks dry-heated BSA/dextran T40 mixture, molar ratio 1 : 5 (Batch 1). dn/dc = 0.165ml/g, all other conditions as described in Figure 5.1
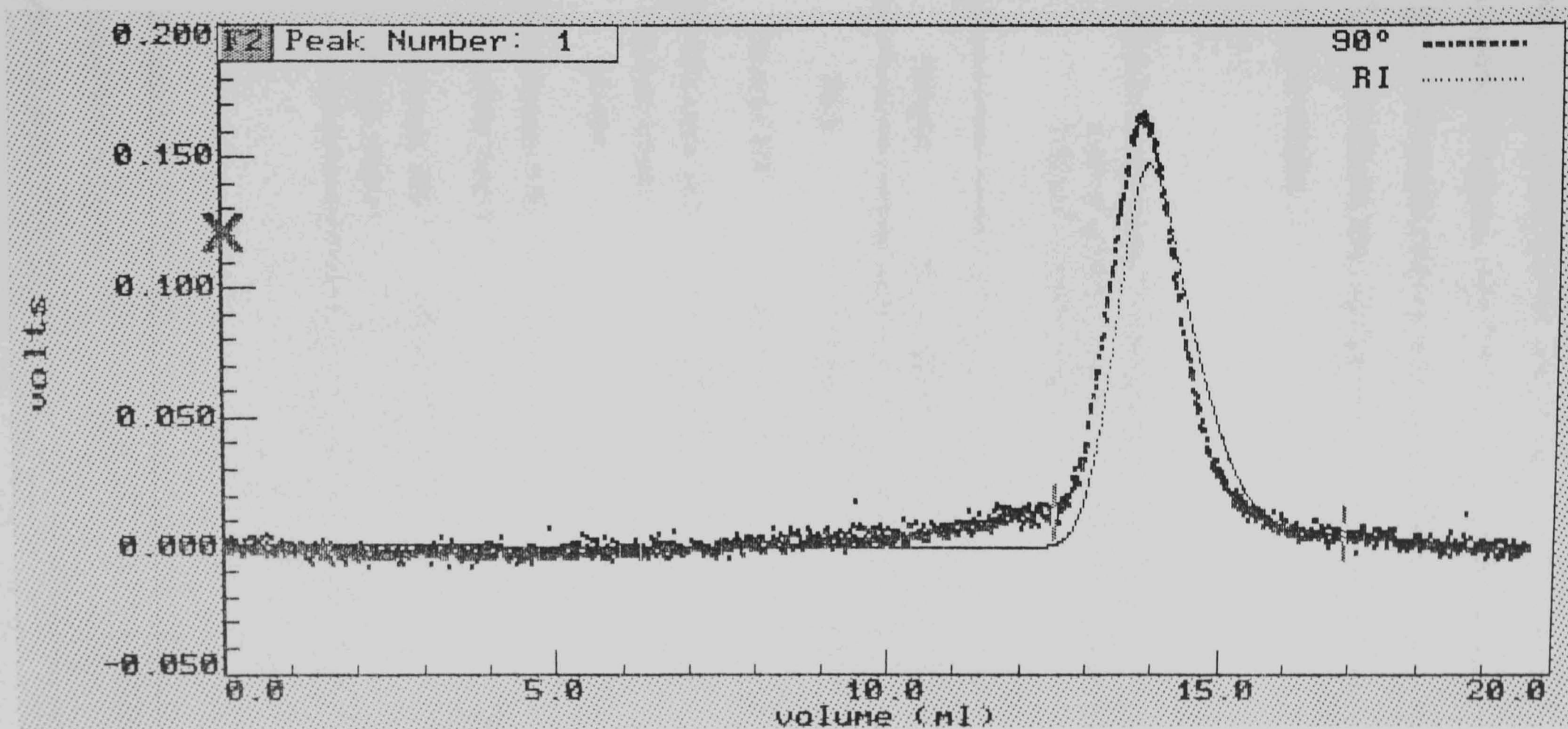
Figure 5.4: Light scattering (90° detector) and refractive index detector elution profiles for non-heat treated BSA/dextran T40 mixture, molar ratio 1 : 5 (Batch 1). dn/dc = 0.165ml/g, all other conditions as described in Figure 5.1

The weight average molecular weight obtained for dextran T40 was a little lower (34 000 g/mol) than the manufacturers value, duplicate runs showed a discrepancy of approx. 10%. This may partly be due to the low molecular weight of the sample causing only low scattering intensities. Signal to noise ratios would also be low, causing relatively large errors in the calculated molecular weights.

Table 5.1: Experimentally determined and calculated weight average molecular weights of BSA/dextran T40 complexes (molar ratios 1:5) and controls (Batch 1)

Sample	M_w by SEC/MALLS	M_w expected
BSA	121 200±2 800	66 700
Dextran T40	34 000±3 000	38 900
BSA/Dextran T40 non-heat treated mixture	44 700±2 300	46 000
BSA/Dextran T40 2 weeks heat treated	70 500±2 900	
BSA/Dextran T40 3 weeks heat treated	67 400±8 400	

There appears to be little difference in the weight average molecular weights obtained for the two and three weeks dry-heated BSA/Dextran T40 mixtures. Table 5.2 shows the predicted weight average molecular weights based on stoichiometric combinations of BSA and dextran T40 and any non-reacted monomers which have not been separated from the main complex. Details of

the calculations are given in section 1.1 (equation [1.2]). Although comparison of experimentally determined data with those in Table 5.2 cannot provide a definite stoichiometric description of the complex, my results are consistent with the hypothesis that a 'Maillard' complex forms involving one molecule of the polysaccharide and one protein molecule. Since dextran contains only one reducing group it seems reasonable that this group is involved.

Table 5.2: Weight average molecular weights of BSA/dextran T40 complexes

Molar ratio	Predicted M_w	
	BSA(monomer)/ dextran T40	BSA(dimer)/dextran T40
1:1	65 900	82 900
1:2	97 300	108 600
1:3	140 400	140 000
1:4	195 000	177 300
1:5	261 200	220 300

A second batch of complexes was prepared in Leeds using BSA/dextran T40 and BSA/dextran T500 in various molar ratios. Weight average molecular weights obtained (using column system 2, see Section 3.3.1) after 3 weeks dry-heating are tabulated in Table 5.3.

The sample with a BSA/dextran T40 ratio of 2:1 showed the highest molecular weight. This was rather surprising as both compounds are of fairly

Table 5.3: Weight average molecular weights of BSA/dextran T40 and BSA/dextran T500 complexes (Batch 2)

Sample, Molar ratio	M_w	
	Experimental value	Predicted values based on assumed stoichiometries
BSA/T40 2:1	447 000	60 400[a]
		90 500[b]
		172 300[c]
BSA/T40 1:3	108 700	49 000[a]
		77 300[b]
		122 100[e]
		183 400[f]
BSA/T500 3:1	390 000	376 200[a]
		471 400[b]
		579 400[c]
		700 100[d]
BSA/T500 1:3	365 400	481 600[a]
		524 100[b]
		885 800[e]
		1 566 700[f]
BSA	86 100±1100	66 700[g]
BSA 3 weeks heat treated	213 000±34 600	no value predicted
Dextran	39 200±800	38 900

a = non-reacted mixture, b = 1:1 (BSA/dextran)

c = 2:1 (BSA/dextran); d = 3:1 (BSA/dextran)

e = 1:2 (BSA/dextran); f = 1:3 (BSA/dextran)

g = value from van Holde (1985)

low molecular weight and a simple 2:1 complex would not be expected to show a molecular weight above 172 300. Linkage of two BSA molecules to one dextran molecule is difficult to envisage however, as dextrans contain only one reducing end group per molecule and it would be difficult for a second BSA molecule to attach itself to the same dextran.

The molecular weight of the BSA/dextran T40 1:3 complex shows that some reaction has taken place, however, it does not appear to have been as extensive as that of the 2:1 mixture. There appears to have been no reaction between BSA and dextran T500 during dry-heating. The molecular weight averages of both dry-heated samples are close to the predicted values for unreacted mixtures - phenomena associated with the larger dextran, could be a possible explanation.

Investigations regarding the BSA/dextran T40 hybrid from dry-heating at 2:1 molar ratio were expanded as this seemed the most interesting system. The average weight average molecular weight determined from 14 repeat injections of this complex was found to be 497 000±80 000 (see Table 5.4). Realistically, a weight average molecular weight of only 90 500 could be expected (ie. a 1 : 1 complex plus 1 mole unreacted BSA).

Elution profiles of native and dry-heated BSA and BSA/dextran T40 2:1 complex from batch 2 (Figure 5.5 to Figure 5.7) show a decrease in elution volume indicating the increasing size of the molecules. These profiles also indicate the polydisperse nature of all three samples. The molecular weight versus elution volume plot for both dry-heated samples (Figure 5.9 and Figure 5.10) show smooth separations in the linear high molecular weight region whereas the plot from the native BSA (Figure 5.8) shows a steep decline in the high molecular weight region and then the molecular weight stabilizes out which supports the suggestion that some of the native BSA is dimerized.

The experimentally obtained value for the dry-heated BSA/dextran T40 2:1

185
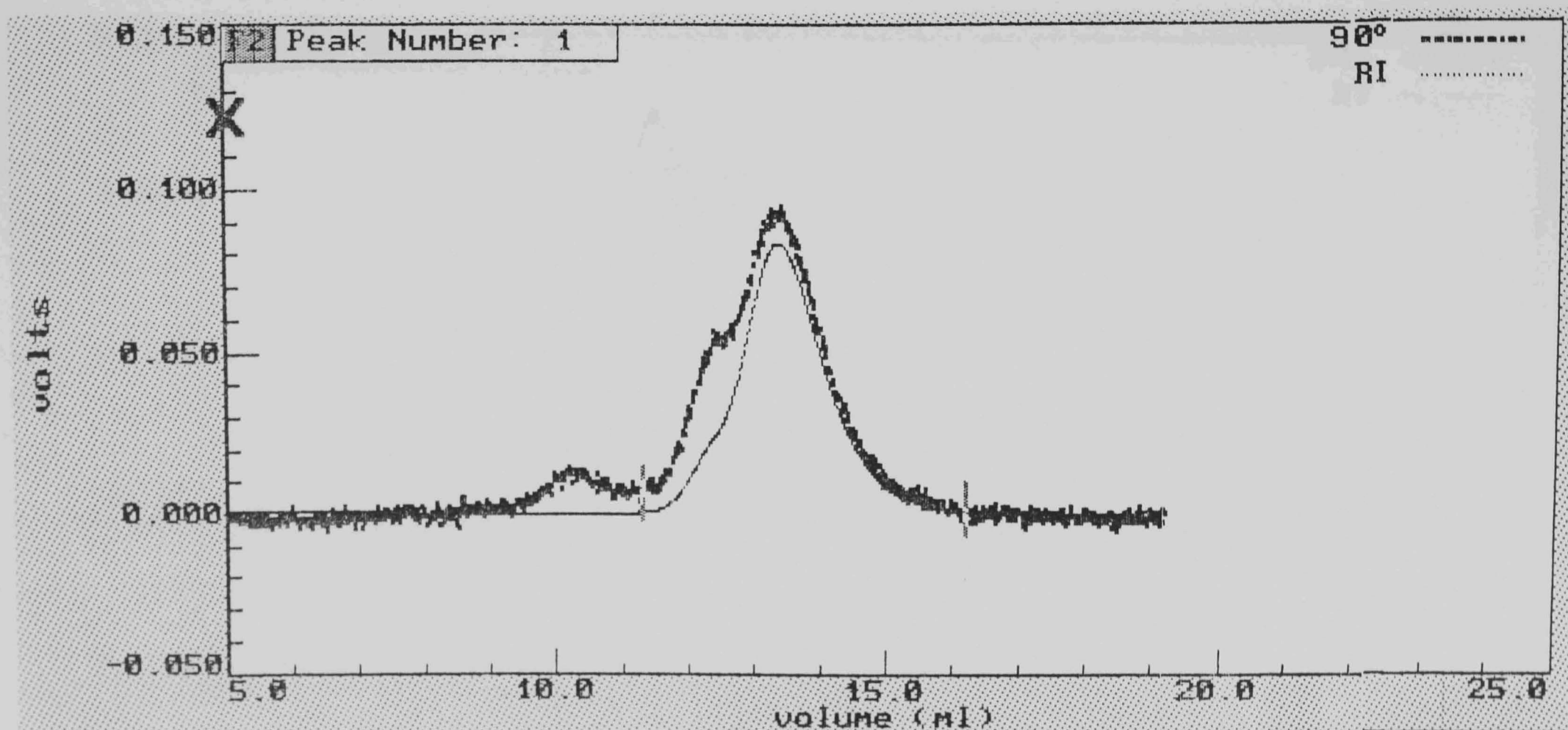
Figure 5.5: Light scattering (90° detector) and refractive index detector elution profiles for native BSA (Batch 2). dn/dc = 0.185ml/g, other conditions as described in Figure 5.1 but used column system 2.
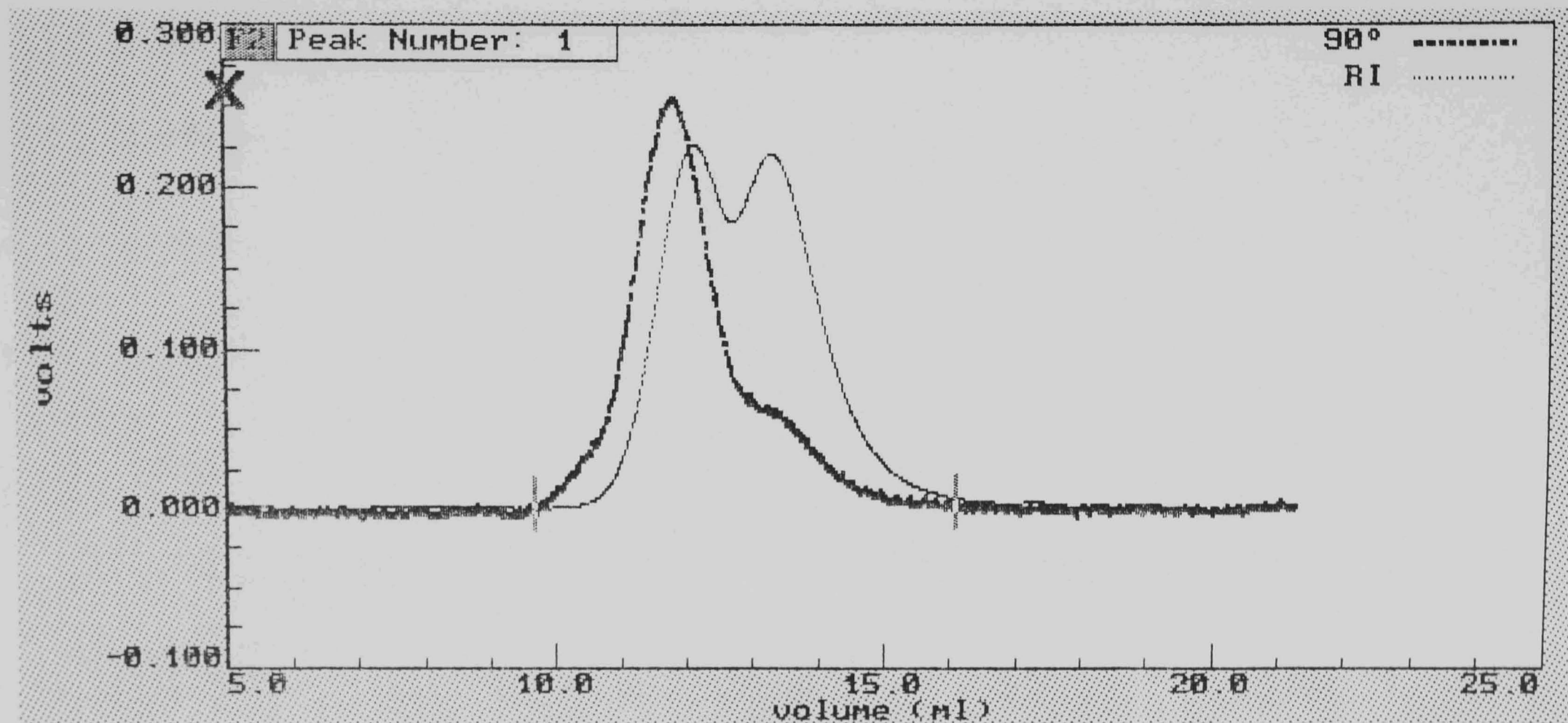
Figure 5.6: Light scattering (90° detector) and refractive index detector elution profiles for 3 weeks dry-heated BSA (Batch 2). dn/dc = 0.185ml/g, other conditions as described in Figure 5.1 but used column system 2.
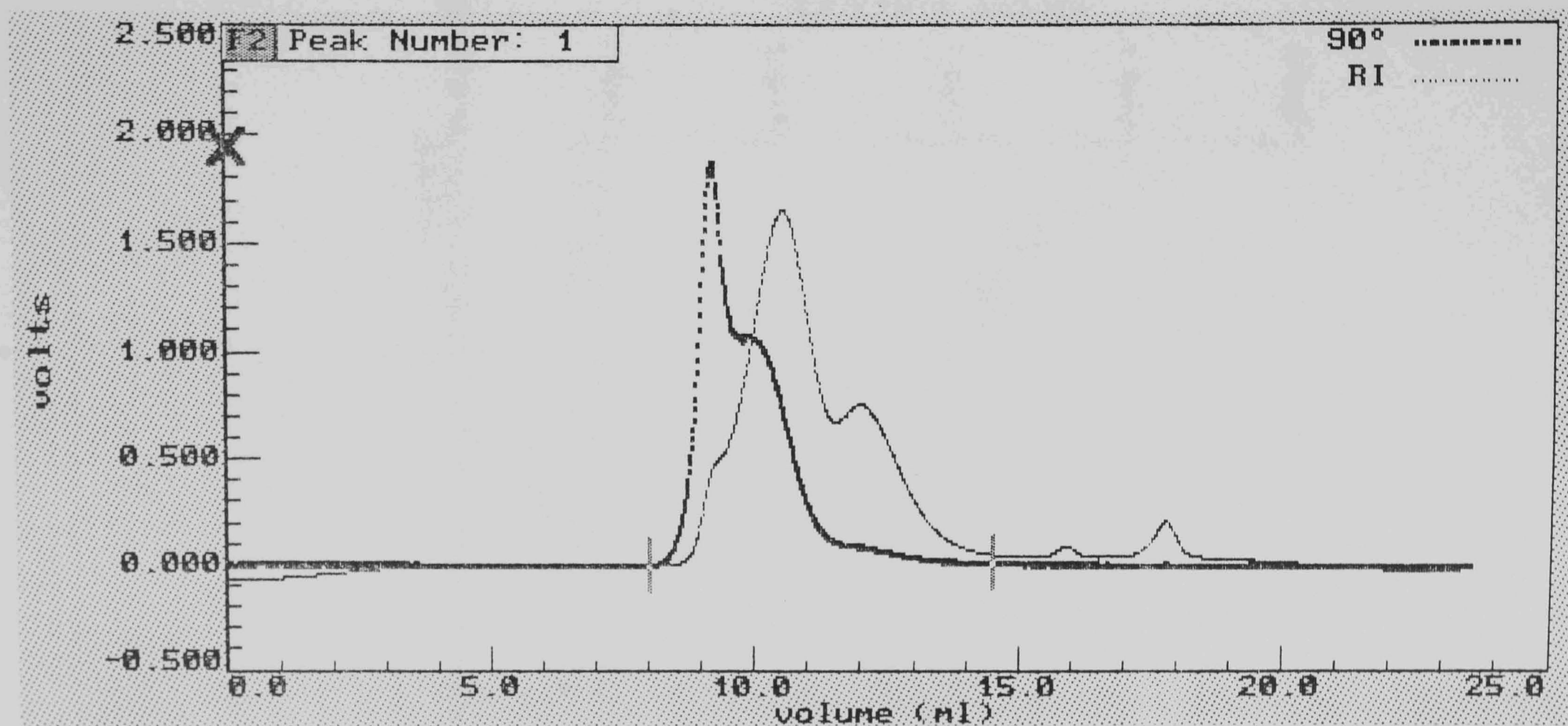
Figure 5.7: Light scattering (90° detector) and refractive index detector elution profiles for 3 weeks dry-heated BSA/dextran T40 (molar ratio 2 : 1) (Batch 2). dn/dc = 0.165ml/g, other conditions as desribed in Figure 5.1, but used column system 2.
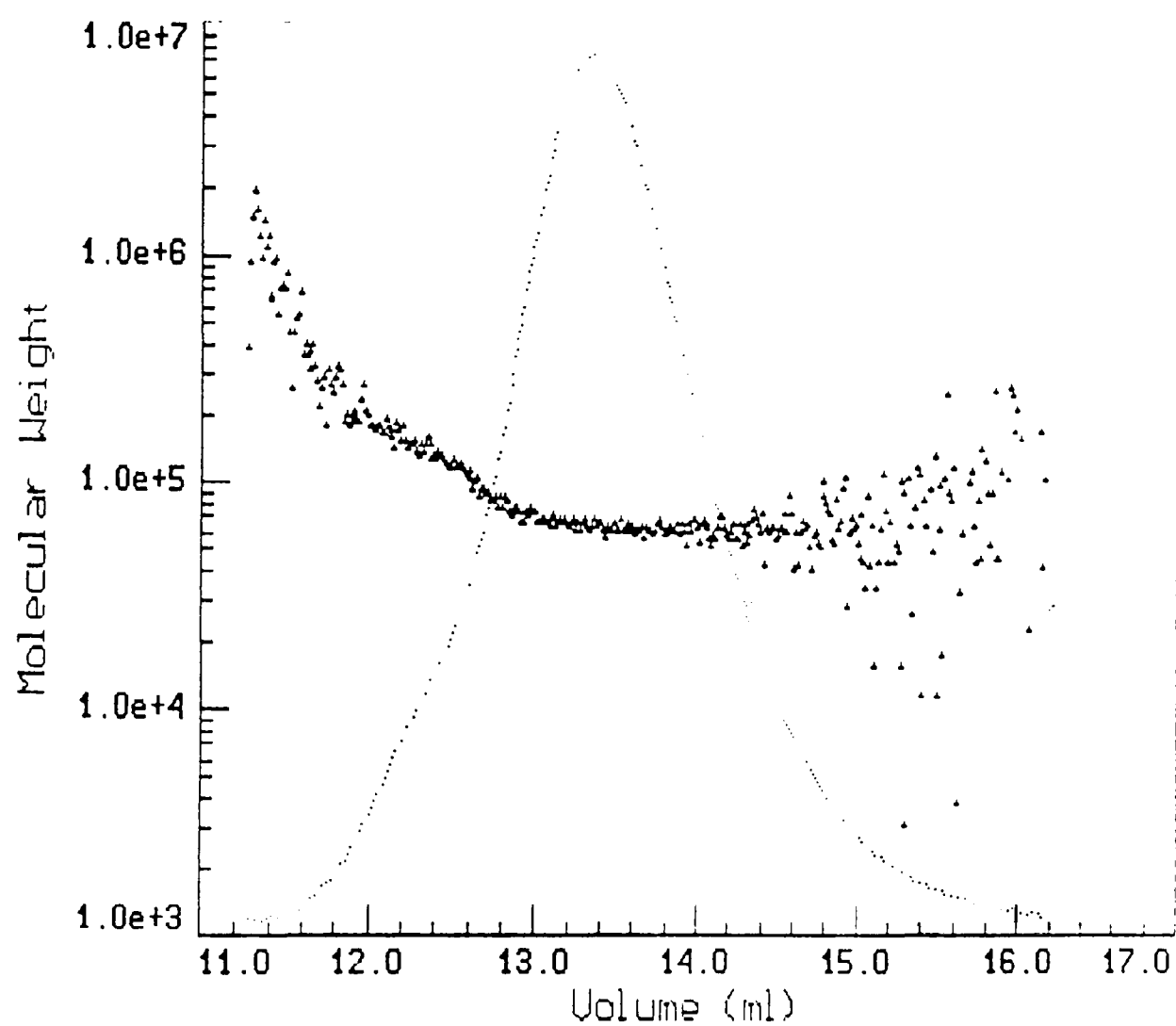
Figure 5.8: Molecular weight versus elution volume plot for native BSA (Batch 2).
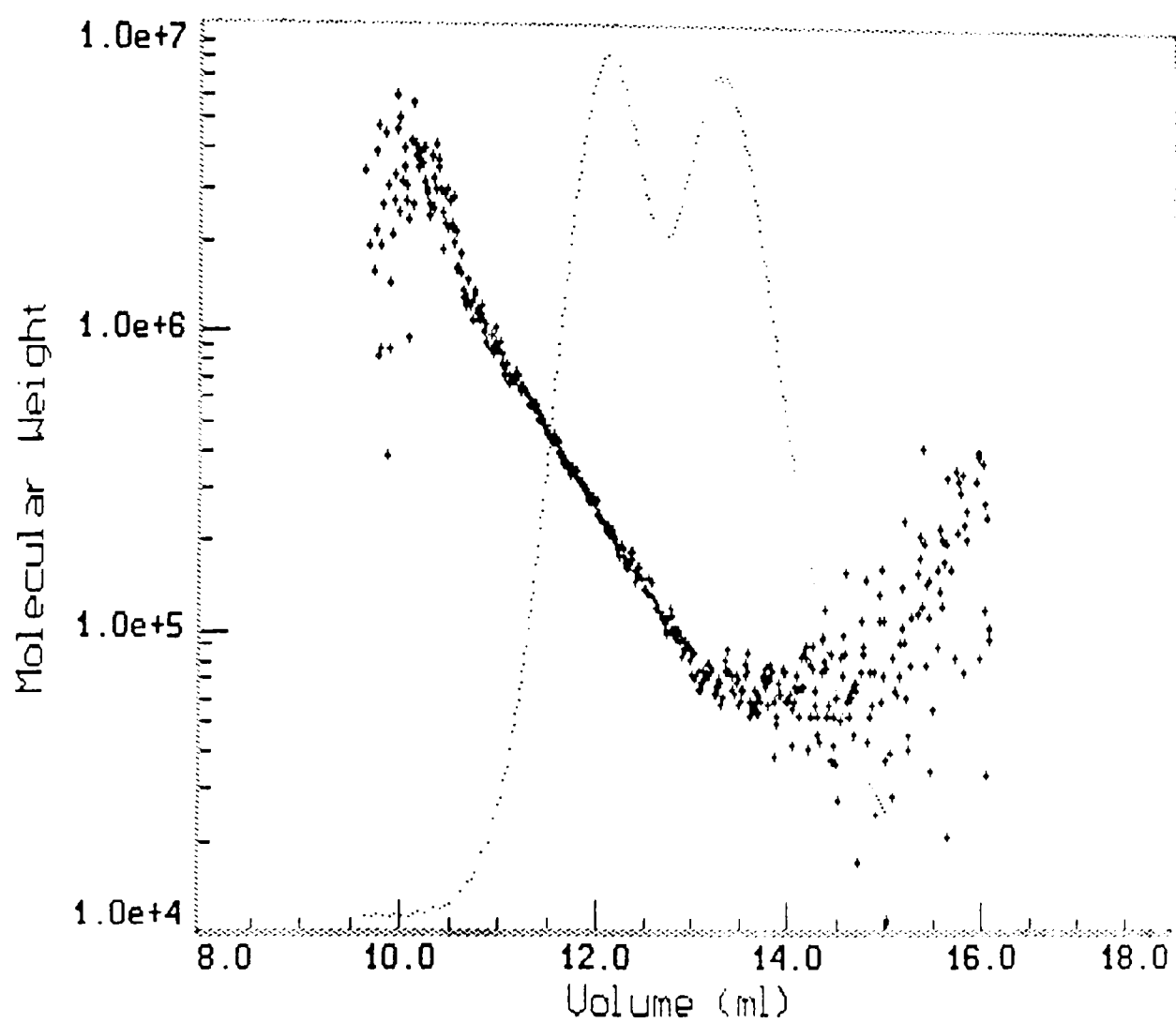
Figure 5.9: Molecular weight versus elution volume plot for 3 weeks dry-heated BSA (Batch 2).
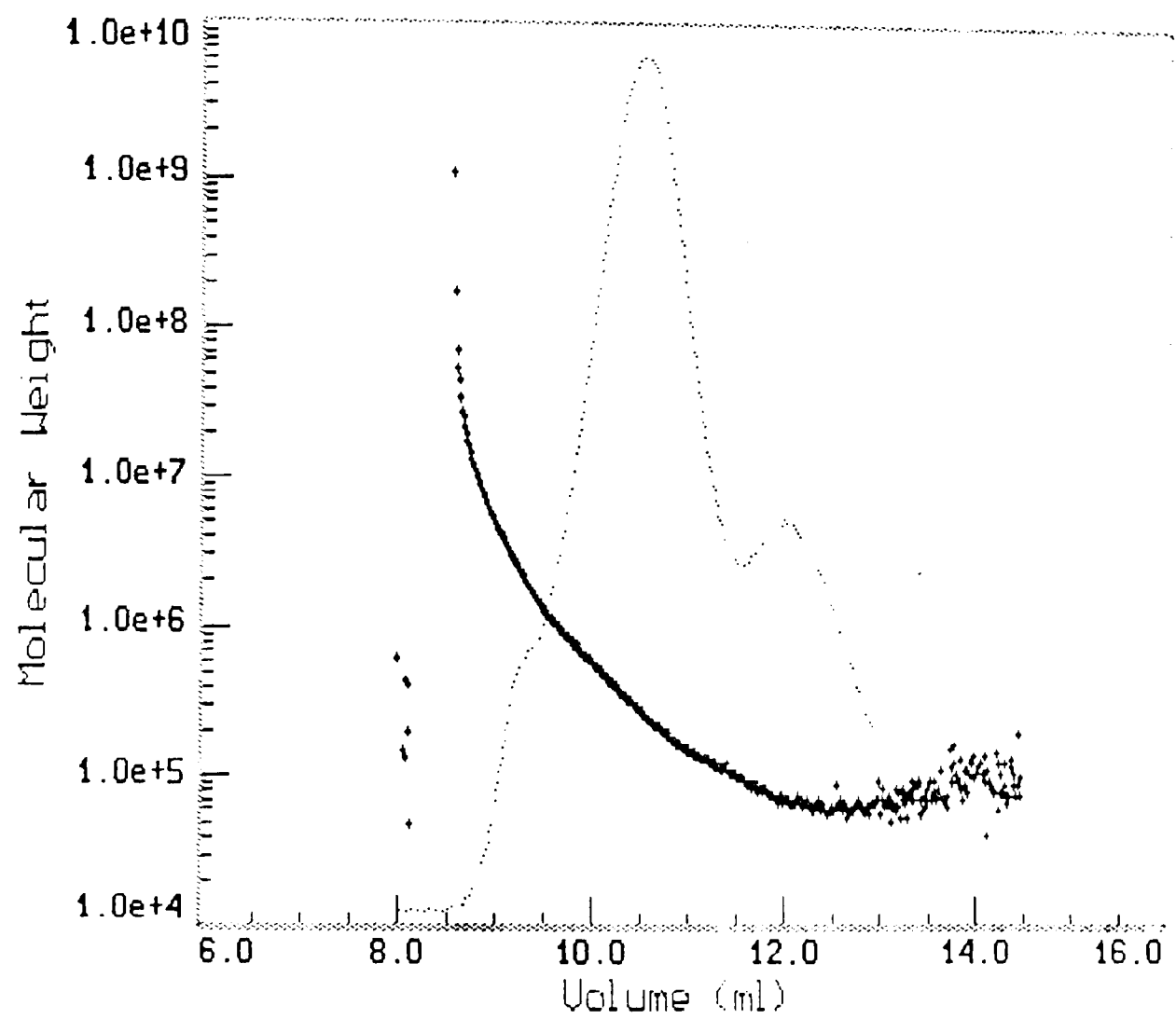
Figure 5.10: Molecular weight versus elution volume plot for 3 weeks dry-heated BSA/dextran T40 (molar ratio 2 : 1) mixture (Batch 2).

complex is thus between 4 and 5 times larger than the predicted value if no interaction took place. Apparent weight average molecular weights from sedimentation equilibrium ultracentrifugation experiments were found to be 450 000±20 000 g/mol. Data from both techniques are therefore in fairly close agreement. Sedimentation coefficients of dry-heated BSA and BSA/dextran T40 (2:1) complex are also shown in Table 5.4. It was not considered necessary to extrapolate $s_{20,w}$ values to infinite dilution, as the values were used for comparison rather than as absolute data. However,

Table 5.4: Comparison of molecular weights, sedimentation coefficients and frictional coefficients from dry-heated BSA and dry-heated BSA/dextran T40 molar ratio 2:1 composite (Batch 2)

Hydrodynamic parameters	BSA, dry-heated (Batch 2)	dry-heated BSA/dextran T40 (molar ratio 2:1, Batch 2)
M_w (g/mol) from SEC/Malls	158 000±10 000	497 000±80 000
M_w (g/mol) from sedimentation equilibrium	130 000±10 000	450 000±20 000
s_{20} (S)	5.43±0.1	4.85±0.1
$s_{20,w}$ (S)	5.56±0.1	4.98±0.1
f/f_0	1.3±0.1	4.5±0.1

these data alone cannot give much information regarding the solution conformation of the samples. Such information is obtained from the frictional ratio, f/f_0, which is obtained using $s_{20,w}$ values (assuming that they are close to values at infinite dilution) in conjunction with molecular weights (Tanford,

1961; van Holde, 1985). An unhydrated, highly symmetrical shape such as a hard sphere will give a frictional coefficient close to unity. The relatively large value for the complex is therefore suggestive of a highly asymmetrical and/or highly hydrated molecule.

The above data could lead to the assumption that some form of aggregation or self-association between the complex molecules and/or the complex and the free BSA has taken place. Self-association of hybrids is a feasible scenario. According to Tanford (1980) amphiphilic molecules have self-associating properties and can form molecular assemblies in aqueous media and if covalent bonding between the hydrophilic dextran and the hydrophobic BSA has taken place, the hybrid will be amphiphilic. A. Kato et al (1992) described similar behaviour of ovalbumin-dextran and lysozyme-dextran complexes which formed micelles in aqueous solvents, with degree of association increasing with increasing salt concentration.

Investigations with new composites continued using only BSA and dextran T40 at various molar ratios, including a fresh preparation of a 2:1 ratio. Molecular weight values from SEC/MALLS determinations are shown in Table 5.5. None of the high BSA content hybrids exhibited molecular weights as high as those shown by the first 2:1 hybrid, but they were found to all have very similar molecular weights (see Figure 5.11). Hybrids from low BSA content mixtures all had much lower molecular weights than their high BSA content counterparts. This could be further evidence for association/aggregation of free BSA molecules to a 1:1 hybrid.

Table 5.5: Weight average molecular weights of BSA/dextran T40 mixtures after dry-heating at various molar ratios (Batch 3)

Molar ratio BSA/Dextran T40	M_w from SEC/MALLS
1:3.4	93 000±7 800
1:3	106 000±1 700
1:1.7	119 000±9 200
1:0.85	166 000±700
2:1	249 000±2 700
3:1	255 000±3 200
4:1	247 000±9 700
6:1	320 000±24 000
10:1	210 000±27 500
BSA 3 weeks heat treated	473 000±63 700[a]
BSA (Batch 1)	85 000±9 600
BSA (Batch 2)	83 300±8700
Dextran T40	37 000±4 200
Dextran T40 heat treated (1 week)	41 700[b]
Dextran T40 heat treated (2 weeks)	46 200[b]
Dextran T40 heat treated (3 weeks)	37 300[b]

[a] Compare with M_w from dry-heated BSA from batch 2 which was found to be 213 000 g/mol (see Table 5.3)

[b] Values from single injections

194
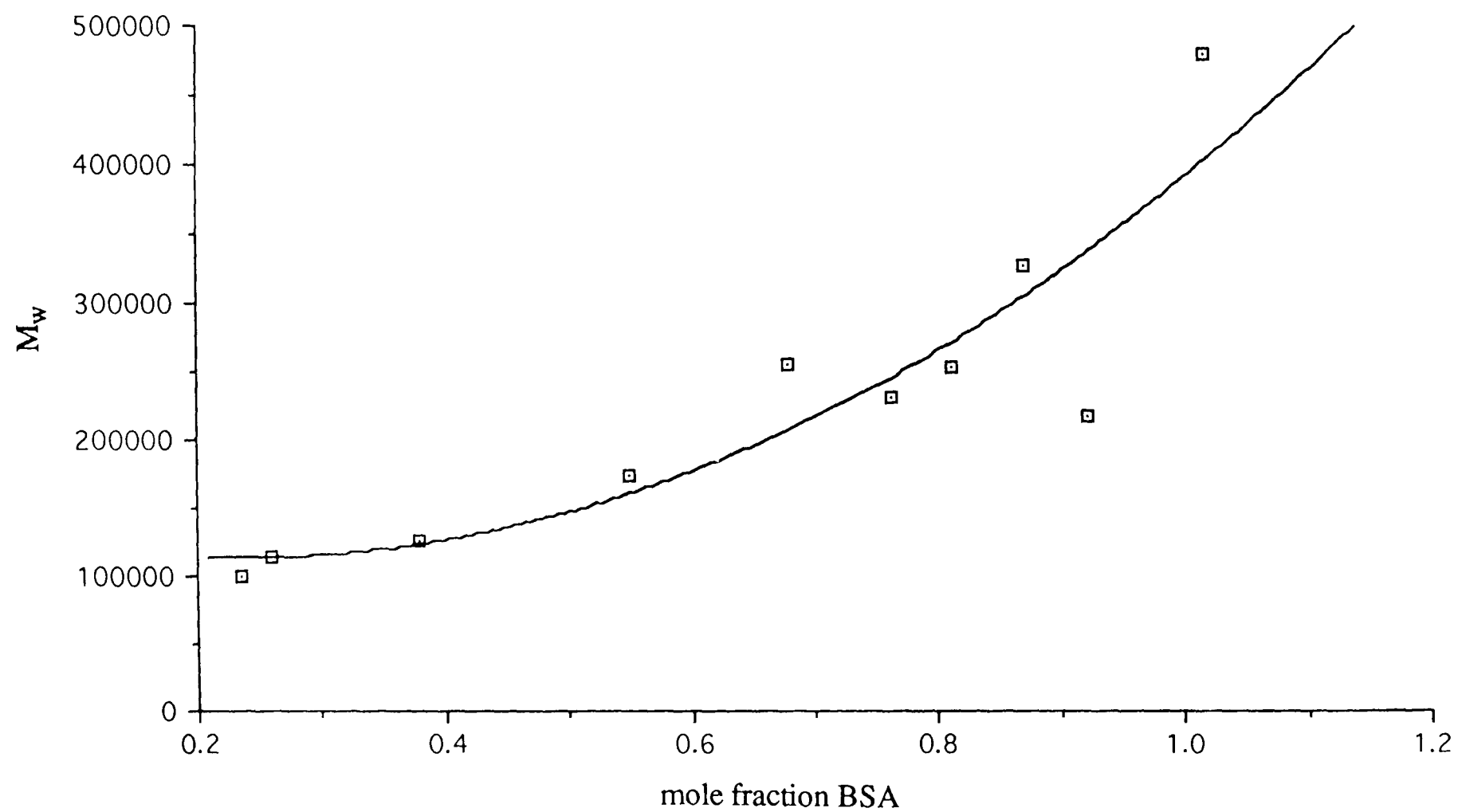
Figure 5.11: Plot of weight average molecular weight from dry-heated BSA/dextran T40 mixtures and BSA (obtained by SEC/MALLS) versus mole fraction BSA (Batch 3)

The work on the dry-heated BSA/dextran mixtures and the controls has provided us with some interesting results about these systems. The weight average molecular weights of the dextran samples were all in good agreement with the expected values (ie. manufacturers values) although the T40 results were slightly lower, possibly because light scattering intensities were getting too low for good signal to noise ratios. The molecular weights of the dry-heated dextran T40 samples were virtually unchanged which is also in keeping with expectations.

The situation with the BSA was found not to be so clear cut. Values were much higher than would be expected for monomer BSA and varied by approx. 10%. The former is suggestive of some dimerization. Similar problems were found with the dry-heated BSA samples. There was strong evidence that aggregation had taken place during the dry-heating process, however, reproducibility of molecular weights from two different batches was not very good.

The unheated mixtures gave the expected molecular weights assuming that the BSA was in the monomeric form and that there was no interaction between the macromolecules.

Dry-heated mixtures containing dextran T500 did not show any evidence of complex formation. However, dry-heated mixtures of dextran T40 did appear to form complexes or at least give larger molecular weights than would be expected even for mixtures of heat aggregated BSA and T40. This is especially the case for the higher BSA levels. The molecular weight of the complex appears to depend on the preparation batch, this is particularly evident for the BSA/T40 2:1 complex which gave a molecular weight of 447 000 g/mol when it was prepared initially and a molecular weight of 249 000 g/mol for the second preparation.

The results suggest that the high molecular weight dextran does not form complexes on dry-heating whereas the low molecular weight dextran does. It

196

is interesting to consider what may be responsible for these effects. The obvious interactions are

(i) Maillard reaction between dextran and protein most probably between a reactive lysine on the BSA and the reducing end group on the dextran

(ii) Possible association of the amphiphilic Maillard complexes in solution to form micellar structures as suggested by A. Kato (1992)

(iii) Non-covalent or S - S mediated associations between the protein molecules

CHAPTER 6

CONCLUDING REMARKS

The work described in this thesis can be separated into two major areas. Firstly, the characterization of the irradiated guar gum samples and, secondly, the work on the dry-heated BSA/dextran complexes. The additional analysis described in Appendix A to C was exclusively performed using SEC/MALLS and although only molecular weight values were obtained, these revealed some interesting results. In the following, I would like to discuss the implications the results have on the use of the materials analysed and make some suggestions for further work.

6.1 IRRADIATED GUAR GUM

The use of ionizing radiation for the disinfestation, sterilization and preservation of foods and food components has been accepted in some countries but is still under review in many others. Disinfestation is frequently still carried out by fumigation with materials such as ethylene oxide, methyl bromide, etc. These chemicals may in themselves be a hazard to the consumer and radiation is a process which is a relatively safe alternative. However, radiation does affect the treated material and in polysaccharides the major feature is the breaking of glycosidic bonds resulting in a decrease in chain length thus inducing changes in their functional properties such as viscosity.

Guar gum has many uses in the food and other industries. Most of these are based on the high viscosities of guar solutions either alone or in synergism with other polysaccharides such as xanthan. A reduction in molecular weight and hence viscosity due to irradiation would therefore be highly undesirable. My results have shown that increasing the radiation dose for dry guar gum samples affects its molecular weight. Radiation doses required to control the infestation of grains rarely requires more than 0.5kGy (Tilton and Brower, 1987) which for guar gum would only mean a slight reduction in its viscosity and may be acceptable to the industry. However, in order to reduce the microbial load, doses between 1 and 10kGy are required and for complete sterilization applications of up to 70kGy may be necessary (Rayas-Duarte and Rupnow, 1989). The latter doses are outside the legal limits at present but my results have shown that there is a significant reduction in molecular weight and viscosity at applications above 1kGy. Similar decreases in viscosity were found for starches irradiated between 5 and 10kGy (Rayas-Duarte and Rupnow, 1989).

The irradiated series of guar gum samples was investigated with respect to molecular weight, viscosity and conformation and although a reduction in the former two properties was found, there was no change in conformation due to radiation.

As indicated above, guar gum is often used in conjunction with, for example, xanthan or carrageenan or other polysaccharides which will act synergistically with respect to viscosity. It may be interesting to investigate the effect of radiation on the synergistic action of guar gum. It is possible that the α-(1->6) galactose residue may be preferentially removed from the polymer chain. A second area of interest may be an investigation of the purified irradiated material. The experiments described in this thesis were all performed on the raw guar gum, with the implications of uncertainty in the amount of material present in the solutions. Purification of samples would increase the accuracy of the results obtained which might enhance the results of the conformational analysis.

It was also mentioned in the discussion of the SEC/MALLS results obtained from the guar gums (page 127ff), that large uncertainties regarding the extrapolations to zero angle were found. These were considered indicative of heterogeneity of the fractions and most likely due to supramolecular structures. For the purpose of the conformational analysis presented in this thesis these components have been ignored, however, in order to give a complete representation of the sample, they would have to be isolated and characterized and the appropriate functions for their inclusion in the zero angle extrapolations would be necessary.

6.2 DRY-HEATED BSA/DEXTRAN COMPLEXES

Although many dry-heated BSA/dextran complexes were investigated using SEC/MALLS, the work described in this thesis gives only a very small indication as to what may be happening during the dry-heating process. The formation of reaction products of BSA and dextran is not a surprise per se - reaction of proteins with reducing sugars is a process which occurs during cooking of foods and is known as the Maillard Reaction. However, some of the molecular weights found for the BSA/dextran T40 complexes were much higher than would be expected from either simple one-to-one reaction products or if the components had reacted in the molar ratios as given in the respective mixture. There is, of course, no need for the materials to react in these ratios, BSA contains many amino-groups which, theoretically, could be available for reaction with a reducing sugar, however, dextrans contain only one reducing end group and it seems highly improbable that more than one BSA could react with one dextran by a Maillard mechanism. However, it was found that the highest molecular weights were obtained when there was more BSA than

dextran present in the mixture (on a mole per mole basis). The situation was further complicated by the large molecular weights obtained from the dry-heated BSA alone and the lack of reproducibility of molecular weight values from one batch of samples to the next (reproducibility within a batch of samples was however found to be good).

It is clear that a full evaluation of the dry-heated composites would require a great deal of further work. Apart from testing the reproducibility of complex formation at one given molar ratio, this should include the determination of free and bound protein and dextran in each preparation. The nature of the bonds between the two components is important and should also be established, furthermore, the suggestion that oligomeric assemblies of the conjugates may be formed in aqueous, ionic solvents (see A. Kato et al, 1992) should be investigated.

6.3 COMMENTS ON THE WORK DESCRIBED IN APPENDIX A TO C

The work described in Appendix A to C has revealed that SEC/MALLS is a quick and (relatively) easy method for establishing purity and molecular weight of a sample provided that it is separable by chromatography. Moreover, the technique also highlights difficulties within particular preparations. For example, the molecular weights obtained for the amylose fractions of whole starches where the amylopectin had been debranched were considerably higher than those quoted in the literature. These results may be a reflection of some non-degraded amylopectin co-eluting with the amylose, it could also be due to the environmental conditions under which the starches investigated were grown, although, the differences between the values obtained and those quoted

201

in the literature are so large as to almost preclude the latter suggestion. Comparison of the molecular weight of amylose fractionated prior to analysis and the amylose fraction from whole starch may give some indication as to the reason for these discrepancies, however, this also causes a dilemma in that the amylose fractions investigated are no longer identical.

The lack of radius of gyration information from the SEC/MALLS experiments was considered a great loss for the analyses performed. The light scattering technique is unique in that it can give the size of a macromolecule without any prior assumptions regarding shape and it may even give information regarding the shape of a macromolecule. That this information was lost in the case of the guar gum samples was acceptable as these were of a highly heterogeneous nature and the proper functions taking the latter into account will have to be established. However, the information was also found to be unreliable for the samples which appeared not to suffer from any non-size exclusion effects (for example the mucin samples discussed in Appendix B). Investigations using well defined standards of known chromatographic behaviour will have to establish whether the reason for this unreliability is insufficient separation or software problems. For this reason, radius of gyration values are not quoted in this thesis.

6.4 FINAL COMMENT

Polysaccharide systems are polydisperse with respect to molecular weight and frequently with respect to conformation unless they have been exhaustively fractionated. They also exhibit highly non-ideal solution behaviour and, as the above studies have shown, there are difficulties in the interpretation for almost every technique that has been used for their characterization. The work

202

described for the guar gum may be taken as an indication of how important it is to realize that they cannot be characterized by a single method, but that it is imperative that results are checked by at least one other independent technique.

BIBLIOGRAPHY

Adam, S. (1983); Recent developments in radiation chemistry of carbohydrates; in 'Recent Advances in Food Irradiation', P.S. Elias and A.J. Cohen (eds.), Elsevier Biomedical Press, Amsterdam

Albersheim, P., Nevins, D.J., English, P.D., Kar, A. (1967); A method for the analysis of sugars in plant cell-wall polysaccharides by gas-liquid chromatography. *Carbohydr. Res.* **5**, 340-345

Asaoka, M., Okuno, K., Konishi, Y., Fuwa, H. (1987); The effect of endosperm mutations and environmental temperature during development on the distribution of molecular weigh of amylose in rice endosperm. *Agric. Biol. Chem.* **51**, 3451-3453

Baker, C.W., Whistler, R.L., (1975); Distribution of D-galactosyl groups in guaran and locust-bean gum. *Carbohydr. Res.* **45**, 237-243

Ball, A., Harding, S.E., Simpkin, N.J. (1990); On the molecular weight distribution of dextran T-500; in, 'Gums and Stabilizers for the Food Industry 5', G.O. Phillips. D.J. Wedlock, P.A. Williams (eds.), IRL Press, Oxford

Banks, W., Geddes, R., Greenwood, C.T., Jones, I.G. (1972); Physicochemical studies on starches. *Starch* **24**(8), 245-251

Banks, W., Greenwood, C.T. (1975); Starch and its components, Edinburgh University Press, Edinburgh

Banks, W., Greenwood, C.T., Sloss, J. (1969); Light-scattering studies on aqueous solutions of amylose and amylopectin. *Carbohydr. Res.* **11**, 399-406

Barth, H.G., Carlin Jr., F.J. (1984) A review of polymer shear degradation in size exclusion chromatography; *J. Liq. Chromatogr.* **7**(9), 1717-1738

Beri, R.G., Walker, J., Reese, E.T., Rollings, J.E. (1993); Characterization of chitosans via coupled size exclusion chromatography and multiple-angle laser light-scattering technique. *Carbohydr. Res.* **238**, 11-26

Berth, G. (1988); Studies on the heterogeneity of citrus pectin by gel permeation chromatography on Sepharose 2B/Sepharose 4B. *Carbohydr. Polym.* **8**, 105-177

Berth, G. (1992); Methodical aspects of characterization of alginate and pectate by light scattering and viscometry coupled with GPC. *Carbohydr. Polym.* **19**, 1-9

Billingham, N.C. (1977); Molar Mass Measurements in Polymer Science, Kogan Page, London

Blake, S.M., Deeble, D.J., Phillips, G.O., DuPlessey, A. (1988); The effect of sterilizing doses of γ-irradation on the molecular weight and emulsification properties of gum arabic. *Food Hydrocoll.* **2**(5), 407-415

Bremecker, K.-D. (1990); Semi-solid aqueous gels as nasal and buccal bioadhesives, in 'Bioadhesion - Possibilities and Future Trends', R. Gurny, H.E. Junginger (eds.), Vol. 25, Wissenschaftliche Verlagsgesellschaft mbH, Stuttgart

Cao, Y., Dickinson, E., Wedlock, D.J. (1991); Influence of polysaccharides on the creaming of casein-stabilized emulsions. *Food Hydrocolloids* **5**(5), 443-454

Carlstedt, I., Sheehan, J.K. (1984); Is the macromolecular architecture of cervical, respiratory and gastric mucins the same? *Biochem. Soc. Trans.* **12**, 615-617

Carlstedt, I., Sheehan, J.K., Corfield, A.P., Gallagher, J.T. (1985); Mucus glycoproteins: A gel of a problem. *Ess. Biochem.* **20**, 40-76

Cassassa, E.F. (1976); Comments on exclusion of polymer chains from small pores and its relation to gel permeation chromatography. *Macromolecules* **9**, 182-185

Cassassa, E.F., Eisenberg, H. (1961); Partial specific volumes and refractive index increments in multicomponent systems. *J. Phys. Chem.* **65**, 427-433

Clegg, R.E., Kertesz, Z.I. (1956); Aftereffect in the degradation of cellulose and pectin by gamma rays. *Science* **124**, 893

Coll, H., Prusinowski, L.R. (1967); Calibration in gel permeation chromatography. *Polym. Lett.* **5**, 1153-1156

Corona, A., Rollings, J.E. (1988); Polysaccharide characterization by aqueous size exclusion chromatography and low angle laser light scattering. *Sep. Sci. Technol.* **23**(8/9), 855-874

Creeth, J.M., Bhaskar, K.R., Horton, J.R. (1977); The separation and characterization of bronchial glycoproteins by density-gradient methods. *Biochem J.*, **167**, 557-569

Creeth, J.M., Cooper, B. (1984); Studies on the molecular weight distribution of two mucins. *Biochem. Soc. Trans.* **12**, 618-621

Creeth, J.M., Harding, S.E. (1982a);A simple test for macromolecular heterogeneity in the analytical ultracentrifuge. *Biochem. J.* **205**, 639-641

Creeth, J.M., Harding S.E. (1982b); Some observations on a new type of point average molecular weight. *J. Biochem. Biophys. Methods* **7**, 25-34

Creeth, J.M., Knight, C.G. (1965); On the estimation of the shape of macromolecules from sedimentation and viscosity measurements. *Biochem. Biophys. Acta* **102**, 549-558

Creeth, J.M., Pain, R.H. (1967); The determination of molecular weights of biological macromolecules by ultracentrifuge methods. *Prog. Biophys. Mol. Biol* **17**, 217-287

Cross, M.M. (1965); Rheology of non-Newtonian fluids: a new flow equation for pseudo-plastic systems. *J. Colloid Sci.*, **20**, 417-437

Dautzenberg, H., Rother, G. (1992); Light Scattering: Theoretical aspects. in, 'Physical Methods for Glycopolymer Characterisation', 7th Harden Discussion Meeting, Eynsham Hall, Oxford

Davis, S.S. (1985); The design and evaluation of controlled release systems for the gastrointestinal tract. *J. Control. Rel.* **2**, 27-38

Dawkins, J.V.(1976); Thermodynamic interpretation of polystyrene retention on crosslinked polystyrene gels in GPC with poor and theta solvents. *J.Polym.Sci.* **14** Part A-2, 569-571

Dea, I.C.M., McKinnon, A.A., Rees, D.A. (1972); Tertiary and quaternary structure in aqueous polysaccharide systems which model cell wall cohesion: reversible change in conformation and association of agarose, carrageenan and galactomannan. *J.Molec. Biol.* **68**, 153-172

Dea, I.C.M., Morris, E.R., Rees, D.A., Welsh, E.J., Barnes, H.A., Price, J. (1977); Association of like and unlike polysaccharides: mechanism and specificity in galactomannans, interacting bacterial polysaccharides, and related systems. *Carbohydr. Res.* **57**, 249-272

Dea, I.C.M., Morrison, A. (1975); Chemistry and interaction of seed galactomannans. *Adv. Carbohydr. Chem. Biochem.* **31**, 241-312

Debye, P. (1944); *J. Appl. Phys.* **15**, 338

Dickinson, E. (1993); Protein-polysaccharide interactions in food colloids; in, 'Food Colloids and Polymers: Stability and Mechanical Properties', E. Dickinson, and P. Walstra (eds.), Royal Society of Chemistry

Dickinson, E., Euston, S.R. (1991); Stability of food emulsions containing both protein and polysaccharide; in, 'Food Polymers, Gels and Colloids', E. Dickinson and S.R. Euston (eds.), Royal Society of Chemistry, Cambridge

Dickinson, E., Galazka, V.B. (1991); Emulsion stabilization by ionic and covalent complexes of β-lactoglobulin. *Fd. Hydrocoll.* **5**(3). 281-296

207

Dickinson, E., Galazka, V.B. (1992); Emulsion stabilization by protein-polysaccharide complexes; in, 'Gums and Stabilisers for the Food Industry 6', G.O. Phillips, P.A. Williams, D.J. Wedlock (eds.), IRL Press, Oxford

Dickinson, E., Galazka, V.B., Anderson, D.M.W. (1991); Emulsifying behaviour of gum arabic. Part 2: Effect of the gum molecular weight on the emulsion droplet-size distribution. *Carbohydr. Polym.* **14**, 385-392

Dickinson, E., Murray, B.S., Stainsby, G. (1988); Protein adsorption at air-water and oil-water interfaces; in 'Advances in Food Emulsions and Foams', E. Dickinson and G. Stainsby (eds.), Elsevier Applied Science, London

Doublier, J.L., Launay, B. (1981); Rheology of galactomannan solutions: comparative study of guar gum and locust bean gum. *J. Text Stud.* **12**, 151-172

Dubois, M., Gilles, K.A., Hamilton, J.K., Rebers, P.A., Smith, F. (1956); Colorimetric method for determination of sugars and related substances. *Anal. Chem.* **28**(3), 350-356

Ebling, P., Hannele, Y.-J., Aro, A., Helve, E., Sinisalo, M., Koivisto, V.A. (1988); Glucose and lipid metabolism and insulin sensitivity in type 1 diabetes: the effect of guar gum. *Am. J. Clin. Nutr.* **48**, 98-103

Edmond, E., Farquhar, S., Dunstone, J.R., Ogston, A.G. (1968); The osmotic behaviour of Sephadex and its effects on chromatography. *Biochem. J.* **108**, 755-763

Einstein, A. (1906); *Ann. Phys.* **19**, 289

Einstein, A. (1910); *Ann. Phys.* **33**, 1275

Einstein, A. (1911); *Ann. Phys.* **34**, 591

Ellis, P.R., Kamalanathan, T., Dawoud, F.M., Strange, R.N., Coultate, T.P. (1988); Evaluation of guar biscuits for use in the management of diabetes: tests of physiological effects and palatability in non-diabetic volunteers. *Europ. J. Clin. Nutr.* **42**, 425-435

Evans, J. H. (1972); Manipulation of light scattering data; in, 'Light Scattering from Polymer Solutions', M.B. Huglin (ed.), Academic Press, London

Fincher, G.B., Stone, B.A., Clarke, A.E. (1983); Arabinogalactan-proteins: structure, biosynthesis and function. *Ann. Rev. Plant Physiol.* **34**, 47-70

Flory, P.J. (1953); Principles of Polymer Chemistry, Cornell University, New York

French, D. (1972); Fine structure of starch and its relationship to the organization of starch granules. *J. Jap. Soc. Starch Sci.* **19**, 8-25

Fujii, M., Honda, K., Fujita, H. (1973); Dilute solutions of amylose in dimethylsulfoxide. *Biopolym.* **12**, 1177-1195

Fujita, H. (1975); Foundations of Ultracentrifugal Analysis; in, 'Chemical Analysis Vol. 42,' P.J. Elving, J.D. Winefordner, I.M. Kolthoff (eds.), Wiley, New York

Gaisford, S.E., Harding, S.E., Mitchell, J.R., Bradley, T.D. (1986); A comparison between the hot and cold water soluble fractions of two locust bean gum samples. *Carbohydr. Polym.* **6**, 423-442

Galliard, T., Bowler, P. (1987); Morphology and composition of starch; in, 'Starch: Properties and Potential', T. Galliard (ed.), John Wiley &Sons, Chichester

Gerken, T.A. (1993); Biophysical approaches to salivary mucin structure, conformation and dynamics. *Crit. Rev. Oral Biol. Med.* **4**(3/4), 261-270

Giddings, J.C. (1982); Analysis of fundamental obstacles to the size exclusion chromatography of polymers of ultrahigh molecular weight. *Adv. Chromatogr.* **10**, 217-258

Giddings, J.C., Kucera, E., Russell, C.P., Myers, M.N. (1968); Statistical theory for the equilibrium distribution of rigid molecules in inert porous networks. Exclusion chromatography. *J. Phys. Chem.* **72**, 4397-4408

Goldstein, A.M., Alter, E.N. (1959); Guar gum; in 'Industrial Gums', R.L. Whistler (ed.), Academic Press, New York

Grasdalen, H., Painter, T. (1980); N.M.R. studies of composition and sequence in legume-seed galactomannans. *Carbohydr. Res.* **81**, 59-66

Green A.A. (1933);The preparation of acetate and phosphate buffer solutions of known pH and ionic strength. *J. Am. Chem. Soc.* **55**, 233-2336

Grice, H.C. (1988); Safety evaluation of butylated hydroxyanisole from the perspective of effects on forestomach and oesophageal squamous epithelium. *Fd. Chem. Toxic.* **26**, 717-723

Grubisic, Z., Rempp, R., Benoit, H. (1967); A universal calibration for gel permeation chromatography. *Polym. Lett.* **5**, 753-759

Gurov, A.N., Nuss, P.V., Gurova, N.V., Dotdaev, S.H. (1988); Equilibrium and non-equilibrium complexes between bovine serum albumin and dextran sulphate. - III Methylene blue binding by equilibrium complexes. *Fd. Hydrocoll.* **2**, 297-310

Hall, L., Yalpani, M. (1980); A high yielding, specific method for the chemical derivatization of D-galactose-containing polysaccharides: oxidation with D-galactose oxidase, followed by reductive animation. *Carbohydr. Res.* **81**, C10-C12

Harding, S.E. (1984); An analysis of the heterogeneity of mucins. *Biochem J.* **219**, 1061-1064

Harding, S.E. (1989); The macrostructure of mucus glycoproteins in solution. *Adv. Carbohydr. Chem. Biochem.* **47**, 345-381

Harding, S.E. (1992); Sedimentation Analysis of Polysaccharides; in, 'Analytical Ultracentrifugation in Biochemistry and Polymer Science', S.E. Harding, A.J. Rowe, J.C. Horton (eds.), Royal Society of Chemistry, Cambridge

Harding, S.E., Berth, G., Ball, A., Mitchell, J.R., Garcia de la Torre, J.G. (1991a); The molecular weight distribution and conformation of citrus pectins in solution studied by hydrodynamics. *Carbohydr. Polym.* **16**, 1-5

Harding, S.E., Horton, J.C., Morgan, P.J. (1992); MSTAR: A FORTRAN program for the model independent molecular weight analysis of macromolecules using low speed or high speed sedimentation equilibrium; in, 'Analytical Ultracentrifugation in Biochemistry and Polymer Science', S.E. Harding, A.J. Rowe, J.C. Horton (eds.), Royal Society of Chemistry, Cambridge, 275-294

Harding, S.E., Rowe, A.J., Creeth, J.M. (1983); Further evidence for a flexible and highly expanded spheroidal model for mucus glycoproteins in solution. *Biochem. J.* **209**, 893-896

Harding, S.E., Varum, K.M., Stokke, B.T., Smidsrod, O. (1991b); Molecular weight determination of polysaccharides. *Adv. Carbohydr. Anal.* **1**, 63-144

Hassid, W.Z. (1970); Biosynthesis of sugars and polysaccharides; in, 'The Carbohydrates: Chemistry and Biochemistry IIA', W. Pigman and D.A. Horton (eds.), Academic Press, New York

Hayashi, K., Kasumi, T., Kubo, N., Haraguchi, K., Tsumura, N. (1989); Effects of N-acetyl muramidase from *Streptomyces rutgersensis* H-4b as a food preservative. *Agric. Biol. Chem.* **53**, 3173-3177

Hizukuri, S. (1985); Relationship between the distribution of the chain length of amylopectin and the crystalline structure of starch granules. *Carbohydr. Res.*, **141**, 295-306

Hizukuri, S. (1986); Polymodal distribution of the chain lengths of amylopectins, and its significance. *Carbohydr. Res.* **147**, 342-347

Hizukuri, S., Kaneko, T., Takeda, Y. (1983); Measurement of the chain length of amylopectin and its relevance to the origin of crystalline polymorphism of starch granules. *Biochim. Biophys. Acta* **760**, 188-191

Hizukuri, S., Takagi, T. (1984); Estimation of the distribution of molecular weight for amylose by the low-angle laser-light-scattering technique combined with high-performance gel chromatography. *Carbohydr. Res.* **134**, 1-10

Hoffman, J., Svensson, S. (1978); Studies of the distribution of the D-galactosyl side-chain in guaran. *Carbohydr. Res.* **65**, 65-71

Holzwarth, G. (1976); Conformation of the extracellular polysaccharide of *Xanthomonas campestris.Biochem.* **15**, 4333-

Hong, H.C., Yu. L.P., Parke, J.T., Rollings, J.E. (1987); Enzymatic depolymerization of heterogeneous biopolymeric substrates. *Ann. N.Y. Acad.* **501**, 426-433

Horton, D., Riley, D.A., Hansen, P.M.T. (1980); Sedimentation-equilibrium studies of the polysaccharide components of *Pseudomonas aeruginosa. Biopolym.* **19**, 1801-1814

Huber, C., Lederer, K.H. (1980); Flow rate dependent degradation of high molecular weight polyisobutylene in GPC. *J. Polym. Sci., Polym Lett. Ed.* **18**, 535-540

Huggins, M.L. (1942); The viscosity of dilute solutions of long-chain molecules. IV. Dependence on concentration. *J.Am.Chem.Soc.*, **64**, 2716-2718

Hutton, D.A., Pearson, J.P., Allen, A., Foster, S.N.E. (1990); Mucolysis of the colonic mucus barrier of faecal proteinases: Inhibition by interacting polyacrylate. *Clin.Sci.,* **78**, 265-271

Imeson, A.P., Ledward, D.A., Mitchell, J.R. (1977); On the nature of the interaction between some anionic polysaccharides and proteins. *J. Sci. Food Agric.* **28**, 661-668

Jackson, C., Nilsson, L.H., Wyatt, P.J. (1989); Characterization of biopolymers using a multi-angle light scattering detector with size exclusion chromatography. *J. Appl. Polym. Sci: Appl. Polym Symp.* **43**, 99-114

Jansson, P.E., Kenne, L., Lindberg, B. (1975); Structure of the extracellular polysaccharide from *Xanthomonas campestris*. *Carbohydr. Res.* **45**, 275-282

Joint FAO/IAEA/WHO Expert Committee (1981); Wholesomeness of irradiated food. Report of Meeting 27 October - 3 November 1980, Geneva. Wld. Hlth. Org. Techn. Rep. Ser. No. 659

Jukes, D.J. (1991); Making food irradiation legal - past, present and future. *Food Sci. Technol. Today* **5**(4), 211-217

Jumel, K., Browne, P., Kennedy, J.F. (1992); The use of low angle laser light scattering with gel permeation chromatography for the molecular weight determination of biomolecules; in 'Laser Light Scattering in Biochemistry', S.E. Harding, D.B. Satelle, V.A. Bloomfield (eds.), Royal Society of Chemistry, Cambridge, Chapter 2

Kang, K.S., Pettitt, D.J. (1993); Xanthan, gellan, welan and rhamsan; in, 'Industrial Gums,' R.L. Whistler, J. BeMiller (eds.), Academic Press, San Diego

Kato, A., Kameyama, K., Takagi, T. (1992); Molecular weight determination and compositional analysis of dextran-protein conjugates using low-angle laser light scattering technique combined with high performance gel chromatography. *Biochim. Biophys. Acta* **1159**, 22-28

Kato, A., Minaki, K., Kobayashi, K. (1993); Improvement of emulsifying properties of egg white proteins by the attachment of polysaccharide through Maillard reaction in a dry state. *J. Agric. Food Chem.* **41**, 540-543

Kato, A., Murata, K., Kobayashi, K. (1988); Preparation and characterization of ovalbumin-dextran conjugate having excellent emulsifying properties. *J. Agri. Food Chem.* **36**, 421-425

Kato, A., Sasaki, Y., Furuta, R., Kobayashi, K. (1990); Functional protein-polysaccharide conjugate prepared by controlled dry-heating of ovalbumin-dextran mixtures. *Agric. Biol. Chem.* **54**(1) 107-112

213

Kato, Y., Matsuda, T., Kato, N., Nakamura, R. (1988); Browning and protein polymerization induced by amino-carbonyl reaction of ovalbumin with glucose and lactose. *J. Agric. Food Chem.* **36**, 806-809

Kato, Y., Matsuda, T., Kato, N., Nakamura, R. (1989); Maillard reaction of disaccharides with protein: suppressive effect of non-reducing end pyranoside groups on browning and protein polymerization. *J. Agric. Food Chem.* **37**, 1077-1081

Kato, Y., Watanabe, K., Sato, Y. (1978); Effect of the Maillard reaction on the attributes of egg white proteins. *Agric. Biol. Chem.* **42**, 2233-

Kato, Y., Watanabe, K., Sato, Y. (1981); Effect of Maillard reaction on some physical properties of ovalbumin. *J. Food Sci.* **46**, 1835-1839

Kawahara, K., Ohta, K., Miyamoto, H., Nakamura, S. (1984); Preparation and solution properties of pullulan fractions as standard samples for water-soluble polymers. *Carbohydr. Polym.* **4**, 335-356

Kaye, W., Havlik, A.J., (1973); Low angle laser light scattering - absolute calibration. *Appl. Opt.* **12**, 541-550

Kaye, W., Havlik, A.J., McDaniel, J.B. (1971); Light scattering measurements on liquids at small angles. *Polym. Lett.* **9**, 695-699

Kennedy, J.F., Cabral, J.M.S., Sa-Correia, I., White, C.A. (1987); Starch biomass: a chemical feedstock for enzyme and fermentation processes; in, 'Starch : Properties and Potential', T. Galliard (ed.), John Wiley & Sons, Chichester

Kennedy, J.F., White, C.A. (1983); Bioactive Carbohydrates, Ellis Horwood, Chichester

King, K., Gray, R. (1993); The effect of gamma irradiation on guar gum, locust bean gum, gum tragacanth and gum karaya. *Food Hydrocoll.* **6**(6), 559-569

Kirk, R.S., Sawyer, R. (1991); Pearson's Composition and Analysis of Foods. Longman Scientific & Technical

Klingler, R.W., Zimbalski, M. (1992); Molekulare Charakterisierung von Amylosen verschiedenen Ursprungs. *Starch* **44**, 414-418

Kontominas, M.G., Kokini, J.L. (1990); Measurement of molecular parameters of water soluble apple pectin using low angle laser light scattering. *Lebensm.- Wiss. u. -Technol.* **23**, 174-177

Kraemer, E.O. (1938); *Ind. Eng. Chem.*, **30**, 1200

Kratochvil, P. (1972); Particle scattering functions; in, 'Light Scattering from Polymer Solutions', M.B. Huglin (ed.), Academic Press, London

Kratochvil, P. (1987); Classical Light Scattering from Polymer Solutions, A.D. Jenkins (ed.), Polymer Science Library 5, Elsevier, Amsterdam

Kusama Y., Kageyama, E., Shimada, M., Nakamura, Y. (1976); Molecular weights and molecular weight distributions of irradiated cellulose fibres by gel permeation chromatography. *J. Appl. Polym. Sci.* **20**, 1679-

Lambert, F., Milas, M., Rinaudo, M. (1982); Gel permeation chromatography of the xanthan gum using a light scattering detector. *Polym. Bull.* **7**, 185-189

Launay, B., Doublier, J.L., Cuvelier, G. (1986); Flow properties of aqueous solutions and dispersions of polysaccharides; in, 'Functional Properties of Food Macromolecules', D.A. Ledward, J.R. Mitchell (eds.), Elsevier, Amsterdam

Laurent, T.C., Killander, J. (1964); A theory of gel filtration and its experimental verification. *J.Chromatog.* **14**, 317-330

Lavrenko, P.N., Linow, K.J., Görnitz, E. (1992); The concentration dependence of the sedimentation coefficient of some polysaccharides in very dilute solution; in, 'Analytical Ultracentrifugation in Biochemistry and Polymer Science', S.E. Harding, A.J. Rowe, J.C. Horton (eds.), Royal Society of Chemistry, Cambridge

Lecacheux, D., Mustiere, Y., Panaras, R., Brigand, G. (1986); Molecular weight of scleroglucan and other extracellular microbial polysaccharides by size exclusion chromatography and low angle laser light scattering. *Carbohydr. Polym, 6*, 477-492

Lecacheux. D., Panaras, R., Brigand, G., Martin, G. (1985); Molecular weight distribution of carrageenans by size exclusion chromatography and low angle laser light scattering. *Carbohydr. Polym. 5*, 423-440

LeCerf, D., Irinei, F., Muller, G. (1991); The effect of gamma irradiation on the water-swelling properties of karaya gum. *Food Hydrocoll. 5*(1/2), 155-157

Ledward, D.A. (1979); Protein-polysaccharide interactions; in, 'Polysaccharides in Food', J.M.V. Blanshard, J.R. Mitchell (eds.), Butterworths, London

leMaire, M., Viel, A., Moller, J.V. (1989); Size exclusion chromatography and universal calibration of gel columns. *Anal. Biochem. 177*, 50-56

Lindberg, B., Lorngren, J., Thompson, J.L., (1973); Degradation of polysaccharides containing uronic acid residues. *Carbohydr. Res. 28*, 351-357

Lopes, I., Andrade, C.T., Milas, M., Rinaudo, M. (1992); Role of conformation and acetylation of xanthan on xanthan-guar interaction. *Carbohydr. Polym. 17*, 121-126

Maier, H., Anderson, M., Karl, C., Magnuson, K., Whistler, R.L. (1993); Guar, locust bean, tara, and fenugreek gums; in 'Industrial Gums, Polysaccharides and their Derivatives'; 3rd Edition, R.L. Whistler and J.N. BeMiller (eds.), Academic Press, San Diego

216

Mauron, J. (1981); The Maillard reaction in food; A critical review from the nutritional standpoint; in, 'Progress in Food and Nutrition Science. Maillard Reactions in Food', Vol 5, C. Eriksson (ed.), Pergamon Press, Oxford

McCleary, B.V. (1979); Enzymatic hdrolysis, fine structure, and gelling interaction of legume-seed D-galacto-D-mannans. Carbohydr. Res. 71, 205-230

McCleary, B.V., Clark, A.H., Dea, I.C.M., Rees, D.A. (1985); The fine structure of carob and guar galactomannans. Carbohydr. Res. 139, 237-260

McCleary, B.V., Matheson, N.K. (1975); Galactomannan structure and β-mannanase and β-mannosidase activity in germinating legume seeds. Phytochem. 14, 1187-1194

McCleary, B.V., Matheson, N.K. (1983); Action patterns and substrate-binding requirements of β-D-mannanase with mannosaccharides and mannan-type polysaccharides. Carbohydr. Res. 119, 191-219

McCleary, B.V., Matheson, N.K., Small, D.M. (1976); Galactomannans and a galactoglucomannan in legume seed endosperms: structural requirements for β-mannanase hydrolysis. Phytochem. 15, 1111-1117

McCleary, B.V., Nurthen, E., Taravel, F.R., Joseleau, J.-P. (1983); Characterization of the oligosaccharides produced on hydrolysis of galactomannan with β-D-mannanse. Carbohydr. Res. 118, 91-109

McLaren, K.G. (1978); Degradation of cellulose in irradiated wood and purified celluloses. Int. J. Appl. Radiat. Isotopes 29, 631

Milas, M., Rinaudo, M. (1979); Conformational investigation on the bacterial polysaccharide xanthan. Carbohydr. Res. 76, 189-196

Moorhouse, R., Arnott, S., Walkinshaw, M.D. (1977); Am. Chem. Soc. Symp. Ser. 45

Morris, E.R. (1979); Polysaccharide structure and conformation in solutions and gels; in, 'Polysaccharides in Food', J.M.V. Blanshard and J.R. Mitchell (eds.), Butterworths, London

Morris, E.R., Cutler, A.N., Ross-Murphy, S.B., Rees, D.A., Price, J. (1981); Concentration and shear rate dependence of viscosity in random coil polysaccharide solutions. *Carbohydr. Polym.* 1, 5-21

Morris, E.R., Rees, D.A., Thom, D., Boyd, J. (1978); Chiroptical and stoichiometric evidence of a specific primary dimerisation process in alginate gelation. *Carbohydr. Res.* 66, 145-154

Morrison, W.R., Karkalas, J. (1990); Starch. *Meth. Plant Biochem.* 2, 323-352

Nakamura, S., Kato, A., Kobayashi, K. (1991); New antimicrobial characteristics of lysozyme-dextran conjugate. *J. Agric. Food Chem.* 39, 647-650

Nakamura, S., Kato, A., Kobayashi, K. (1992a); Bifunctional lysozyme-galactomannan conjugate having excellent emulsifying properties and bactericidal effect. *J. Agric. Food Chem.* 40, 735-739

Nakamura, S., Kato, A., Kobayashi, K. (1992b); Enhanced antioxidative effect of ovalbumin due to covalent binding of polysaccharide. *J. Agric. Food Chem.* 40, 2033-2037

Nakano, A., Minovra, Y. (1975); Relationship between hydrodynamic volume and the scission of polymer chains by high-speed stirring in several solvents. *Macromolecules* 8, 677-680

Nakano, A., Minovra, Y. (1978); Degradation of aqueous poly(acrylic acid) and its sodium salt solutions by high-speed stirring. *J. Appl. Polym. Sci.* 22, 2207-2215

Nikuni, Z. (1978); Granule and amylopectin structures. *Starch* 30, 105-111

Norton, I.T., Goodall, D.M., Frangon, S.A., Morris, E.R., Rees, D.A. (1984); Mechanism and dynamics of conformational ordering in xanthan polysaccharide. *J. Mol. Biol.* **175**, 371-394

Ouano, A.C. (1976); Gel permeation chromatography. XII. Computer assissted gel permeation chromatography and low angle laser light scattering photometry. *J. Chromatogr.* **118**, 303-312

Painter, T.J. (1967); Random depolymerisation of heteropolysaccharides. Part I. Dependence of yield and average molecular weight of homooligosaccharides upon monosaccharide distribution. J. Chem. Soc. C922-927

Phillips, G.O. (1961); Radiation chemistry of carbohydrates. *Adv. Carbohydr. Chem. Biochem.* **16**, 13-58

Phillips, G.O. (1972); Effects of ionizing radiations on carbohydrate systems. *Radiat. Res. Rev.* **3**, 335-351

Phillips, G.O. (1980); in 'The Carbohydrates', W. Pigman and D. Horton (eds.), Academic Press, New York

Porath, J., Flodin, P. (1959); Gel filtration: A method for desalting and group separation. *Nature*, **183**, 1657-1659

Price, N.C., Dwek, R.A. (1986); Principles and Problems in Physical Chemistry for Biochemsits, 2nd Ed., Oxford Science Publications, Clarendon Press, Oxford

Raffi, J., Agnel, J.P., Dauberte, B., Saint-Lebe, L. (1981a); Gamma radiolysis of starches derived from different foodstuffs. Part I. Study of some induced carbonyl derivatives. *Starch* **33**, 188-192

Raffi, J., Agnel, J.P., Dauberte, B., d'Urbal, M., Saint-Lebe, L. (1981b); Gamma radiolysis of starches derived from different foodstuffs. Part III. Study of induced hdrogen peroxide. *Starch* **33**, 269-271

Raffi, J., Frejaville, C., Dauphin, J.F., Dauberte, B., d'Urbal, M., Saint-Lebe, L. (1981c); Gamma radiolysis of starches derived from different foodstuffs. Part II. Study of induced acidities. *Starch* **33**, 235-240

Ralston, G. (1993); Introduction to Analytical Ultracentrifugation. Beckman Instruments Inc. Fullerton.

Raman, C.V. (1927); *Indian. J. Phys.* **2**, 1

Rayas-Duarte, P., Rupnow, J.H. (1989); Some physical and chemical properties of gamma irradiated food starches, in 'Frontiers in Carbohydrate Research 1 - Food Applications', R.P. Millane, J.N.BeMiller, R. Chandrasekaran (eds.), Elsevier Applied Science, London

Rinaudo, M., Desbriers, J. (1980); Aqueous gel permeation chromatography of polyelectrolytes and salt exclusion effects. *Europ. Polym. J.* **16**, 849-854

Robin, J.P., Mercier, C., Charbonniere, R., Guilbot, A. (1974); Litnerized starches. Gel filtration and enzymatic studies of insoluble residues from prolonged acid treatment of potato starch. *Cereal Chem.* **51**, 389

Robin, J.P., Mercier, C., Duprat, F., Charbonniere, R., Guilbot, A. (1975); Amidons Lintnérisés. *Stärke* **75**, 36-45

Robinson, G., Ross-Murphy, S.B., Morris, E.R. (1982); Viscosity-molecular weight relationships, intrinsic chain flexibility, and dynamic solution properties of guar galactomannan. *Carbohydr. Res.* **107**, 17-32

Rowe, A.J., Wynne Jones, S., Thomas, D., Harding, S.E. (1989); Analysis of solute concentration and concentration derivative distribution by means of frameshift Fourier and other algorithms applied to Rayleigh interferometric and Fresnel fringe patterns. *SPIE* **1163**, 138-148

Sato, T., Norisuye, T., Fujita, H. (1984); Double-stranded helix of xanthan: dimensional and hydrodynamic properties in 0.1M aqueous sodium chloride. *Macromol.* **17**, 2696-2700

Seymour, G.B., Harding, S.E. (1987); Analysis of the molecular size of tomato (*Lycopersicon esculentum* Mill) fruit polyuronides by gel filtration and low speed sedimentation equilibrium. *Biochem. J.* **245**, 463-466

Sharman, W.R., Richards, E.L., Malcolm, G.N. (1978); Hydrodynamic properties of aqueous solutions of galactomannans. *Biopolymers* **17**, 2817-2833

Sheehan, J.K., Carlstedt, I. (1984); Hydrodynamic properties of human cervical-mucus glycoproteins in 6M-guanidinium chloride. *Biochem. J.* **217**, 93-101

Silberberg, A., Meyer, F.A. (1982); Structure and function of mucus: in, 'Mucus in Health and Disease - II', E.N. Chantler, J.B. Elder, M. Elstein (eds.), Plenum Press, New York

Sjöberg, A.-M. (1987); The effects of γ-irradiation on the structure of apple pectin. *Food Hydrocoll.* **1**(4), 271-276

Smidsrod, O., Andresen, I.-L. (1979); Biopolymerkemi, Tapir, Trondheim

Sommermeyer, K., Cech, F., Pfitzer, E., Rössler, K. (1992); Characterisation of polymers by size exclusion chromatography using multiple detection. Investigations on the determination of structural differences of hydroxyethyl starches. *Chromatographia* **33**(3/4), 151-153

Spiller, G.A., Farquhar, J.W., Gates, J.E., Nichols, S.E. (1991); Guar gum and plasma cholesterol. *Arterisc. Thromb.* **11**, 1204-1208

Stainsby, G. (1980); Proteinacous gelling systems and their complexes with polysaccharides. *Food Chemistry* **6**, 3-14

Stenlund, B.(1976); Polyelectrolyte effects in gel chromatography. *Adv. Chromatogr.* **14**, 37-74

Strutt, J.W. (Lord Rayleigh) (1871); *Phil.Mag.* **41**, 107

Stuting, H.H., Krull, I.S., Mhatre, R., Krzysko, S.C., Barth, H.G. (1989); High performance liquid chromatography of biopolymers using on-line laser light scattering photometry. *LC-GC* **7**(5), 402-417

Sullivan, C.R., Corona, A., Rollings, J.E. (1992); Chromatographic technologies for macromolecular starch characterization; in, R.J. Alexander, H.F. Zobel (eds.), Developments in Carbohydrate Chemistry, American Association of Cereal Chemists, St. Paul

Swallow, A.J. (1977); Chemical effects of irradiation; in, 'Radiation Chemistry of Major Food Components', P.S. Elias, A.J. Cohen (eds.), Elsevier, Amsterdam

Takagi, T. (1990); Application of low angle laser light scattering detection in the field of biochemistry. Review of recent progress. *J. Chromatogr.* **506**, 409-416

Takagi, T., Hizukuri, S. (1984); Molecular weight and related properties of lily amylose determined by monitoring of elution from TSK-Gel PW high performance gel chromatography columns by the low-angle laser light scattering technique and precision differential refractometry. *J. Biochem.* **95**, 1459-1467

Takeda, Y., Hizukuri, S., Juliano, B.O. (1986); Purification and structure of amylose from rice starch. *Carbohydr. Res.* **148**, 299-308

Takeda, Y., Shitaozono, T., Hizukuri, S. (1988); Molecular structure of corn starch. *Starch* **40**, 51-54

Tako, M., Nakamura, S. (1984); Rheological properties of deacetylated xanthan in aqueous media. *Agr. Biol. Chem.* **48**, 2987-2993

Tanford, C. (1961); Physical Chemistry of Macromolecules, Wiley, New York

Tanford, C. (1980); The Hydrophobic Effect, 2nd Ed., Wiley, New York

222

Tilton, E.W., Brower, J.H. (1987); Ionizing radiation for insect control in grain and grain products. *Cer. Fds. Wrld.* 32(4), 330-335

Tombs, M.P. (1970); Alterations to proteins during processing and the formation of structures, in, 'Proteins as Human Food', R.A. Lawrie (ed.), Butterworths, London

Van Holde, K.E. (1985) Physical Biochemistry, 2nd Edition, Prentice-Hall Inc., Englewood Cliffs

Vijayendran, B.R., Bone, T (1984); Absolute molecular weight and molecular weight distribution of guar by size-exclusion chromatography and low-angle laser light scattering. *Carbohydr. Polym.* **4**, 299-313

von Sonntag C. (1980); Free radical reactions of carbohydrates as studied by radiation techniques. *Adv. Carbohydr. Chem Biochem.* **37**, 7-77

von Sonntag, C. (1987); The Chemical Basis of Radiation Biology, Taylor & Francis, London

Wales, M., van Holde, K.E. (1954); *J. Polym. Sci.* **14**, 81

Watanabe, K., Sato, Y., Kato, Y., (1980); Chemical and conformational change of ovalbumin due to the Maillard reaction. *J. Fd Proc. Preserv.* **3**, 263-274

Weiss, A.R., Cohn-Ginsberg, E. (1970); Calibration of gel-permeation columns with unfractionated polymers. *J. Polym. Sci.* **8** Part A-2, 148-152

Whistler, R.L., Hymowitz, T.(1979); Guar: Agronomy, Production Industrial Use and Nutrition, Purdue University Press, West Lafayette

Whistler, R.L., Ingle, T.R. (1965); in 'Starch chemistry and technology', R.L. Whistler, and E.F. Paschall (eds.), Academic Press, New York

Wielinga, W.C. (1990); Production and application of seed gums; in, 'Gums and Stabilizers for the Food Industry 5', G.O. Phillips, D.J. Wedlock, P.A. Williams (eds), Oxford University Press, Oxford, 383-403

Williams, D.L., Pretus, H.A., Browder, I.W. (1992); Application of aqueous gel permeation chromatography with in-line multi-angle laser light scattering and differential viscometry detectors for the characterization of natural product carbohydrate pharmaceuticals. *J. Liq. Chromatogr.* **15**(13), 2297-2309

Woodward, J.R., Phillips, D.R., Fincher, G.B. (1983); Water soluble (1->3), (1->4)-β-D-glucans from barley (*Hordeum vulgare*) endosperm. I. Physicochemical properties. *Carbohydr. Polym.* **3**, 143-156

Wyatt, P.J. (1993); Light scattering and the absolute characterization of macromolecules. *Anal. Chim. Acta* **272**, 1-40

Wyatt, P.J., Jackson, C., Wyatt, G.K. (1988) Part I. Absolute GPC determination of molecular weights and sizes from light scattering. *Am. Lab.* **20**, 86-91

Yau, W.W., Bly, D.D. (1980); in Size exclusion chromatography; T. Provder (ed.), *Amer. Chem. Soc. Sym. Ser.* **138**, Washington D.C.

Yau, W.W., Kirkland, J.J., Bly, D.D.(1979); Modern Size Exclusion Chromatography, Wiley, New York

Yau, W.W., Malone, C.P., Fleming, S.W. (1968); The equilibrium distribution coefficient in gel permeation chromatography. *J. Polym. Sci.* Part B **6**, 803-807

Yau, W.W., Malone, C.P., Suchan, H.L. (1970); Separation mechanism in gel permeation chromatography. *Sep. Sci.* **5**, 259-271

Yu, L.P., Rollings, J.E. (1987); Low angle laser light scattering - aqueous size exclusion chromatography of polysaccharides: Molecular weight distribution and polymer branching determination. *J. Appl. Polym. Sci.* **33**. 1909-1921

Zimm, B.H. (1945); *J. Chem. Phys.* **13**, 141

Zimm, B.H. (1948); *J. Chem. Phys.* **16**, 1099

Zobel, H.F. (1992); Starch granule structure; in, 'Developments in Carbohydrate Chemistry', R.J. Alexander, H.F. Zobel (eds.), American Association of Cereal Chemists, St. Paul

225

APPENDIX A: SEC/MALLS STUDIES ON STARCH

Four starch samples, cassava, wheat, potato and waxy rice, were analysed as part of the investigation into the fine structure of amylopectin by M.H. Ong. The debranched amylopectin fractions are of relatively low molecular weight and their light scattering intensities were too low for reliable absolute molecular weight determination, attention was therefore focussed on the amylose fraction of these starch samples.

Elution profiles for the samples investigated are shown in Figures A.1 to A.4. The light scattering peaks of the amylose fractions were very large in all cases and in order to see the corresponding concentration detector traces these had to be expanded (Figure A.5 to Figure A.8). From these traces the separation between the amylose fraction and the various amylopectin fractions are evident.

Weight average molecular weights as determined by SEC/MALLS and calculated degrees of polymerisation (DPw) thereof for the different amyloses (Table A.1) were higher than would usually be expected from amylose. However, there is considerable discrepancy between molecular weight values found by different workers in the literature. Asaoka et al (1987) found DPw's ranging from 2000 to 3800 for rice starches grown under different environmental conditions, using the same debranching regime and SEC columns as in our experiments. The DPw values for isolated amyloses from potato and rice starches obtained by Takeda et al (1988) were found to be much lower than our results. There is still a difference in opinion as to whether isolation of amylose by precipitation or extraction procedures results in the pure material. Klingler and Zimbalski (1992) found that isolated amylose fractions did not represent all the amylose present in the various starches and /or that some residual amylopectin was present. They suggested

Figure A.1: Elution profile from light scattering detector (90° detector) for cassava starch. Initial starch concentration = 15mg/ml, injection volume = 100µl, dn/dc = 0.15ml/g, flow rate = 0.5ml/min, eluent = sodium phosphate buffer, pH 8.6, column system 3.

Figure A.2: Elution profile from light scattering detector (90° detector) for wheat starch. Initial starch concentration = 15mg/ml, injection volume = 100µl, dn/dc = 0.15ml/g, flow rate = 0.5ml/min, eluent = sodium phosphate buffer, pH 8.6, column system 3.
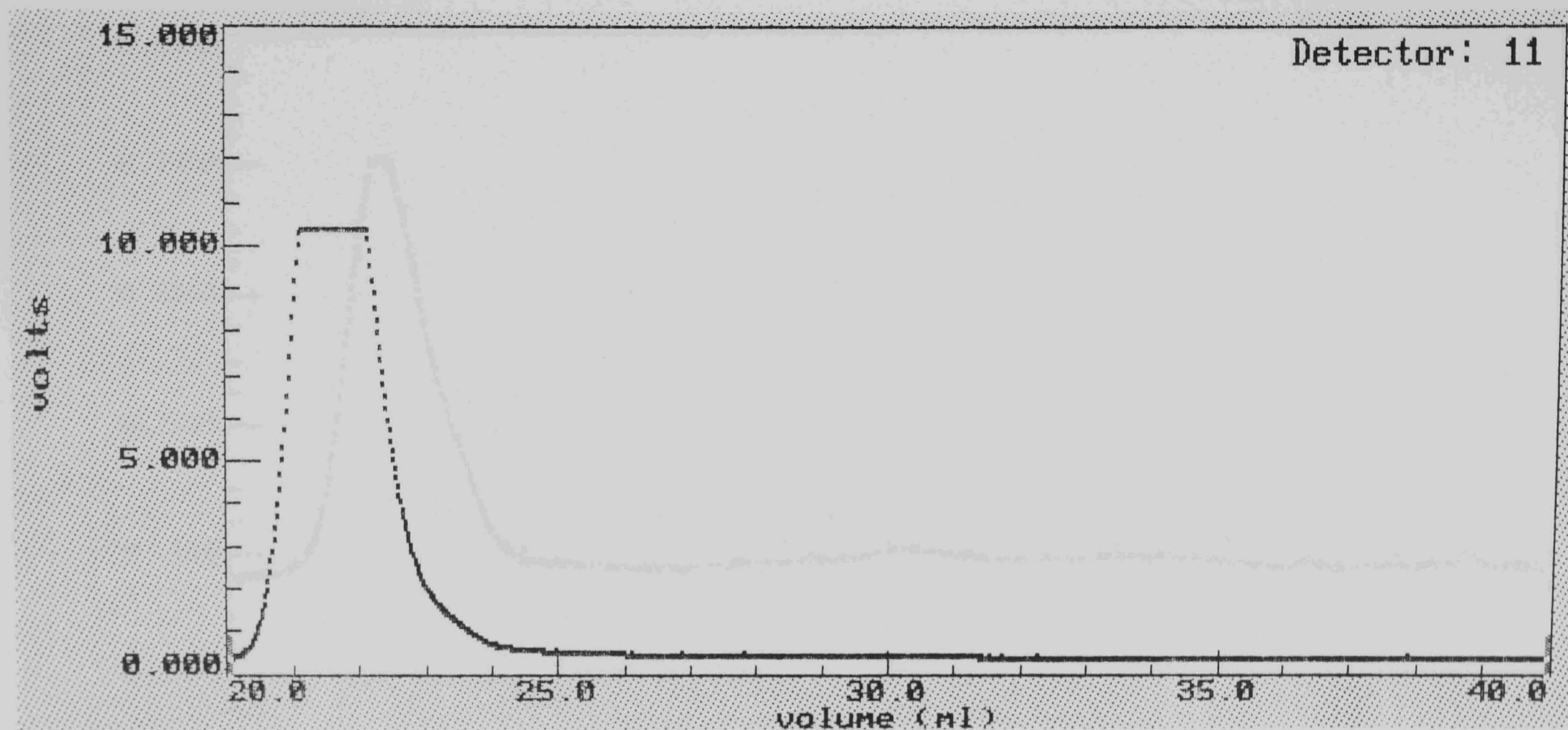
Figure A.3: Elution profile from light scattering detector (90° detector) for potato starch. Initial starch concentration = 15mg/ml, injection volume = 100µl, dn/dc = 0.15ml/g, flow rate = 0.5ml/min, eluent = sodium phosphate buffer, pH 8.6, column system 3.
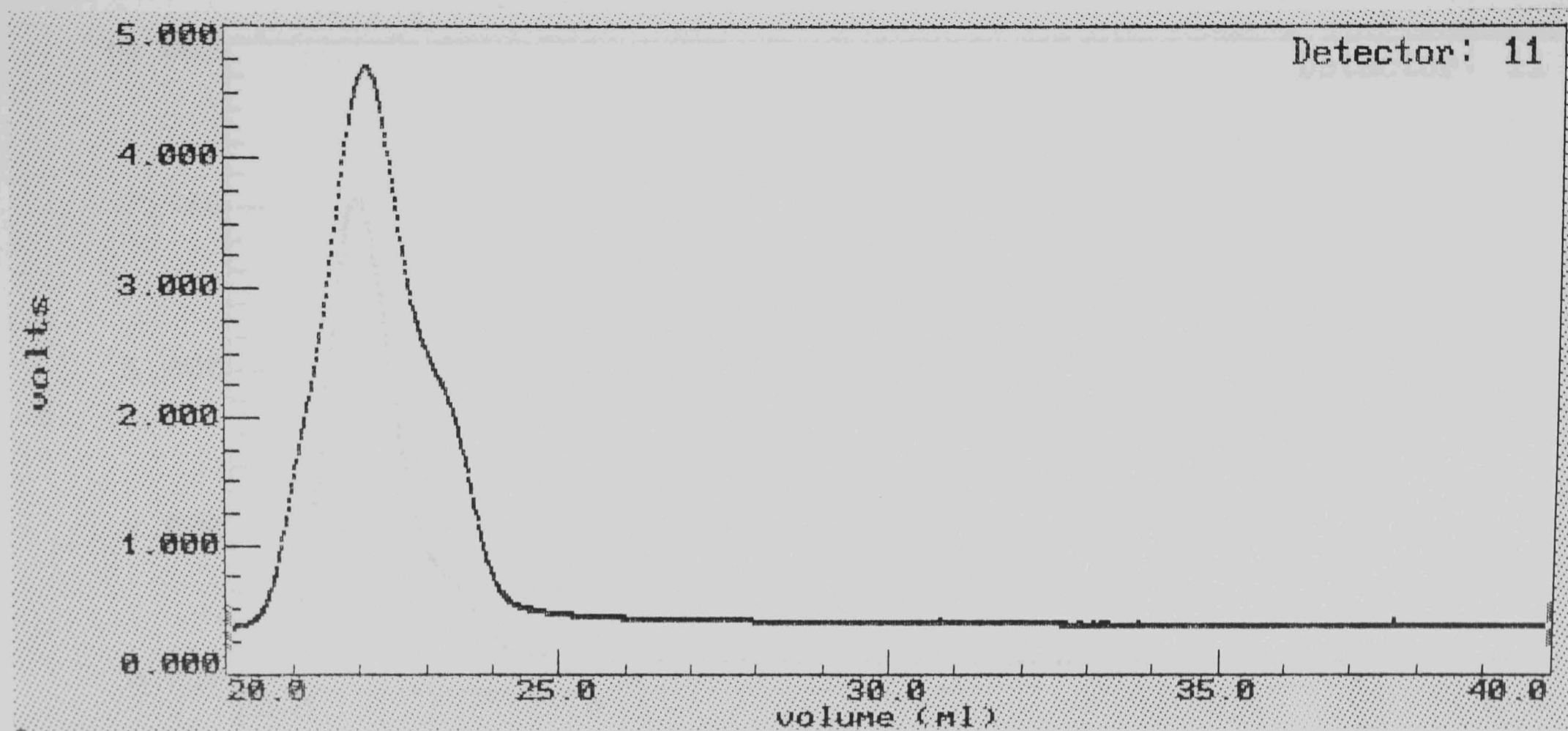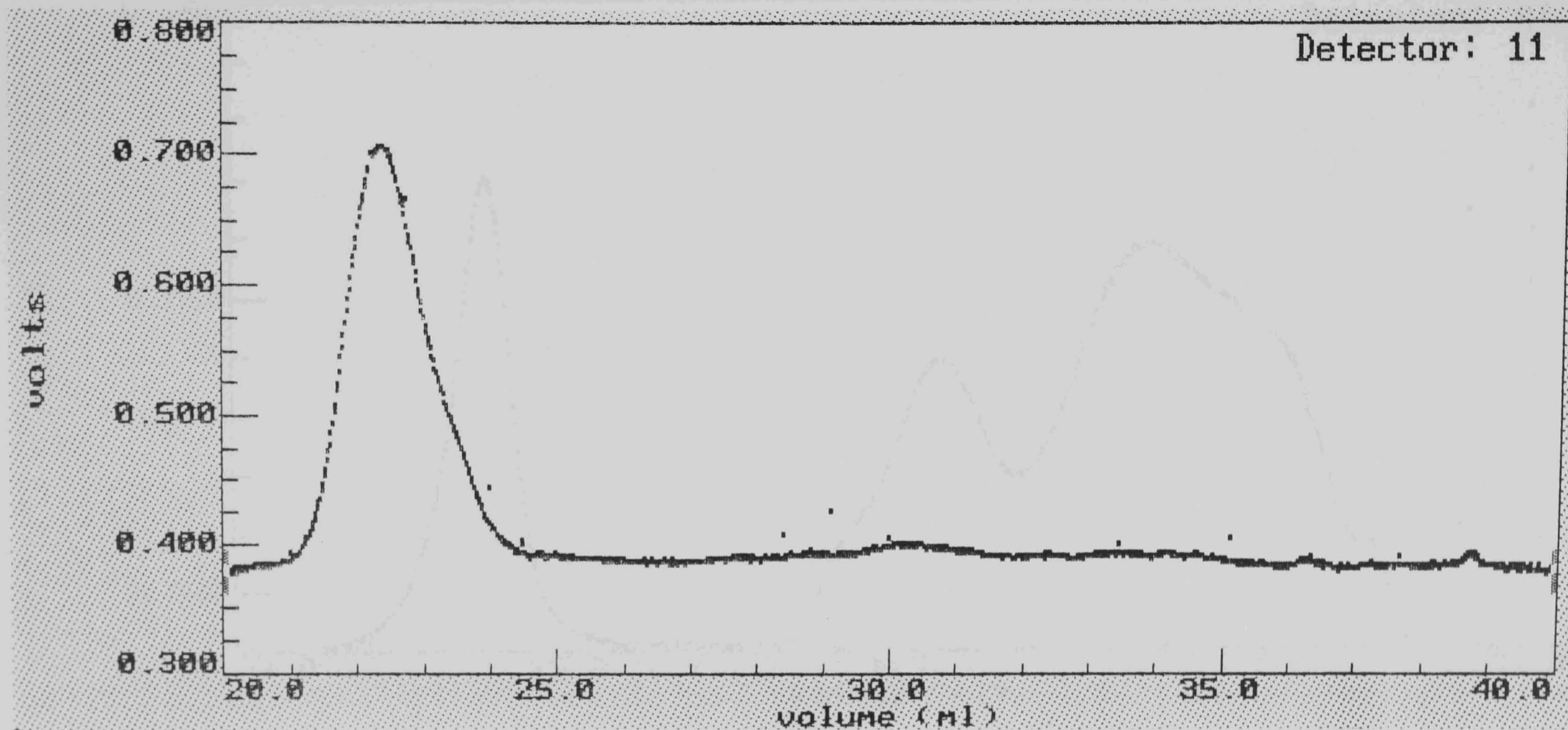
Figure A.4: Elution profile from light scattering detector (90° detector) for waxy rice starch. Initial starch concentration = 15mg/ml, injection volume = 100µl, dn/dc = 0.15ml/g, flow rate = 0.5ml/min, eluent = sodium phosphate buffer, pH 8.6, column system 3.
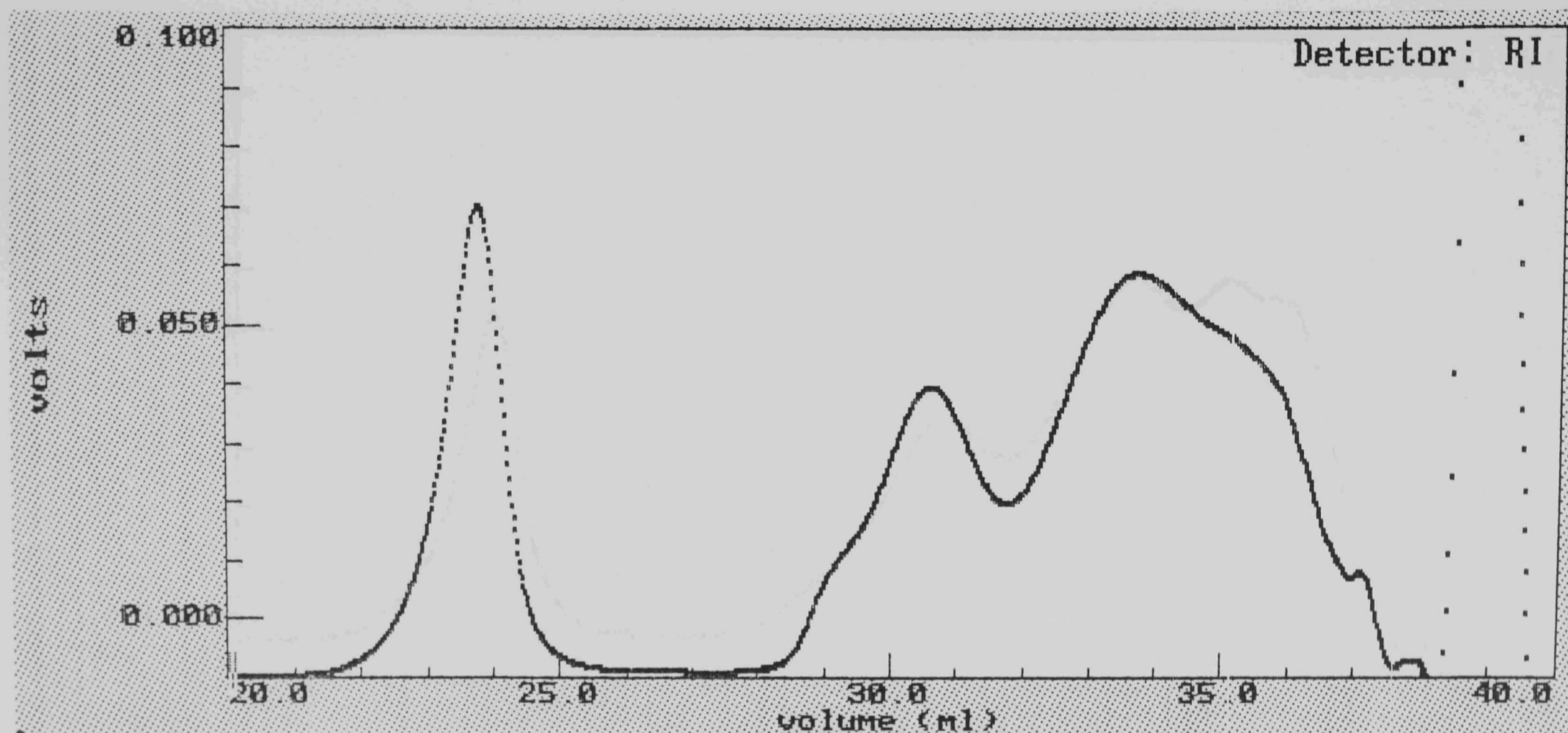
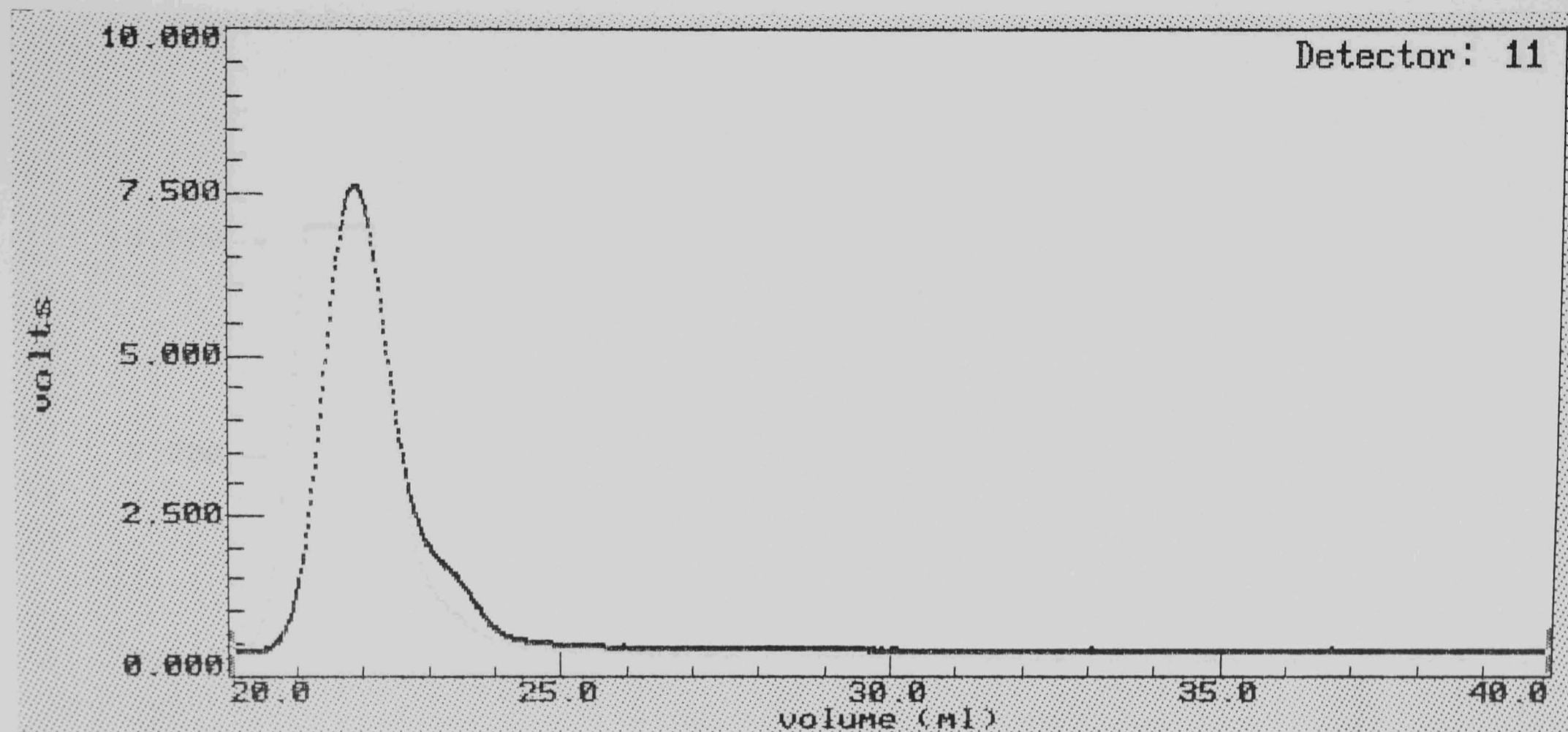**Figure A.5**: Elution profile from concentration detector (RI detector) for cassava starch. Chromatographic conditions as in Figure A.1
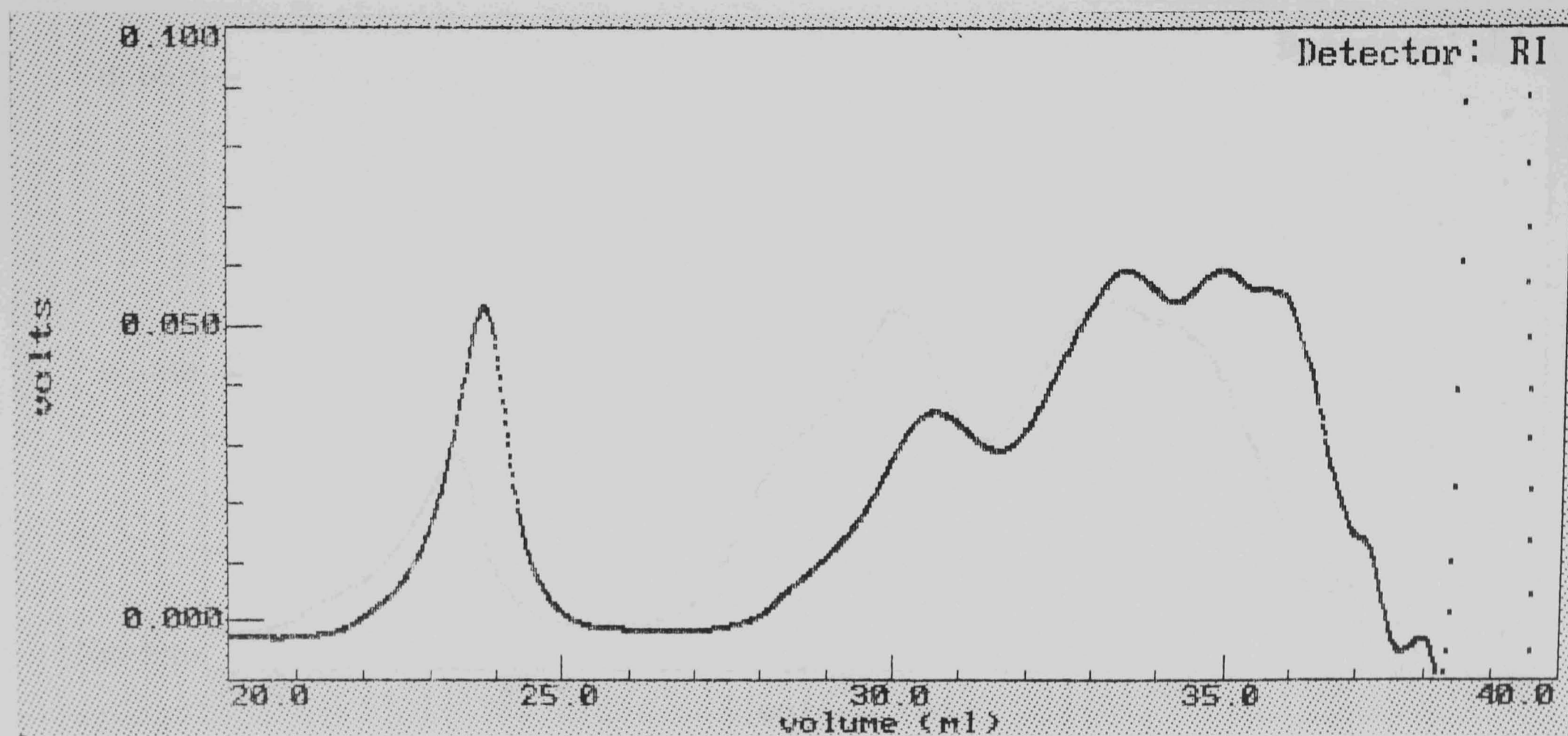
Figure A.6: Elution profile from concentration detector (RI detector) for wheat starch. Chromatographic conditions as in Figure A.2

232
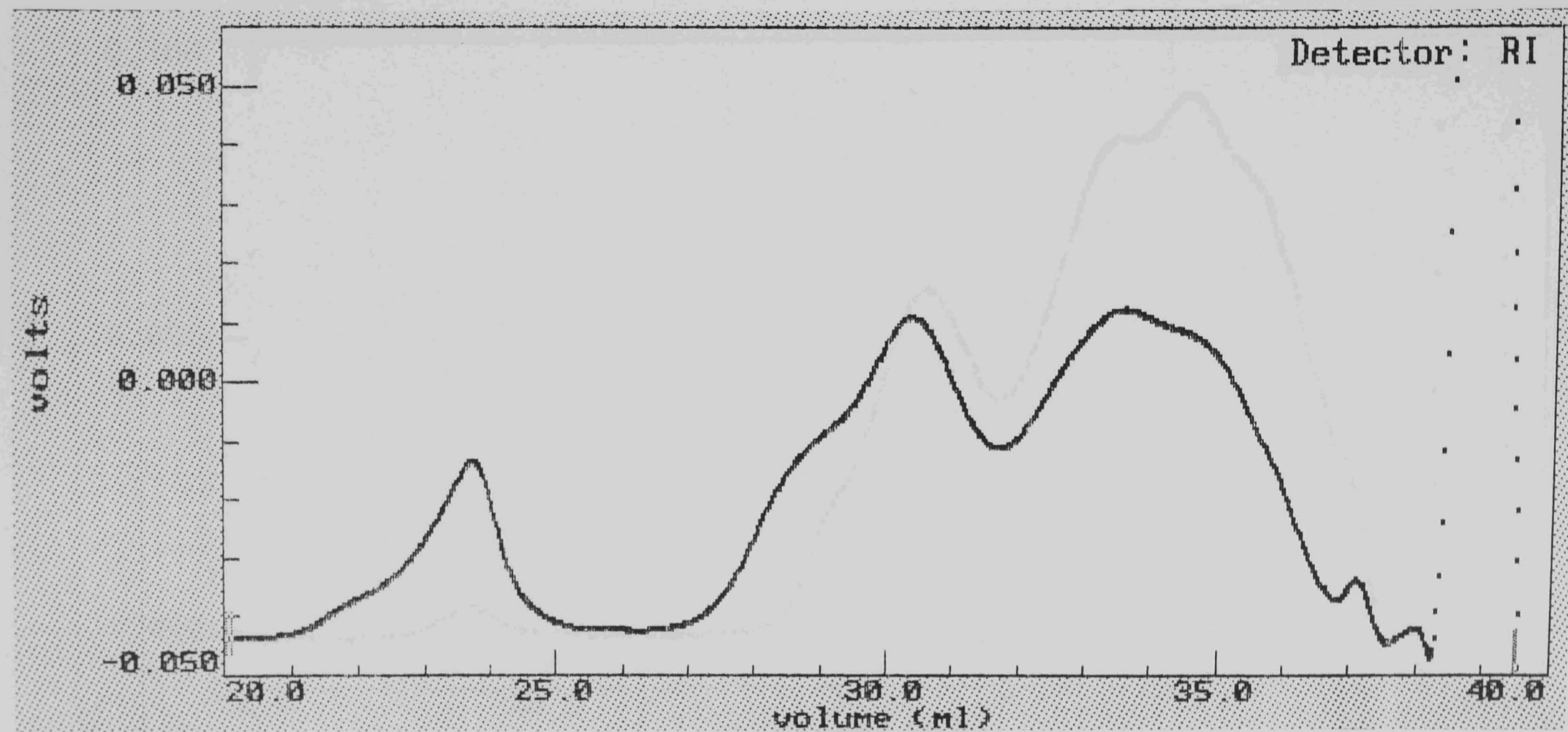
Figure A.7: Elution profile from concentration detector (RI detector) for potato starch. Chromatographic conditions as in Figure A.3

233
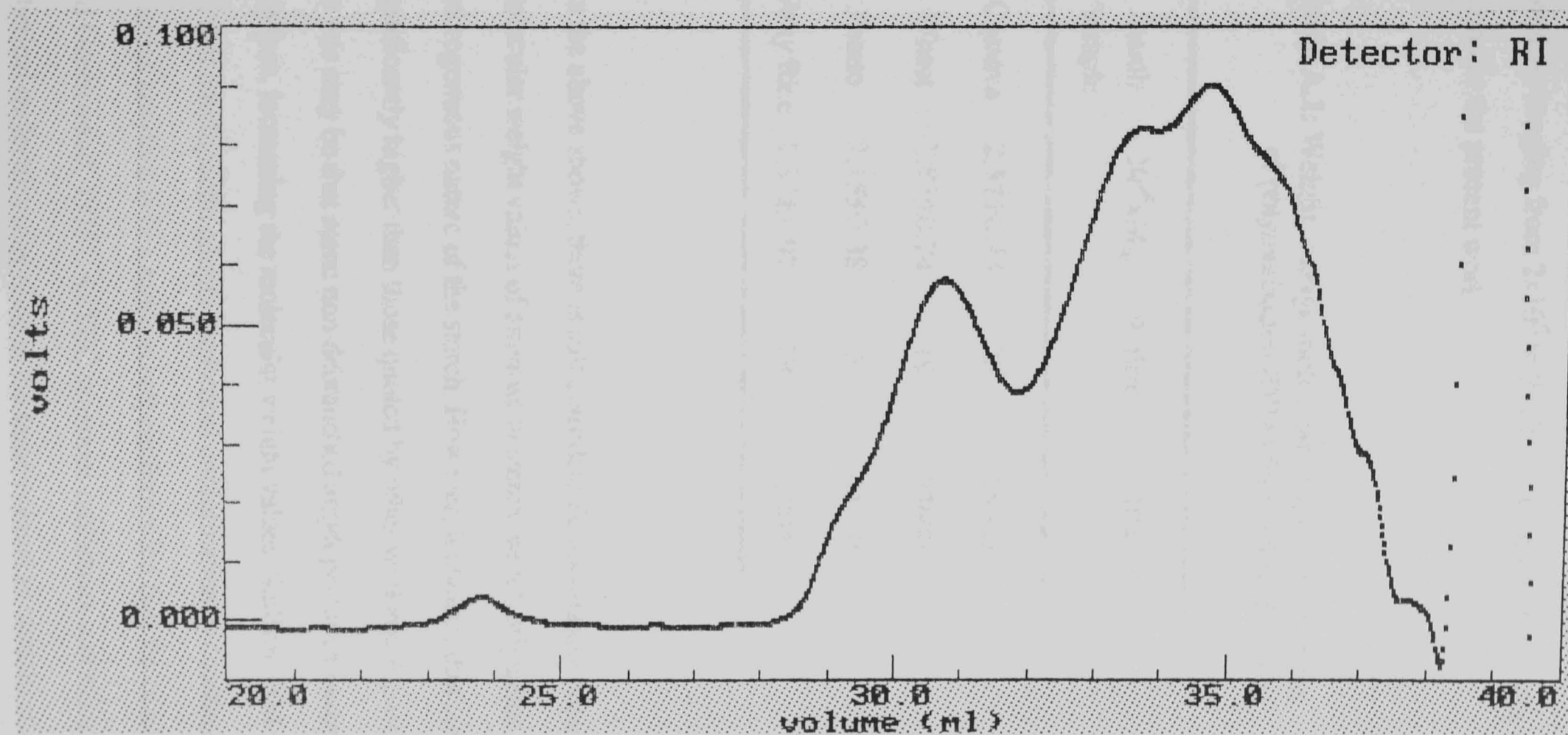
Figure A.8: Elution profile from concentration detector (RI detector) for waxy rice starch. Chromatographic conditions as in Figure A.4

that SEC of the whole starch would be the best method for investigating amylose and amylopectin and obtained weight average molecular weights for amylose ranging from 2×10^5 to 9×10^5, ie. considerably lower than those found in the present work.

Table A.1: Weight average molecular weights and degrees of polymerization (DPw) for amylose fractions

Starch sample	$10^{-6} \times M_w$	% Error	DPw
Cassava	2.57 ± 0.73	28	15900
Wheat	3.83 ± 0.74	19	23600
Potato	7.15 ± 0.38	5	44100
Waxy Rice	1.31 ± 1.02	79	8000

As the above shows, there is still considerable uncertainty regarding molecular weight values of amylose in starch, which originates from the heterogeneous nature of the starch. However, it appears that our values are significantly higher than those quoted by other workers. A possible reason for this may be that some non-debranched amylopectin co-eluted with the amylose, increasing the molecular weight values. Sullivan et al (1992) point out that amylopectin adopts a spherical conformation in aqueous media whereas amylose is in a random coil conformation (see for example Banks and Greenwood, 1975). As SEC separates molecules according to size, spherical molecules may elute at the same volume as random coils having lower molecular weights. A second possibility for the high molecular weight

values and the discrepancies between the different injections is that the amylose may have retrograded between the two runs - typical run times were approx. one hour.

The molecular weight versus elution volume profiles of the amylose fractions of our starches (Figure A.9 to Figure A.12) indicate good, linear separation of the molecules but also some heterogeneity. This is particularly evident for the potato starch (Figure A.10) which also displays a shoulder on the high molecular weight side in the concentration trace.

The above results show that there is significant uncertainty regarding the molecular weight values from the amylose fractions and debranching of amylopectin may have complicated the separation of the two starch components. Further detailed research is therefore required before definite conclusions can be drawn.

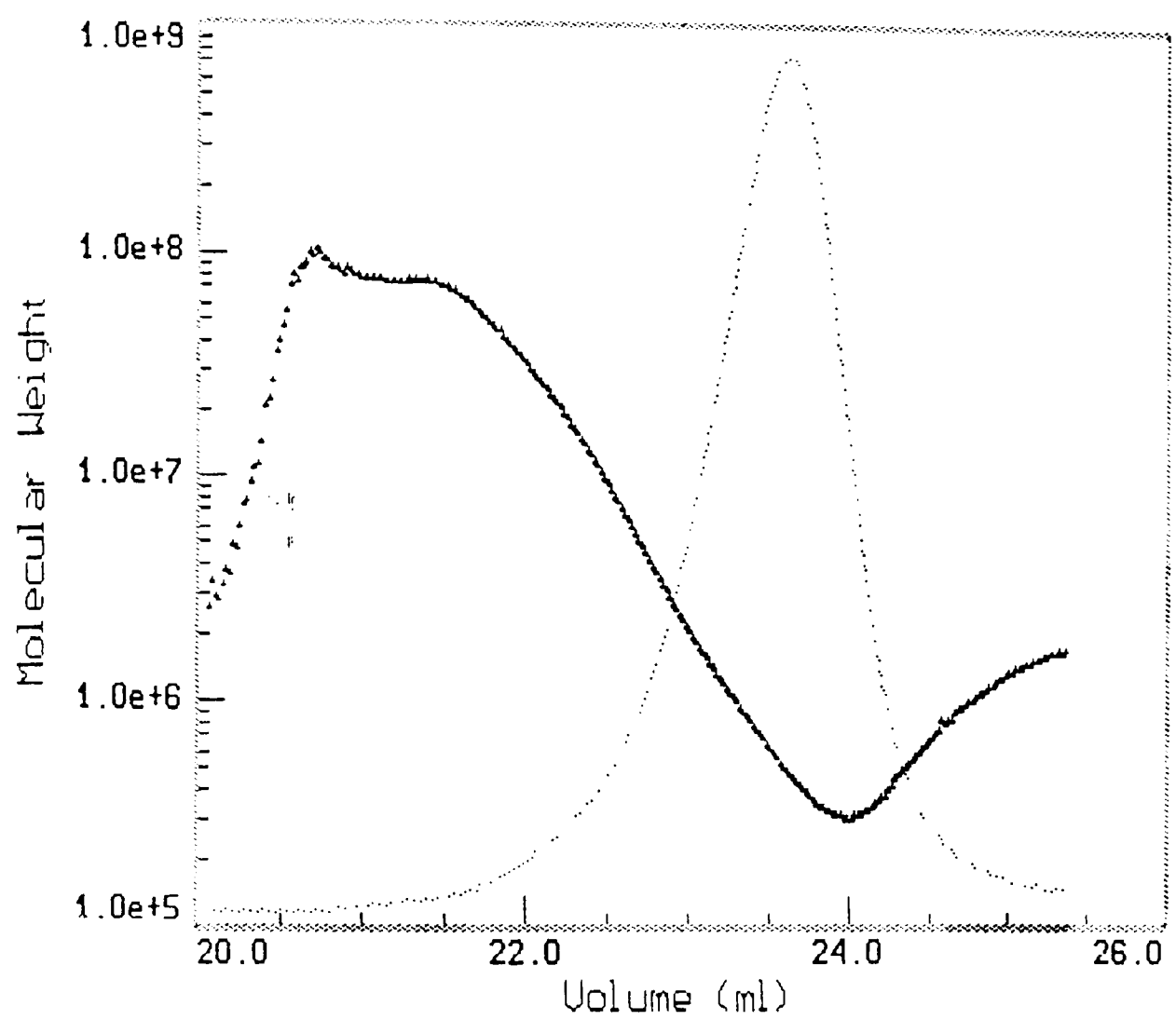**Figure A.9**: Plot of molecular weight versus elution volume for amylose fraction from cassava starch
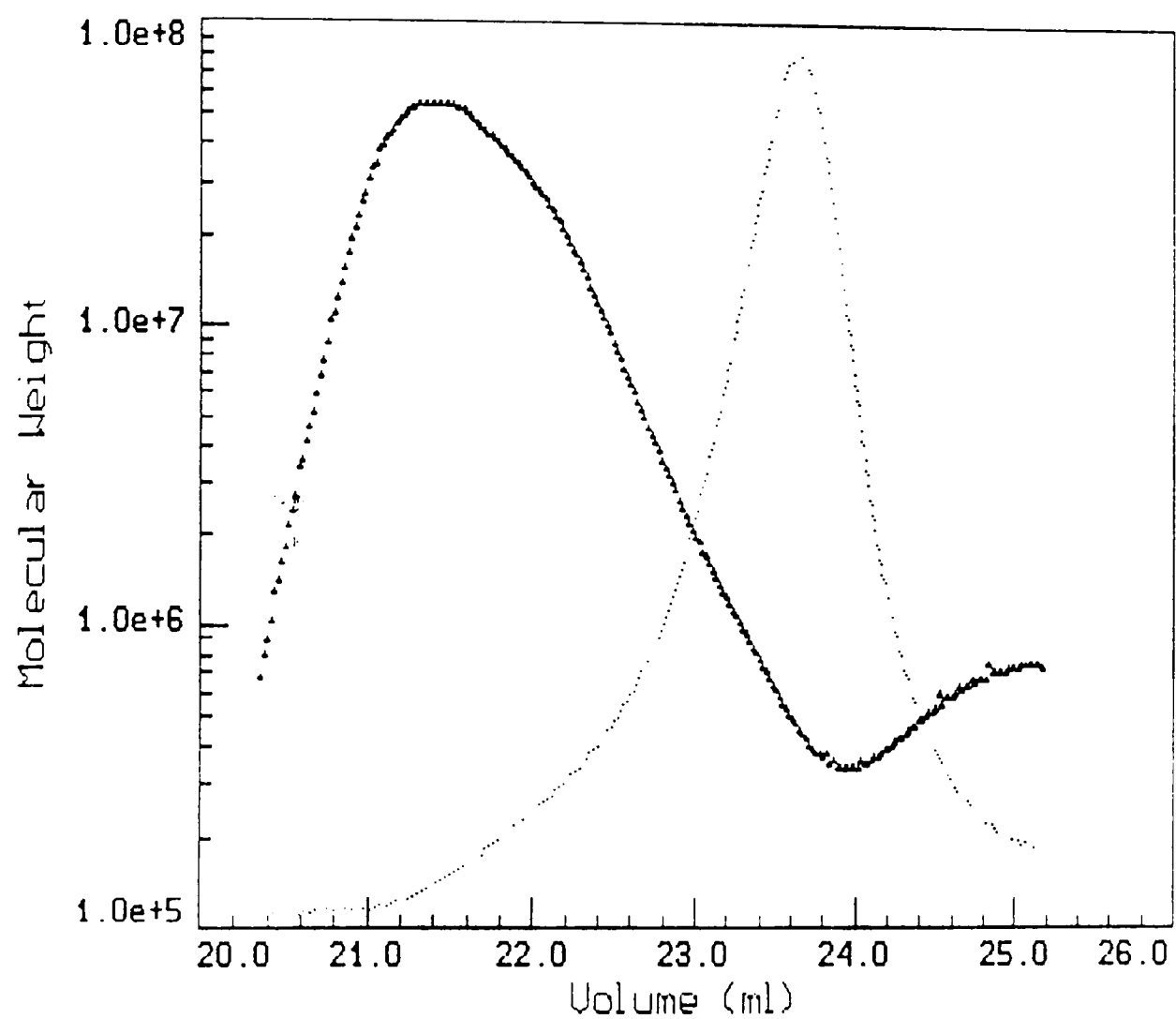
Figure A.10: Plot of molecular weight versus elution volume for amylose fraction from wheat starch
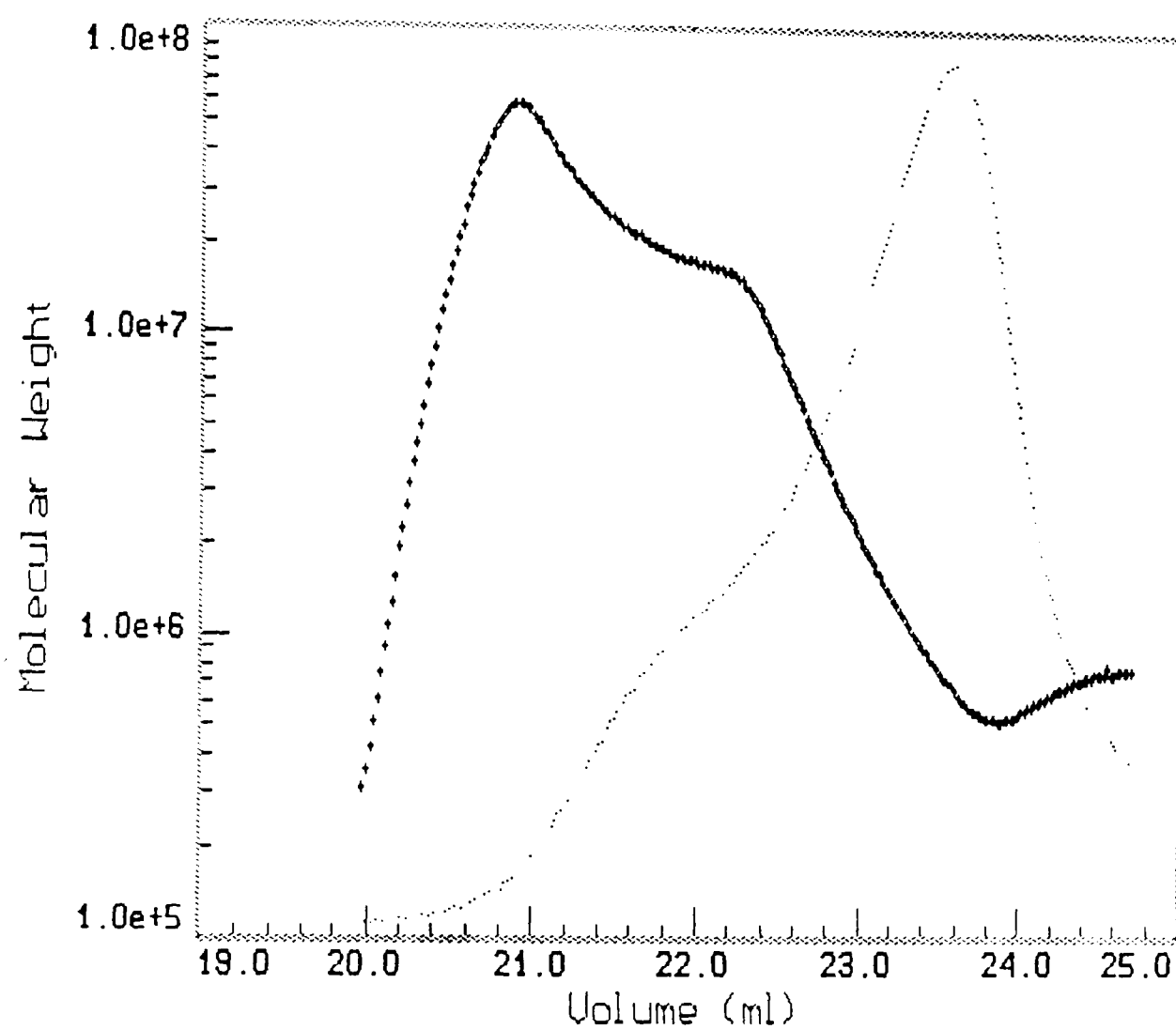
Figure A.11: Plot of molecular weight versus elution volume for amylose fraction from potato starch
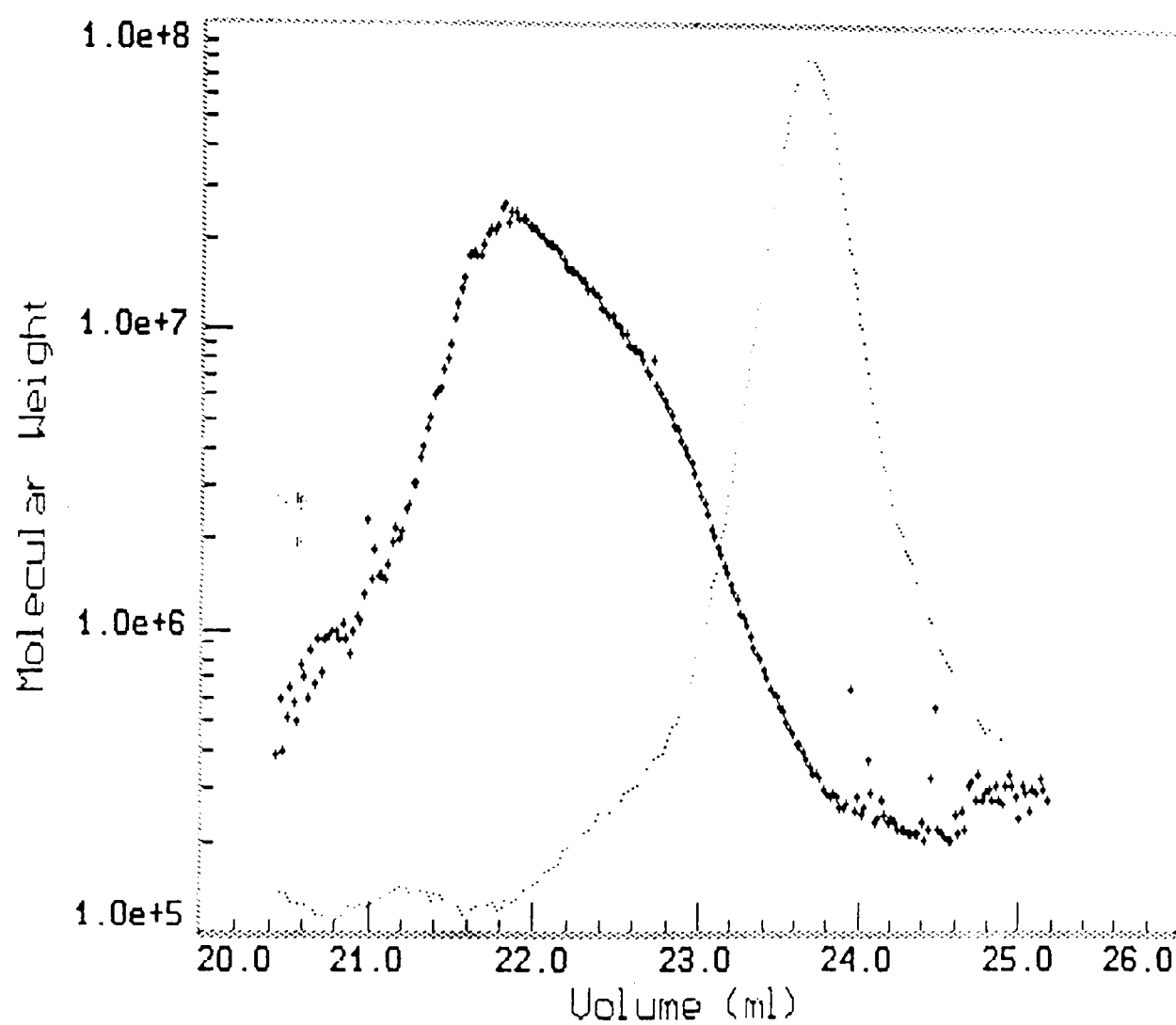
Figure A.12: Plot of molecular weight versus elution volume for amylose fraction from waxy rice starch

APPENDIX B: SEC/MALLS STUDIES ON MUCINS

B.1 Pig Gastric Mucin

The delay of the transit of a pharmaceutical dosage form within the gastro intestinal tract is often considered desirable, particularly in systems which are intended as controlled drug release systems (Davis, 1985). One way of delaying the transit of a pharmaceutical formulation within the gastro intestinal tract could be the inclusion of bioadhesive agents into the formulation which can adhere to the mucosal surface of the gastro intestinal tract (Bremecker, 1990). Mucus polysaccharide (or mucin) is the major component of the mucosal layer of the gastro intestinal tract and is therefore used as a model compound for bioadhesive studies. Prior to these studies it is important to characterize the physical properties and hydrodynamic behaviour of the model compound and this has been done by Mr. I. Fiebrig (Pharmaceutical Sciences, Nottingham University). As part of his characterization program, the molecular weights of several mucin samples at various purification stages were determined by SEC/MALLS. The results are shown in Table B.1.

The commercial samples (PGM 1, 2 and 3) exhibited relatively low weight average molecular weights and as the elution traces show (Figure B.1 is a representative example), there is a large shoulder on the main peak which is not removed even after extensive ultrafiltration (Figure B.2). These materials are frequently not sufficiently pure (for example, proteases may still be present) and should not be used as model compounds for bioadhesive studies (personal communication, I. Fiebrig). Clearly, the model compounds should be of high molecular weight and highly purified and such material was

241

Figure B.1: Elution profiles from light scattering (90° detector) and differential refractive index detectors for PGM 1 mucin sample. Sample concentration = 1mg/ml, injection volume = 100µl, dn/dc = 0.165ml/g, flow rate = 0.8ml/min, eluent = phosphate/chloride buffer (I = 0.1, pH6.8) as described in Section 3.1.4.1, column system 2.

Figure B.2: Elution profiles from light scattering (90° detector) and differential refractive index detectors for PGM 2 sample. Conditions as in Figure B.1

freshly prepared by I. Fiebrig as described in Section 3.1.4.1. The weight average molecular weights of these samples are much higher than the commercial samples. The elution trace of the crude sample (ie. after preparation as described in Section 3.1.4.1) (Figure B.3) still has a shoulder on the low molecular weight side of the peak and the weight average molecular weight is only approx. 3.5×10^6. Purification of this sample by preparative SEC led to a weight average molecular weight of 5.1×10^6 and complete removal of the lower molecular weight component (see Figure B.4). After a second caesium chloride density gradient ultracentrifugation purification the increase in the weight average molecular weight of the purified fraction was not considered significant for the purpose of the

Table B.1: Weight average molecular weight values for pig gastric (PG) mucins.

Sample	$10^{-6} \times M_w$ (1st investigation)	$10^{-6} \times M_w$ (2nd investigation)
Commercial samples		
PGM 1	$1.25 \pm 0.01^*$	$1.54 \pm 0.01^*$
PGM 2	$1.33 \pm 0.01^*$	1.68
PGM 3	0.67	-
Freshly prepared samples		
PGM 4A	3.49	-
PGM 4B	5.10	-
PGM 4C	$5.75 \pm 0.03^*$	-
PGM 5B1	$9.28 \pm 0.1^*$	-
PGM 5B2	$7.18 \pm 0.19^*$	-

* Results are average of duplicate runs.

Figure B.3: Elution profiles from light scattering (90° detector) and differential refractive index detectors for PGM 4A sample. Conditions as in Figure B.1
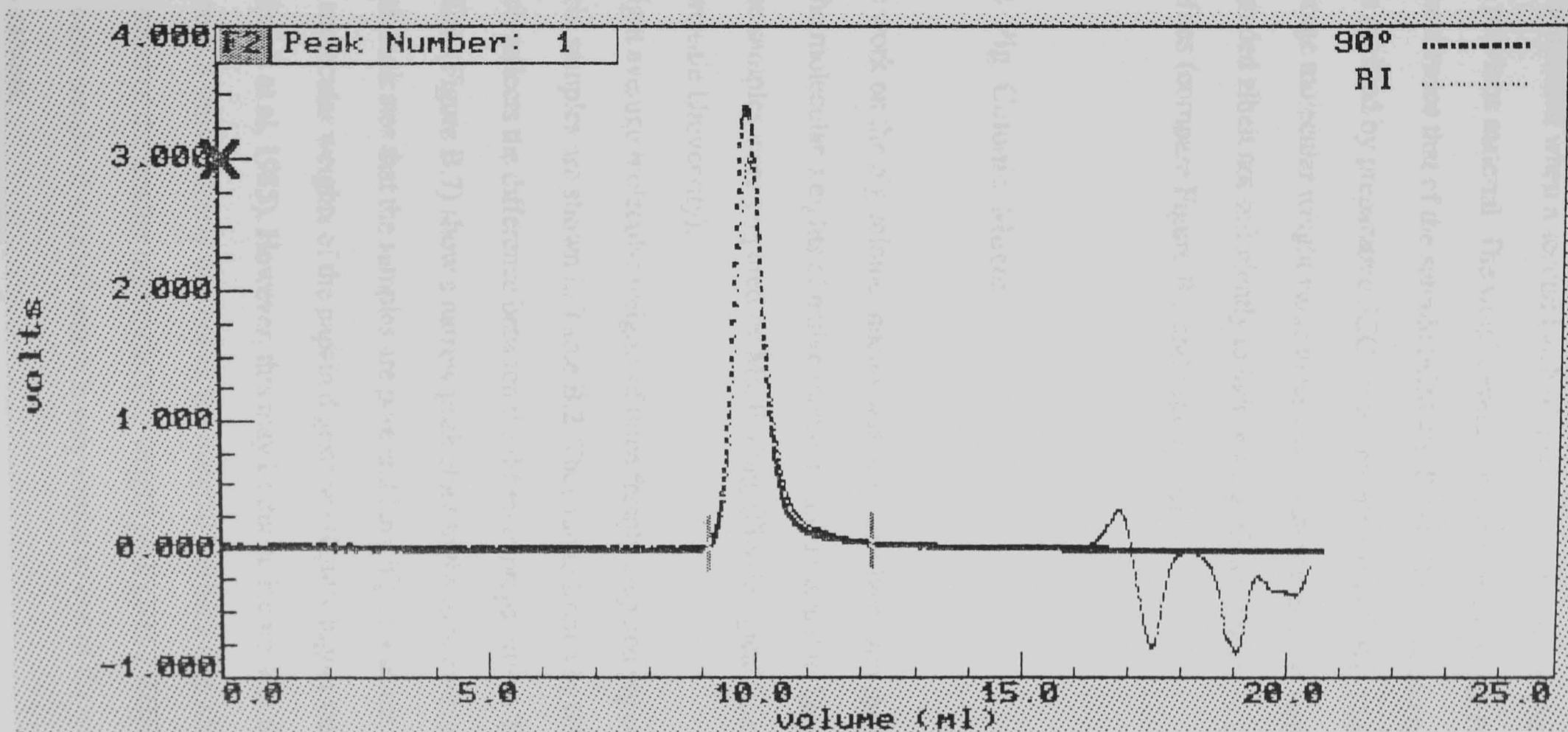
Figure B.4: Elution profiles from light scattering (90° detector) and differential refractive index detectors for PGM 4B sample. Conditions as in Figure B.1
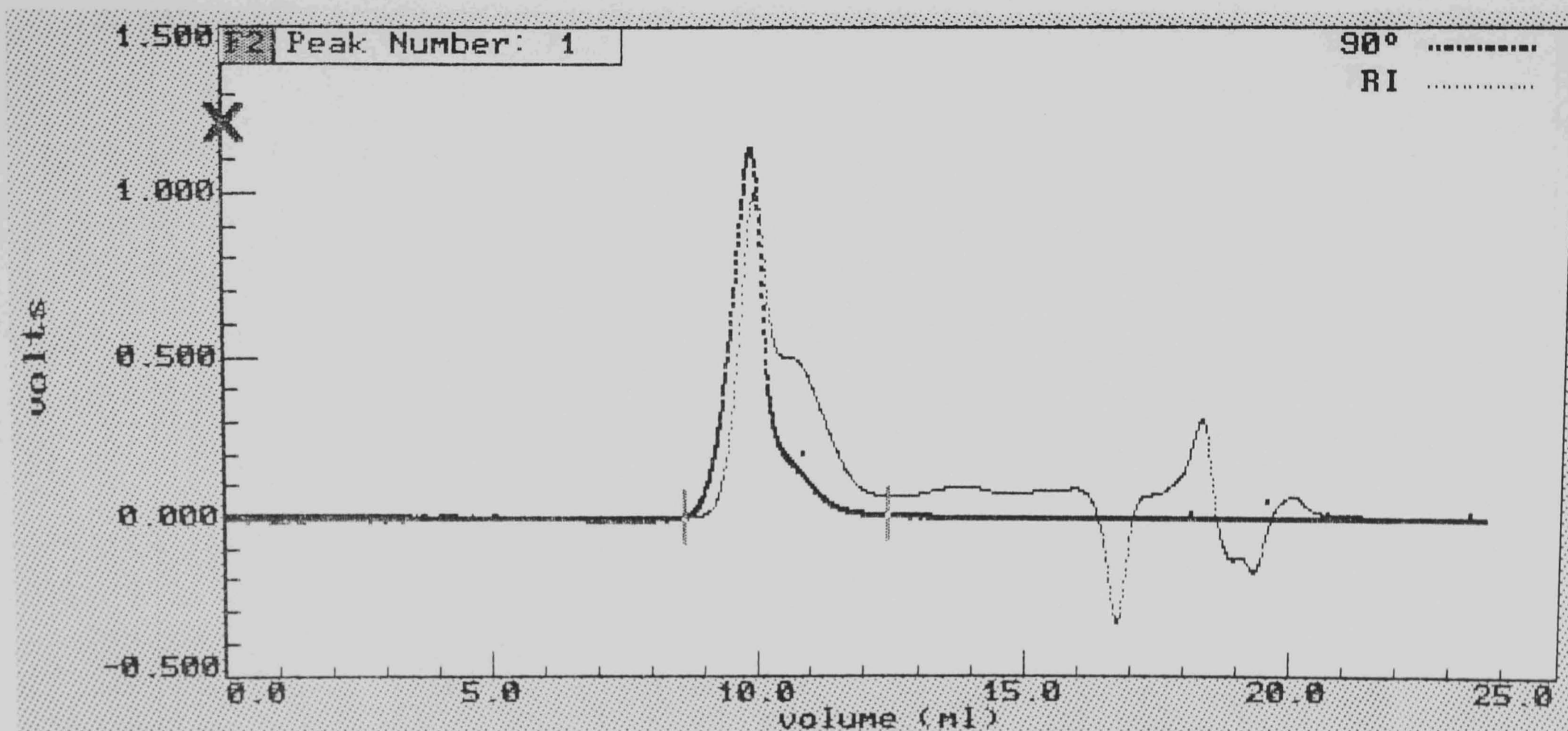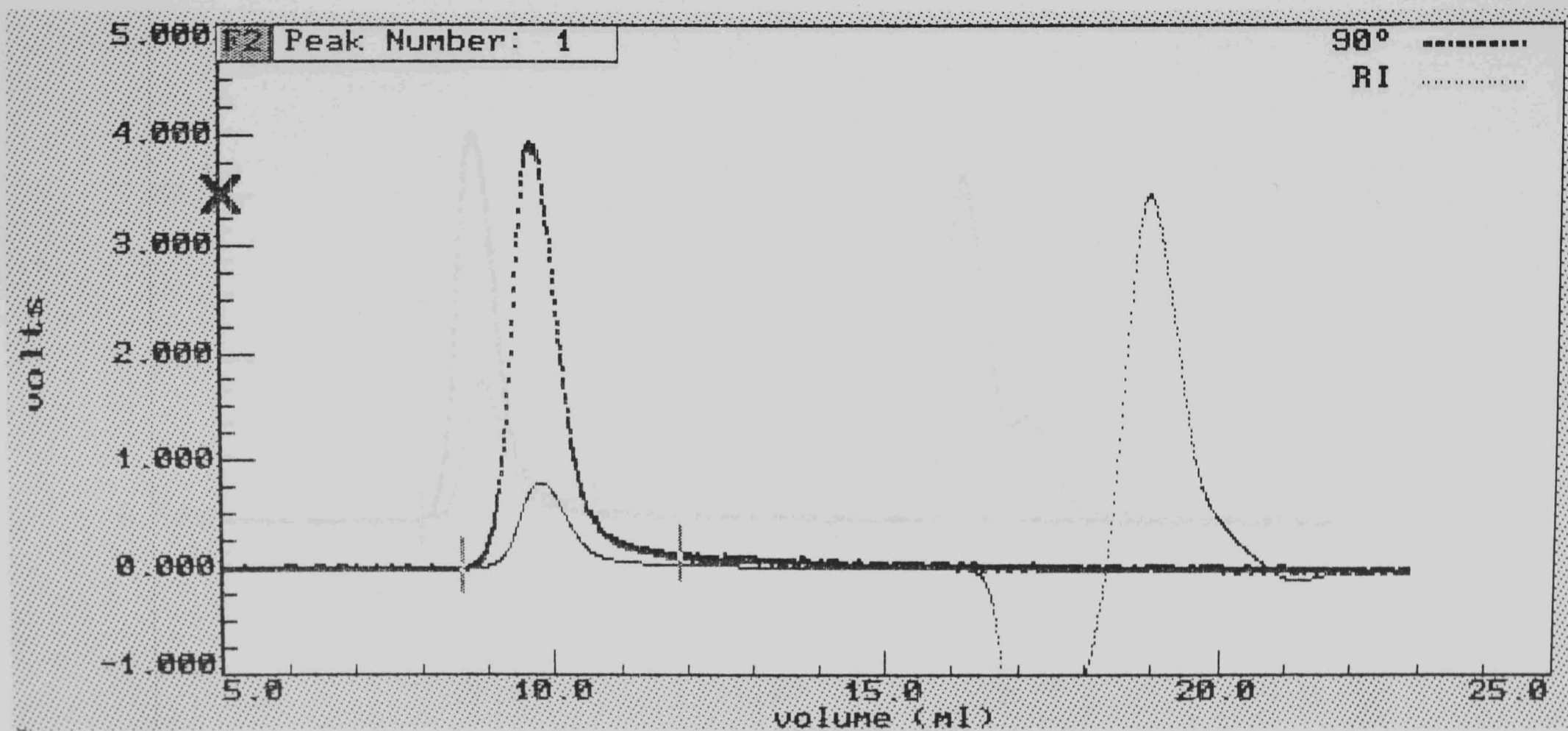
Figure B.5: Elution profiles from light scattering (90° detector) and differential refractive index detectors for PGM 5B1 sample. Conditions as in Figure B.1
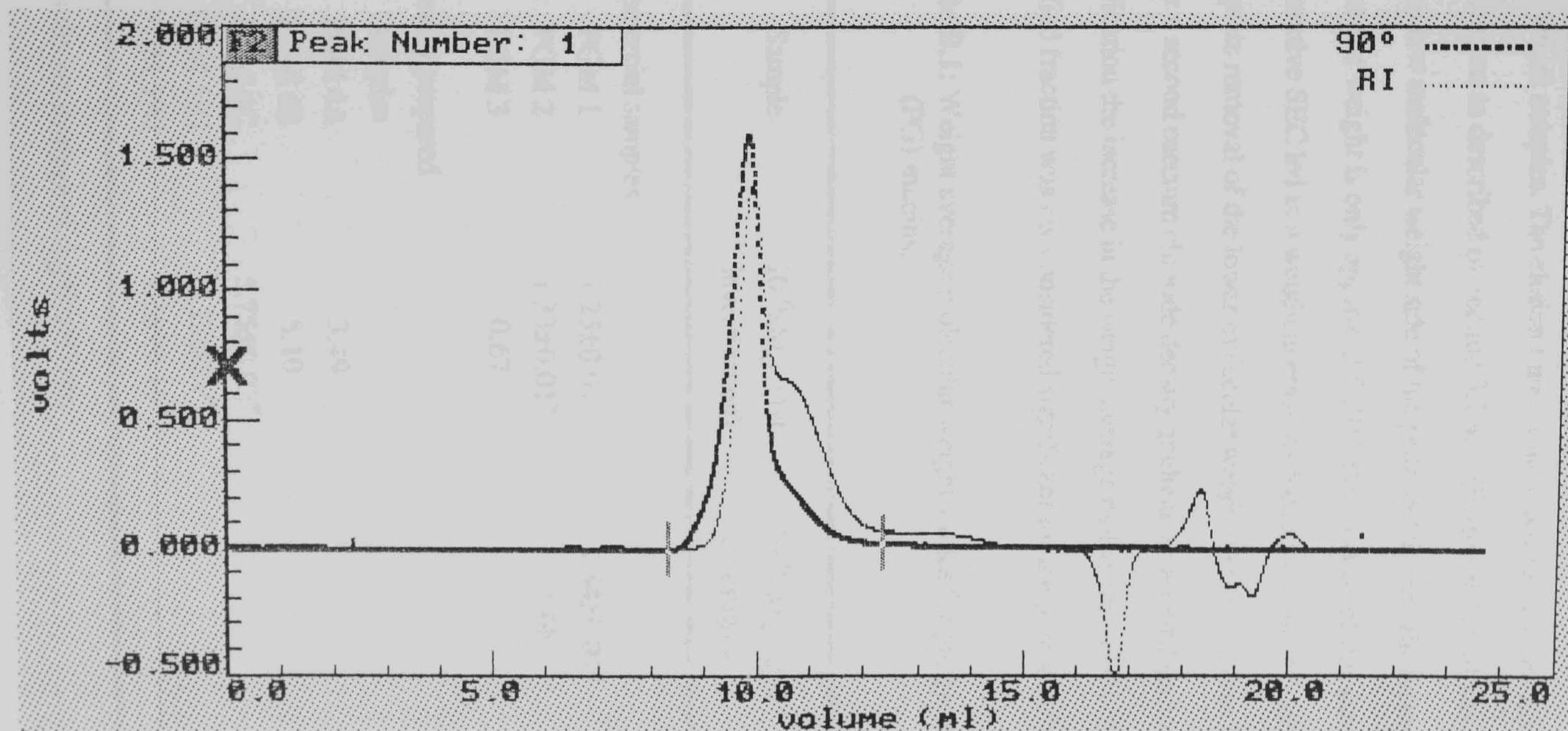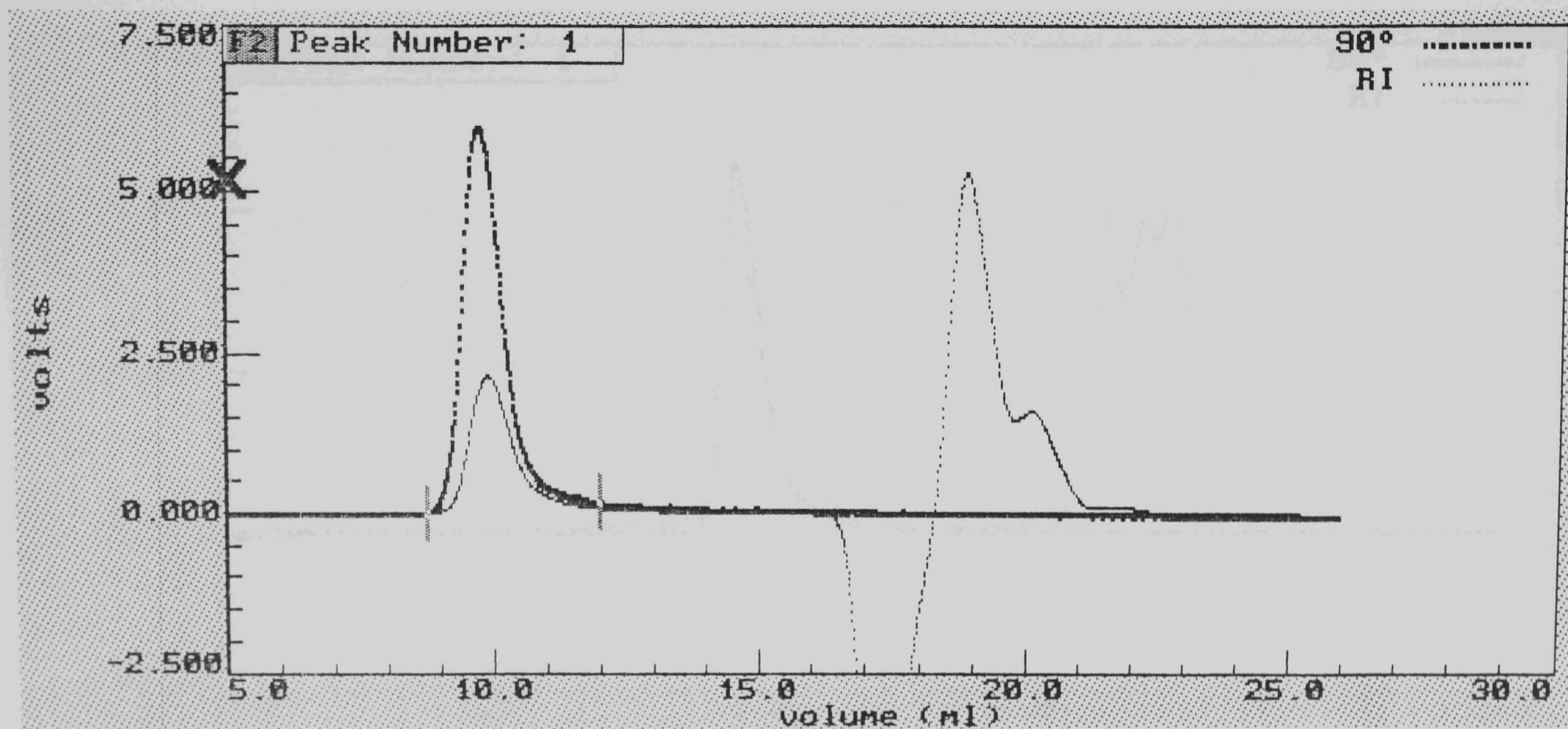
Figure B.6: Elution profiles from light scattering (90° detector) and differential refractive index detectors for PGM 5B2 sample. Conditions as in Figure B.1
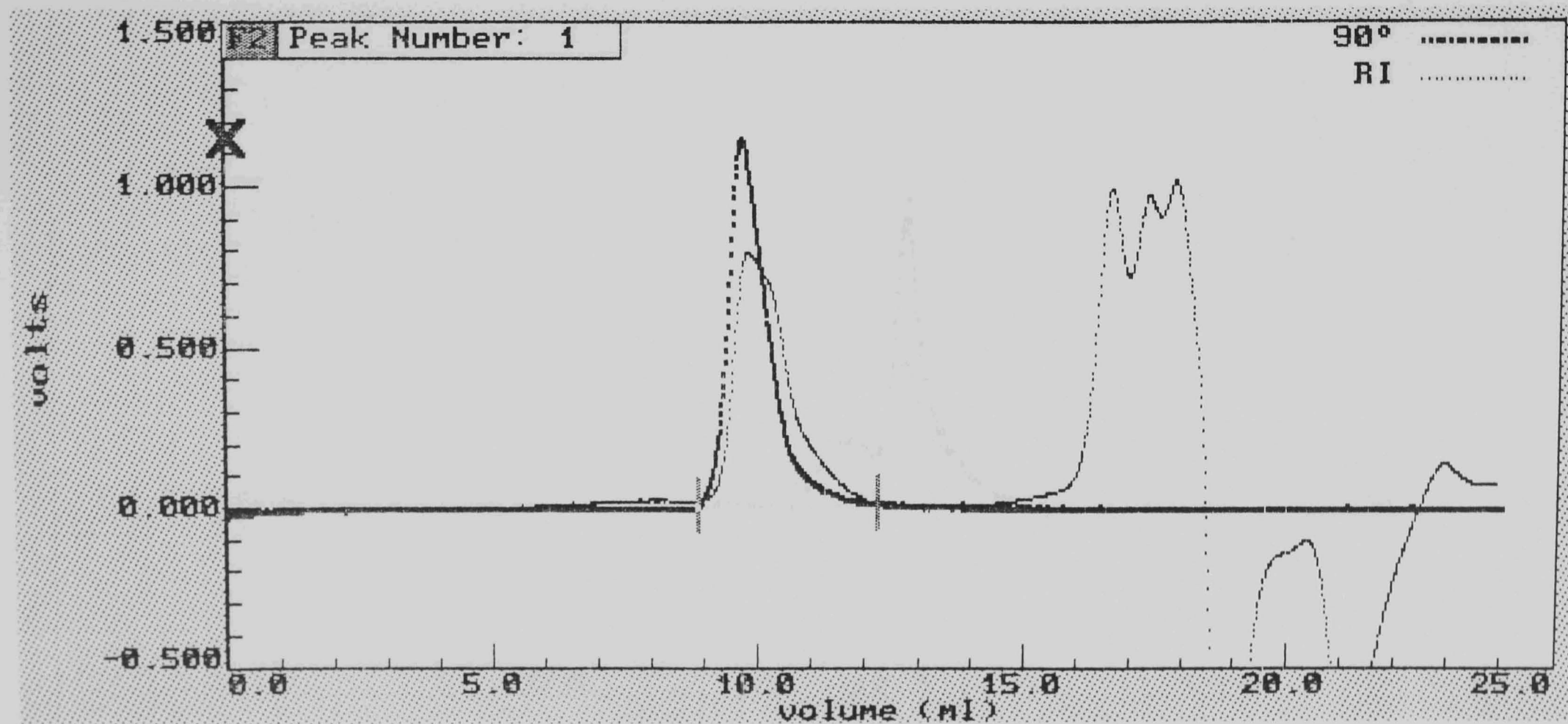
Figure B.7: Elution profiles from light scattering (90° detector) and differential refractive index detectors for PCM A1 sample. Conditions as in Figure B.1
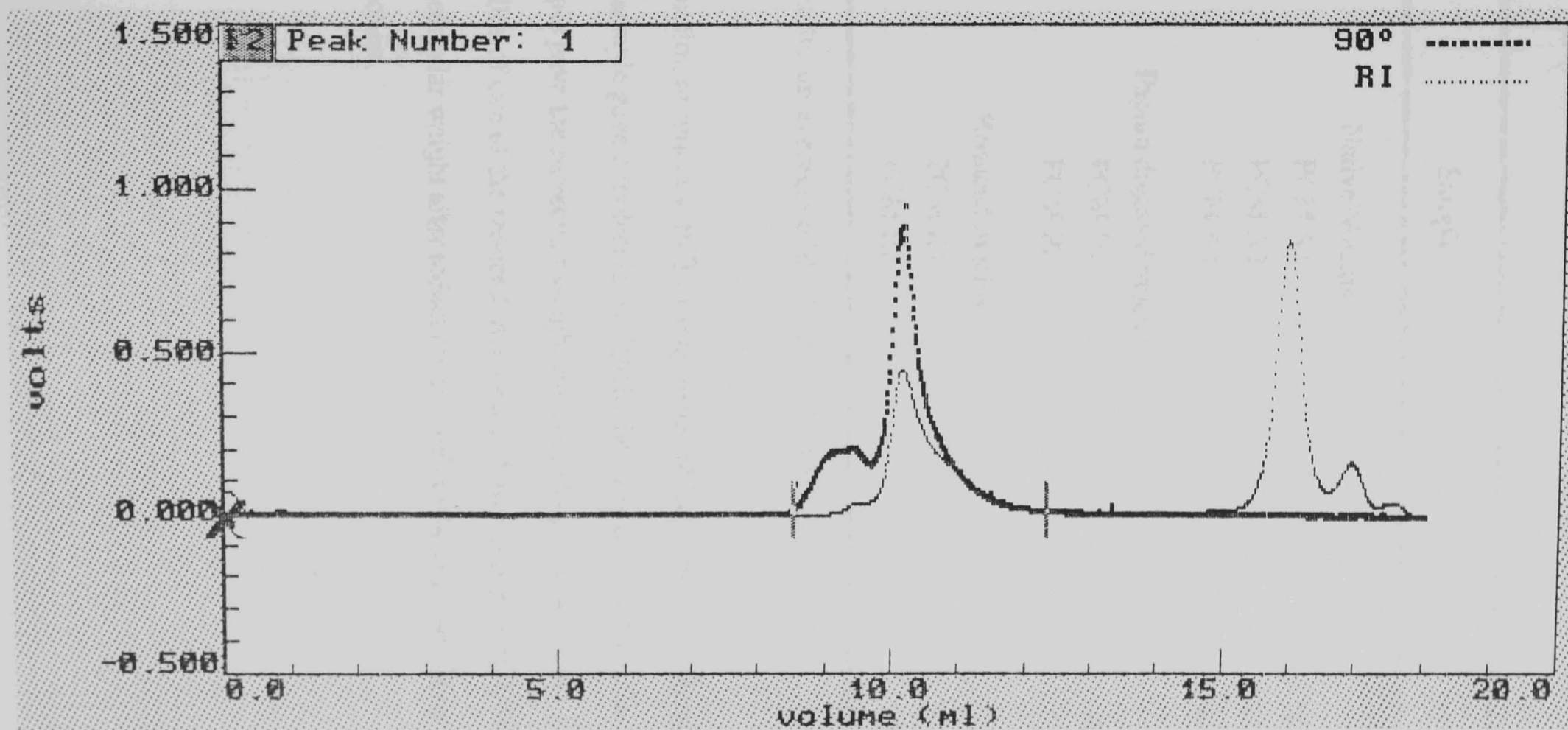
Figure B.8: Elution profiles from light scattering (90° detector) and differential refractive index detectors for PCM P2 sample. Conditions as in Figure B.1

Table B.2: Weight average molecular weights of native and degraded pig colonic mucins using SEC/MALLS

Sample	$10^{-6} \times M_w$
Native Mucins	
PCM A1	$5.56 \pm 0.16^*$
PCM A2	$4.89 \pm 0.19^*$
PCM A3	$6.41 \pm 0.24^*$
Papain digested mucins	
PCM P1	0.672
PCM P2	0.800
Reduced mucins	
PCM R1	0.501
PCM R2	3.77

* Results are averages of duplicate SEC/MALLS runs.

Reduction of mucin with β-mercaptoethanol led to two very different results, one sample gave a molecular weight higher than expected and the second sample gave the molecular weight corresponding to a basic unit. Elution profiles of one of the reduced mucins are shown in Figure B.9. The variation in molecular weight after reduction may reflect the non-specificity of the thiol reduction.
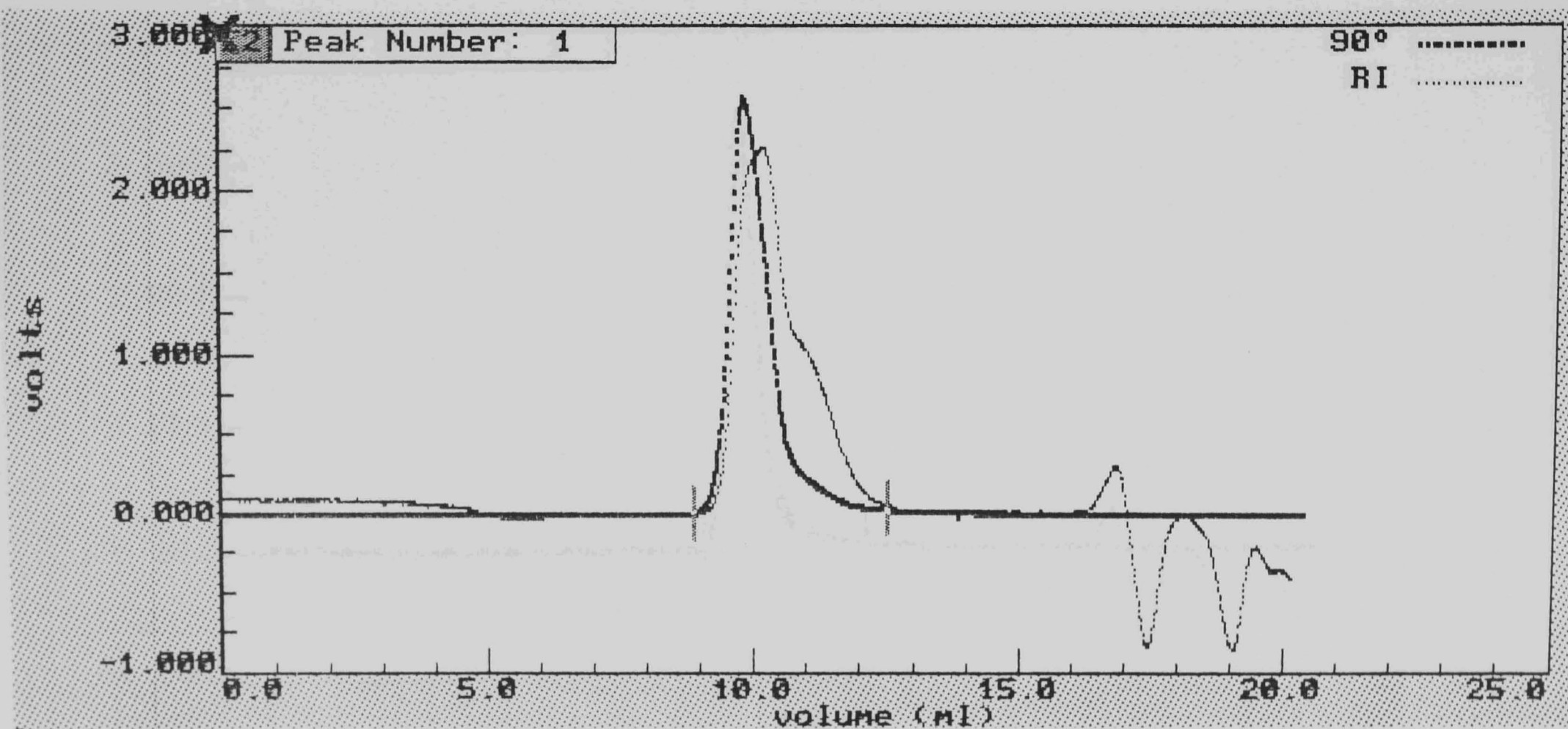
Figure B.9: Elution profiles from light scattering (90° detector) and differential refractive index detectors for PCM R2 sample. Conditions as in Figure B.1

APPENDIX C: SEC/MALLS STUDY ON XANTHAN

The xanthan samples were gifts from Kelco International and were analysed by SEC/MALLS as part of Mr. R. Dhami's characterization work of xanthan. SEC/light scattering analyses have been carried out by a number of workers (for example Lecacheux et al, 1986, Lambert et al, 1982; Milas and Rinaudo, 1979). However, SEC of xanthan is problematic due to the very large size of the molecules and there are not many packing matrices which have pores sufficiently large to allow separation of xanthan.

The chromatograms of the three xanthans investigated are shown in Figure C.1 to Figure C.3. There are two striking features of these chromatograms. Firstly, the very steep rise at the total exclusion volume which indicates that a large amount of material is eluting at the total exclusion volume. Secondly, both the light scattering and concentration traces take a very long time to return to the baseline - such behaviour is usually interpreted as one of the signs for adsorption. The molecular weight versus elution volume trace (Figure C.4) for the Keltrol BT sample confirms this suspicion. Material starts eluting at the exclusion volume, however, instead of the molecular weight decreasing with increasing elution volume, an increase of molecular weight with elution volume is found. Such behaviour is feasible when molecules of different conformations co-elute, however, coupled with the information from the elution traces it seems more likely, that non-size exclusion effects such as adsorption have taken place.

The weight average molecular weight values obtained for the xanthan samples fall within the range quoted by other workers (Lecacheux et al, 1986; Lambert et al, 1982; Milas and Rinaudo, 1979) and it would be expected that with an absolute detector the average molecular weight values are still correct
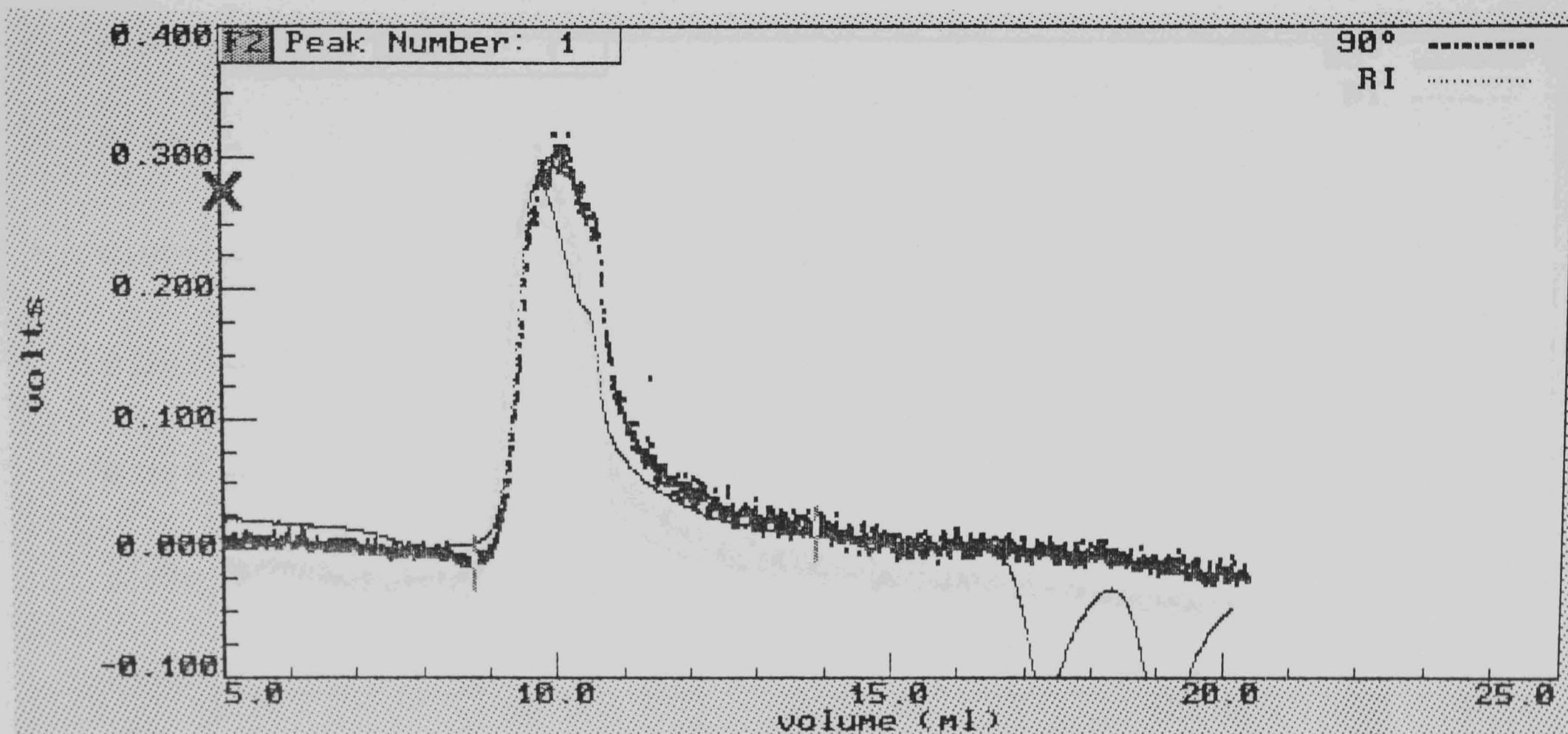
Figure C.1: Elution profiles from light scattering (90° detector) and differential refractive index detectors for Keltrol RD sample. Sample concentration = 1mg/ml, injection volume = 100µl, dn/dc = 0.164ml/g, flow rate = 0.5ml/min, eluent = phosphate/chloride buffer (I = 0.3, pH6.8) according to Green (1933), column system 2.
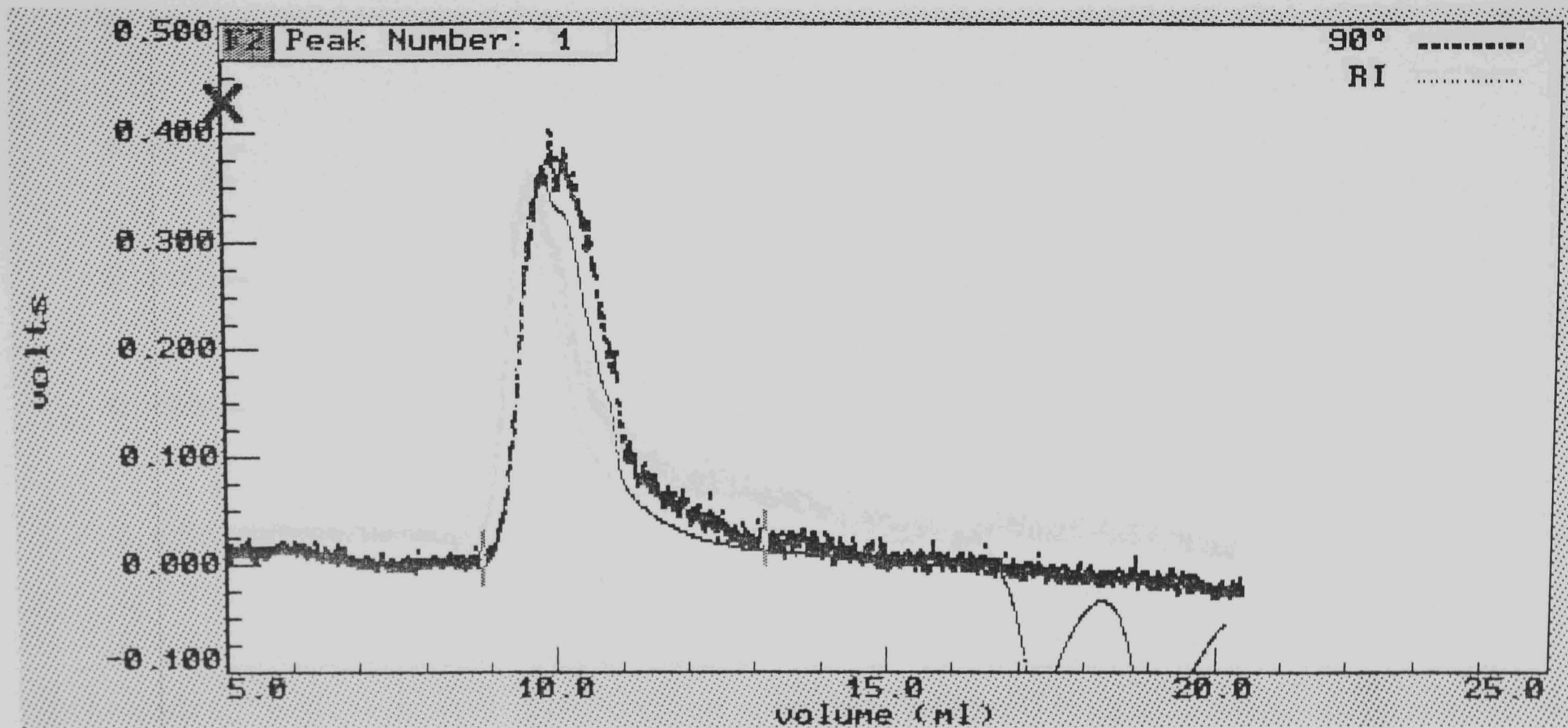
Figure C.2: Elution profiles from light scattering (90° detector) and differential refractive index detectors for Keltrol BT sample. Conditions as in Figure C.1.

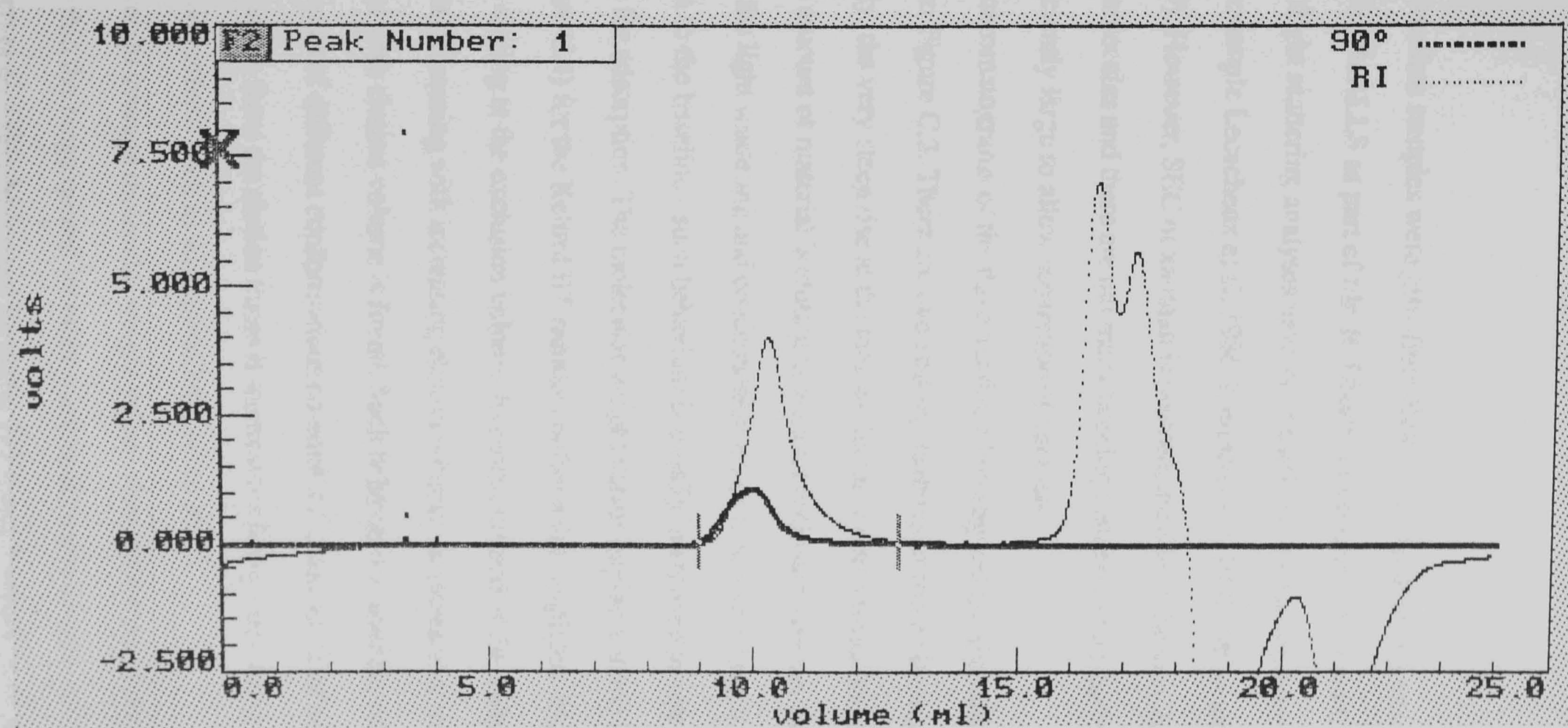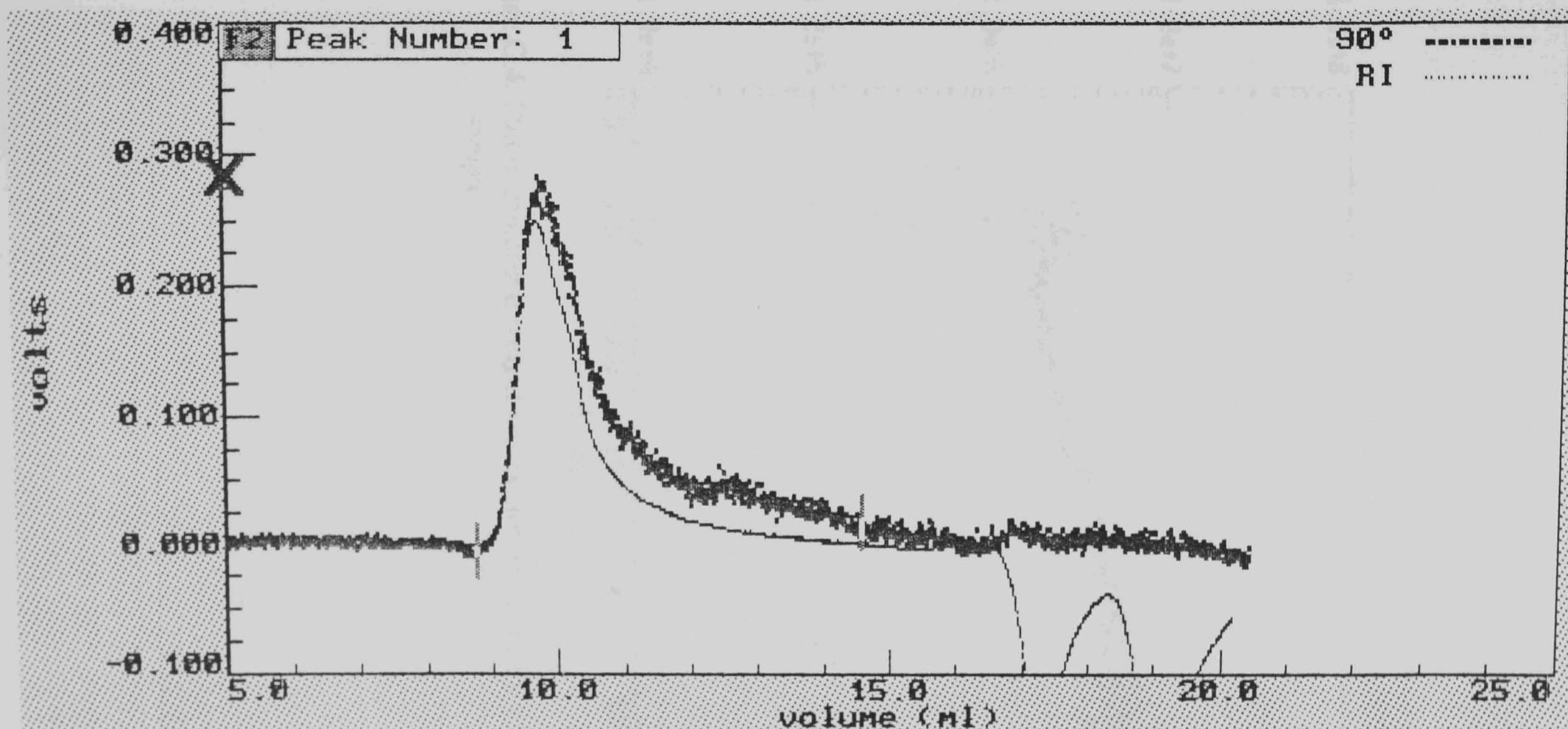**Figure C.3**: Elution profiles from light scattering (90° detector) and differential refractive index detectors for Keltrol FG sample. Conditions as in Figure C.1.
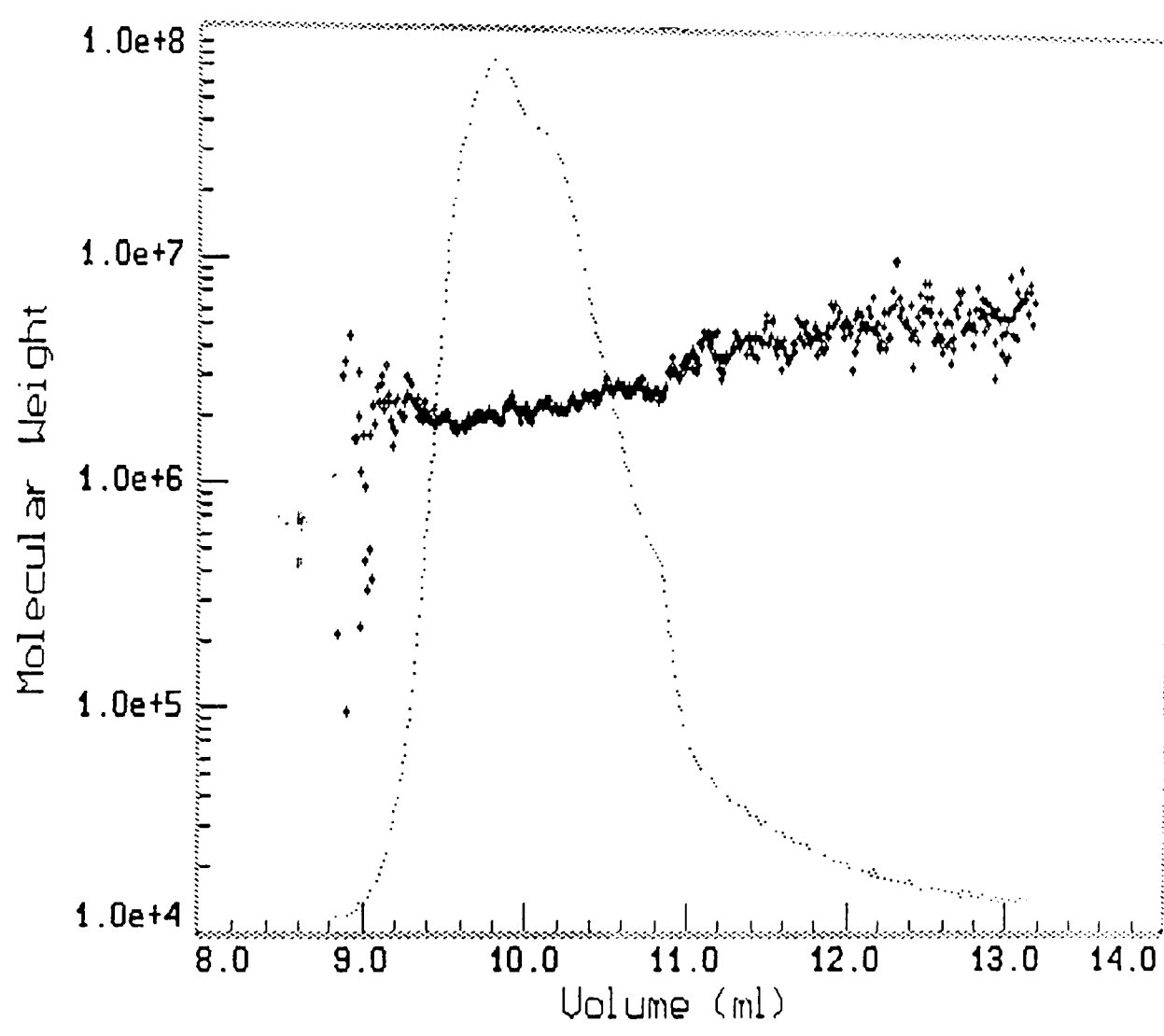
Figure C.4: Plot of molecular weight versus elution volume for Keltrol BT sample

as there is no elution volume dependence of this parameter. However, there is a large difference between the molecular weight averages for the samples which were run twice (see Table C.1) which may be indicative of adsorbed material from a previous run being slowly released. The weight average molecular weight values quoted here are therefore subject to these limitations. Further work with xanthan on SEC/MALLS was abandoned as it appeared futile with regards to improving results and possibly very costly with regards to SEC columns. The samples were characterized by sedimentation equilibrium techniques by Mr. R. Dhami and the results are included for comparison in Table C.1.

Table C.1: Weight average molecular weights of commercial xanthan samples

Sample	$10^{-6} \times M_w$ (from SEC/MALLS)[a]	$10^{-6} \times M_w$ (from sed. equilibrium)[b]
Keltrol BT	2.60	2.45
Keltrol FG	2.43 3.62	3.16
Keltrol RD	1.98 2.99	4.89

[a] Individual results from each SEC/MALLS run

[b] Personal communication from Mr. R. Dhami

PUBLICATIONS

Jumel, K., Harding, S.E., Mitchell, J.R., Dickinson, E. (1993): Evidence for Protein-Polysaccharide Complex Formation as a Result of Dry-heating of Mixtures; in, 'Food Colloids and Polymers: Stability and Mechanical Properties', E. Dickinson and P. Walstra (eds.), Royal Society of Chemistry, Cambridge, 157-160

Harding, S.E., Jumel, K., Kelly, R., Gudo, E., Horton, J.C., Mitchell, J.R. (1993); The Structure and Nature of Protein-Polysaccharide Complexes; in, 'Food Protein Structure and Functionality', K.D. Schwenke, and R. Mothes (eds.), VCH, Weinheim, 216-226

Mitchell, J.R., Hill, S.E., Jumel, K., Harding, S.E., Aidoo, M. (1992); The Use of Anti-Oxidants to Control Viscosity and Gel Strength Loss on Heating of Galactomannan Systems; in, 'Gums and Stabilizers for the Food Industry 6', G.O. Phillips, P.A. Williams, D.J. Wedlock (eds.), Oxford University Press, Oxford, 303-310

Evidence for Protein–Polysaccharide Complex Formation as a Result of Dry-heating of Mixtures

By K. Jumel, S. E. Harding, J. R. Mitchell, and Eric Dickinson[1]

DEPARTMENT OF APPLIED BIOCHEMISTRY AND FOOD SCIENCE, UNIVERSITY OF NOTTINGHAM, SUTTON BONINGTON, LOUGHBOROUGH, LEICESTERSHIRE LE12 5RD, UK
[1]PROCTER DEPARTMENT OF FOOD SCIENCE, UNIVERSITY OF LEEDS, LEEDS LS2 9JT, UK

1 Introduction

The complexes produced by the dry-heating of the globular protein bovine serum albumin (BSA) and the non-ionic polysaccharide dextran have been shown recently to have excellent emulsion stabilizing properties.[1,2] This short paper presents experimental data on the molecular weight of complexes formed by dry-heating mixtures of BSA and dextran T40 (4×10^4 daltons) as determined by gel permeation chromatography with light-scattering detection (GPC/MALLS) and ultracentrifugation.

2 Experimental

Protein–polysaccharide complexes were prepared by dry heating various molar ratios of BSA and dextran T40 at 60 °C for 3 weeks as described previously.[1] The samples were dissolved in phosphate/chloride buffer (pH 7.0, ionic strength 0.1 M). Weight-average molecular weights of samples of various molar ratios were determined by GPC/MALLS (sample concentration 3 mg ml^{-1}).[3] The BSA–dextran complex of molar ratio 2:1 in a solution of concentration 0.5 mg ml^{-1} was investigated under conditions of low-speed sedimentation equilibrium in a Model E analytical ultracentrifuge. The sedimentation coefficient of this same complex (sample concentration 2 mg ml^{-1}) was determined using a Beckman XL-A analytical ultracentrifuge.

3 Results and Discussion

Figure 1 shows the weight-average molecular weight M_w of various BSA–dextran complexes as determined by GPC/MALLS. We see that, of the various samples investigated, only the complex with a composition of 33 mol % dextran has a molecular weight substantially greater than that for the native protein. Table 1 compares the value of M_w obtained from GPC/MALLS for this 2:1 molar ratio complex with that from low-speed sedimentation equilibrium. Also shown for comparison are M_w values for the heat-treated pure BSA (same heating conditions). The results indicate that, although some aggregation of the BSA itself occurs during the
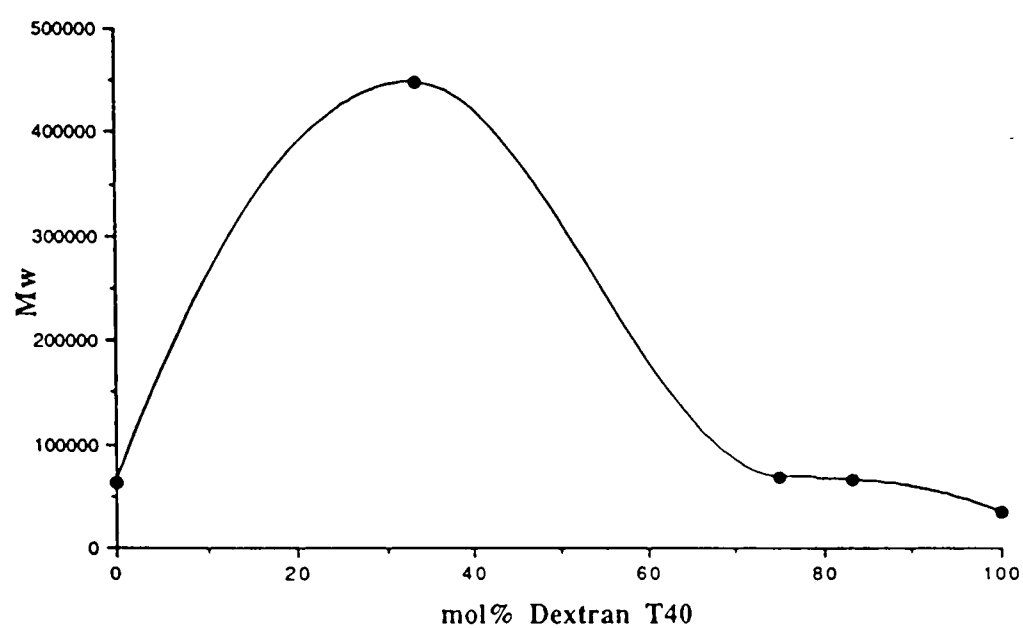
mol% Dextran T40

Figure 1 *Weight-average molecular weight M_w of complexes obtained by dry-heating of mixtures of BSA and dextran T40 at various molar ratios*

Table 1 *Molecular weight, sedimentation coefficients, and frictional coefficients*

Sample	M_w (daltons) GPC/MALLS	M_w (daltons) Model E	s_{20} (S)	$s_{20,w}$(S)	f/f_0
BSA native	62 700 ± 5 000	66 700[a]	3.93 ± 0.1	4.04 ± 0.1	1.3 ± 0.1
BSA heat-treated (3 weeks)	158 000 ± 10 000	130 000 ± 10 000	5.43 ± 0.1	5.59 ± 0.1	1.3 ± 0.1
BSA/T40 complex 2:1 ratio	450 000 ± 20 000	330 000 ± 20 000	4.85 ± 0.1	4.98 ± 0.1	3.4 ± 0.1

[a] Value from: K. E. van Holde, 'Physical Biochemistry', Prentice-Hall, 1971

dry-heating process, this does not account for the much larger average molecular weight of the complex. The general trends of behaviour detected by GPC/MALLS and ultracentrifugation are the same. The slight discrepancy in the numerical values can be accounted for by noting that the light-scattering results may be affected to some, extent by additional aggregated material co-existing with the protein–polysaccharide complex, whereas such material might have moved to the cell base in ultracentrifugation measurements and would therefore not have contributed to the weight-average molecular weight.

Figure 2 compares chromatographic elution profiles for the BSA–dextran complex (2:1 molar ratio) with those for the native BSA and the heat-treated BSA. We note the different position of the complex peak (lower elution volume) from that for the protein alone, both from light-scattering analysis and differential refractive index analysis. The peak shape shows that the complex is not a single species but is polydisperse. Figure 3 shows the movement of the sedimenting boundary for the BSA–dextran complex (2:1 molar ratio). The presence of a single sedimenting boundary suggests that the polydispersity is more of a quasi-continuous character than a paucidisperse one.

Sedimentation coefficients of complex, native BSA and heated BSA are also given in Table 1. From the molecular weight and the $s_{20,w}$ value, we can estimate the frictional ratio f/f_0. Assuming that the $s_{20,w}$ value measured is not too far from the infinite dilution value, the large value of f/f_0 derived for the complex is suggestive of either a highly asymmetric or a highly hydrated entity.
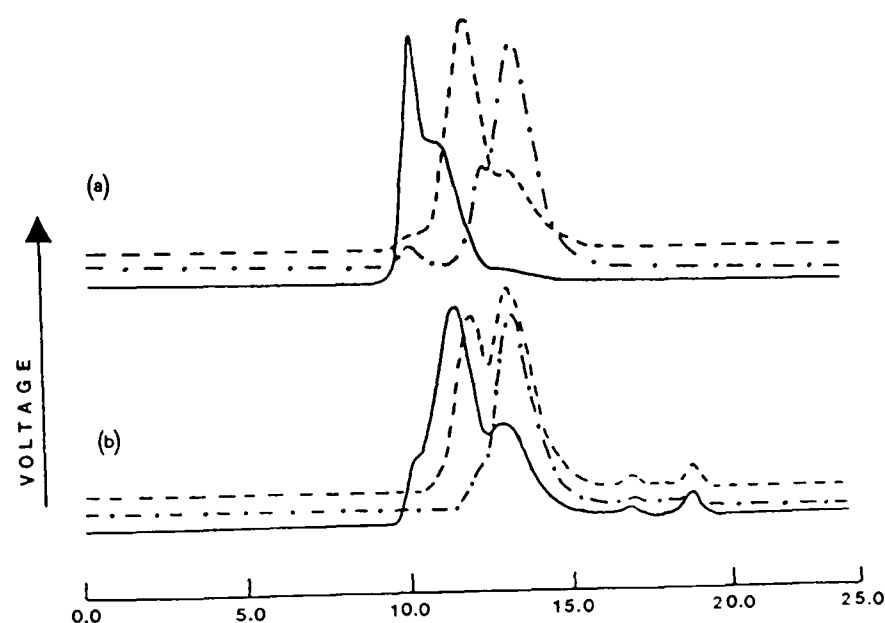
Figure 2 (a) *Light-scattering chromatograms (obtained from 90° detector) and (b) Differential refractive index chromatograms:* - - - - -, *native BSA;* - - -, *heat treated BSA;* —, *BSA/dextran T40 (2:1) complex*
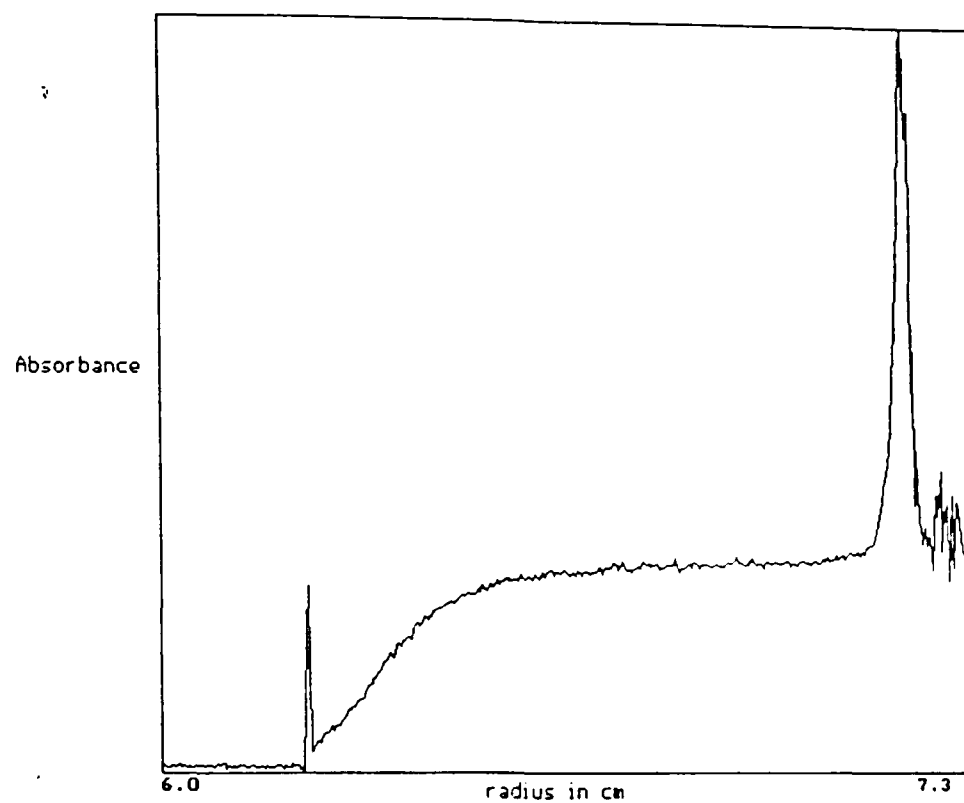
Figure 3 *Sedimenting boundary of BSA/dextran T40 (2:1) complex*

References

1. E. Dickinson and V. B. Galazka, in 'Gums and Stabilisers in the Food Industry',
   ed. G. O. Phillips, D. J. Wedlock, and P. A. Williams, Oxford University Press,
   1992, Vol. 6, p.351.
2. E. Dickinson and M. G. Semenova, *Colloids Surf.*, 1992, 64, 299.
3. P. J. Wyatt, in 'Laser Light Scattering in Biochemistry', ed. S. E. Harding,
   D. B. Satelle, and V. A. Bloomfield, Special Publication No. 99, Royal Society
   of Chemistry, Cambridge, 1992, p. 35.

The Structure and Nature of Protein-Polysaccharide Complexes

Stephen Harding, Kornelia Jumel, Rachel Kelly, Elias Gudo,
John C. Horton and John R. Mitchell

University of Nottingham, School of Agriculture,
Sutton Bonington LE12 SRD, England

Summary

Many food systems consist of mixtures of protein and polysaccharide and many are also thermally processed. Potential interaction phenomena in solutions of protein and polysaccharide are described using the following probes: sedimentation velocity and sedimentation equilibrium analytical ultracentrifugation, dynamic light scattering and total intensity light scattering coupled to an on-line gel permeation chromatography system. Specifically the following mixtures were studied: (i) unheated and heated solutions containing mixtures of bovine serum albumin (BSA) and a highly characterised alginate; (ii) unheated and heated solutions of BSA with a well characterised pectin; (iii) solutions of dry heated mixtures of BSA with a dextran. In (i) a strong dependence on heating temperature is demonstrated; in (ii) no interaction is observed, rather the pectin itself appears thermally unstable; in (iii) the size of the complex appears to depend critically on the molar ratio of BSA to dextran.

1. Introduction

For many years our laboratory has been interested in the solution sizes, shapes and interactions of glycopolymers - that is glycoproteins and polysaccharides - but quite recently we have branched out into the relatively dangerous world of glycopolymer-protein interactions, and in this paper we will describe our work on three types of food protein-polysaccharide systems which we have been focussing on over the last eighteen months or so.

A fundamental complication when attempting to study possible interaction phenomena in protein-polysaccharide mixtures is that although one entity in the mixture is usually well characterised and well behaved - namely the protein component - the other, the polysaccharide, is not. Solutions of polysaccharides are usually highly non-ideal in the thermodynamic sense through exclusion volume and polyelectrolyte effects; they are also usually highly polydisperse (i.e. consist of non-interacting components of different molecular weight and density). Finally, some can also have the potential to perform self-association reactions in solution.

All these properties of polysaccharides make it very difficult to try and describe potential interactions with proteins in terms of stoichiometries and interaction constants - sometimes the best we can hope for is to semi-quantify average effects. This means that

when dealing with solutions of polysaccharides mixed with proteins we cannot use the so-called "high resolution" techniques of nmr, X-ray diffraction or computer molecular modelling but instead have to use the classical "low-resolution" solution techniques such as analytical ultracentrifugation and light scattering.

We have been looking at potential interactions in three types of mixture. First, unheated solutions of a well characterised alginate with bovine serum albumin (BSA). Secondly, mixtures of the same alginate and also pectin with BSA where the solution had previously been given various degrees of heat treatment. Finally we looked for interactions in a system where a dry mixture of a polysaccharide and a protein had been heat-treated prior to being brought into solution. It is worth pointing out that many food systems consist of mixtures of protein with polysaccharide and many are thermally processed, so seeing what happens under solution heating or dry heating conditions is, one would think, quite relevant. However we would like to stress that all the studies we have done so far on these systems have been under dilute solution conditions: it could well be the situation we see is quite different at higher concentrations.

2. Methodology

There are three principal "low-resolution" techniques we have used to study these interactions: analytical ultracentrifugation (in two formats), dynamic light scattering and finally total intensity (or classical) light scattering coupled to on-line GPC.

2.1. Analytical Ultracentrifugation

We used two types of analytical ultracentrifuge experiment. In "sedimentation velocity" the rate of movement of a sedimenting boundary is measured to obtain the sedimentation coefficient which is a function of the size, shape and interaction properties of the system. We use both absorption optics and "refractive index gradient" (or Schlieren) optics. At the much slower speeds in a "sedimentation equilibrium" experiment, which is used to measure molecular weights and - for protein systems - to quantify interaction parameters, we can record the final distribution of solute in the centrifuge cell using either Rayleigh interference optics or absorption optics (the latter is used if we are only focussing on the behaviour of the protein component of the mixture).

Three analytical ultracentrifuges were used for this work. (i) An MSE (Crawley, U.K.) Centriscan equipped with scanning absorption and scanning Schlieren optics. This is dedicated to sedimentation velocity work and is particularly useful for detecting interactions between species which have different chromophores by looking for co-sedimentation. Sedimentation coefficients were evaluated off line using a computer graphics digitising tablet interfaced to an Apple IIE microcomputer. (ii) A Beckman (Palo Alto, USA) Model E equipped with Rayleigh interference optics and a laser light source

and which is dedicated to sedimentation equilibrium measurements. Rayleigh interference solute distribution records are captured off line via an LKB laser densitometer and converted to a record of relative concentration versus radial distance via a UCSD PASCAL Fourier series PC routine ANALYSE2 [1]. These ASCII data are then passed onto a mainframe IBM 3084/Q and molecular weight analysis performed using a FORTRAN routine MSTAR (see, e.g. [2]). (iii) An Optima XL-A. This is the newest analytical ultracentrifuge from Beckman instruments [3] from whom we are privileged to have received an evaluation model. In this study, this instrument was used only for sedimentation equilibrium work with (protein) solute distributions recorded using absorption optics at 278 nm. ASCII records of solute absorbance versus distance from the interfaced PC were passed to the IBM 3084/Q and analysed as above.

2.2. Dynamic Light Scattering

For the dynamic light scattering we use a Malvern 4700 instrument with a 25 mW laser (see e.g. [4]) at a scattering angle of 90°. The data are analysed only to give simple apparent diffusion coefficient measurements at a temperature of 25°C from the slope of the log of the normalised autocorrelation function against delay time (or equivalently channel number). This gives a rough measure of particle size (without correction of the apparent translational diffusion coefficient to zero angle, zero sample time or zero concentration) and, from comparison of the goodness of linear and quadratic fits, a rough idea of sample polydispersity via the so-called "polydispersity factor" (see, e.g., [5]).

2.3. Total Intensity Light Scattering (TILS)/ Gel Permeation Chromatography (GPC)

The other light scattering instrument which we have used is a total intensity (or classical) light scattering photometer from Wyatt instruments (see, e.g., [6]). A cleverly constructed array of detectors allows simultaneous intensity measurements for a range of angles. More significant is the provision of a flow cell which allows the instrument to be coupled on-line to gel permeation chromatography - we use this total set-up as a second independent technique from sedimentation equilibrium for molecular weight work. The idea of a scattering cell as a flow cell coupled directly on-line to GPC separation columns and associated filters is in our opinion a superb one for (i) circumventing the well-known but, these days, ill-reported dust problem of light scattering and (ii) fractionating a heterogeneous system directly prior to molecular weight analysis. It appears to give reliable results - as checked by sedimentation equilibrium - but with only a fraction of the time and effort, as will be seen below.

3. Solution Heated Mixtures of BSA with an Alginate

We will first consider mixed solutions of a well-characterised protein - BSA - with a well characterised, highly purified and fractionated alginate polysaccharide called Pronova (Protan Ltd., Drammen, Norway). This is an alginate extensively studied by groups at Trondheim and Trieste [7] using light scattering and osmometry and by ourselves [8,9] using analytical ultracentrifugation and total intensity light scattering/gel permeation chromatography. We have a consensus molecular weight of just over ~200,000 for this substance. Solutions (each of concentration 2 mg/ml) of BSA (Sigma, Poole, UK) and alginate dispersed in a phosphate chloride buffer (pH = 6.8, I = 0.1) were mixed together in a 1:1 ratio and then studied either as made up or after being heated for 30 minutes at various temperatures. The aim was to search for changes in apparent molecular size, sedimentation coefficient or molecular weight and from these to obtain a qualitative idea of the strength of any interaction as a function of temperature. All the *measurements* were done at a temperature of 25.0°C.

3.1. Mean size

Mean size was estimated in terms of the effective hydrodynamic diameter from dynamic light scattering measurements as described above.

MEAN SIZE (DYNAMIC L.S.): ALGINATE + BSA

Fig. 1.
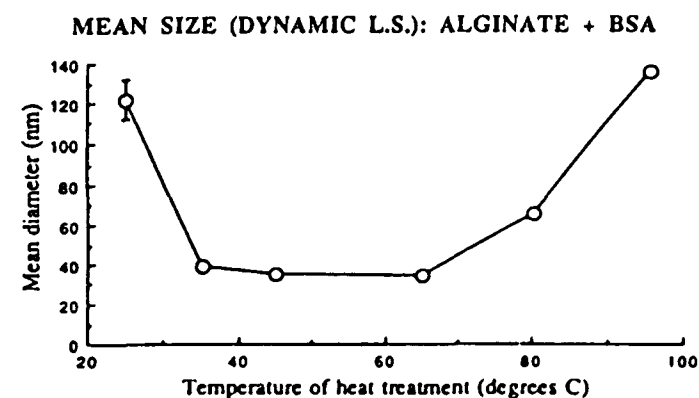Effective hydrodynamic diameter of solution heated mixtures of BSA with pro-nova alginate. All measurements performed at a temperature of 25.0°C.

Fig. 1 shows an interesting trend of a drop in size after mild heat treatment compared with its value when no heat treatment was applied. Between treatment temperatures of 70 and 80°C the size increases again to over three times the previous size at a treatment

temperature of 95°C. The alginate control shows no change in effective diameter {~(70+10) nm} whereas the BSA control shows an increase from about 10 nm to about 50 nm beyond its denaturing temperature (~55°C). It would appear therefore *on the basis of this data alone* that we have an interaction with no heat treatment, destroyed by mild treatment - the bottom plateau level appears to be approximately a weighted average of the alginate and BSA species -until beyond the thermal denaturation temperature of the protein the interaction process becomes significant again.

3.2. Sedimentation velocity

Now you can never trust one technique in isolation in this business -especially if it's a light scattering one. Sedimentation velocity however appears to confirm the above observations. Consider for example a Schlieren diagram for the non-heat treated mixture (Fig. 2) showing two clear components, one sedimenting at 1.5 S, presumably unbound alginate, the other moving down much faster at 10.6 S, far faster than even dimeric BSA: and this is a complex. Indeed the sedimentation coefficient of the faster component measured at 25°C as a function of treatment temperature appears to reproduce the trend observed with the dynamic light scattering data, with a drop in s value for mild heat treatment and a steady increase beyond the thermal denaturation temperature of the BSA when presumably more potentially interactive groups are exposed.
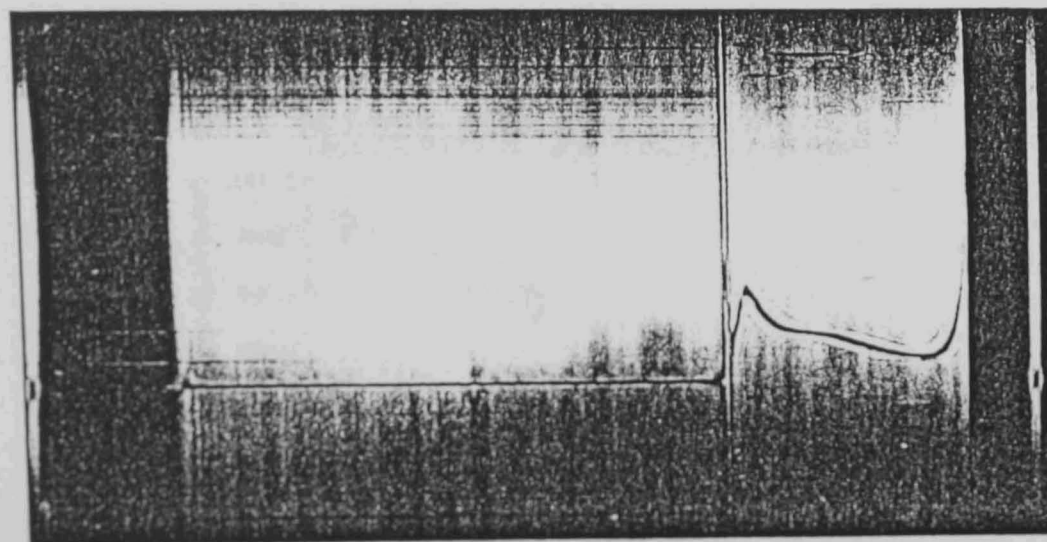

Fig. 2.
Sedimentation diagram for a solution containing 1 mg/ml BSA and 1 mg/ml pro-nova alginate, after no prior heat treatment.
Rotor speed 34790 rev/min. Direction of sedimentation is from left to right.

In fact, if we combine the sedimentation data with the dynamic light scattering diffusion data, then, notwithstanding the fact that we haven't corrected our results properly to standard solvent conditions or extrapolated to zero solute concentration, we can get a *relative* estimate of the weight average molecular weight of the mixtures' components. This is shown in Fig. 3 with values hovering around the unbound alginate value of ~200000 between temperatures of 35°C to 55°C reaching up to 10 times this value at either extreme.
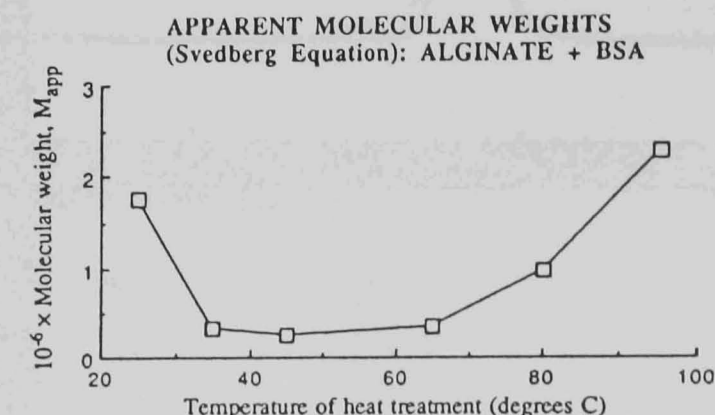

Fig. 3.
Apparent molecular weights of solution heated mixtures of BSA with pro-nova alginate evaluated from the Svedberg equation. All measurements performed at a temperature of 25.0°C.

4. Solution Heated Mixtures of BSA with a Pectin

If we replace the alginate by a highly characterised pectin { "GENU" pectin with a degree of esterification ~70% [10] } we get quite a different picture. The apparent mean size from dynamic light scattering drops and continues to drop with increasing temperature of heat treatment (Fig. 4a). We believe this proves that the interaction of BSA is more specific to alginate and that the pectin itself is thermally unstable as shown in the control of Fig. 4b. Perhaps a native pectin molecule is not a simple covalent entity but made up of smaller non-covalent basic units. This view appears to be confirmed by measurement of (apparent) molecular weights (at a loading concentration of ~0.5 mg/ml) as determined directly by low speed sedimentation equilibrium (Fig. 4c).

This marks the present extent of our work on heated solution mixtures. Obviously we need to look at a range of concentrations and for a range of solvent conditions (pH, ionic strength etc.) to understand better what exactly is happening.

(a)

MEAN SIZE (DYNAMIC L.S.): BSA + PECTIN

(b)

MEAN SIZE (DYNAMIC L.S.): PECTIN ONLY

(c)

APPARENT MOLECULAR WEIGHTS
(SEDIMENTATION EQUILIBRIUM): PECTIN
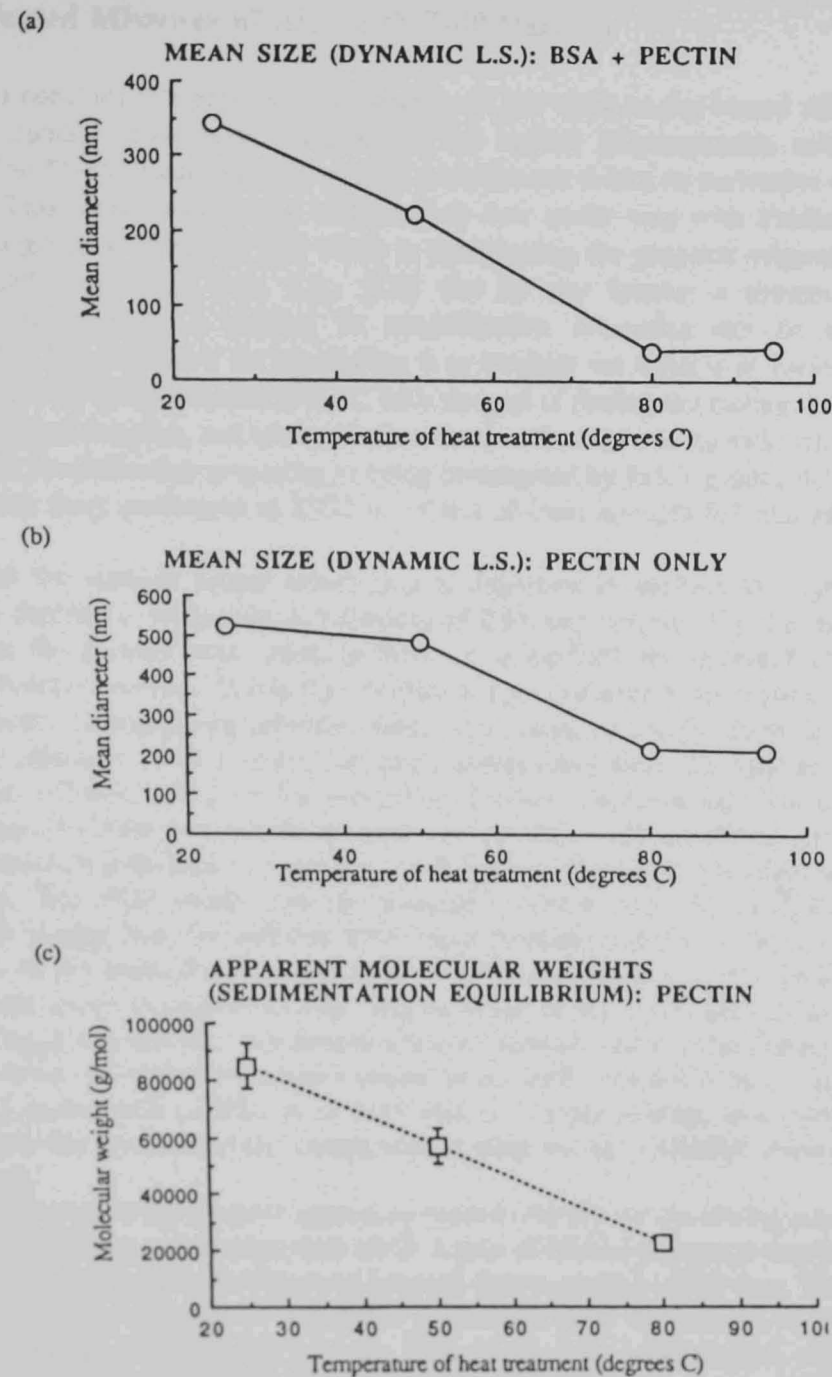
Fig. 4.
Effective hydrodynamic diameter of (a) solution heated mixtures of BSA with GENU pectin and (b) solution heated GENU pectin. (c) Apparent molecular weights (at a loading concentration of 0.5 mg/ml) for GENU pectin. All measurements performed at a temperature of 25.0°C.
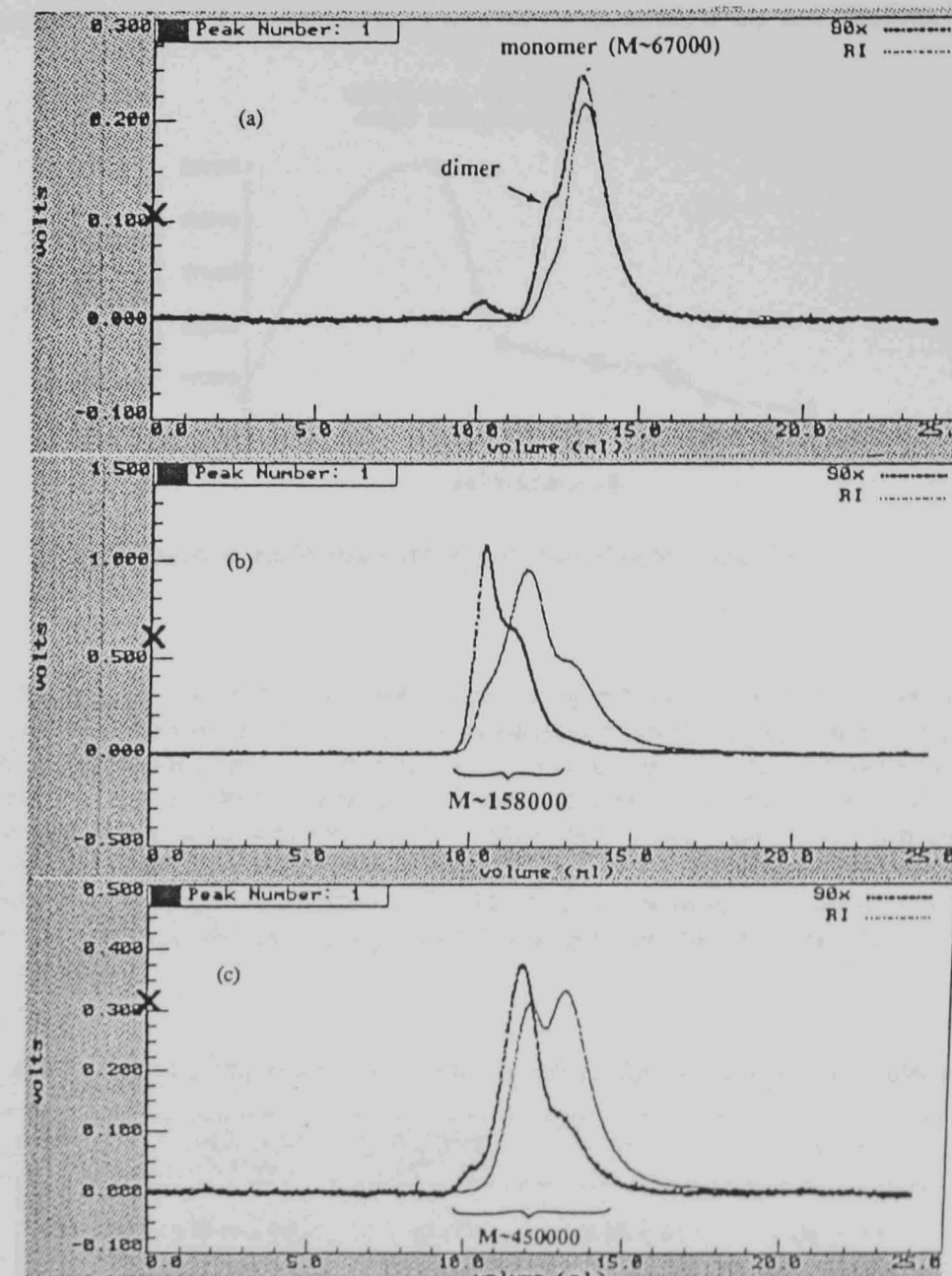
Fig. 5.
Total intensity light scattering/gel permeation chromatography 90° scattering angle intensity (solid lines) and refractive index (lighter lines) versus elution volume profiles for solutions of
(a) native BSA (b) dry heated BSA
(c) dry heated mixture of BSA (T-40 dextran at a molar mixing ratio of 2:1.

5. Dry Heated Mixtures of BSA with T-40 Dextran

We will conclude this paper with a summary of our work on dry heated mixtures of BSA with another fairly well characterised but neutral polysaccharide called T-40 dextran. (The "T-40" means the commercial manufacturer thinks its molecular weight is ~40000.) This work is part of a collaboration now under way with Professor Eric Dickinson's group at Leeds [11,12] which is investigating the proposal originally made by Kato and co-workers (see, e.g., [13]) that by dry heating a protein with a polysaccharide such as a dextran its emulsification properties can be enhanced considerably. The procedure for dry heating is to incubate the mixture at various molar ratios for a period of three weeks at 60°C with the goal of finding the mixing ratio which gives the biggest complex, and seeing if this corresponds to the mixing ratio which gives the optimum emulsification properties as being investigated by Eric's group. All solution measurements were performed at 25°C in solvent of ionic strength 0.1 and pH 6.8 as above.

As with the solution heated mixtures it is important to perform the appropriate controls to determine the individual behaviour of BSA and dextran. Fig. 5a shows two traces from the Dawn-F total intensity light scattering-GPC for unheated BSA as a function of elution volume. One is the intensity of light scattered at an angle of 90° and the other is the corresponding refractive index (concentration) profile. Most of the BSA appears as monomer (with a molecular weight extrapolated from the angular intensity envelope of ~67000) with a smaller proportion of dimer. The same experiment on BSA that had been dry heated before being made up into dilute solution shows, as with the solution heated material before, a tendency to dimerise or form high molecular weight n-mers (Fig. 5b). The weight average molecular weight over the macromolecular distribution eluting from the columns (PSS Hema Biolinear and Hema Bio40 in series) comes out to 2-3 times the monomer value. Similar experiments on the T-40 dextran control yield weight average molecular weights of just under 40000 and no tendency to aggregate upon dry heating. Dry heated mixtures however show a clear disposition to aggregate over and beyond the small increase for the BSA, and this is shown in Fig. 5c for a 2: 1 molar ratio of BSA to dextran with the weight average molecular weight coming over the macromolecular components coming out as ~450000, averaged over several runs.

In fact the size of the complex appears to depend critically on the mixing ratio (rather like antigen-antibody interactions) with the 2: 1 ratio of BSA to dextran giving by far the largest size (Fig. 6) as based on the total-intensity light scattering / GPC data. This seems to be reproducible. Because of this rather remarkable value we've tried to check this using independent sedimentation methods. First of all using sedimentation equilibrium performed using the new Optima XL-A, we find a value for the apparent weight average molecular weight from the M* procedure [14] of ~330000 for the 2: 1 complex and ~130000 for heat treated BSA, both in good agreement with the light scattering results (bearing in mind that the sedimentation equilibrium results correspond to a loading

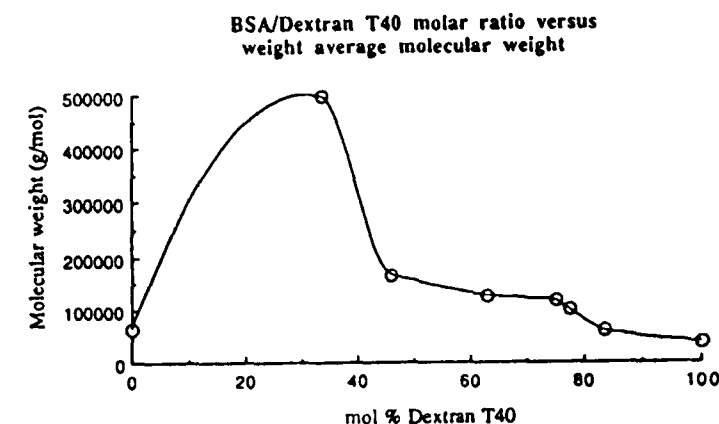concentration of ~0.5 mg/ml and not corrected for thermodynamic non-ideality).

Fig. 6.
Molecular weight of BSA/T-40 complex as a function of molar mixing ratio.

This concept of a strong interaction at the mixing ratio of 2: 1 was confirmed by co-sedimentation experiments (see, e.g., [15]) using sedimentation velocity and a mixture of Schlieren and absorption optics. Finally, Table 1 summarises the clear difference in size between the 2:1 dry heated mixture compared with native and heat treated BSA and native and with heat treated T-40 dextran as supported by two independent techniques, namely light scattering and analytical ultracentrifugation.

With that philosophical statement of the importance of the virtue of combining results from independent techniques together when handling tricky systems such as these, we close this paper.

Table 1. Dry heated BSA dextran T-40 mixture - molecular weights and sedimentation coefficients.

Sample	M_w (g/mol) TILS/GPC	M_w (g/mol) Sed. eqm	s_{20} (S)	$s_{20,w}$ (S)
BSA native	62700 ± 5000	66700*	3.93 ± 0.1	4.04 ± 0.1
head treated	158000 ± 10000	130000 ± 10000	5.43 ± 0.1	5.59 ± 0.1
BSA/T40	450000 ± 20000	330000 ± 20000	4.85 ± 0.1	4.98 ± 0.1
2:1 ratio	37100 ± 3000	·	~2.0	~2.0
T40 native heat treated	37300 ± 3000	·	·	·

* Value from Physical Biochemistry, K. E. van Holde, Prentice-Hall, 1971.
* For 3 weeks at 60°C

6. References

[1] S.E. Harding and A.J. Rowe, Optics andLasers in Engineering 8 (1988) 83-96.
[2] S.E. Harding, J.C. Horton and P.J. Morgan in S.E. Harding, A.J. Rowe and J.C. Horton (Eds.),
Analytical Ultracentrifugation in Biochemistry and Polymer Science, Royal Society of Chemistry,
Cambridge, U.K., 1992, Chapter 15.
[3] R. Giebler in (2), Chapter 2.
[4] A.D. Molina-Garcia, S.E. Harding and R.S.S. Fraser, Biopolymers 29 (1990) 1443-1452.
[5] P.N. Pusey in H.Z. Cummings and E.R. Pike (Eds.),
Photon Correlation and Light Beating Spectroscopy, Plenum Press, New York, 1974, p. 387.
[6] P.J. Wyaa (1992) in S.E. Harding, D.B. Sattelle and V. Bloomfield (Eds.), Laser Light Scattering
in Biochemistry, Royal Society of Chemistry, Cambridge, U.K., Chapter 3.
[7] A. Martinsen, G. Sjåk-Bræk, 0. Smitisrød, F. Zanetti and S. Paoletti,
Carbohydrate Polym. 15 (1990) 171.
[8] J.C. Horton, S.E. Harding and J.R. Mitchell, Biochem. Soc. Trans. 19 (1991) 510-511.
[9] J.C. Horton, S.E. Harding, J.R. Mitchell and D.F. Morton-Holmes,
Food Hydrocolloids 5 (1991) 125-127.
[10] M.A.V. Axelos, G. Berth, J.P. Busnel, D. Duranti, S.E. Harding, C. Rolin, J.C. Horton
and J.F. Thibault, Pure and Applied Chemistry (1993) manuscript submitted.
[11] E. Dickinson and V.B. Galazka, Food Hydrocolloids 5 (1991) 281-296.
[12] K. Jumel, S.E. Harding, J.R. Mitchell and E. Dickinson
in E. Dickinson (Ed.), Food Colloids and Polymers: Stability and Mechanical Properties, 1993
[13] S. Nakamura, A. Kato and K. Kobayashi, J. Agric. Food Chem. 40 (1992) 735-739.
[14] J.M. Creeth and S.E. Harding, J. Biochem. Biophys. Meth. 7 (1982) 25-34.
[15] E.N. Marsh and S.E. Harding, Biochem. J. (1993) in press.

The use of anti-oxidants to control viscosity and gel strength loss on heating of galactomannan systems

J.R.MITCHELL, S.E.HILL, K.JUMEL, S.E.HARDING and M.AIDOO

Department of Applied Biochemistry and Food Science, University of Nottingham, Sutton Bonington, nr Loughborough, Leicestershire LE12 5RD, UK

SUMMARY

Viscosity loss on autoclaving guar gum solutions can be substantially reduced by the addition of mixtures of the antioxidants, sodium sulphite and propyl gallate. There appears to be a strong synergistic interaction between the two materials with the maximum affect occurring at ratios of sulphite to gallate of about 3:1. Total antioxidant levels required for substantial protection at pH 7.0 are of the order~100ppm. The antioxidant combination is also effective in reducing the loss in gel strength which results from autoclaving mixtures of carrageenan and locust bean gum. The similar optimum ratio of sulphite to gallate to that found with the guar system and the small influence of the antioxidants on carrageenan alone suggests that in this mixed system the antioxidants function primarily by protecting the locust bean gum. The results favour a specific interaction rather then "phase separated" model for the mixed gel system. It is possible some of the reported interactions between polysaccharides and other food ingredients can be understood in terms of the antioxidant properties of the ingredients rather than biopolymer association or phase separation.

INTRODUCTION

Polysaccharides are extensively used as thickeners and gelling agents in heat sterilised foods. It is well established that heat treatment can result in substantial decreases in viscosity and gel strengths the decrease being strongly dependent on pH (Pilnik and MacDonald,(1)).In general viscosity and gel strength loss on heating is far lower at neutral pHs then acid pHs which is indicative of the importance of acid hydrolysis. The exception is pectin where β-elimination dominates. However even at neutral pHs polysaccharides will degrade as a result of oxidative reductive depolymerisation (ORD) reactions. This form of degradation can be controlled by the addition of antioxidant systems. The work that has been carried out has mainly been concerned with the stabilisation of polymers used in oil field applications, e.g. Wellington (2), and little attempt has been

made to extend this approach to food systems using non-toxic antioxidants. Recently, (3) , we have reported some preliminary work which demonstrated that galactomannans, in particular, can be effectively stabilised by low levels of combinations of sodium sulphite and propyl gallate. These materials are allowed as additives in some food products. In this paper we demonstrate that there is a very strong synergism between the two antioxidants and extend the work to the mixed carrageenan/locust bean gum gel systems to determine if the substantial gel strength loss that occurs on autoclaving (Ainsworth and Blanshard (4)) can be prevented.

MATERIALS AND METHODS

Polysaccharides

Guar gum, locust bean gum and carrageenan (described predominantly as kappa) were obtained from the Sigma Chemical Company and used without any further purification.

Other Chemicals

Propyl gallate was obtained from the Sigma Chemical Company. Potassium dihydrogen orthophosphate (SLR grade), disodium hydrogen orthophosphate (SLR grade) potassium chloride (AR grade) and sodium sulphite (AR grade) were obtained from Fisons plc.

Preparation of Solutions and Gels

Unless otherwise stated solutions and gels were prepared in a mixed phosphate buffer of pH 7.0 (9.09 g/l KH_2PO_4, 11.88 g/l Na_2HPO_4). In some cases KCl was added and/or the pH altered by changing the ratio of the two phosphate salts. The anti-oxidants were incorporated into the buffer prior to the addition of the polysaccharide. Guar gum was added at ambient temperature using a high shear mixer to give a concentration (w/v) of 0.8%. Carrageenan and locust bean gum were added to the buffer at a temperature of 80°C to give a total polysaccharide concentration of 0.8%. Cans (diameter 72 mm and height 58 mm) were filled with the guar or carrageenan-locust bean gum mixture and seamed leaving no headspace. Following retorting (120 C for 60 minutes) the cans were water cooled and allowed to stand at ambient temperature for approximately 24 hours prior to viscosity and gel strength measurement. Some measurements were also made on non-retorted controls.

Viscosity

Viscosities were determined at 20°C using a Deer rheometer equipped with cone and plate geometry (cone angle 4°) or concentric cylinder geometry (radius of inner cylinder = 2.8 cm, radius of outer cylinder = 2.9 cm). Measurements were generally

made at five different applied stresses.

Gel Strength

Gel strength measurements were made directly in the can at ambient temperature using a TAXT2 Texture Analyser (Stable Microsytems Ltd, Haslemere, Surrey, England). The lid of the can was removed and a 1.20 cm diameter plunger was used to penetrate the gel at a speed of 2 cm/sec to a distance of 25 mm. The maximum force recorded was taken as the gel strength in Newtons. Following texture measurement, the pH of the gel was recorded.

RESULTS AND DISCUSSION

Figure 1 displays the viscosity of the 0.8% guar solutions following retorting as a function of antioxidant ratio at a total antioxidant level of 200 ppm (0.02%). The data shows very strong synergism between the two additives. It has been reported that the addition of sulphite enhances the thermal stability of guar gum (Rodriguez (5)) but it is clear that the binary system suggested from Wellington's (2) work with xanthan gum is very much more effective. The optimum ratio of the two additives is about 3:1 sulphite to gallate, gallate on its own having little effect.

There is some scatter in Figure 2 but this suggests that the stabilising effect of the additives levels off at concentrations of about 200 ppm. This is consistent with our preliminary work on this system (3) although in the current investigation the maximum viscosity obtained after retorting was about half that of the unretorted control, whereas previously complete stability was claimed. The reason for the difference is that in this case the concentration was well above c* and hence the viscosity will be far more strongly molecular weight dependent then in the previous case where measurements were being made on 0.2% solutions.

It is interesting to compare the effect of the antioxidants on the thermal stability of guar with their ability to prevent the breakstrength loss which occurs on autoclaving mixed carrageenan locust bean gum gels. Figure 3 shows a somewhat similar dependence on additive ratio to that observed for the viscosity of guar gum solutions. There is some suggestion that the sulphite: gallate ratio required for optimum gel strength is higher then that required for control of guar viscosity. Thus replacing 15ppm (0.0015%) of sulphite by gallate in the formulation doubles the gel strength. It is clear that the gel strength can be enhanced by a factor of about 4 compared with the system containing no additives although the strength of the non-retorted system is not achieved.

The effect of total additive concentration at ratios of 17:3 gallate to sulphite is displayed in Figure 4. This set of data implies that retorted gel strength does not reach a maximum
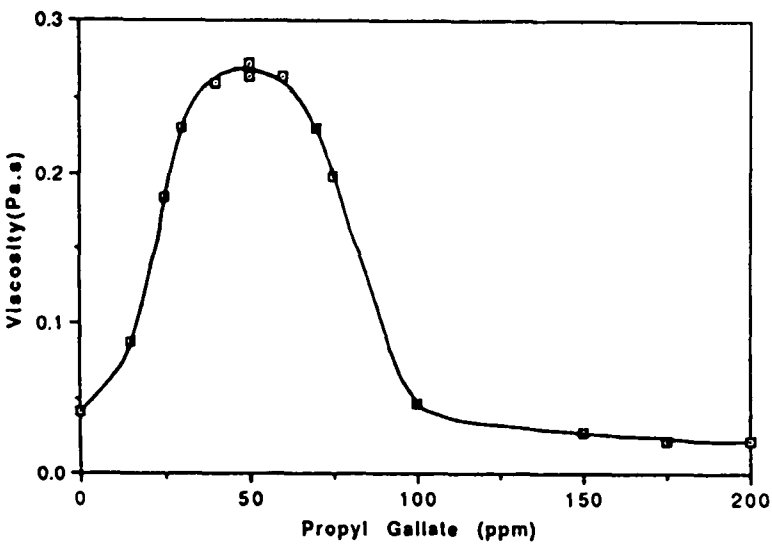
Figure 1. Effect of Antioxidant Ratio on the Viscosity (measured at 20°C and 50s⁻¹) of a 0.8% Guar Gum Solution at pH 7.0. The Total Antioxidant Concentration (Gallate plus Sulphite) was 200 ppm and Numbers on the Abscissa are the Propyl Gallate Concentration. The Viscosity of an Unretorted Control Containing no Additives was 0.55 Pa.s.
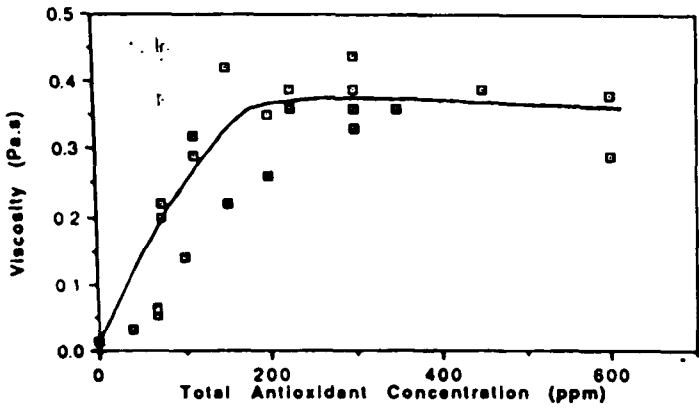

Figure 2. Effect of Total Antioxidant Concentration at a Sulphite:Gallate Ratio of 15:5 on Viscosity of Retorted Guar Solutions. Other Details as in the Legend to Figure 1.
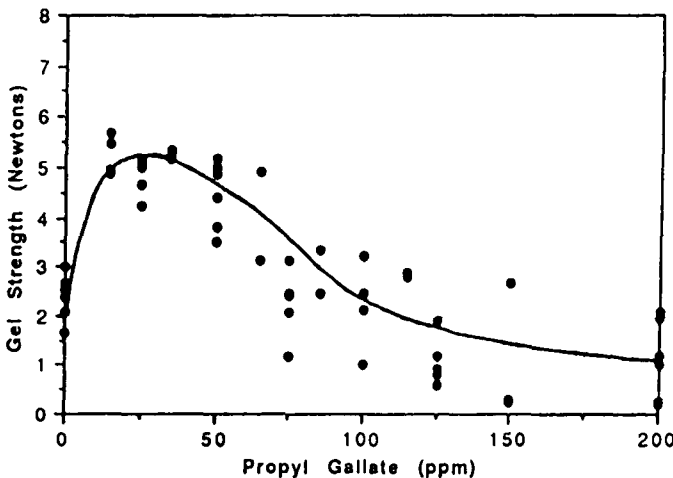

Figure 3. Effect of Antioxidant Ratio on the Strength of Retorted Gels at pH 7.0 Containing 0.4% Locust Bean Gum and 0.4% Carrageenan. The Total Antioxidant Concentration (Gallate plus Sulphite) was 200 ppm and Numbers on the Abscissa Represent the Concentration of Gallate . The Strength of a Retorted Control Containing no Antioxidants was 1.11 N (Five Measurements, Lowest-0.57N, Highest-1.73N) and a Non-Retorted Control with no Antioxidants was 7.0N (6.5N, 7.5N).
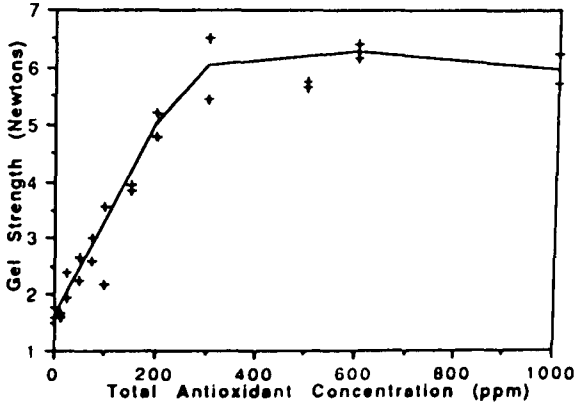

Figure 4. Effect of Total Antioxidant Concentration at a Sulphite:Gallate Ratio of 17:3 on Strength of Retorted Gels. Other Details as in Legend to Figure 3.
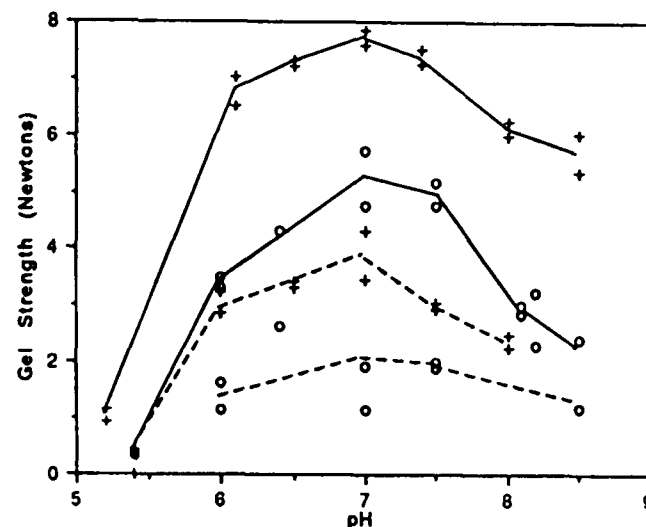
Figure 5. Effect of pH and KCl Addition on the Strength of Retorted Gels. ——— With Antioxidants (200 ppm of Sulphite and Gallate. Ratio 17:3). - - - - Without Antioxidants. ,+, With 0.1M KCl. ,o, No KCl. Other Details as in the Legend to Figure 3.
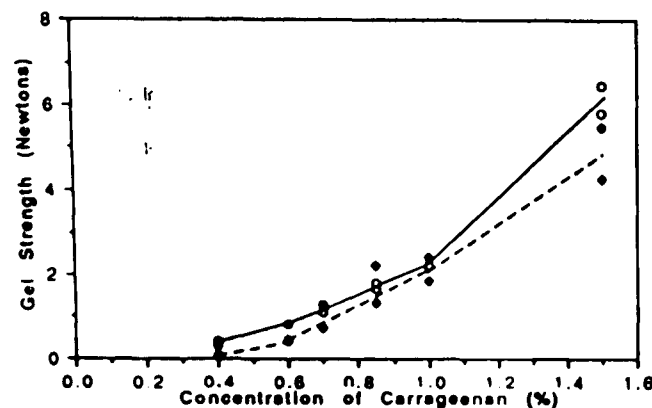

Figure 6. Retorted Gel Strength as a Function of Carrageenan. Concentration Alone (pH 7.0, no added KCl). - -●- - - No Antioxidants. ——o—— With 200 ppm of Sulphite plus Gallate (Ratio 17:3).

until the additive level exceeds 300 ppm although substantial improvement is obtained at far lower levels.

It is well recognised that the strength of these systems is strongly influenced by pH and by K $^+$ level. Figure 5 shows that gel strength is enhanced by the presence of KCl, however in the presence of KCl the antioxidant systems still have a substantial beneficial affect which in % or ratio terms is comparable to that obtained when there is no added K$^+$. Maximum gel strength is obtained near neutral pH and below pH 5 a solid gel is not obtained after retorting whether or not the antioxidants are present. This is presumably because at the lower pHs hydrolysis becomes far important as a degradation mechanism compared with ORD reactions.

Retorted gels containing carrageenan alone are not stabilised to anything like the same extent (Figure 6) compared with the mixed polysaccharide system and this suggests that what is important is the role of the antioxidants in protecting the galactomannans against degradation. This is of course consistent with our original work showing that compared with some other other food polysaccharides these materials are particularly receptive to protection by antioxidants.

A number of models have been suggested to explain the synergistic interaction between carrageenan and locust bean gum. The early suggestions that there was a specific association between unsubstituted regions of the mannan chain and carrageenan junction zones (Dea et al, (6)) have been challenged mainly on the basis that X-ray diffractograms on mixtures can be explained by the addition of carrageenan and mannan patterns and do not reveal a new ordered form (Cairns et al, (7)). A picture where locust bean gum associates with the carrageenan junction zones at only a small number of points on the galactomannan chain with the long flexible galactomannan chains making a small entropic contribution to the modulus but a major contribution to the rupture strength by holding the network together while carrageenan junctions reform on deformation would seem easier to reconcile with the strong dependence of brittleness on locust bean gum molecular weight implied by this work than would be the case for a phase separated picture.

Finally we would wish to make the point that we have shown that in simple aqueous systems very small amounts of antioxidants can drastically effect the "functionality" of polysaccharides. There will be antioxidant activity associated with many natural food ingredients. Some of the interations/synergisms reported between food ingredients e.g. galactomannans and milk, may be explained by the antioxidant capability of the ingredients included with the polysaccharide rather then a "non-chemical" macromolecular interaction.

ACKNOWLEDGEMENTS

REFERENCES

1. Pilnik, W. and McDonald, R.A. (1968) Gordian 12, 531

2. Wellington, S.L. (1983) Soc. Pet. Eng. J 9296, 901-912.

3. Mitchell, J.R., Reed,J., Hill, S.E. and Rogers, E. (1991) Food Hydrocolloids 5, 141-144

4. Ainsworth, P.A. and Blanshard, J.M.V. (1979) J. Food Technology 14, 141-147.

5. Rodriguez, P. (1985) US Patent 4514318.

6. Dea, I.C.M., McKinnon, A.A., and Rees, D.A. (1972) J. Mol. Biol. 68, 153-172

7. Cairns, P., Miles, M.J. and Morris, V.J. (1986) Int. J. Biol. Macromolecules 8, 124-127